NAVAL POSTGRADUATE SCHOOL
Monterey, California

THESIS

POWER RECOVERY OF RADIATION-DAMAGED
GALLIUM ARSENIDE AND
INDIUM PHOSPHIDE SOLAR CELLS

by

Corinne Cypranowski

December 1989

Thesis Advisor: Sherif Michael

Unclassified
SECURITY CLASSIFICATION OF THIS PAGE

REPORT DOCUMENTATION PAGE

Form Approved
OMB No. 0704-0188

1a. REPORT SECURITY CLASSIFICATION UNCLASSIFIED	1b. RESTRICTIVE MARKINGS NONE
2a. SECURITY CLASSIFICATION AUTHORITY	3. DISTRIBUTION/AVAILABILITY OF REPORT Approved for public release; Distribution is unlimited.
2b. DECLASSIFICATION/DOWNGRADING SCHEDULE	
4. PERFORMING ORGANIZATION REPORT NUMBER(S)	5. MONITORING ORGANIZATION REPORT NUMBER(S)
6a. NAME OF PERFORMING ORGANIZATION Naval Postgraduate School 6b. OFFICE SYMBOL (If applicable) 72	7a. NAME OF MONITORING ORGANIZATION Naval Postgraduate School
6c. ADDRESS (City, State, and ZIP Code) Monterey, Ca 93943-5000	7b. ADDRESS (City, State, and ZIP Code) Monterey, Ca. 93943-5000
8a. NAME OF FUNDING/SPONSORING ORGANIZATION 8b. OFFICE SYMBOL (If applicable)	9. PROCUREMENT INSTRUMENT IDENTIFICATION NUMBER
8c. ADDRESS (City, State, and ZIP Code)	10. SOURCE OF FUNDING NUMBERS PROGRAM ELEMENT NO. / PROJECT NO. / TASK NO / WORK UNIT ACCESSION NO.

11. TITLE (Include Security Classification)
POWER RECOVERY OF RADIATION-DAMAGED GALLIUM ARSENIDE AND INDIUM PHOSPHIDE SOLAR CELLS

12. PERSONAL AUTHOR(S)
Cypranowski, Corinne

13a. TYPE OF REPORT	13b. TIME COVERED	14. DATE OF REPORT (Year, Month, Day)	15. PAGE COUNT
Master's Thesis	FROM _____ TO _____	1989 December	156

16. SUPPLEMENTARY NOTATION The views expressed in this thesis are those of the author and do not reflect the official policy or position of the Department of Defense or the U.S. Government.

17. COSATI CODES		
FIELD	GROUP	SUB-GROUP

18. SUBJECT TERMS (Continue on reverse if necessary and identify by block number)
Minority carrier injection annealing of GaAs and InP solar cells

19. ABSTRACT (Continue on reverse if necessary and identify by block number)

Radiation damaging to on-orbit solar arrays was found to significantly decrease power output and efficiency. By a process of annealing, these cells can recover some of the initial performance parameters. Gallium Arsenide (GaAs) and Indium Phosphide (InP) solar cells were subjected to 1 MeV electron radiation by a Dynamitron linear accelerator at two fluence level of 1E14 and 1E15 electrons/cm^2. The annealing process was varied by temperature, amount of forward biased current, light conditions and time. Both types of cells were found to be hardened to radiation; however, the InP cells were superior over the two. Multiple cycles of irradiating and annealing were performed to observe the amount of degradation and recovery The results prove that substantial recovery will occur, particularly with the InP cells. Applying this process to on-orbit spacecraft utilizing solar arrays as the main source of power will significantly increase mission life and potentially decrease cost of the on-board power system.

20. DISTRIBUTION/AVAILABILITY OF ABSTRACT ☒ UNCLASSIFIED/UNLIMITED ☐ SAME AS RPT. ☐ DTIC USERS	21. ABSTRACT SECURITY CLASSIFICATION Unclassified
22a. NAME OF RESPONSIBLE INDIVIDUAL Sherif Michael	22b TELEPHONE (Include Area Code) (408)-646-2252 22c. OFFICE SYMBOL 62Mi

DD Form 1473, JUN 86 *Previous editions are obsolete.* SECURITY CLASSIFICATION OF THIS PAGE

Approved for public release; distribution is unlimited.

Power Recovery of Radiation-Damaged Gallium Arsenide
and Indium Phosphide Solar Cells

by

Corinne Cypranowski
Lieutenant, United States Navy
B.S., Northern Illinois University
M.S.S.M., University of Southern California

Submitted in partial fulfillment
of the requirements for the degree of

MASTER OF SCIENCE IN ELECTRICAL ENGINEERING

from the

NAVAL POSTGRADUATE SCHOOL
December 1989

Author: 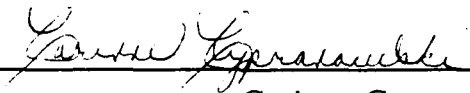

Corinne Cypranowski

Approved by: 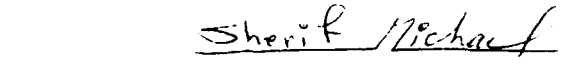

Sherif Michael, Thesis Advisor

Rudolph Panholzer, Second Reader

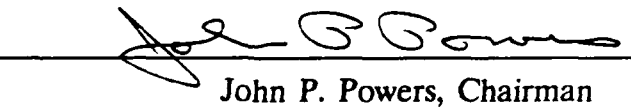

John P. Powers, Chairman
Department of Electrical and Computer Engineering

ABSTRACT

Radiation damaging to on-orbit solar arrays was found to significantly decrease power output and efficiency. By a process of annealing, these cells can recover some the initial performance parameters. Gallium Arsenide (GaAs) and Indium Phosphide (InP) solar cells were subjected to 1 MeV electron radiation by a Dynamitron linear accelerator at two fluence levels of 1E14 and 1E15 electrons/cm^2. The annealing process was varied by temperature, amount of forward-biased current, light conditions and time. Both types of cells were found to be hardened to radiation; however, the InP cells were superior over the two. Multiple cycles of irradiating and annealing were performed to observe the amount of degradation and recovery. The results prove that substantial recovery will occur, particularly with the InP cells. Applying this process to on-orbit spacecraft utilizing solar arrays as the main source of power will significant increase mission life and potentially decrease cost of the on-board power system.

TABLE OF CONTENTS

I. INTRODUCTION

A. DEVELOPMENT OF SPACE POWER SYSTEMS

Electrical power, the life-line of all spacecraft, has been a critical issue since the beginning of space exploration. Without sufficient power, an orbiting spacecraft could not operate its subsystems or payloads and mission life would be drastically reduced. As space exploration progressed, spacecraft capabilities have expanded and the need for electrical power has increased; therefore, the development of power systems have become more sophisticated and efficient.

A new era called the "space age" began with Sputnik I on October 4, 1957. Chemical batteries supplied the power needed to this spacecraft, but soon this would not suffice. Technology has progressed rapidly and the need for more power while on orbit is a necessity. Engineers looked to the sun to supply this additional energy and, in 1958, the first solar array was deployed and operated in space. Vanguard I was the vehicle for testing this new power system and was able to produce less than 1 watt of power over a life of 6 years. [Ref. 1:p. 1.1-1]

The small 23 inch diameter satellites used primarily for space exploration grew into the technologically sophisticated satellites of today which require thousands of watts of power. Solar arrays were able to satisfy those needs and became the primary power source for most spacecraft.

Array designs have grown in size and complexity with efficiency reaching up to the 20% range. Solar cell assemblies mounted on the exterior surface of the satellite was a means of utilizing available surface to increase the total output power which is needed on orbit. This simple design matured into the telescopic cylinders and deployable accordion-type panels which we are utilizing today. These creative designs have increased the power supplied to the spacecraft and have expanded our capabilities in space. [Ref. 2:p. 10]

In 1962, a high-altitude nuclear explosion took place and approximately 10^{25} fission electrons were trapped in the lower region of the Van Allen radiation belts. The Transit 4B was in orbit at this time and transmission ceased 24 days after the nuclear test. The electrons trapped within the belts caused a degradation of the solar cells and on-board electronics. [Ref. 2:p. 10]

Since then, radiation damage has become a critical issue. Various means of improving cell resistivity were explored. A change from p-on-n to n-on-p cells increased base resistivity. It was found that by increasing the thickness of the coverglass on the cell, the cells were shielded from the bombarding electrons to a limited extent. It was also found that low energy protons trapped in the outer regions of the Van Allen belts caused rapid degradation of bare cells by damaging the junctions. [Ref. 2:p. 14]

Despite the problems encountered, solar cell arrays provide an economical and safe source of electrical power. However, the decreased output of the

radiation-damaged cells can no longer provide the required power to an otherwise healthy spacecraft and designers need to over-design the power system to meet the end-of-life requirements. This resulted in larger, heavier and less cost-efficient arrays which would degrade over the mission life. Reversing the damage done to the cells while on orbit would eliminate the requirement of extra power at the beginning of life in order to complete its' mission.

An on-orbit damage annealing process was found to recover the electrical degradation experienced when the cells were subjected to the radiation belts [Ref 3]. The magnitude of recovery was enough to significantly increase the life of the cell while maintaining near peak performance. This is a very attractive prospect by which mission life can be extended for numerous years, particularly for those spacecraft spending the majority of its orbit inside the Van Allen belts. Despite the high exposure of damaging electrons and protons, the utility of the satellite would be extended years beyond their previous design lifetimes.

The success of this phenomena would have multiple implications on the design criteria of future spacecraft. First, the power supplied to the spacecraft could be maintained at the beginning-of-life level for prolonged periods of time, thereby eliminating the need to over-design a system. Secondly, the mission life of a spacecraft would be much longer which would ultimately decrease the cost of satellite operations. Thirdly, the size and weight of the on-board arrays would be reduced since a smaller array could maintain a near-beginning-of-life performance

level by periodically annealing sections of the arrays after a specified level of degradation occurred. The size and weight reduction would also translate into launch cost savings.

B. RESEARCH APPROACH AND GOALS

Various methods of annealing Silicon (Si) and Gallium Arsenide (GaAs) cells have been attempted in the past with limited success. Research has shown that a cell irradiated once with 1 MeV electrons at fluences in the range of 1E14 to 1E15 electrons/cm^2 will exhibit a significant amount of degradation [Ref.3] . The loss of capabilities can then be recovered by applying heat, light or current as the annealing mechanism. Conclusions were drawn that Si and GaAs solar cells can be annealed successfully after a one time irradiation.

In 1986, Clark [Ref. 3] investigated minority carrier injection with a forward bias current as a potential annealing mechanism. A group of cells were damaged and annealed once, while varying the amount of applied current and temperature. His results showed that approximately 28-30% recovery of lost power took place after 48 hours of annealing at 90 C with 0.5 A/cm^2 of continuous current. When the annealing was continued past 48 hours, no additional recovery was observed. Annealing with 1.0 A/cm^2 of forward-biased current showed cell degradation after 48 hours.

Staats [Ref. 4] continued Clark's thesis research to include forward bias current annealing of Si solar cells. This time, specified cells were irradiated with 1 MeV or 20 MeV electrons and annealed with current densities ranging from 0.125 A/cm^2 to 1.250 A/cm^2. The temperature parameter was also varied from 90 C to 140 C. His results verified that GaAs cell capabilities were recovered when annealed with current densities below 1.0 A/cm^2 and thermal annealing begins at 150 C. This experiment was also conducted for one irradiating and annealing cycle.

We now know that annealing of Si and GaAs cells will successfully recover lost capabilities after being subjected to radiation damage only once; however, a more important question is what will happen after multiple cycles of irradiating and annealing? The goal of this thesis is to investigate the long-term effects of such a process and to determine the optimum annealing mechanism to maintain near-peak performance of a cell over extended periods of time.

For the first time, concurrent forward-bias current and heat annealing of the state-of-the-art Indium Phosphide (InP) and GaAs cells was investigated. This research pioneered into the area of repetitive irradiating and annealing cycles of both types of cells while varying current density and time.

C. ORGANIZATION

The remaining contents of this thesis will address topics ranging from on-orbit conditions for satellite operations to the results of repetitive irradiating/annealing cycles of the state-of-the-art solar cells. Chapter 2 contains information on the space environment and the fundamental limitations it presents in relation to the operation of solar arrays. Chapter 3 addresses the state-of-the-art in solar cell technology and the areas of pursuit by industry for resolution of the problems that the environment is causing. The next chapter develops the theory of annealing and the physical defects in the cells which are caused by trapped electron and protons in the radiation belts. Chapters 5 and 6 outline the test plan and experimental results of the GaAs and InP cells subjected to various irradiation fluences and annealing conditions. Lastly, conclusions and recommendations for future research are results presented in the previous chapters. All experimental data obtained in this research is included in Appendices A-D.

II. SPACE ENVIRONMENT

The earth is enveloped by a dynamic environment. It is subjected to rotations, magnetic fields, anomalies, temperature and light variations, disturbances due to solar flares and is bombarded with gases, particles and winds. These disturbances are not only due to the earth's presence, but from other planets and stars in the solar system.

The earth's atmosphere extends to approximately 750 km from its' surface. It consists of the troposphere (containing weather phenomena), the stratosphere (ozone layer), the mesosphere (middle atmosphere with falling temperatures and noctilucent clouds), the thermosphere (region of heating due to absorption of radiation) and the exosphere (which is the escape from the atmosphere). The upper limit of the atmosphere is dependent on the amount of solar activity. As activity increases, the atmosphere will swell in the outward direction. This will cause on-orbit satellites to experience greater drag, thereby reducing the orbit size and increasing the energy lose rate. [Ref. 5: p. 127-143]

In the upper atmosphere there is a conducting region known as the ionosphere. It begins at 50 km above the earth's surface and extends to approximately 2000 km. At short wavelengths, solar radiation causes photoionization of the upper atmosphere. Large numbers of free electrons exist

where the gas density is very low, but the concentration is also dependent on the time of day, season and geomagnetic latitude. [Ref. 6:p. 65]

The ionosphere is divided into three regions according to latitude: high, mid- and low. The low latitude region experiences an equatorial electrojet due to the horizontal magnetic field at the equator. During the daylight hours, this current sheet flows from west to east while the electric fields drive plasma convection westward. At night, the directions reverse and the electron concentration decreases dramatically.[Ref. 6:p. 78]

Approximately 3 to 6 earth radii outward from the magnetic equator is a ring current which moves particles around the earth. Particles cross the earth's magnetic field lines with electrons moving eastward and ions westward resulting in a dusk-to-dawn westward current. The energy range of the ring current particles are 10-100 KeV with a density of 10^{-8}A-m^{-2}. The intensity of the current changes with the amount of plasma sheet particles injected during magnetic storms. [Ref. 6:p. 49]

The mid-latitude region of the ionosphere is free from the influences of energetic particle precipitation, the horizontal magnetic fields along the equator, and the electric fields in the earth's auroral zone. This region parallels the classic ionospheric models. [Ref. 6:p. 65]

Phenomena associated with the high latitude ionosphere originate from the magnetosphere-ionosphere interactions. A two-cell convection patter is produced by the electric fields due to the interaction of the geomagnetic and interplanetary

magnetic fields. The current flow is better known as the auroral electrojet which is responsible for the heating of the neutral atmosphere. The auroral oval and dayside cusp are two high latitude regions in which particle precipitation takes place. The main electron density trough concentration is high poleward and decreases as you move toward the equator. At the polar cap, high energy protons are absorbed due to incoming solar flares. [Ref. 6:p. 82]

Beyond the ionosphere, there is a region of highly active plasma called the magnetosphere. It is formed by the interaction of incoming solar winds and the earth's magnetic fields. These winds consist mainly of 1 KeV protons with a density of $10/cm^3$ and will form a shock wave which in turn forms the magnetosphere [Ref. 7:p. 5-2]. The earth's magnetic field will then experience turbulence due to the plasma of the solar winds passing through the shock wave. This turbulent region is called the magnetosheath and is highly irregular. The magnetopause then forms to create a boundary between the plasma of the solar wind and the magnetosphere. The shape of the magnetopause is depressed on the sunward side due to the high pressures of the solar winds.

Within this region, the Van Allen radiation belts can be located. These belts trap both electrons and protons which are damaging to spacecraft solar arrays. Figure 2.1 is an illustration of the magnetosphere and the location of the radiation belts. Figures 2.2 and 2.3 illustrates the distribution of the trapped particles for the inner and outer belts. The inner belt is characterized by high energy (20 to 200

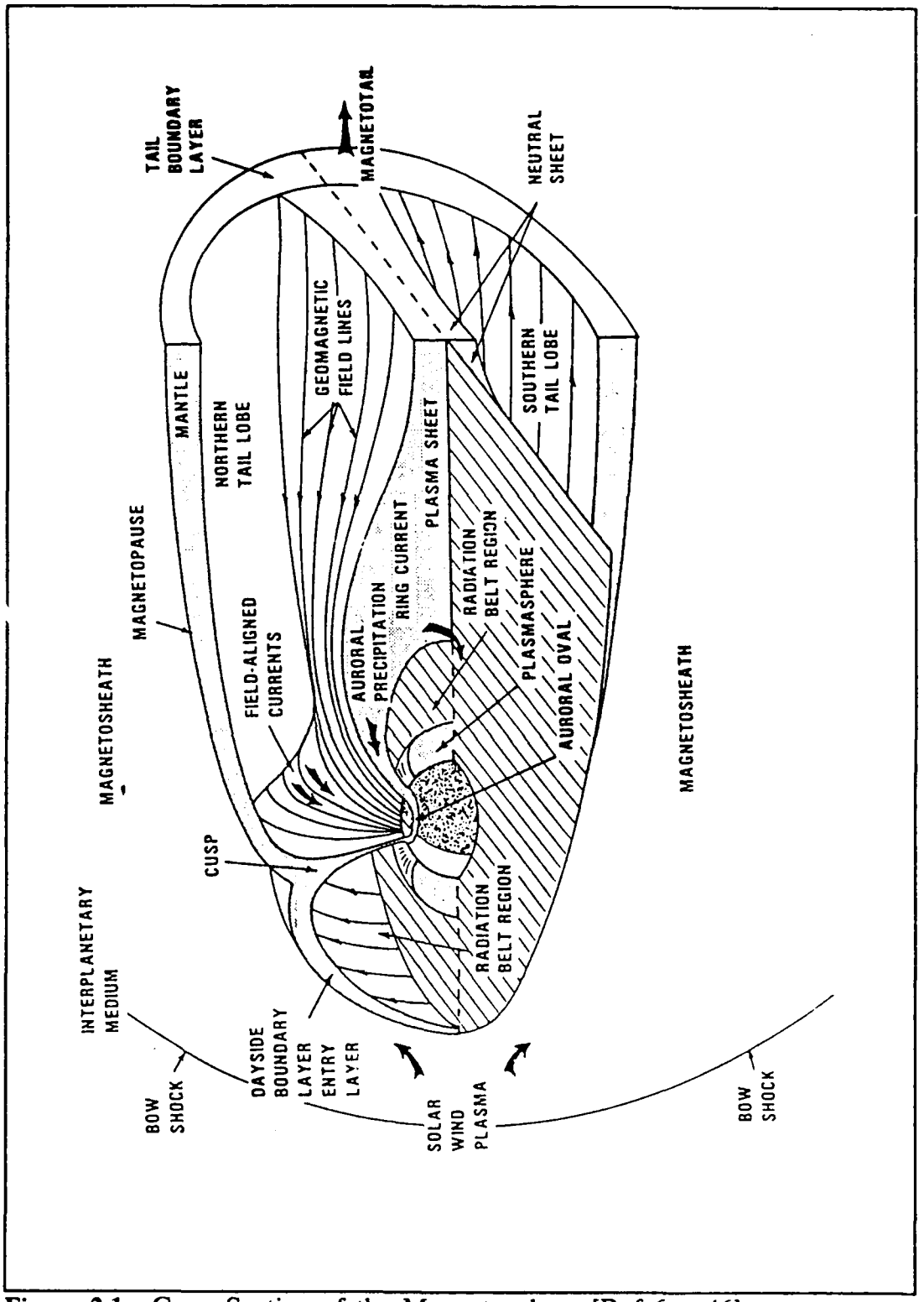

Figure 2.1. Cross Section of the Magnetosphere [Ref 6:p. 46].

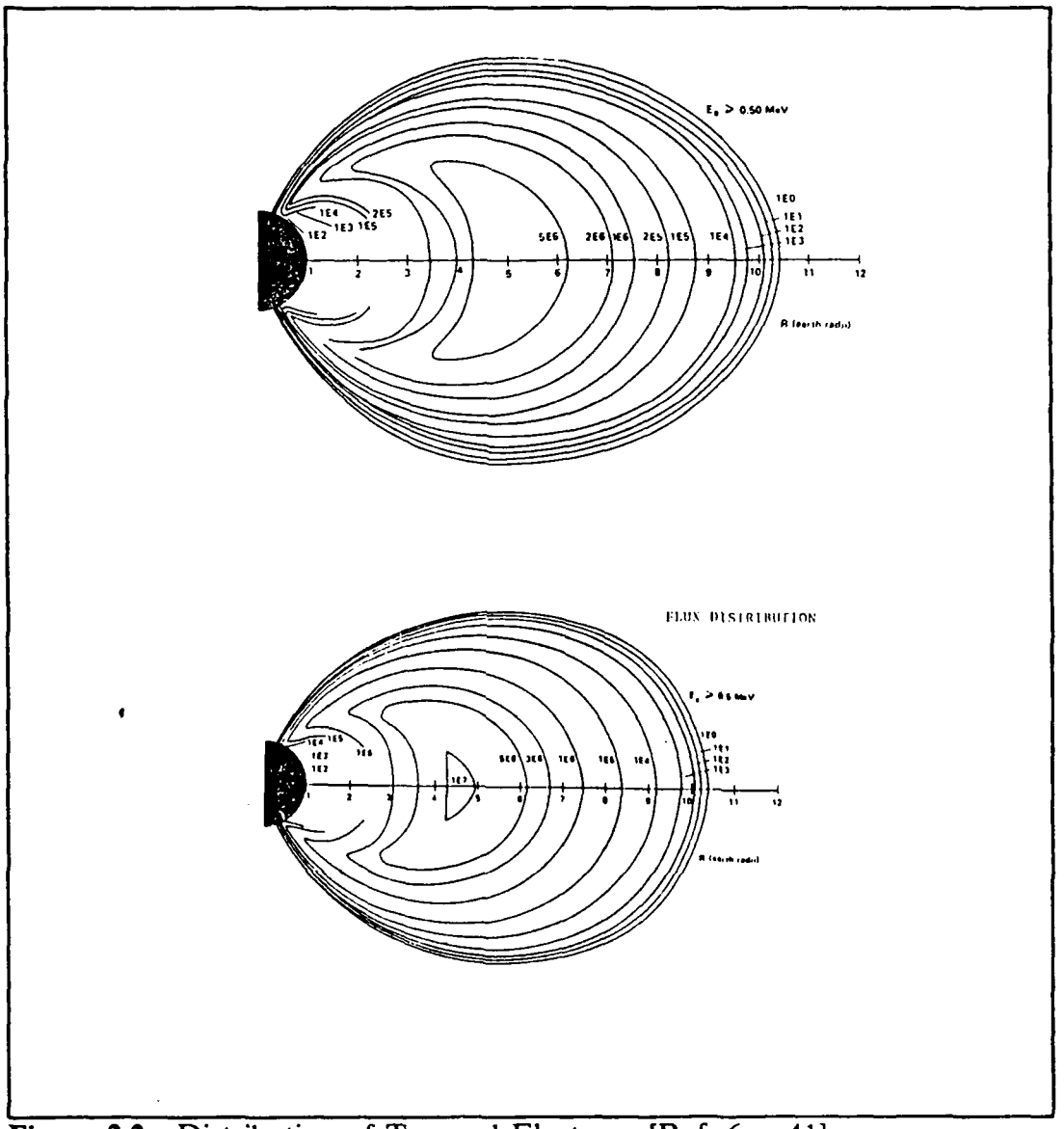

Figure 2.2. Distribution of Trapped Electrons [Ref. 6:p. 41]

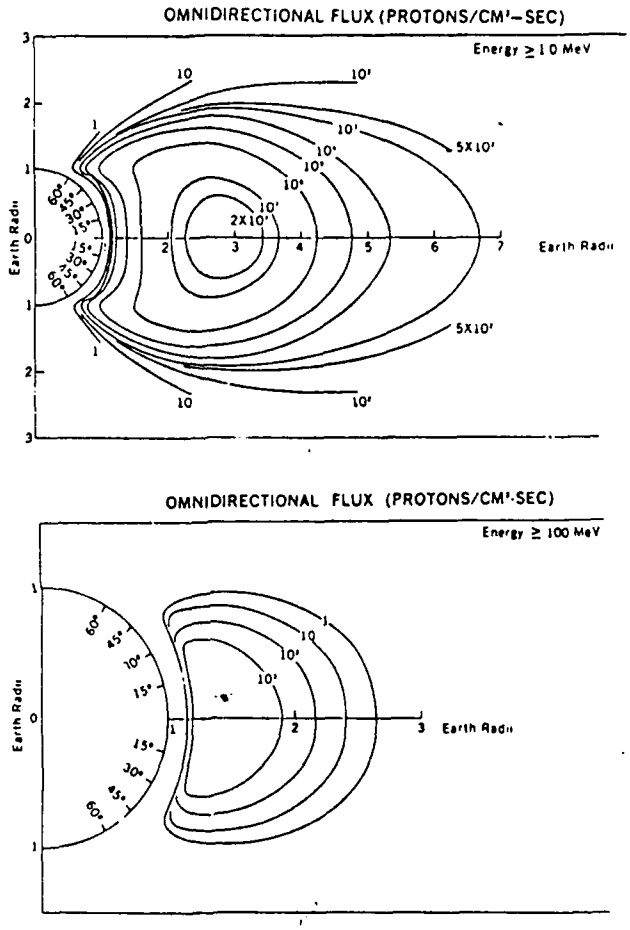

Figure 2.3. Distribution of Trapped Protons [Ref. 6:p. 42]

MeV) protons with a density of about 10^4 protons/cm^2-sec. The outer belt has high energy electrons (1 to 2 MeV) with a density of 10^4-10^5 electrons/cm^2-sec. [Ref. 8:p. 149] Magnetic disturbances, variations in the solar cycle and time of day affect this distribution. [Ref. 6:p. 41].

Operational satellites continually pass through the radiation belts and the amount of radiation damage is dependent on the orbit. A geosynchronous satellite at 0 degree inclination, utilizing a 10 ohm-cm resistive cell with a coverglass shielding of 0.015 cm in thickness, will experience a 1 MeV fluence of 2.48E13 electrons/cm^2-yr due to trapped electrons and protons [Ref. 7:p. 6-12]. GaAs solar cell degradation can be estimated to be approximately a 2.5% loss of power in the first year. [Ref. 1-:p. 554]

The NAVSTAR Global Positioning Satellite (GPS) is in a 20,200 km orbit with an inclination of 55 degrees [Ref. 9:p. 1-2]. This orbital plane passes through the radiation belts and exposes the spacecraft to high levels of radiation damage. A 20,372 km circular orbit at 60 degrees inclination has a damage equivalent fluence due to electrons of 5.26E13 electrons/cm^2-yr and 2.19E11 electrons/cm^2-yr due to protons, totaling 5.28E13 electrons/cm^2-yr. The calculated damage equivalent fluences can then be utilized to determine mission life and power degradation that the spacecraft will experience over its mission life. For the GPS satellite, this dose will result in approximately a 9% degradation in cell efficiency. After seven years

of mission life, the power output of the on-board Si cells will drop to approximately 78% of its initial capabilities [Ref. 10:p. 554].

III. STATE-OF-THE-ART IN SOLAR CELL TECHNOLOGY

The need for power has been increasing with every generation of satellites. The power system must provide the current needs while operating in various environments indicative to that particular orbit. These systems must operate in orbits with different sunlight-eclipse ratios and power profiles. The state-of-the-art systems must accommodate these needs by new array configurations or new types of solar cells.

In the area of silicon cell development, there have been numerous technologies employed to increase the cell output and efficiencies. The technologies are in the areas of crystal growth, dopant and diffusion.

Gallium arsenide cells are becoming more popular due to their higher resistivity to radiation damaging and higher conversion efficiencies compared to their silicon counterparts. However, the disadvantages are higher cost and weight per unit cell. Once the GaAs cells are in full-scale production, additional design changes will be considered, such as a change in material processing to produce a purer material which will improve cell efficiency, greater control in the layer thickness and changing the bandgap located in the photovoltaic active regions [Ref. 11:p. 24]. As with the silicon cells, areas of research are in crystal growth, dopants,

diffusion plus $Ga_{1-x}Al_xAs$ windows to overcome difficulties due to surface recombination. They are also looking for new III-V semiconductor materials.

Heterojunctions and Schottky barriers, antireflective coatings and ohmic contacts are also in the research process to improve on GaAs solar cell output. [Ref. 8:p. 199]

Cadmium sulfide solar cells are being investigated because of their high efficiency per unit cost. The cost of these cells are significantly less than those on the market due to production techniques. Instead of single crystals, the cells are manufactured with simple steps of evaporating thin layers of the material over substrate in large sheets. The CdS cells do have some disadvantages. Degradation problems due to various environmental conditions are the most prominent and delamination of the plastic encapsulation causing the cell contacts to separate. [Ref. 8:pp. 196-197]

Organic solar cells have been around for quite some time; however, no serious research has been conducted due to their low power conversion efficiencies. An advantage to these cells are their simple production procedures and low cost. [Ref. 8:p. 211]

Today the state-of-the-art solar cell is considered to be Indium Phosphide. They are significantly more resistive to radiation damaging due to less degradation of the bases' minority carrier lifetime which then decreases the degradation of Voc [Ref 12:p. 939]. Power degradation is also significantly less than its Si and GaAs

counterparts. InP cells have also demonstrated a higher level of energy conversion with 16.5% conversion efficiency when illuminated under AM0 conditions. Because of the higher efficiency and resistance to radiation damage, the protective coverglass thickness can be reduced which in turn will reduce the overall weight of the array and eliminate the need for shunt circuits. [Ref. 13:p. 1]

It has been reported that radiation-damaged InP cells are more responsive to the annealing process than Si or GaAs cells. For the first time, minority-carrier injection with a low current density at room temperature exhibited enhanced defect annealing and recovery of the cells properties. [Ref. 14:p. 433]

Further observations found that when degraded InP cells were stored at room temperature following irradiation, annealing took place and recovery of cell parameters was noted. This observation of defect annealing applied to both p-type and n-type InP cells. Room temperature recovery is accredited to the changes in deep level trap densities and the minority carrier diffusion length in the active region of the solar cell and the carrier concentration of InP. [Ref. 15:p. 1207]

Some other appealing characteristics of the InP cells are the low temperature required for annealing, the ability to increase radiation resistance by increasing the doping concentration (for p-type bases only) and the possibility of decreasing the array size and weight due to smaller degradation of the cells' output compared to the beginning-of-life capabilities. All of these characteristics indicate that InP cells show great promise and is a strong contender for future space applications.

IV. THEORY OF ANNEALING

A. RADIATION-INDUCED DEFECTS

The basis of solar cell operation is the conversion of solar energy into electrical energy by photovoltaic conversion. In order to maintain its photovoltaic capabilities, the structure of the cell must be able to withstand the hostile environment outside of the earth's atmosphere. The cells are constructed of a substrate (a semiconductor material) which is covered with a coverglass for shielding and an anti-reflective coating. The substrate is made up of atoms with valence electrons which characterizes the material's thermal and electrical properties. In a semiconductor, the energy gap between the valence band and conduction band is small in comparison to an insulator; therefore, the energy required to raise a valence electron in a semiconductor into its conduction band is greater and requires an external field [Ref. 16:p. 325].

The valence electrons of neighboring atoms bond together and form a crystal lattice structure. When light rays with an energy level greater than the energy gap of the solar cell strike the cell, an electron will separate from the bond leaving an electron-hole pair. The electron-hole pairs are separated by the potential barrier at the p/n junction with electrons migrating to one the n-side of the cell and holes

to the p-side. This creates a voltage difference between terminals and can drive an electric current [Ref. 16:p. 326].

During operation, a spacecraft will continually pass through a space radiation environment. This environment consists of cosmic rays, electromagnetic radiation, Van Allen belt radiation, auroral and solar flare particles. The Van Allen belts are in the earth radiation zone which is made up of trapped electrons and protons. The on-orbit solar cells are irradiated by these electrons and protons and damage the cell causing degradation of its energy conversion capabilities [Ref 1:pp. 2.5-1-2.5-5].

As radiative particles enter a solar cell, the depth of penetration depends on the energy level and wavelength of the particle. A low energy electron or proton can only penetrate the surface of the cell, restricting the damage to this area. On the other hand, high energy particles penetrate deep into the cell's substrate causing greater damage. [Ref. 8:pp. 154-155]

Cell penetration by low energy particles are restrained by the protective coverslip. This is a transparent piece of glass that is bonded by a transparent adhesive to the surface of the cell. The greater the density and thickness of the coverslip, the greater the protection and less degradation of the cell. As the lower energy particles bombard the cell, the protective coverslips will degrade. Ionization will cause the adhesive to darken, thereby increasing the light absorption. This increase in absorption causes a decrease in illumination of the cell and an increase

in operating temperature of the array which in turn decreases efficiency. It was discovered that, by adding certain impurities to the coverslip material, it will become more resistive to darkening. [Ref. 8:p. 161-162]

High energy particles will penetrate deep into the cell and causes greater damage. The lattice structure of the substrate will be degraded, resulting in vacancies and interstitials, vacancy-impurities complexes and defect clusters [Ref. 8:p. 149]. These defects act as an impurity compensator. By the carrier removal process, the majority carriers are eliminated for the specific energy band. This process causes an increase in the cell's base resistivity and a lowering of Voc and Isc [Ref 8:p. 156]. The lattice breakdown is also related to the decrease in carrier concentration and to the minority carrier diffusion length which lowers the photocurrent [Ref. 17:p. 1433]. Deep penetration resulting in lattice structure damage will degrade the lifetime of the cell to various degrees depending on the radiation particles and their energies.

B. ANNEALING OF SOLAR CELLS

Defect annealing of solar cells is a process by which the addition of heat and/or current will raise the energy level of the cell. The increase in energy will cause the substrate electrons to become excited and move into new positions within the atomic structure. The holes created by the damaging irradiation are now filled

by the excited electrons and the crystal lattice structure is restored to initial conditions.

Annealing generally takes place at temperatures above 20 C; however, increased temperatures will accelerate the process. This thesis investigated the outcome of annealing cells more frequently at lower temperatures when the amount of damage is rather small; therfore, only minimal recovery is needed to return the cell to its initial conditions.

Solar cells can be annealed by periodic thermal annealing, continuous annealing or injection annealing. Periodic thermal annealing is a repetitive process by which the cell is irradiated at room temperature and isothermally annealed at a specified temperature for a short period of time. Continuous annealing is when the cell is subjected to damaging irradiation and the annealing process simultaneously. Minority carrier injection annealing is the application of a forward bias current to the cells' junction. It was discovered that minority carrier injection annealing accelerated the rate of recovery when a forward bias current was applied to the cells junction at 100 C. The energy needed for this thermal process was reduced by the same amount of energy needed for transition of the non-radiation electron-hole recombination. [Ref 18:p. 35-36]

Minority carrier injection annealing can be accomplished by two different methods. One is by photo-injection which requires the surface of the cell to be

illuminated by a very strong light source. This causes the minority carrier density to increase which then enhances damage recovery. [Ref. 3:p.48]

The other method is forward bias injection which was used in the research of this thesis. As a forward bias potential is created across the cell, a current begins to flow. The forward current increases exponentially as the potential increases; therefore, the power dissipated by the cell increases proportionally. [Ref. 3:p. 49]

GaAs cells have demonstrated favorable recovery utilizing all three of the above mentioned annealing procedures. Previous experiments have shown that GaAs cell irradiated with 1 MeV electrons will exhibit marginal recovery with thermal annealing at temperatures above 300 C [Ref 19:p. 924]. It was also shown that minority carrier injection at near room temperatures will result in annealing. [Ref. 20:p. 1106]

Loo, Knechtli and Kamath [Ref 18:p. 36] observed an accelerated annealing rate when forward bias was applied to the damaged cell at a temperature of 100 C. Recovery time of the Voc was faster with greater power restored.

Annealing experiments with InP cells revealed substantially greater recovery than its GaAs counterparts. These cells have shown to be more resistive to 1 MeV electron and 10 MeV proton irradiation and will anneal at much lower temperatures. Research has shown that recovery will occur with thermal annealing at 100 C and minority carrier injection with a forward bias current. [Ref. 12:p. 937]

InP cells will degrade approximately 10% from their initial efficiency after irradiation with 1 MeV electrons with a fluence of 1E15 electrons/cm^2 and a 7% degradation of Voc [Ref. 12:p. 939]. Recovery of these capabilities were found to be due to room-temperature annihilation within the substrate layer. It has also be accredited to the concentration of the substrate carrier in the InP cell. [Ref. 15:p. 1207]

V. GALLIUM ARSENIDE SOLAR CELLS

A. GaAs CELL CHARACTERISTICS

GaAs solar cells have been proven to have one very important advantage over Si cells, they have a higher resistivity to radiation damaging. They have also been shown to be more efficient than Si since the peak efficiency of the solar spectrum and the energy level needed to free a valence electron is approximately the same. Thermal stability is another advantage for GaAs cells. They exhibit about half the efficiency degradation of Si per degree rise in temperature. It has also been shown that GaAs cells respond better to annealing.

The disadvantages of using GaAs cells over Si are high production costs, higher mass ratio and availability.

The GaAs cells used in this research were 2 x 2 cm in dimension and of the n-p type. They were manufactured by the Applied Solar Energy Corporation and were obtained through Wright-Patterson. Ten cells total were used throughout the experiment and were subjected to various annealing parameters.

The initial electrical characteristics of the cells can be found in the initial I-V curves in Appendix A.

B. TEST PLAN

The first objective of the test plan was to determine the optimum damaging fluence for GaAs cells. This fluence would produce significant degradation of the cells' capabilities, yet still be able to recover approximately to its initial level through annealing. The 1 MeV electron irradiation took place at the Jet Propulsion Laboratory in Pasadena with the Dynamitron linear accelerator.

The two fluences levels that were chosen to begin testing were 1E14 and 1E15 electrons/cm^2. These values were determined from previous research [Refs. 3 and 4]. Of the ten cells available for testing four would be irradiated at each of these levels.

The sequence of testing began with a initial I-V curve which established the baseline for beginning of life capabilities. The I-V curves were constructed under AM0 conditions produced by a Kratos solar simulator at the Jet Propulsion Laboratory. The cells were then irradiated at the specified fluences, followed by the construction of a post-irradiation current-voltage (I-V) curves. Each cell was then annealed and a post-annealing I-V curve was taken. This was done for multiple cycles to determine the possible amount of degradation and recovery while varying irradiation fluence and annealing parameters.

All eight cells were annealed using forward-biased current and heat. The variable annealing parameters were heat, current, illumination and time; however, the temperature variable was maintained at 90 C which was considered a practically

achievable temperature for on-orbit annealing. Annealing took place in darkness which is considered as worse-case conditions.

C. EXPERIMENTAL PROCEDURE AND RESULTS

Cells numbered 133, 136, 139 and 140 were irradiated at 1E14 electrons/cm^2 fluence level for each cycle,throughout the experiment. They were annealed at 90 C with 0.5 A/cm^2 in darkness for up to 48 hours. This was repeated for four cycles, considering only annealing time as the only variable. The I-V curves are illustrated in Appendix A, Figures A.1-A.11.

Open circuit voltage (Voc), short circuit current (Isc), maximum power (Pmax) and percent efficiency (% Eff) at each stage was plotted for cells 133, 136, 139 and 140 and can be found in Appendix B, Figures B.1-B.16. Voc had very little degradation and was able to maintain better than 90% of its initial value after receiving an accumulative dose of 4E14 electrons/cm^2. Isc also recovered with every annealing cycle and maintained approximately 94% of its initial value.

The maximum power showed some initial degradation, but was able to recover with annealing at the specified parameters. Figures B.3, B.7, B.11,and B.15 in Appendix B graphically shows the cells' response. Figure 5.1 is a normalized plot of the maximum power of cell 136 and shows that, after an accumulated dose of 4E14 electrons/cm^2, the cell was able to maintain 89.19% of the initial maximum power. The normalized plot of % Eff of the same cell is illustrated in Figure 5.2.

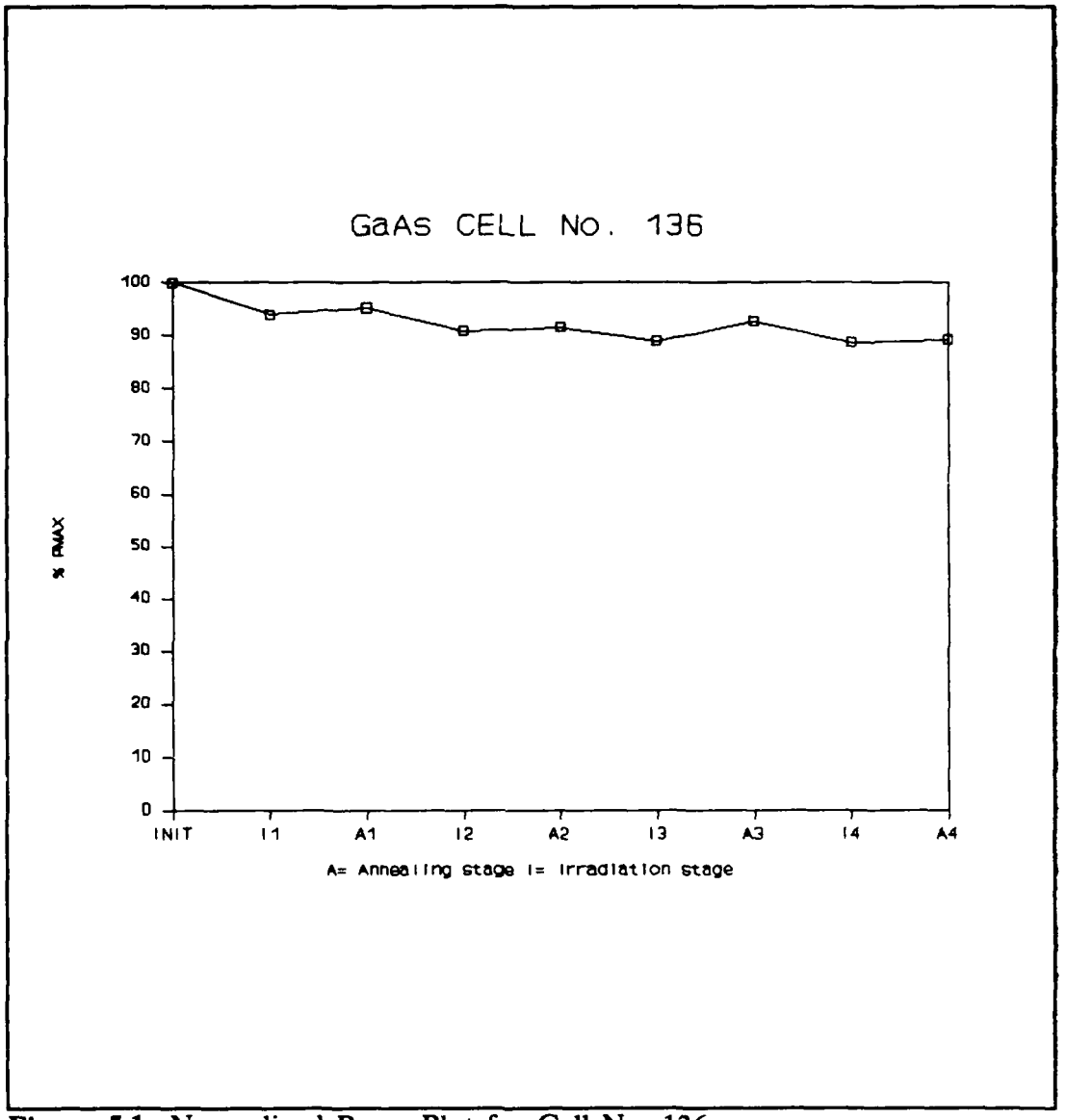

Figure 5.1 Normalized Pmax Plot for Cell No. 136

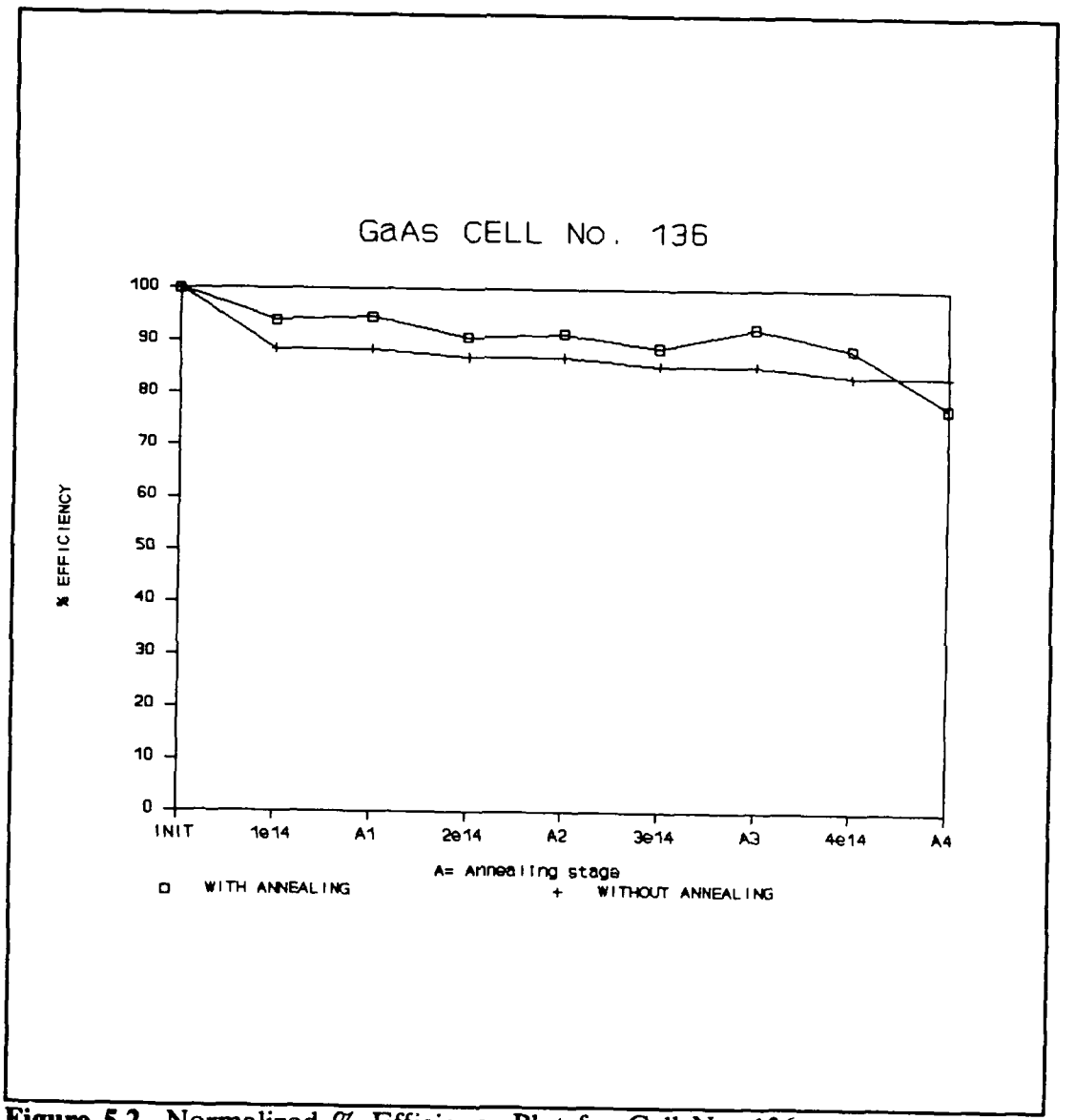

Figure 5.2 Normalized % Efficiency Plot for Cell No. 136

Cells number 148, 149, 152 and 153 were irradiated with 1E15 electrons/cm^2. The were annealed at 90 C with 0.5 A/cm^2 in darkness with time as a varying parameter between 19 and 48 hours. The I-V curves are contained in Appendix A and illustrated that an approximate three-fold degradation occurred when irradiating at 1E15 compared to 1E14 electrons/cm^2. The irradiating and annealing cycle was repeated up to three times with the maximum recovery taking place when annealed for 48 hours.

Voc, Isc, Pmax and % Eff of each stage was plotted for each cell and can be found in Appendix B, Figures B.17-B.32. With the exception of cell number 148, Voc had very little degradation and recovery took place when annealed. The Voc value was maintained at approximately 89.0% or better of its initial value after receiving an accumulative dose of 3E15 electrons/cm^2. Isc also recovered with every annealing cycle, but maintained only 78.2% or better of its initial value.

The maximum power showed initial degradation just as the cells irradiated at 1E14 electrons/cm^2; however, recovery did take place when annealed. Figures B.19, B.23, B.27 and B.31 in Appendix B graphically illustrates the cells' response. Figure 5.3 is a normalized plot of the maximum power of cell number 152 which was able to maintain 70.6% of its initial power. The normalized plot of % Eff of the same cell (Figure 5.4) shows that 70.6% of its efficiency was maintained at the end of three irradiating/annealing cycles.

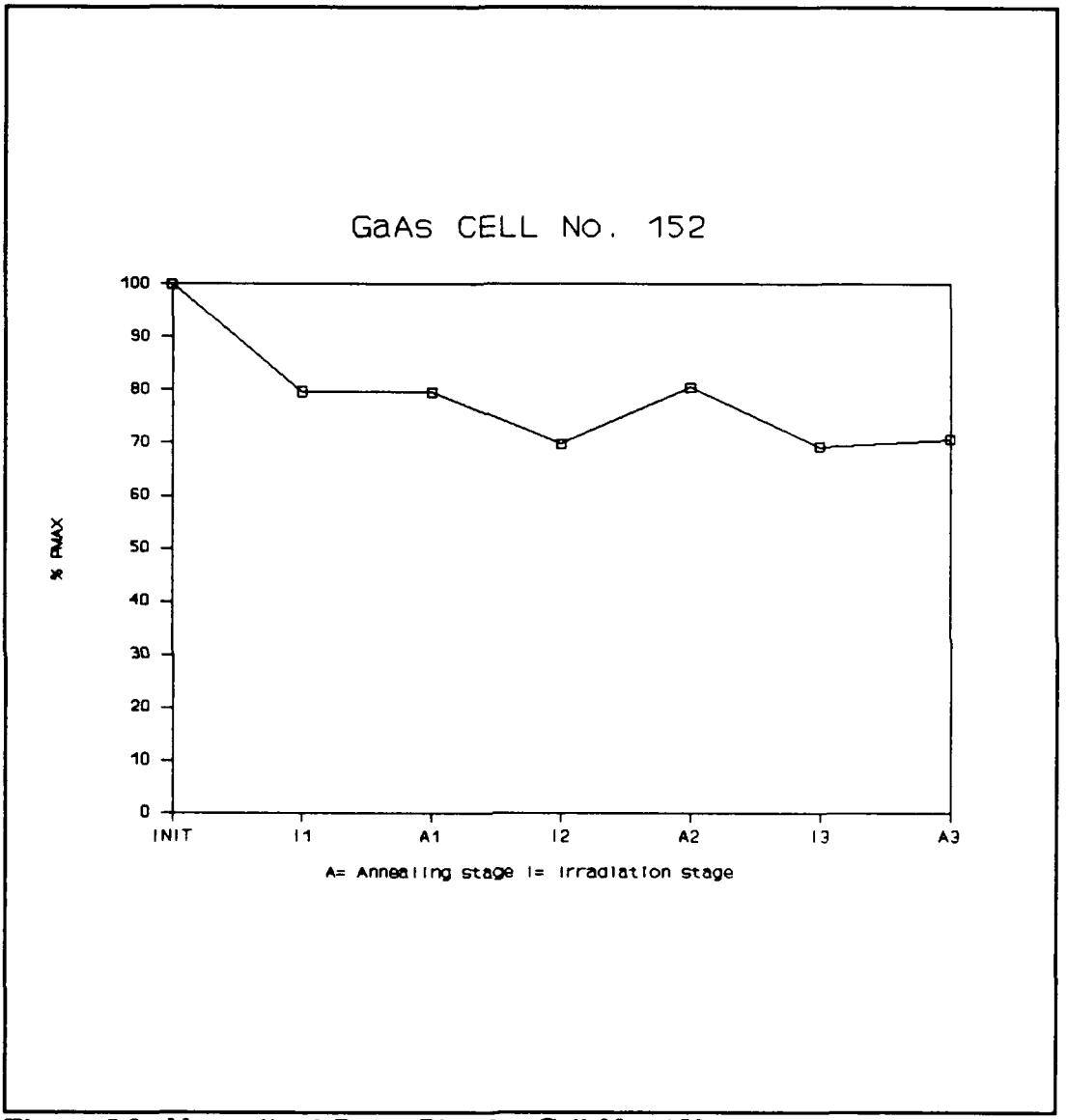

Figure 5.3 Normalized Pmax Plot for Cell No. 152

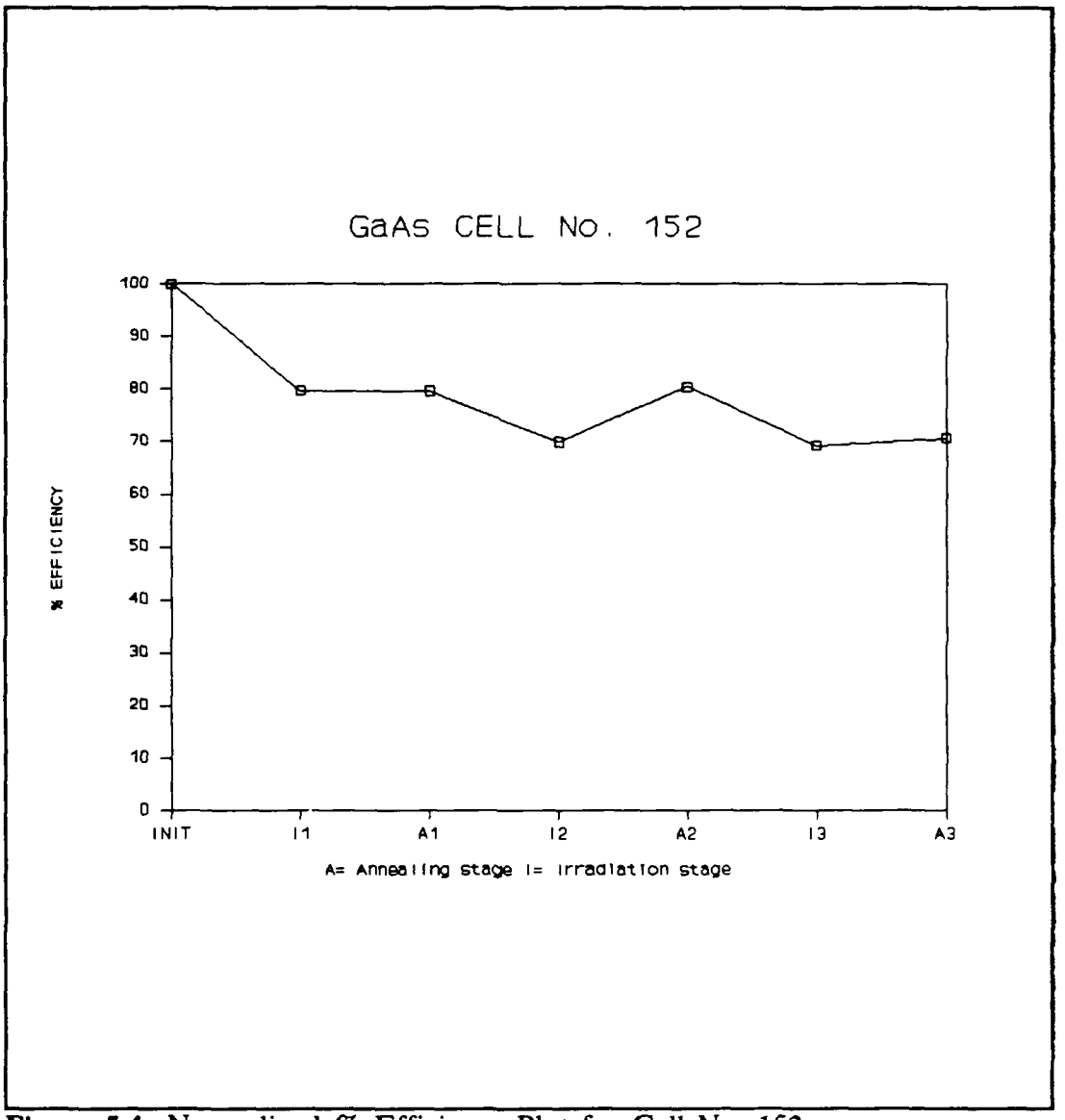

Figure 5.4 Normalized % Efficiency Plot for Cell No. 152

Cell number 119 was irradiated at 1E15 electrons/cm^2 and annealed with heat alone. The annealing cycle lasted for 24 hours at 90 C and no significant recovery took place. Figure A.25 in Appendix A illustrates the results.

Figure 5.5 illustrates the comparative results of Weinberg, Swartz, Hart and Statler [Ref. 10:p. 554] when Si, GaAs and InP cells were continuously irradiated under various conditions. The results confirm that GaAs and InP cells are more resistant to radiation with InP being more robust than all of its counterparts. The GaAs -p+n curve from Figure 5.5 has been plotted in Figure 5.2 in order to compare the results of this research where the cells are annealed after every irradiation and when the cells are continually irradiated without annealing. The actual data with annealing curve shows that annealing will significantly increase the % Eff which can be maintained after an accumulated dose of 4E14 electrons/cm^2.

The above test results indicated that the optimum fluence for irradiating GaAs solar cells is in the range of 1 E14 to 1E15 electrons/cm^2. By altering the annealing parameters, it was concluded that heat and forward-biased current annealing for 48 hours gave the best recovery. Also, the smaller the amount of damage incurred by the cell before annealing will result in a high level of power and % efficiency recovered.

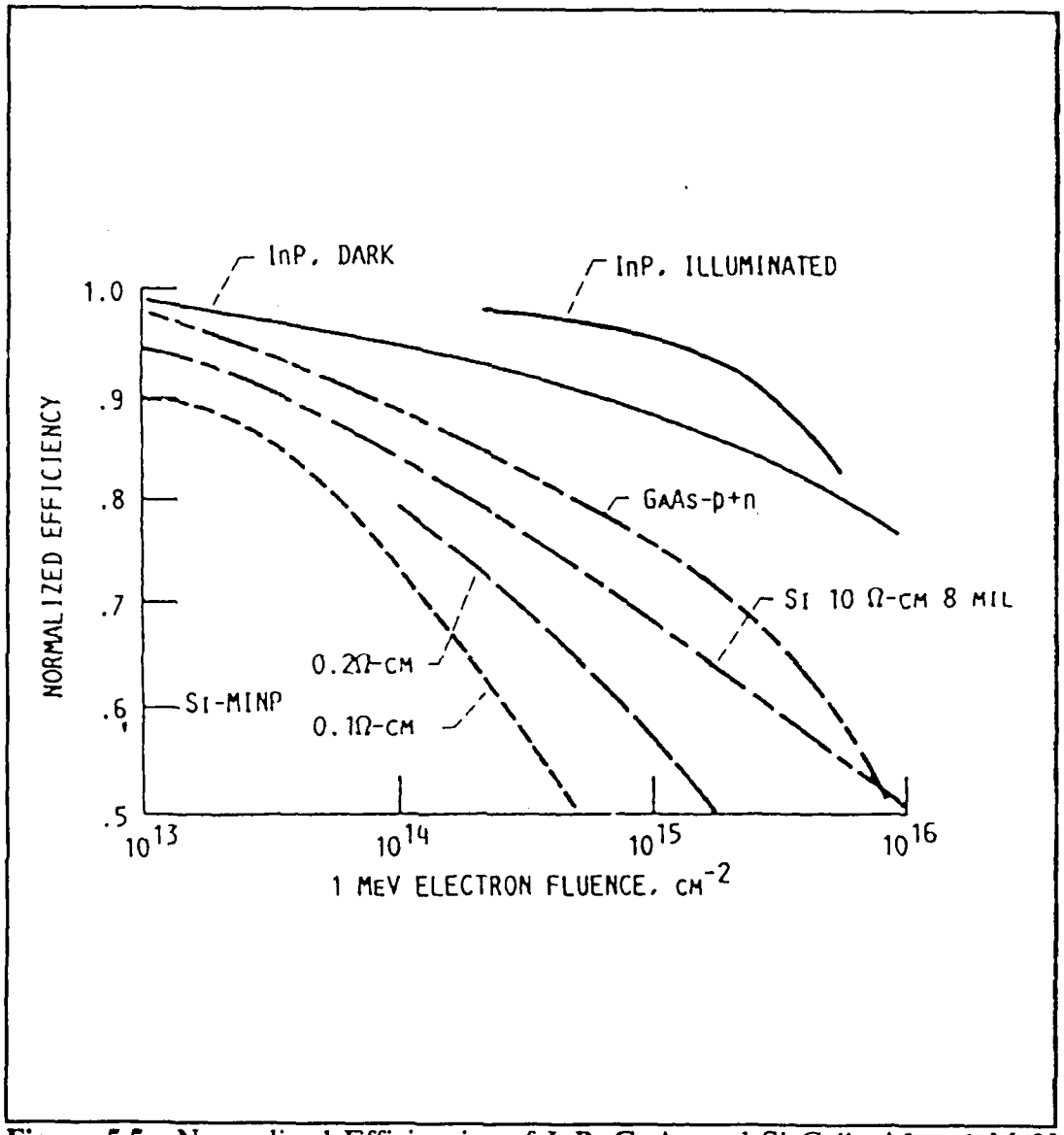

Figure 5.5. Normalized Efficiencies of InP, GaAs and Si Cells After 1 MeV Electron Irradiation [Ref. 10:p. 554]

D. PROTON IRRADIATION

In addition to electron damaging, one cycle of proton damaging was conducted. The equivalent of 1 MeV electrons were used to irradiate two cells at the CalTech facility. The fluence at which the irradiation took place was randomly selected at 7E11 protons/cm^2. Figures A.23 and A.24 in Appendix A graphically shows the amount of degradation which took place. It was found that protons at this fluence degraded the cell about twice as much as electrons at 1E15 electrons/cm^2 fluence. These cells were annealed at 90 C with a forward-biased current of 0.5 A/cm^2 in darkness for 24 hours. Very little recovery took place (approximately 15%) which may indicated that the fluence level used was too high and the damage was irreversible. A lower fluence level should be used for future testing in this area.

VI. INDIUM PHOSPHIDE SOLAR CELLS

A. InP CELL CHARACTERISTICS

InP cells exhibit characteristics which make them advantageous for space applications. They have been shown to be highly radiation resistant compared to Si and GaAs cells and show significantly lower power degradation than their Si or GaAs counterparts. They have typical conversion efficiences of about 16.5% (AM0) which allows the manufacuturers to reduce the cell thickness and weight of the coverslips which provides protection for the cell. InP cells are now being mass produced with excellent uniformity.

The cells used in this research were manufactured by Nippon Mining Company and are available in two sizes, 1 x 2 cm^2 (NS-12B) and 2 x 2 cm^2 (NS-22B). Ten 1 x 2 cm^2 cells were used in the experiments for this thesis.

Typical properties of InP cells are shown in Figure 6.1 as a result of research conducted at NASA Lewis Research Center. These properties were measured when the cell was under zero air mass conditions and held at 25 C.

B. TEST PLAN

The first objective of the test plan was to determine the optimum damaging fluence in which a cell could recover its initial capabilities. When irradiated at the

selected fluence, the cell should exhibit a significant degradation; however, it should not exceed the limit where the damage is irreversible through the annealing process.

Secondly, a testing sequence was derived to determine the long-term effects of multiple cycles of irradiating and annealing. The annealing conditions were varied with every cycle to determine the optimum annealing mechanisms while keeping within an achievable range of temperature and current which can be obtained during orbit.

C. RESULTS

The testing sequence began with determining the initial cell characteristics by developing an I-V curve using a Kratos ss2500 AM0 light source and a Tektronics controlled current sinking IV tester at the Jet Propulsion Laboratory. Next, two of the ten 1 x 2 cm Indium Phosphide (InP) cells were irradiated at 1E14 electrons/cm^2. Figures C.1 and C.7 in Appendix C are the post-irradiation I-V curves for cells 1051 and 1052 and show a minimal amount of degradation. These cells were then annealed by storing them at room temperature in darkness for approximately 30 days. Figures C.2 and C.8 in Appendix C illustrate that the cells recovered almost to the initial capabilities.

The fluence for all InP irradiations was then changed to 1E15 electrons/cm^2 so that degradation and recovery could be measured more accurately and significant changes observed. InP cells numbered 1051-1054, 1056, 1072-1076 were irradiated

at this fluence and post irradiation I-V curves were taken. The average degradation of the maximum power that took place was approximately 9% which is less than one-half the degradation experienced by GaAs cells at this fluence.

The cells were then annealed by various means. Cells numbered 1051-1054 were annealed at 28 C, forward biased with 0.25 A/cm^2 and illuminated under AM0 conditions for 17.8 hours. Figures C.2, C.8, C.10 and C.15 in Appendix C are the post annealing I-V curves which shows approximately a 27% recovery rate for Isc and 32% recovery of the maximum power.

Cells numbered 1056 and 1072 were annealed at 90 degrees C in darkness for 18.5 hours. Figures C.18 and C.22 in Appendix C are the post annealing I-V curves and graphically illustrates approximately a 68% recovery of Isc and a 58% recovery of maximum power.

Annealing with heat at 90 C and a forward bias current of 0.25 A/cm^2 in darkness for 16.5 hours was applied to cells numbered 1073-1074. Figures C.26 and C.31 in Appendix C displays the maximum recovery seen of the three annealing parameters tested. The maximum power recovered was 62% which is 97% of its initial capacity and Isc recovered 83% of its loss.

Since the combination of heat and forward-bias current gave the most promising results, the remaining annealing cycles were conducted with both mechanisms while varying the time parameter. It was found that annealing for 48 hours gave a significant recovery; however, the possibility of recovery taking place

within a matter of minutes was investigated. Cells numbered 1051, 1053, 1073 and 1074 were irradiated at 1E15 electrons/cm^2 and annealed for 15, 30, 60, 75 and 120 minutes. The results are illustrated in Figures C.4, C.12, C.28 and C.33 in Appendix C which verify that the majority of the annealing process takes place within the 2 hour timeframe. These results confirm the exponential annealing and recovery theory, where the exponential time constant can be easily calculated and a model for cell recovery can be easily derived.

Voc, Isc, Pmax and % Eff was plotted for each of the annealing and irradiating stages for all InP cells. These plots can be found in Appendix D. Figure 6.1 is a representative sample of the normalized Voc plots and shows very little degradation in the Voc values throughout the sequential cycles. A normalized Isc plot is shown in Figure 6.2 and has minimal fluctuations. Figure 6.3 is a normalized plot of the maximum power for cell number 1074. It shows that after the cell has been subjected to an accumulative dose of 4E15 electrons/cm^2, the maximum power is still at 89.5% of its initial capabilities.

Previous testing of InP cells have indicated that these cells are more resistant to radiation damage when illuminated. This was confirmed when cells numbered 1051, 1053, 1073 and 1074 were irradiated under AM0 conditions. The results are illustrated in Figures C.6, C.14, C.30 and C.35 in Appendix C.

Figure 6.4 contains the results of Weinberg, Swartz, Hart and Statler [Ref. 10:p. 554] for the InP cell irradiated in darkness without annealing. Comparing the

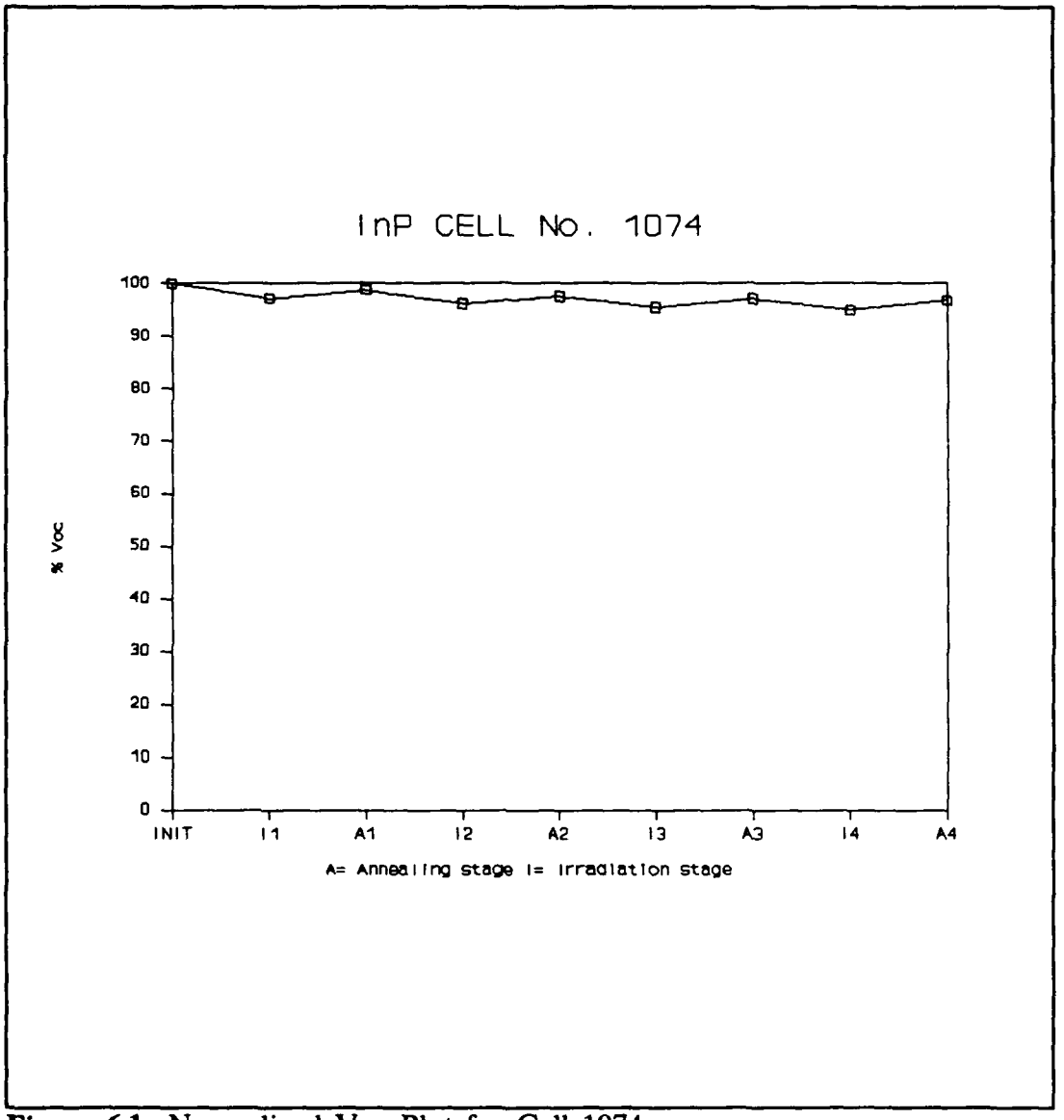

Figure 6.1 Normalized Voc Plot for Cell 1074

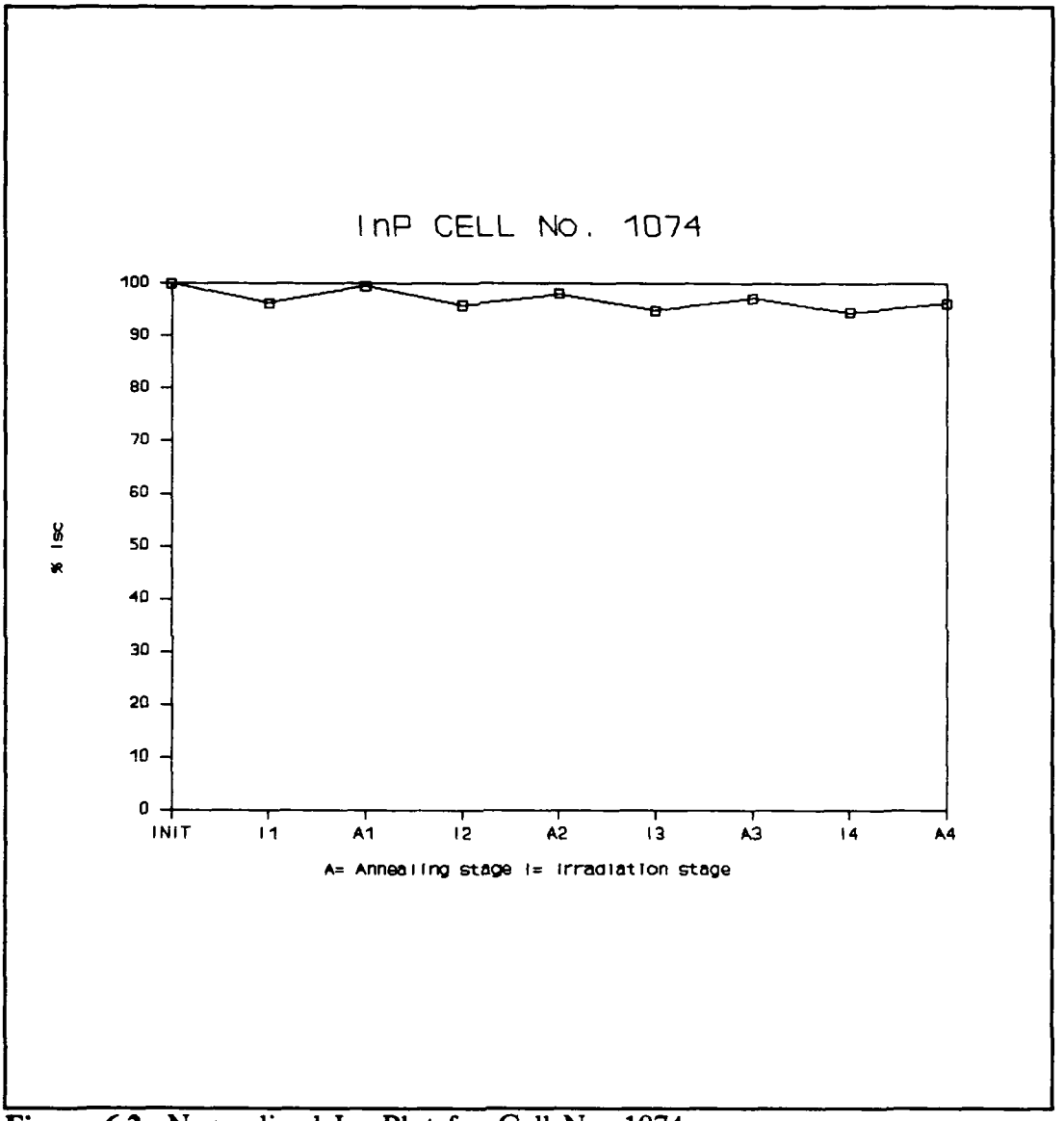

Figure 6.2 Normalized Isc Plot for Cell No. 1074

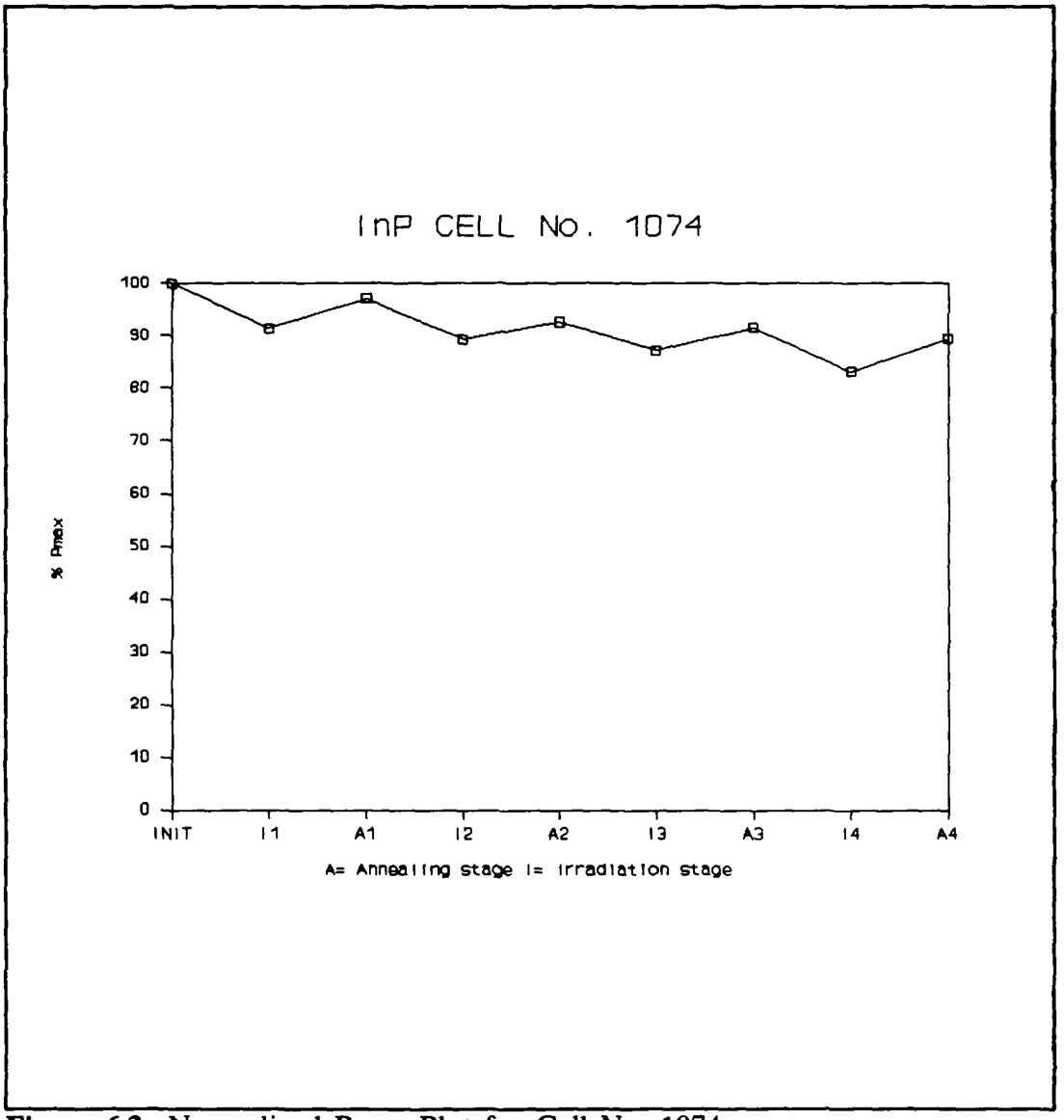

Figure 6.3 Normalized Pmax Plot for Cell No. 1074

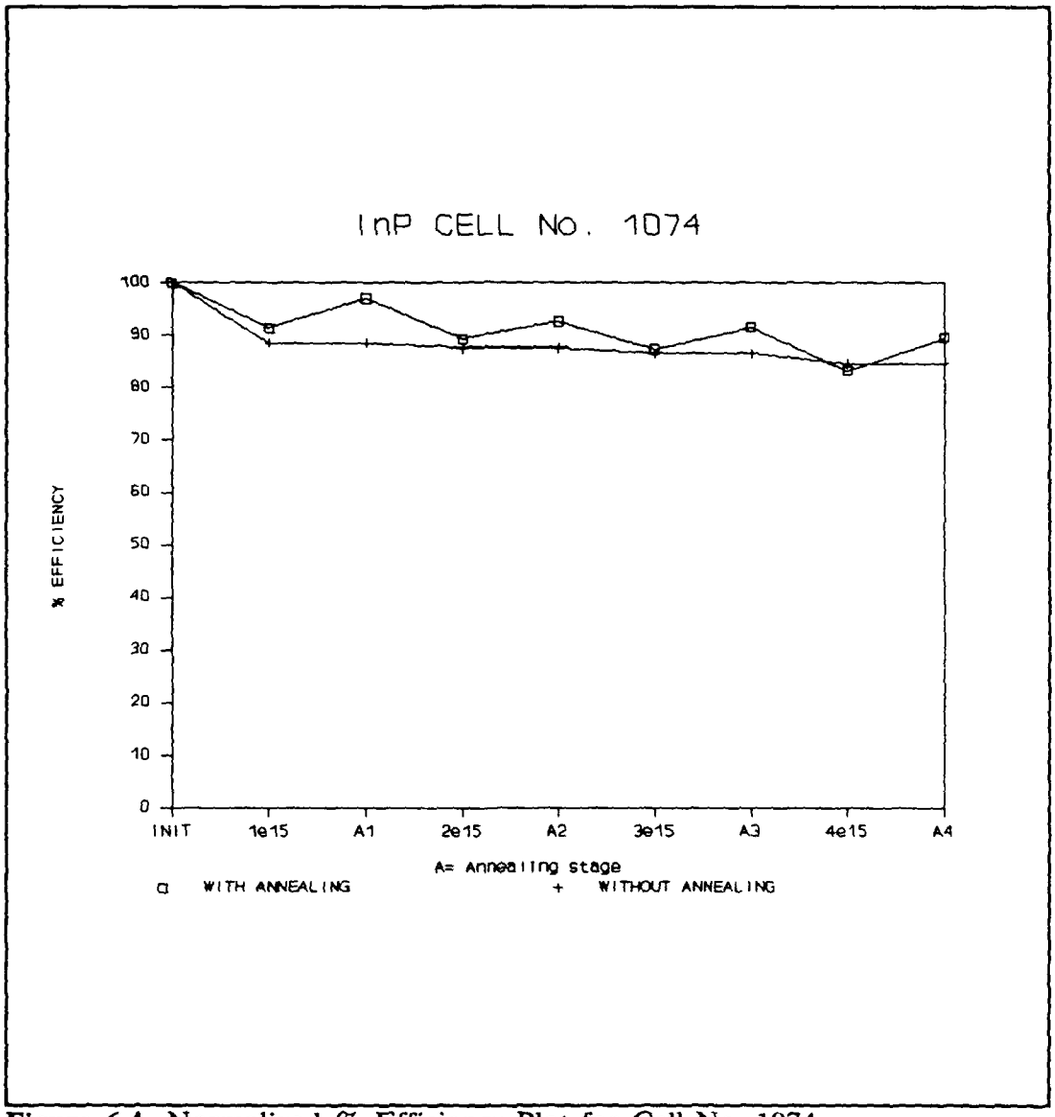

Figure 6.4 Normalized % Efficiency Plot for Cell No. 1074

actual data with annealing curve to the without annealing curve, recovery of the cell's initial efficiency took place with every annealing cycle. This comparison indicates that annealing after irradiation will recover the cell's capabilities and maintain a higher level of its initial capabilities over an extended period of time.

InP cells were proven to be more robust than its GaAs counterparts and were resistive to radiation damage. They were able to withstand higher fluence levels of irradiation and recovered their power and efficiency through annealing. The combination of forward bias current and heat annealing mechanisms gave the best recovery and the majority of annealing took place in the first 2 hours.

D. PROTON IRRADIATION

Cells numbered 1075 and 1076 were subjected to proton damaging with 1 MeV equivalent fluence of 7E11 protons/cm^2. Figures C.36 and C.37 in Appendix C contain the I-V curves from its inital condition through annealing. It was observed that protons are more damaging to the InP cells than electrons which was the same observation with the GaAs cells. The first annealing attempt was at 90 C with 0.25 A/cm^2, in darkness for 2 hours. This produced approximately 20% recovery of the Isc and Pmax loss. Annealing was continued under the same conditions for a total of 4 hours and the recovery was minimal. The amount of forward bias current was increased to 0.5 A/cm^2 for 18 hours and again there was no substantial recovery. The total maximum power recovery was approximately

35% with a minimal increase after 2 hours of annealing. Since the recovery was not very good, it is evident that the fluence level was too high and a threshold was reached whereby damage reversal was not possible.

VII. CONCLUSIONS AND RECOMMENDATIONS

After numerous cycles of irradiating and annealing of GaAs and InP cells, the optimum fluence level was found to be between 1E14 and 1E15 electrons/cm^2. At this level, degradation was within the limits of still being able to reverse the damage caused by trapped electrons and protons in the radiation belts surrounding the earth. The annealing processes used in the testing sequence resulted in recovery of the cells initial capabilities.

Greater recovery was observed when the annealing mechanism consisted of both heat and forward bias current. However, the InP cells responded better to heat alone (90 C) than did the GaAs cells. The GaAs cells were able to maintain over 70% of their initial capabilites after receiving an accumulative dose of 4E15 electrons/cm^2. The InP cells were able to maintain over 87% of its initial capabilities after the same accumulative dose as the GaAs cells.

When comparing the amount of recovery of the GaAs cells to the InP cells, it was observed that the InP cells were in fact more robust and resistive to radiation damage. The InP cells degraded approximately one-third the amount that the GaAs cells degraded at the same fluence level.

The annealing parameters which were varied throughout the testing sequence were temperature, forward bias current, illumination and time. The range of temperature and current used were those which were achievable on orbit; therefore,

this method of irradiating and annealing at the specified levels can be accomplished while on orbit with on-board hardware.

It was shown that mission life extension of various operational satellites is possible. The synchronous satellite with 0 degree inclination referred to in Chapter 2, experiencing a total dose of 2.48E13 electrons/cm^2 could have an extended mission life of approximately 162 years based on the results of an accumulative dose of 4E15 electrons/cm^2. The 1110 km circular orbit with 90 degree inclination would be extended by 49 years and the GPS orbit satellite would be extended approximately 75 years.

This research is just the beginning of investigating this application. Further research into the InP annealing parameters is necessary in order to determine the optimum and most efficient levels of heat and current to be used. Increasing current and reducing temperature or increasing the frequency of annealing at lower levels of degradation may increase recovery to even higher levels of the cells' inital maximum power and efficiency.

Continued research in the area of proton damaging is also a necessity. It was found that the heavier proton particles caused more damage and recovery was more difficult. Additional testing at lower fluence levels are needed to determine the optimum damaging fluence in order to achieve the maximum power recovery of the cell. Again, by varying the annealing parameters, an optimum mechanism can be determined.

Trapped electrons and protons in the radiation belts are only one source of damaging particles. Solar flares are another contributor to the degradation of on orbit arrays. By correlating the solar cycle with the time on orbit of a particular spacecraft, the possibility of a solar flare and the total dose of 1 MeV equivalent electrons can be determined. This in turn can be used to determine the amount of degradation the array will experience during that time.

A proof-of-concept prototype would verify the research done in this area. A mini-array prototype including annealing system and test connections should be fabricated. The mini-array can be operated in the linear accelerator while being subjected to a simulated space environment. The system should be irradiated and annealed under AM0 conditions for multiple cycles. I-V curves should be constructed before and after irradiation and after annealing to verify power recovery of the cells.

APPENDIX A. GaAs CELL I-V CURVES

This appendix contains the I-V curves for multiple cycles of irradiating and annealing of the individual cells. Each curve is labeled with the amount of radiation the cell was subjected to and the conditions of annealing.

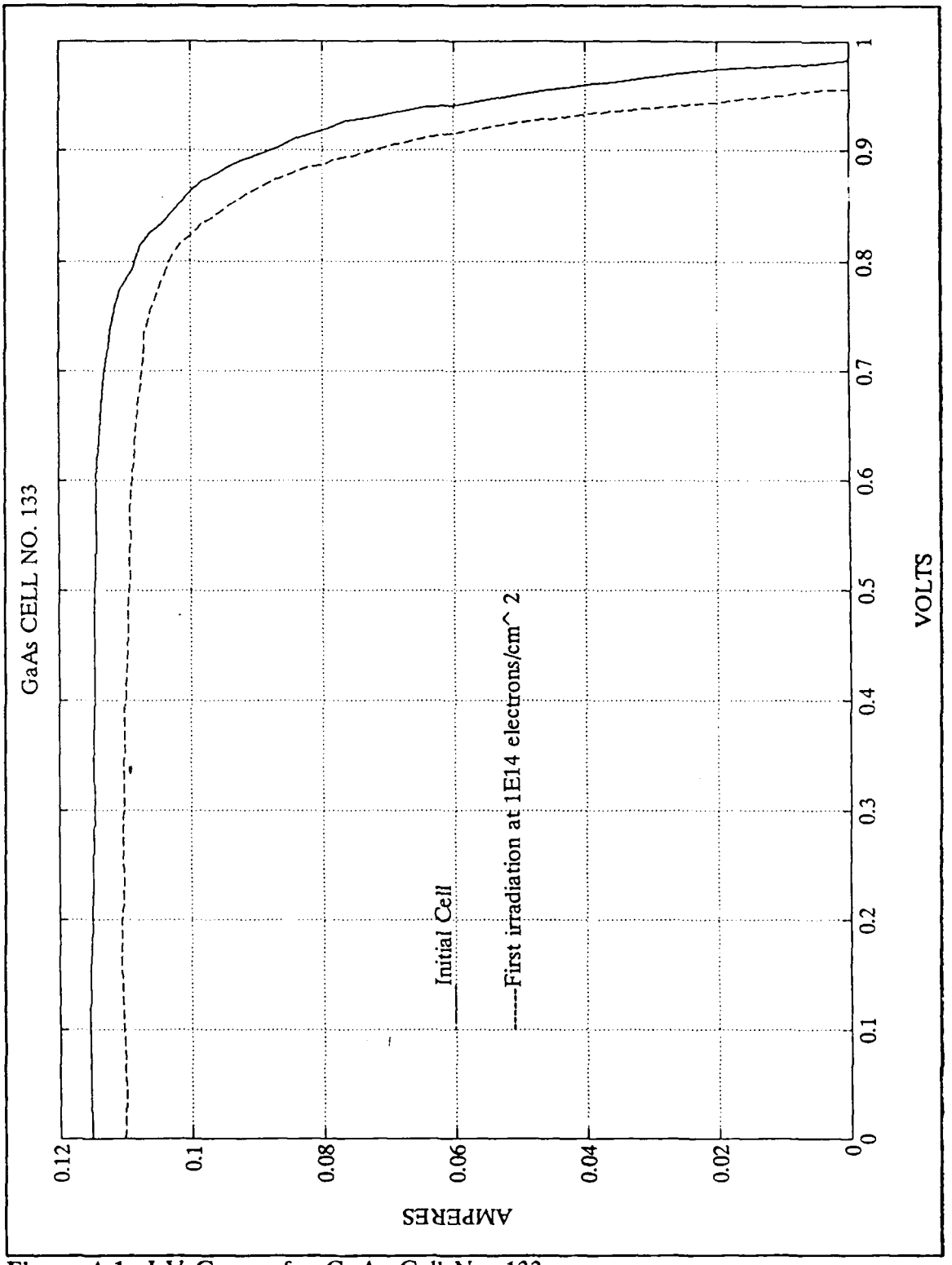

Figure A.1 I-V Curves for GaAs Cell No. 133

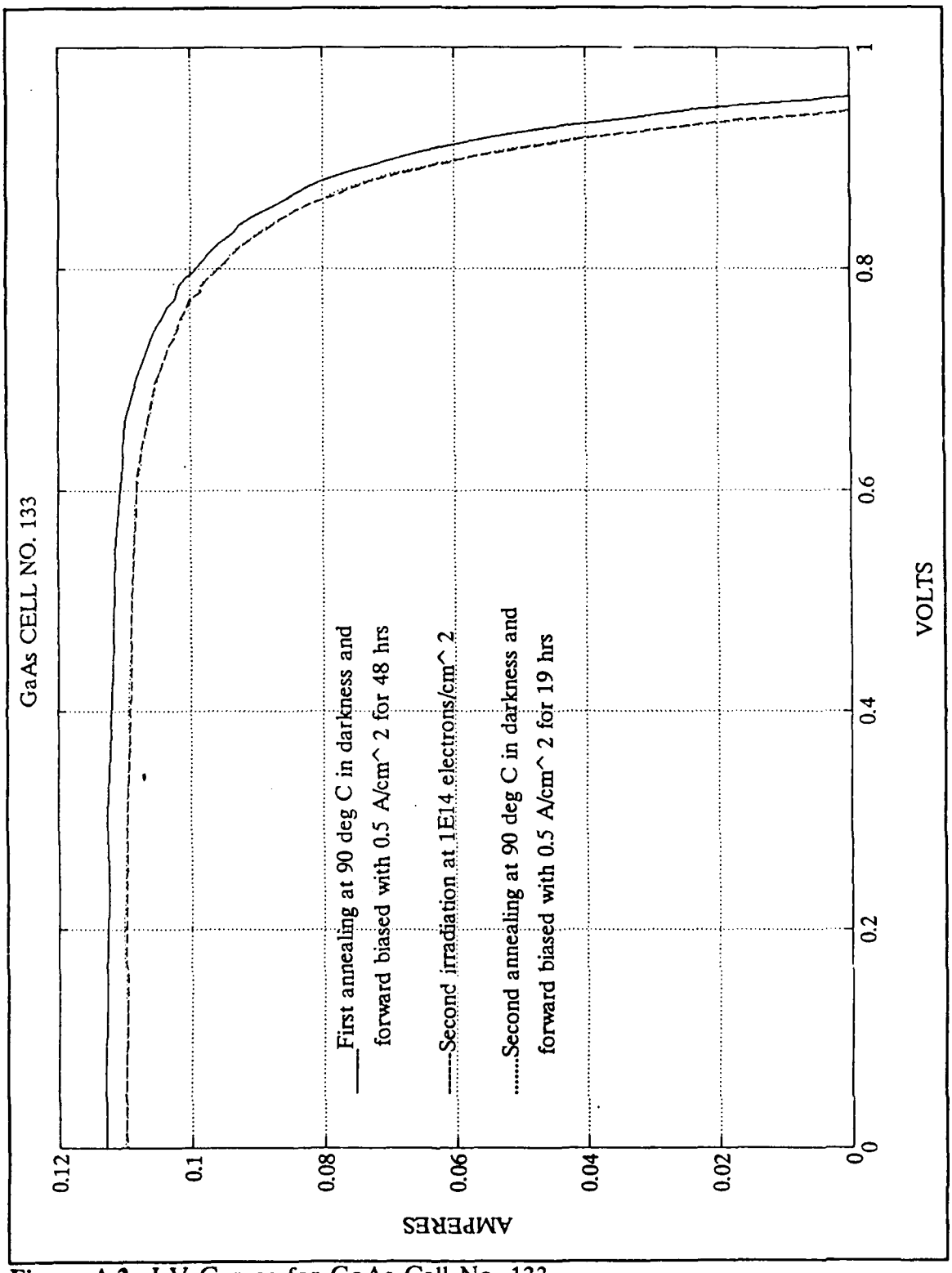

Figure A.2 I-V Curves for GaAs Cell No. 133

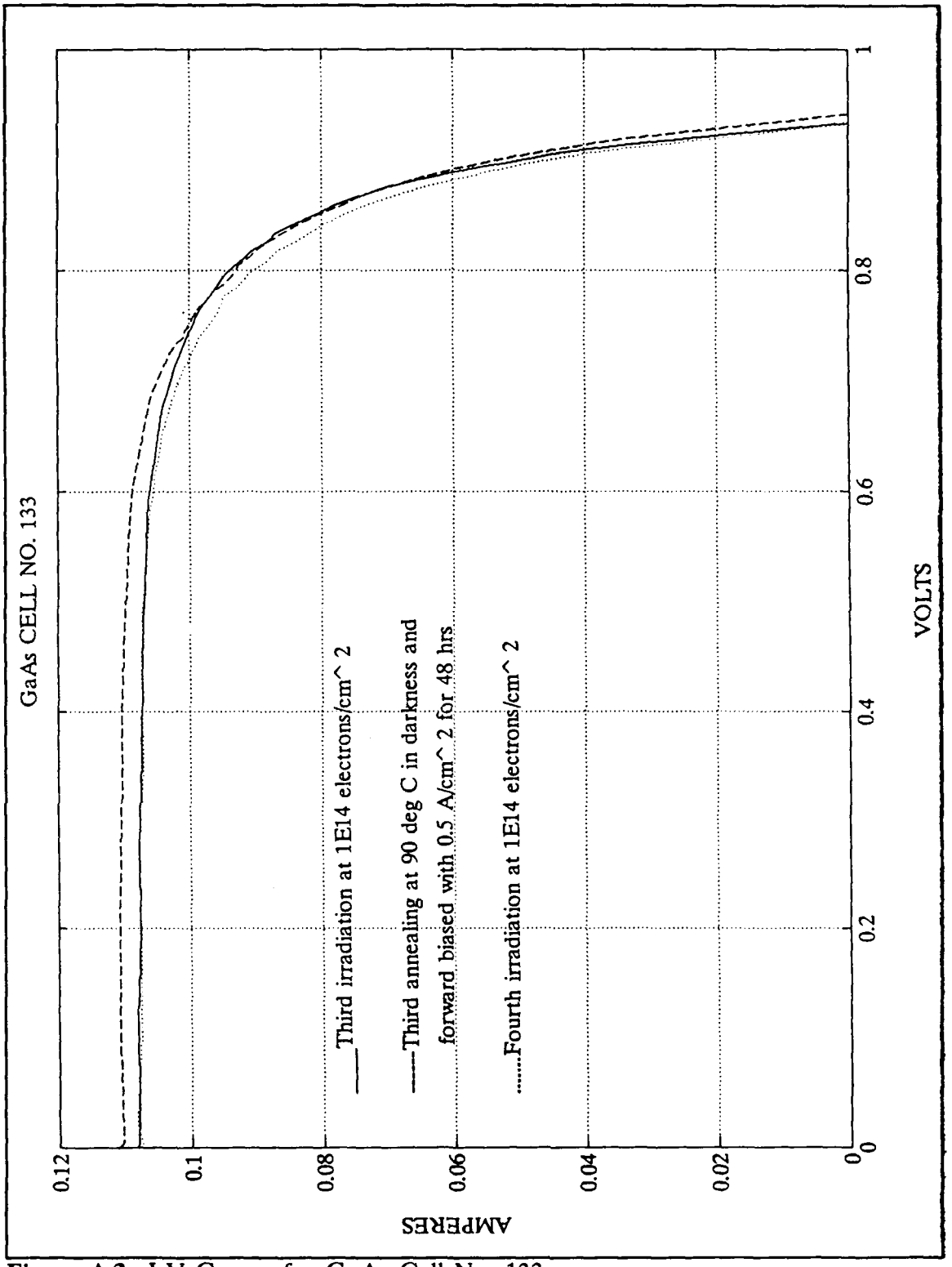

Figure A.3 I-V Curves for GaAs Cell No. 133

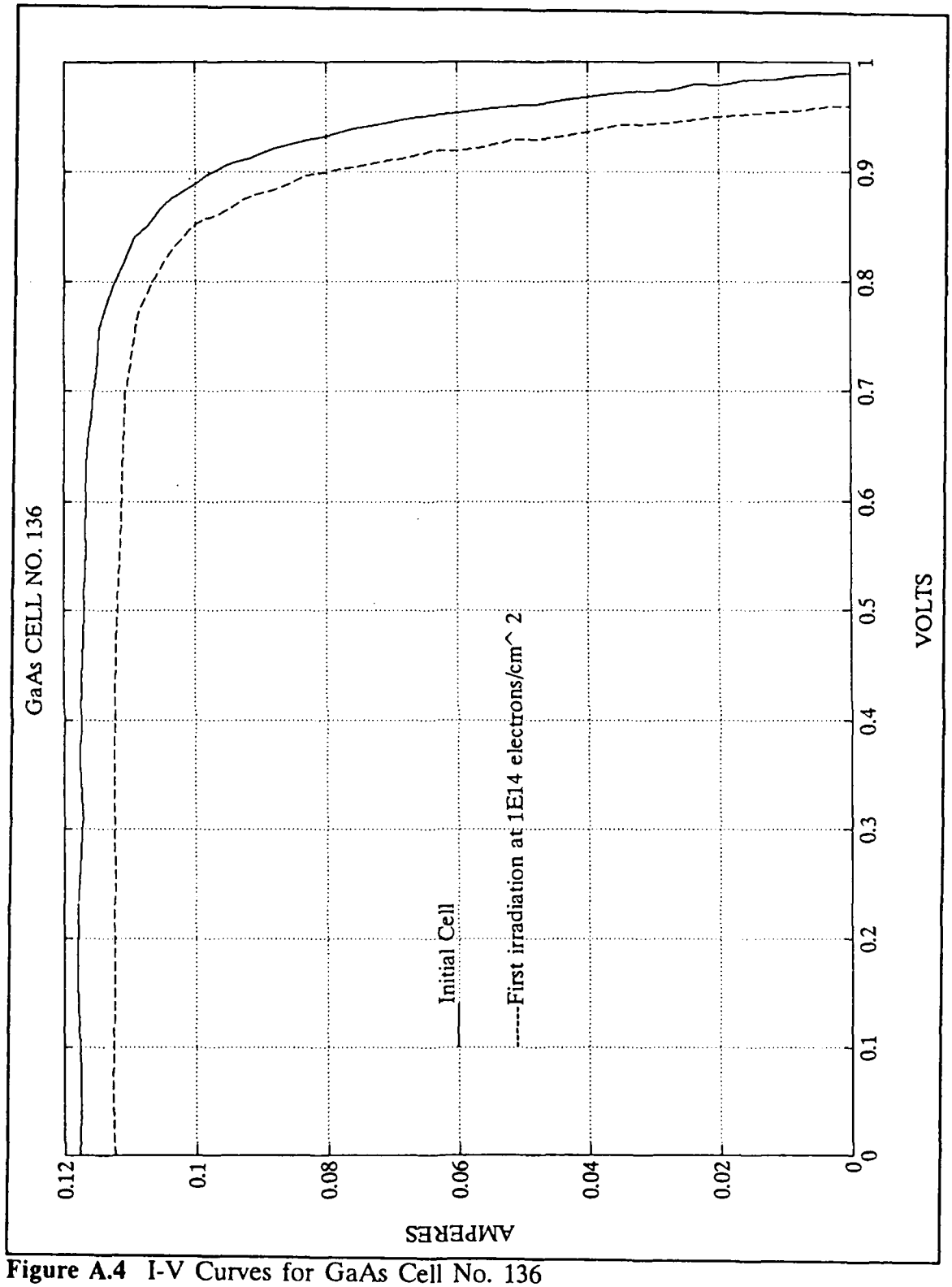

Figure A.4 I-V Curves for GaAs Cell No. 136

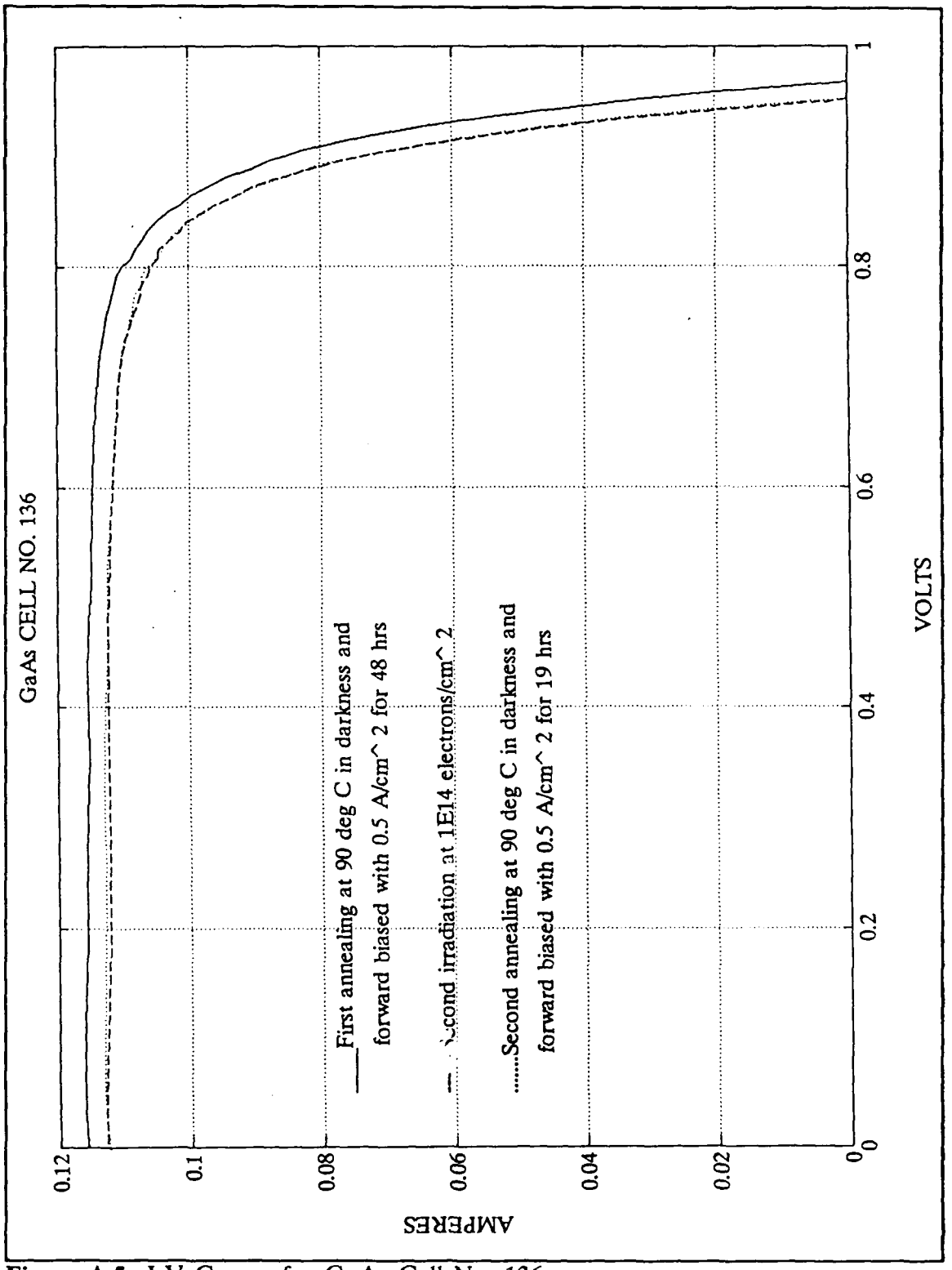

Figure A.5 I-V Curves for GaAs Cell No. 136

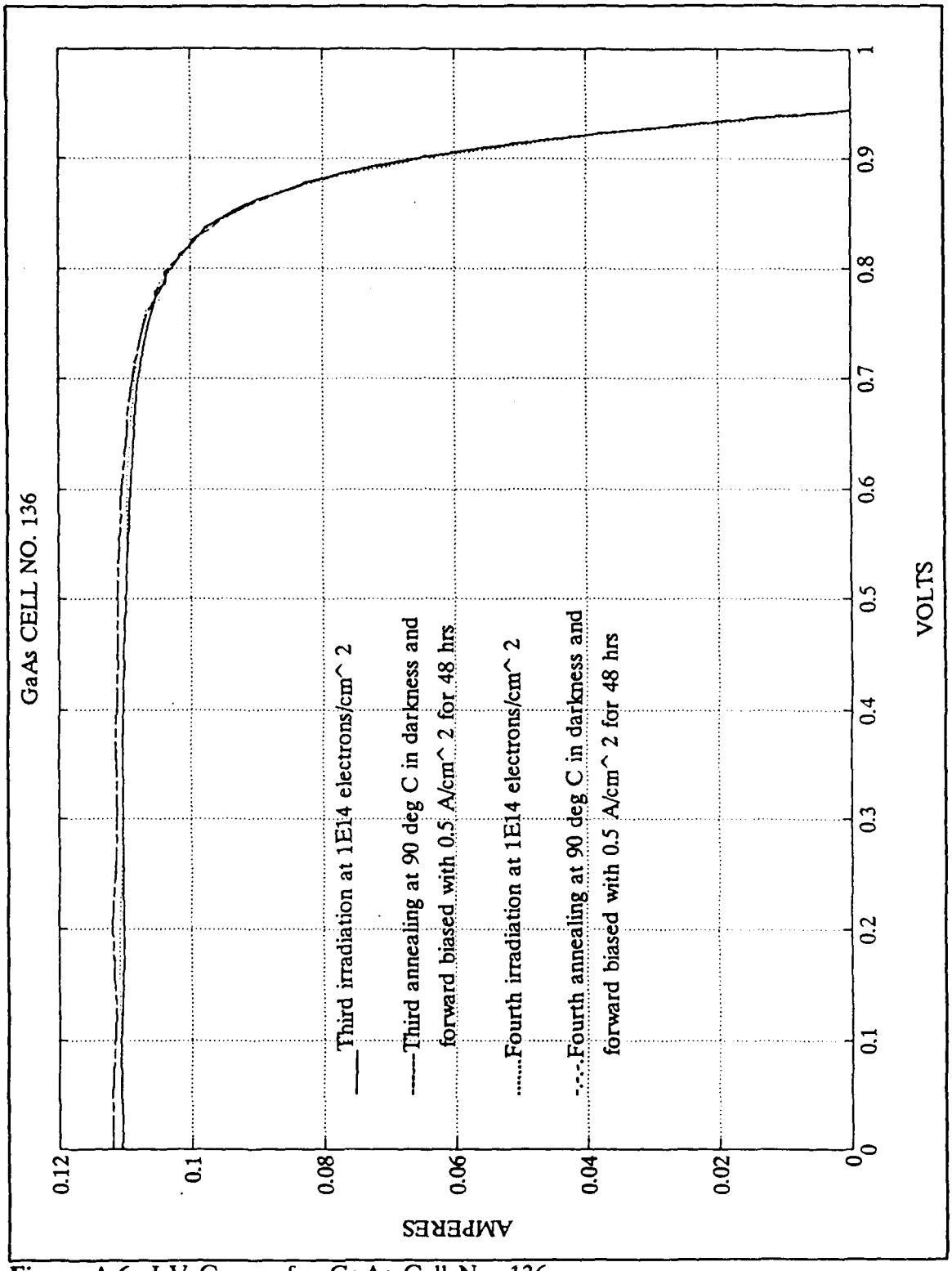

Figure A.6 I-V Curves for GaAs Cell No. 136

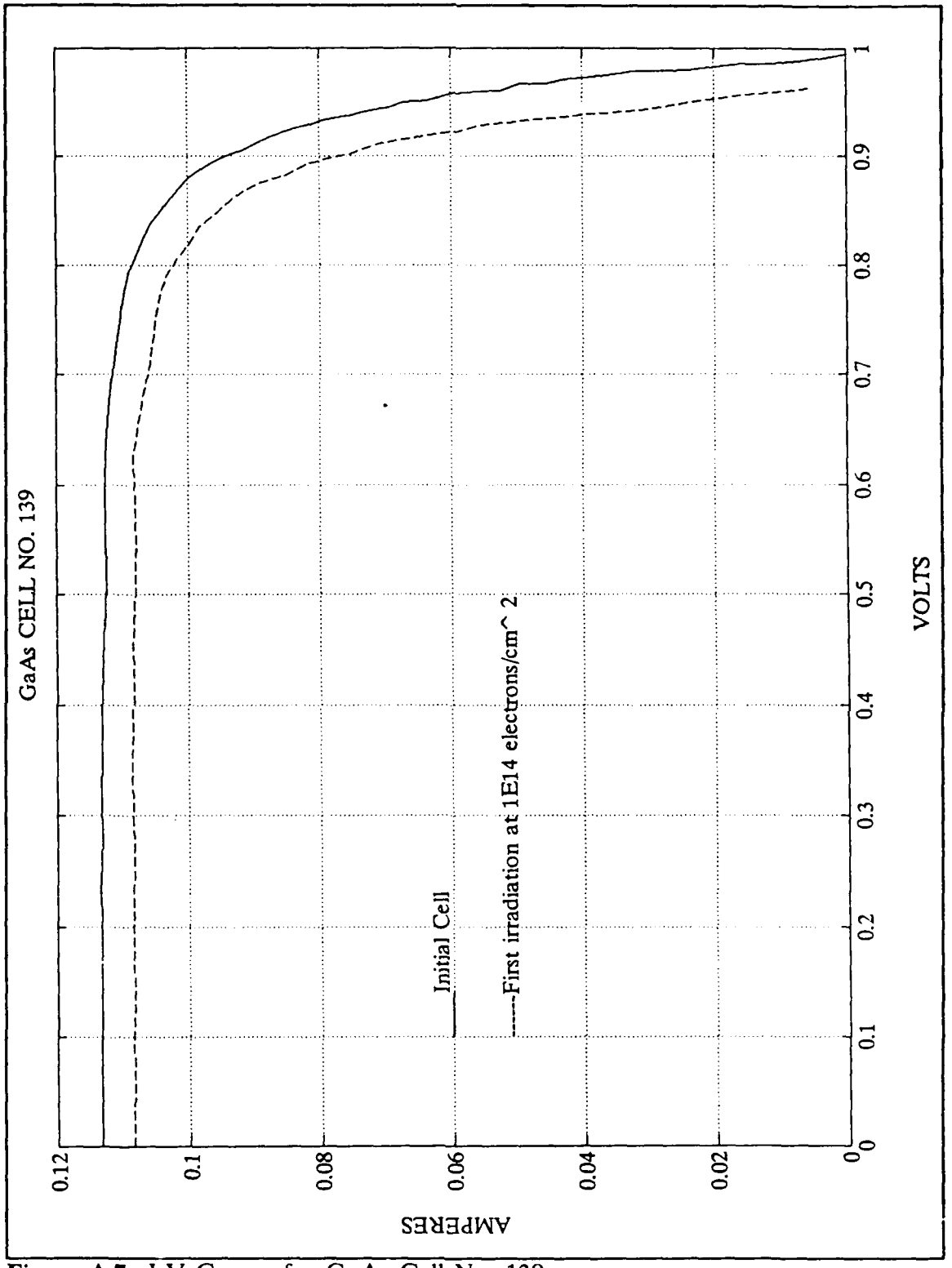

Figure A.7 I-V Curves for GaAs Cell No. 139

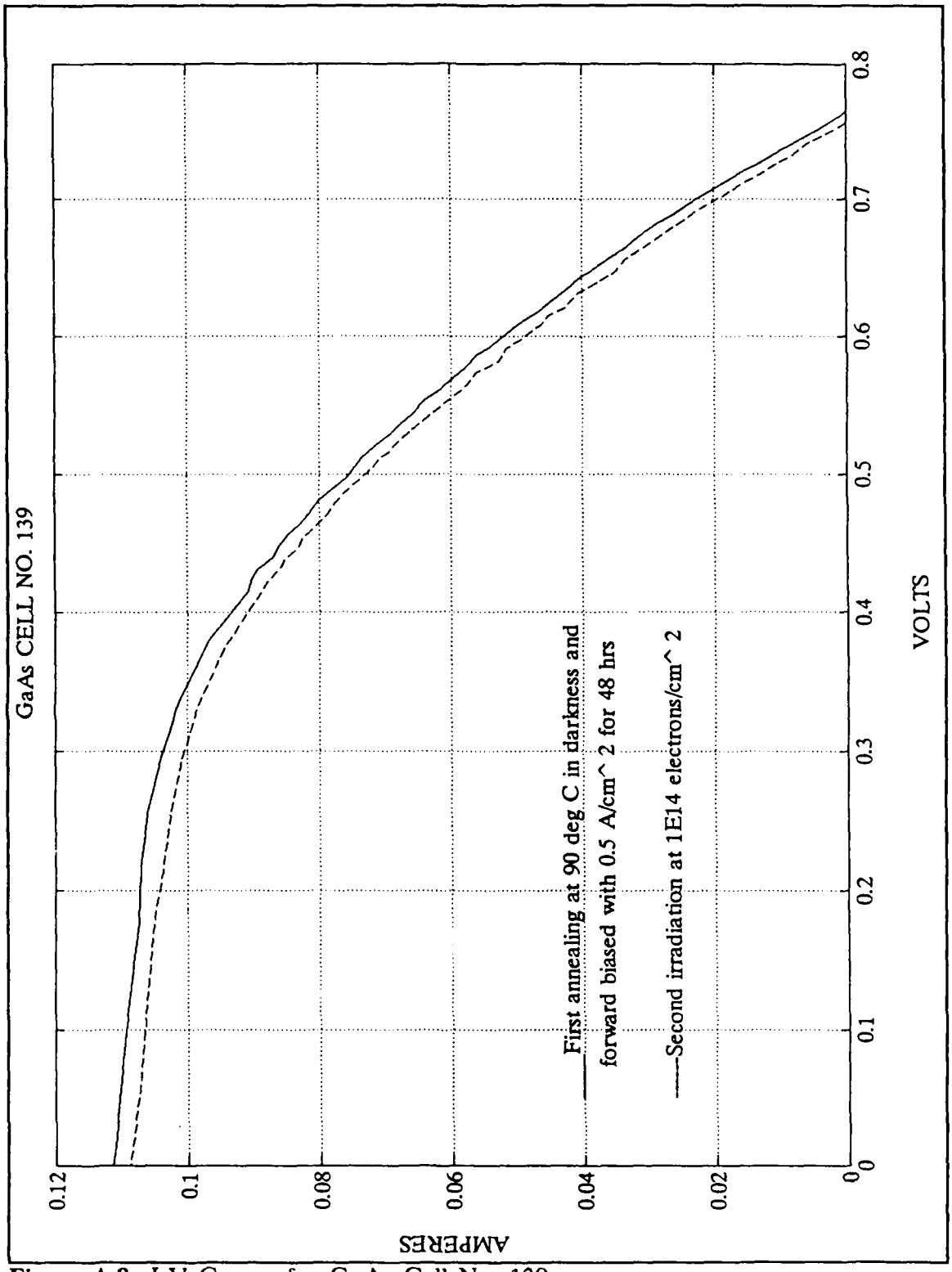

Figure A.8 I-V Curves for GaAs Cell No. 139

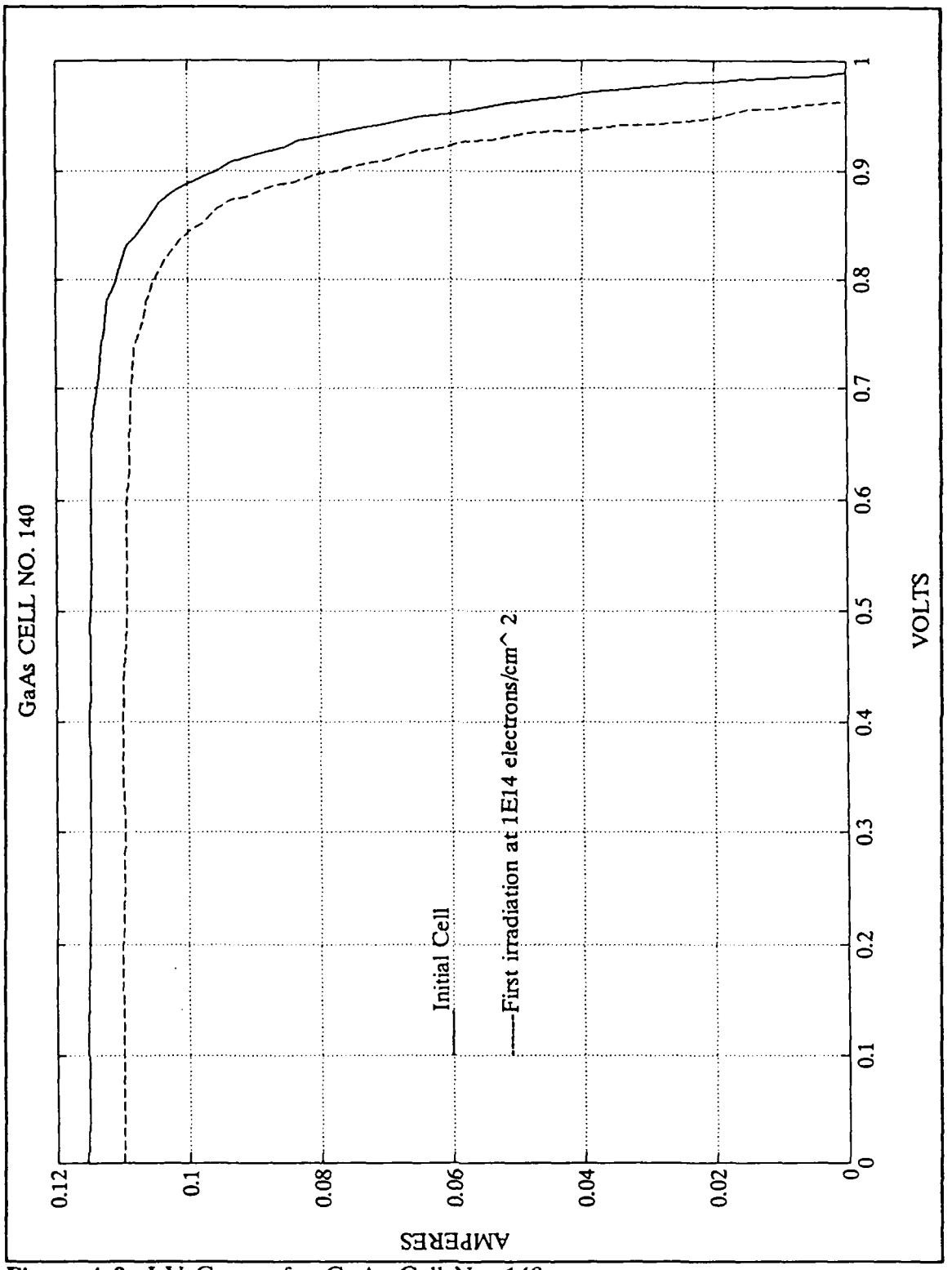

Figure A.9 I-V Curves for GaAs Cell No. 140

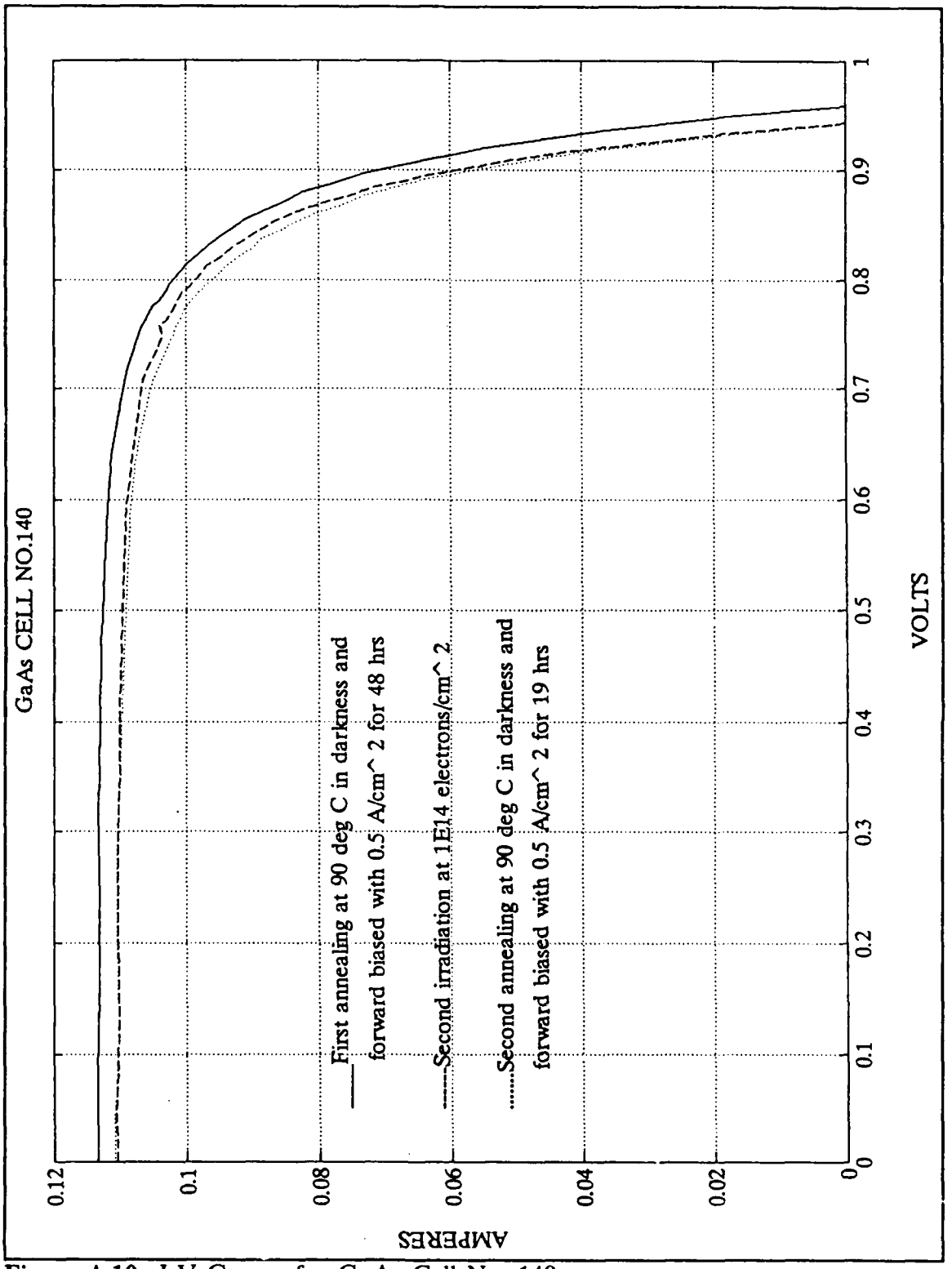

Figure A.10 I-V Curves for GaAs Cell No. 140

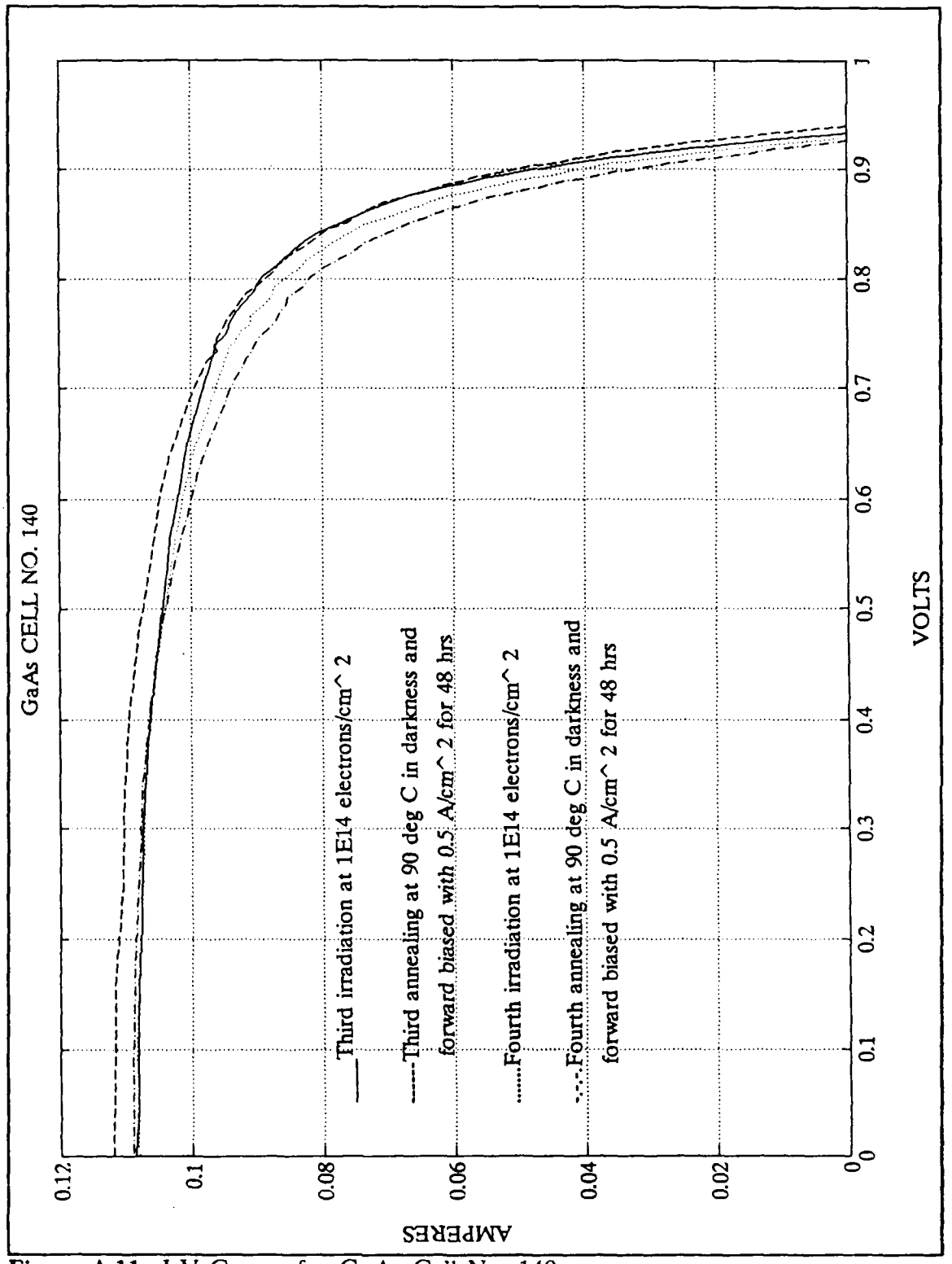

Figure A.11 I-V Curves for GaAs Cell No. 140

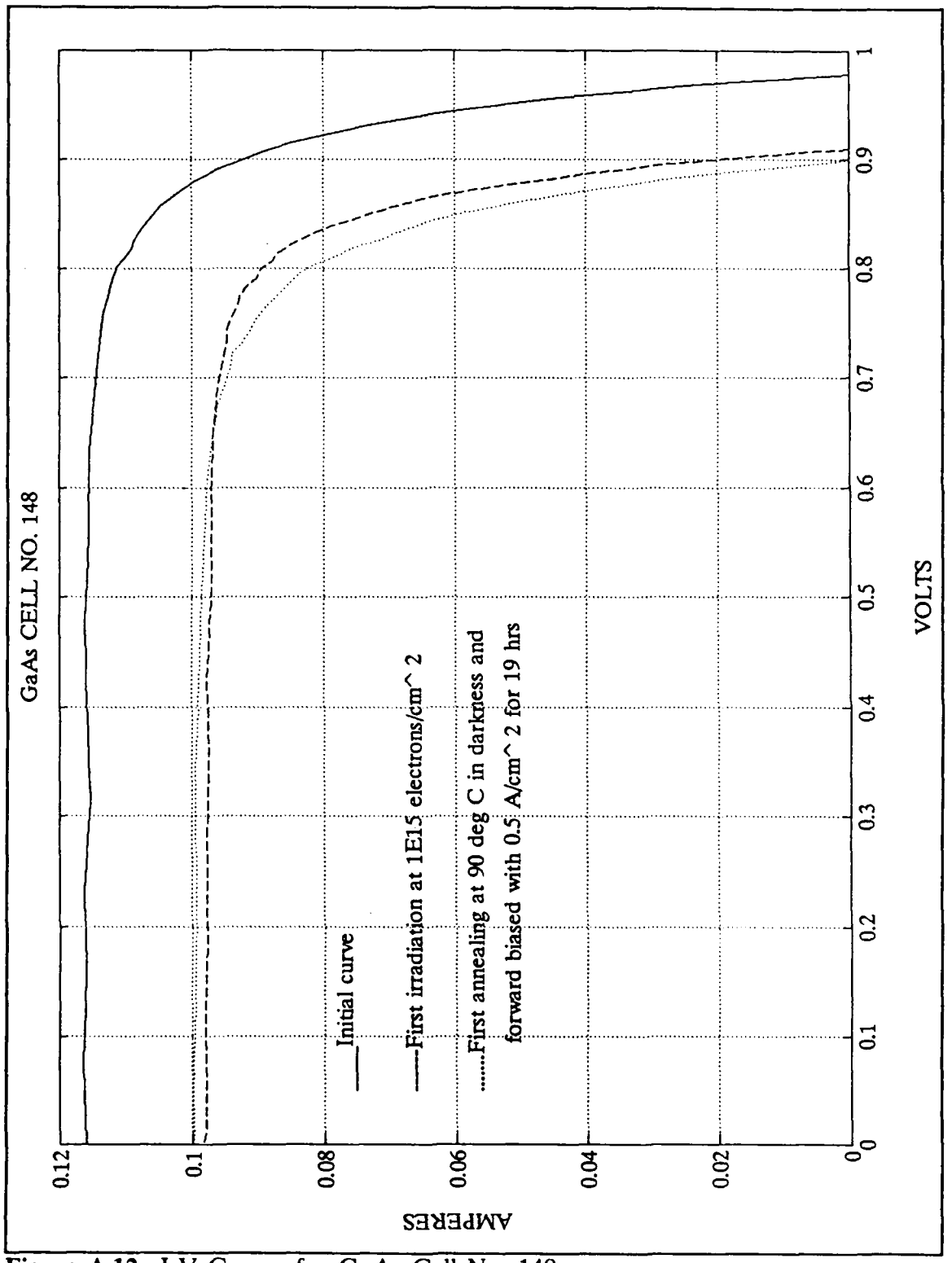

Figure A.12 I-V Curves for GaAs Cell No. 148

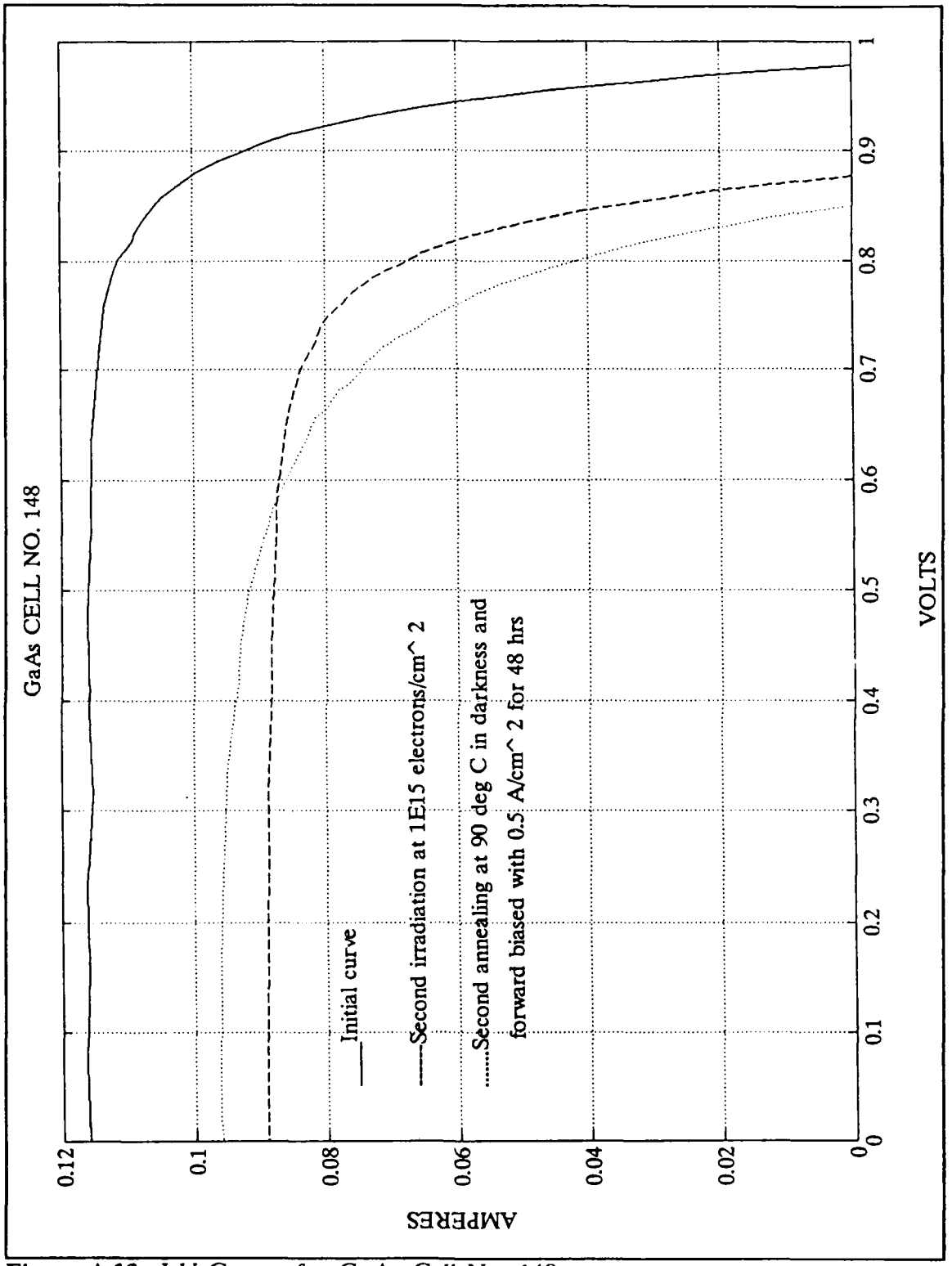

Figure A.13 I-V Curves for GaAs Cell No. 148

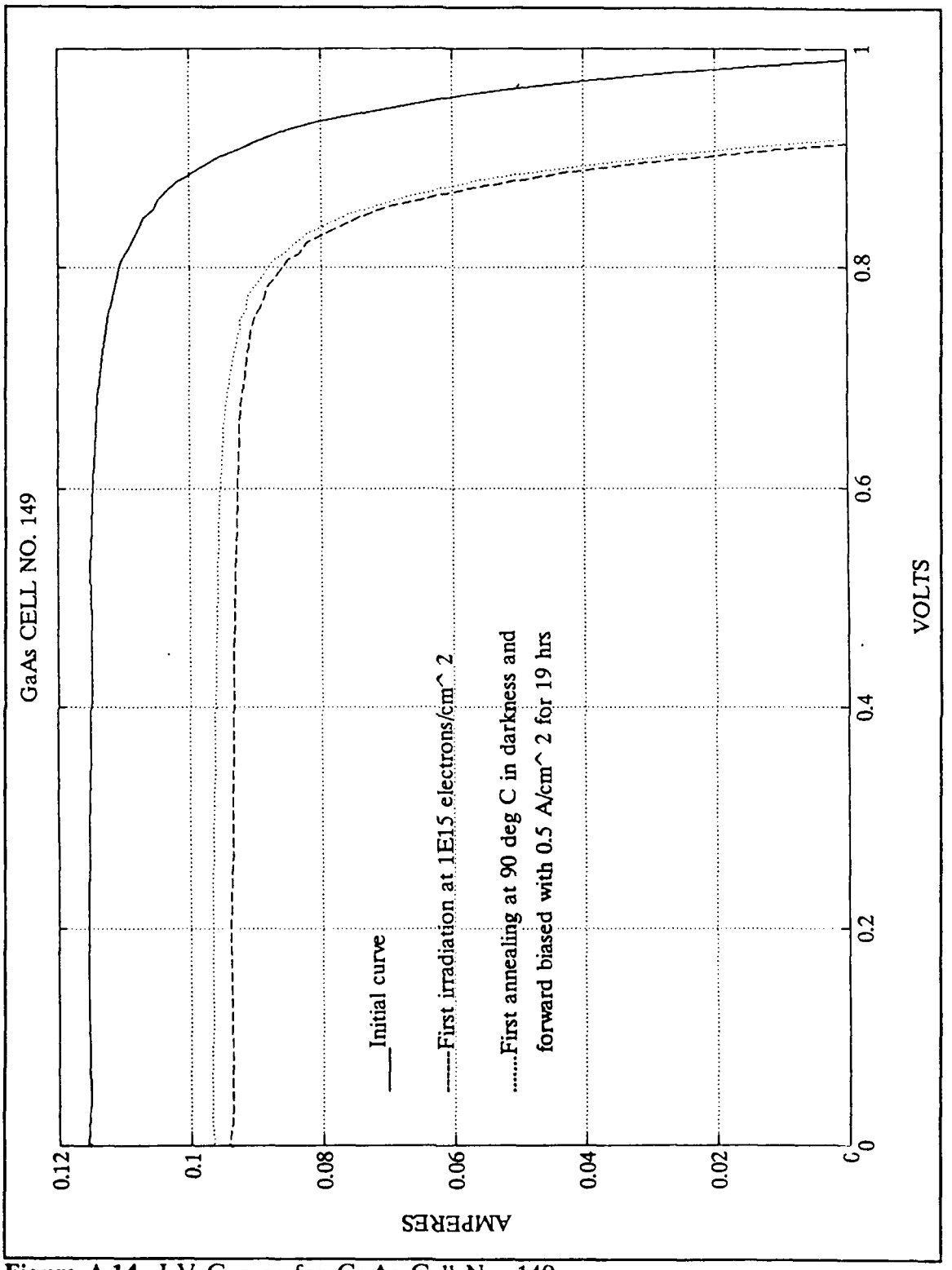

Figure A.14 I-V Curves for GaAs Cell No. 149

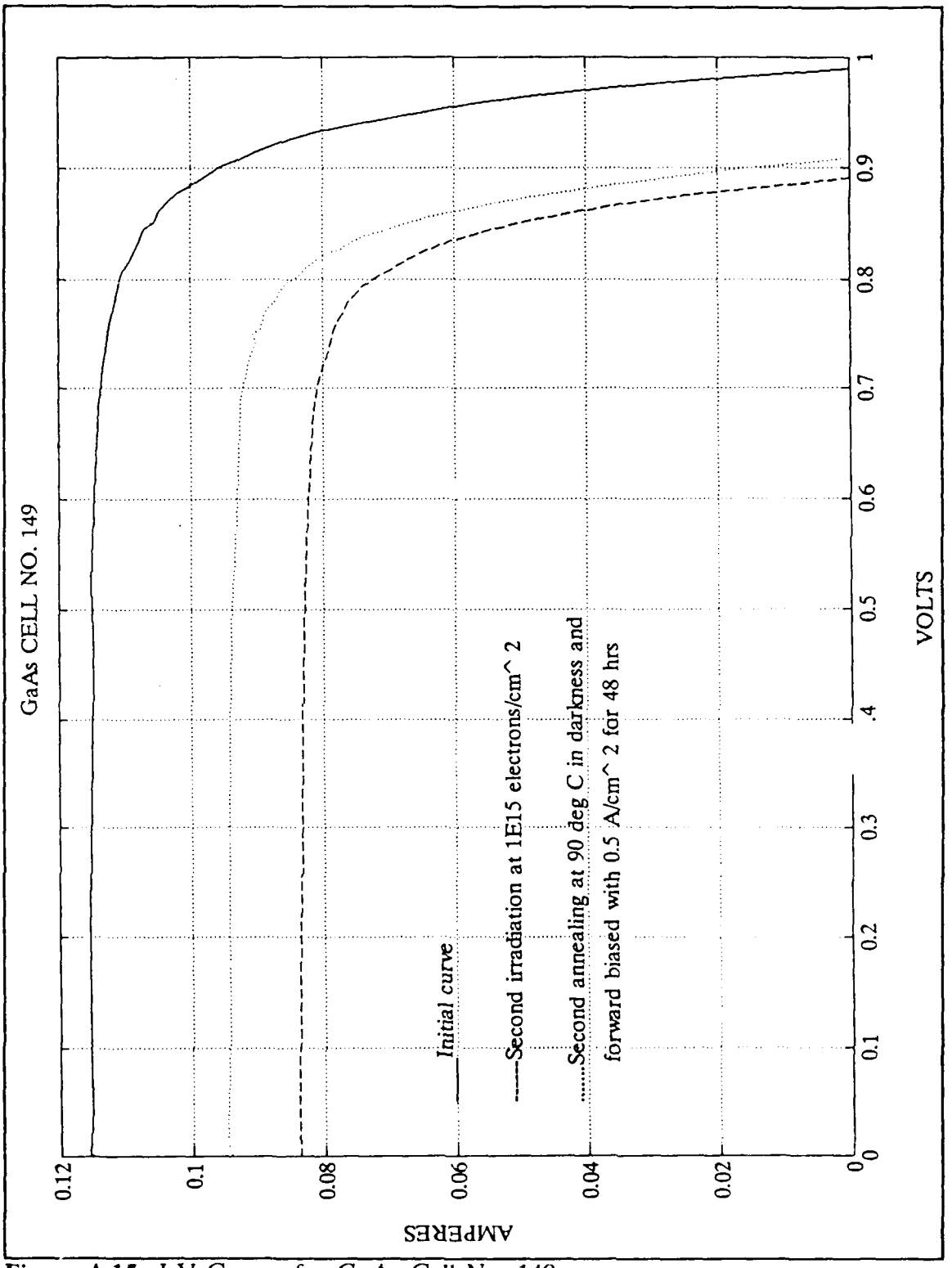

Figure A.15 I-V Curves for GaAs Cell No. 149

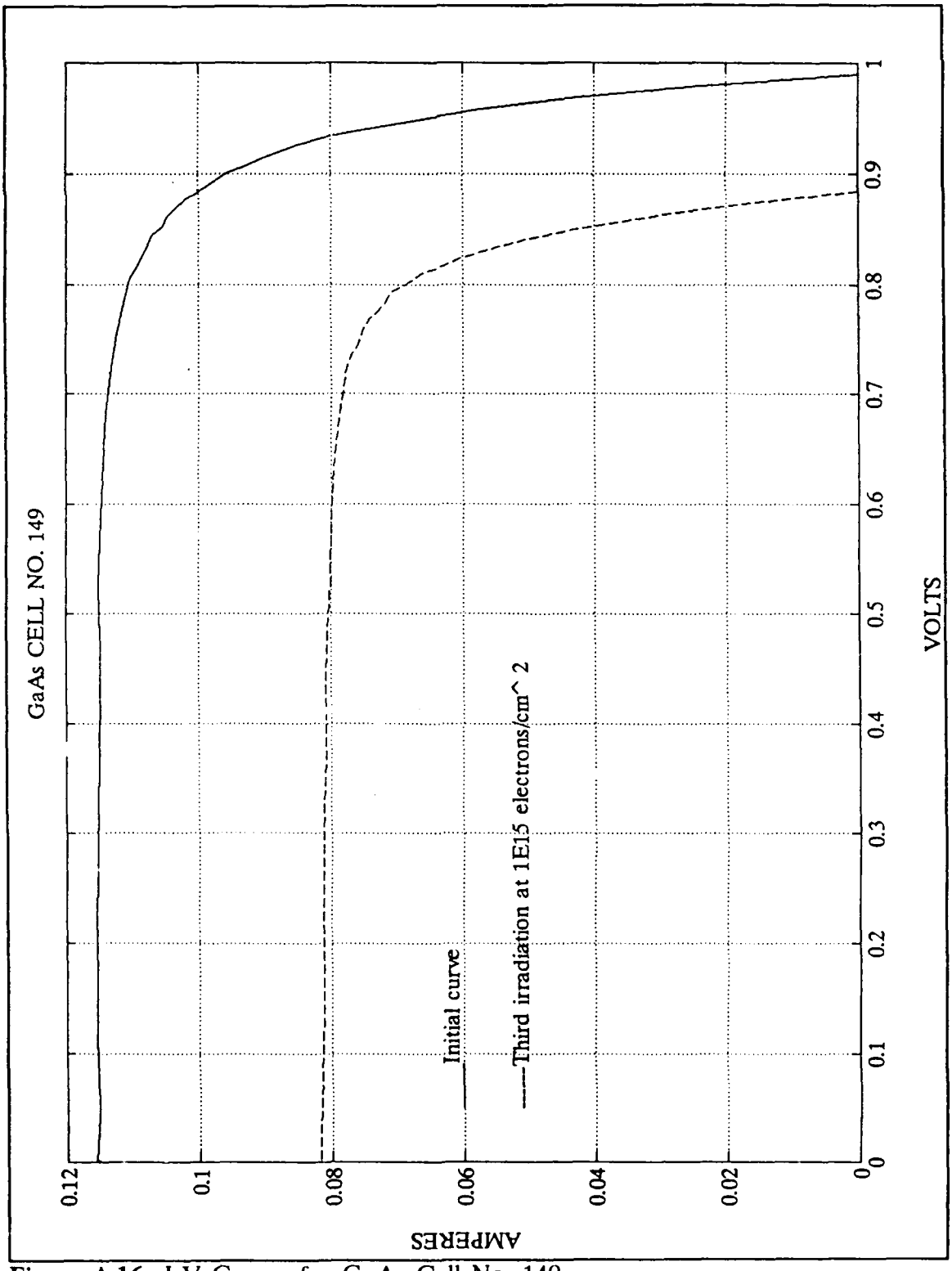

Figure A.16 I-V Curves for GaAs Cell No. 149

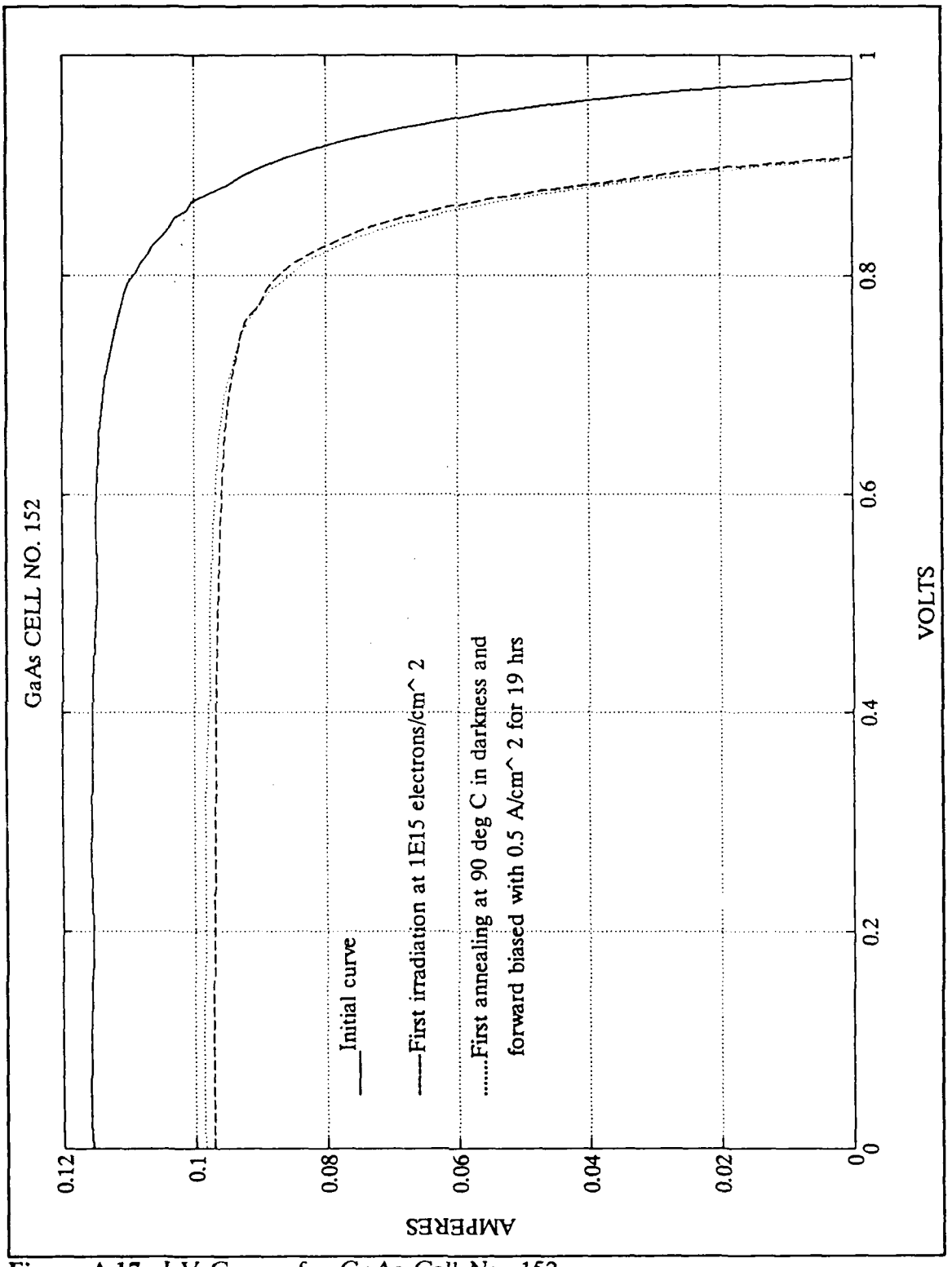

Figure A.17 I-V Curves for GaAs Cell No. 152

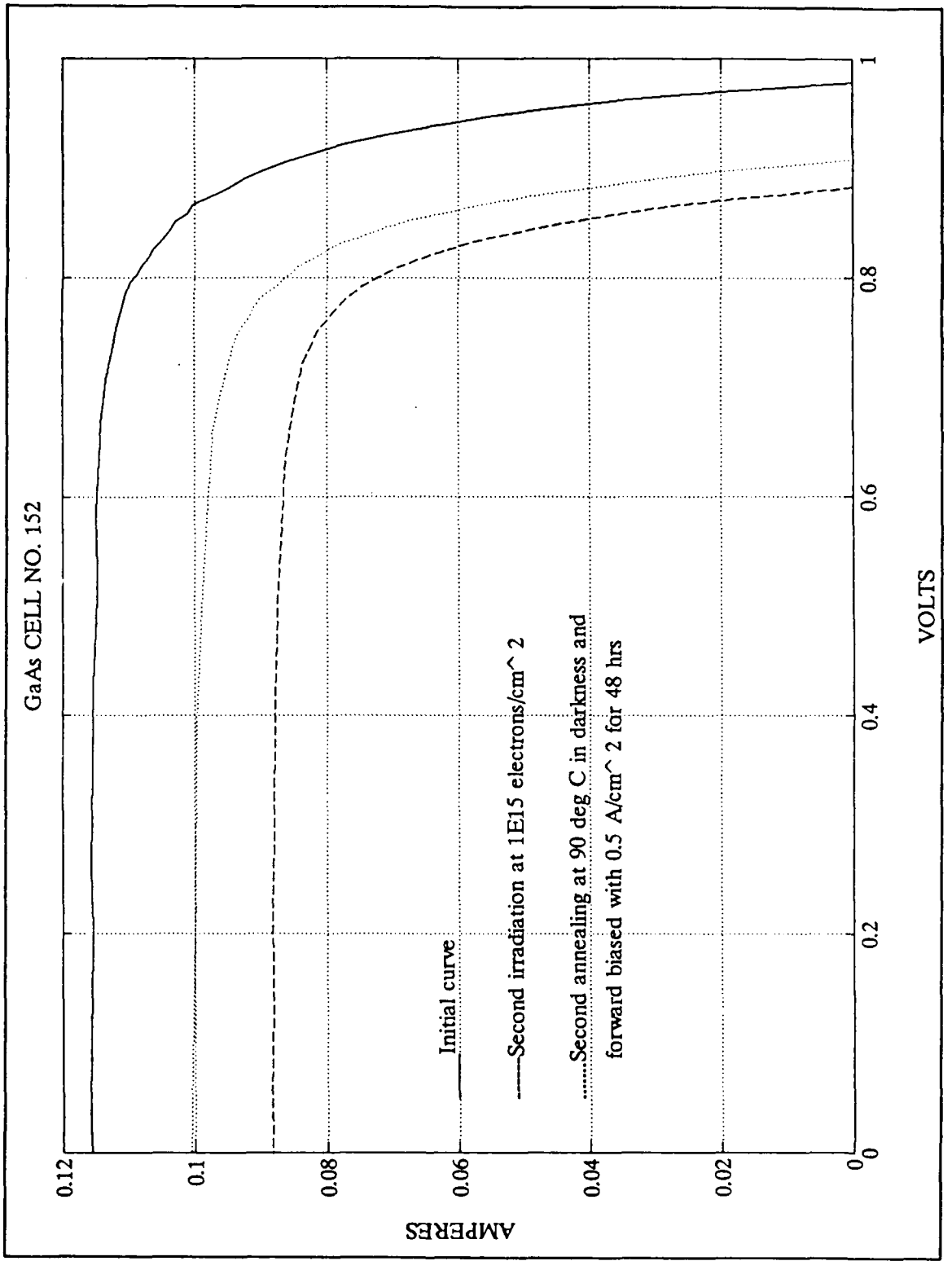

Figure A.18 I-V Curves for GaAs Cell No. 152

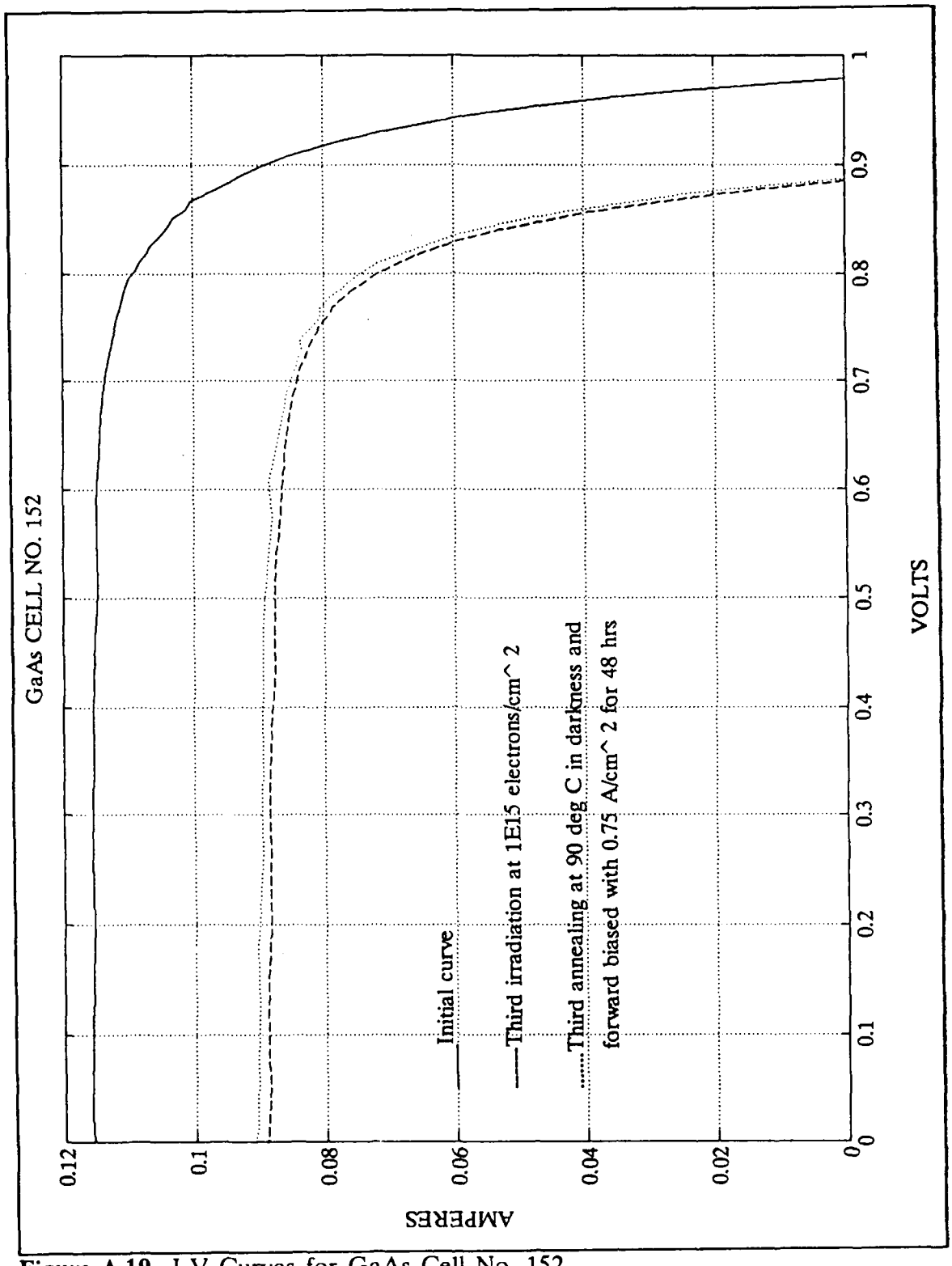

Figure A.19 I-V Curves for GaAs Cell No. 152

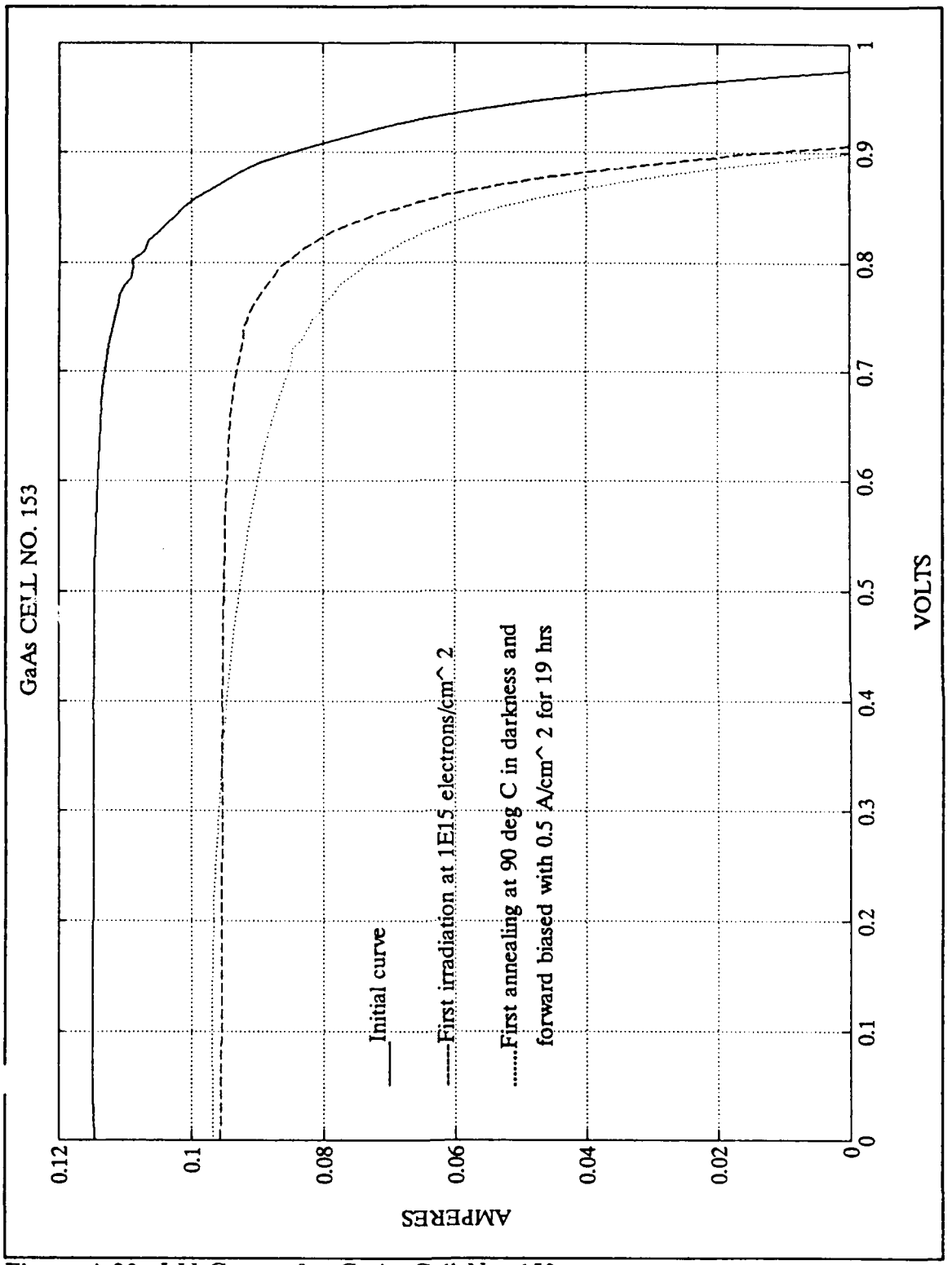

Figure A.20 I-V Curves for GaAs Cell No. 153

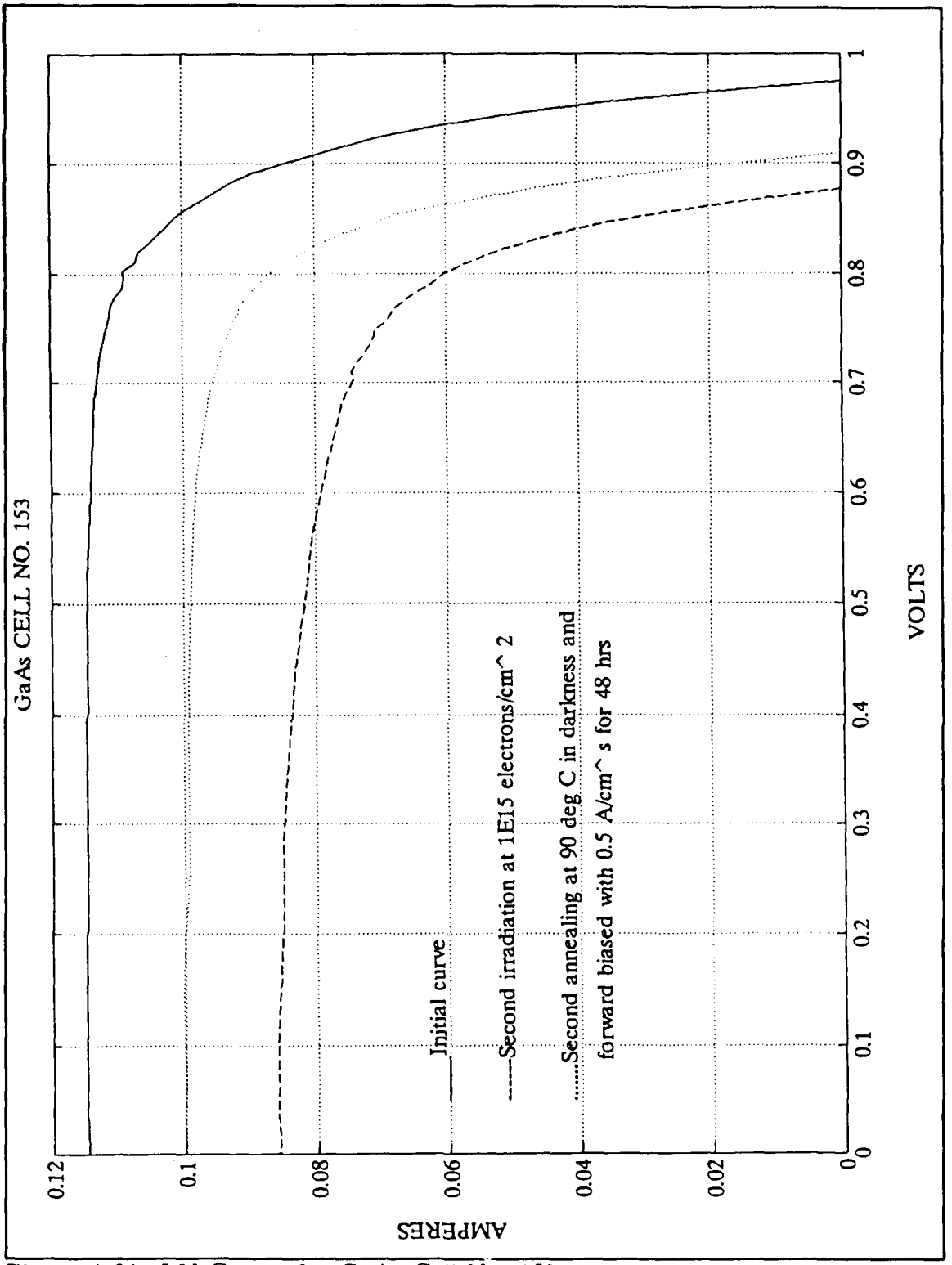

Figure A.21 I-V Curves for GaAs Cell No. 153

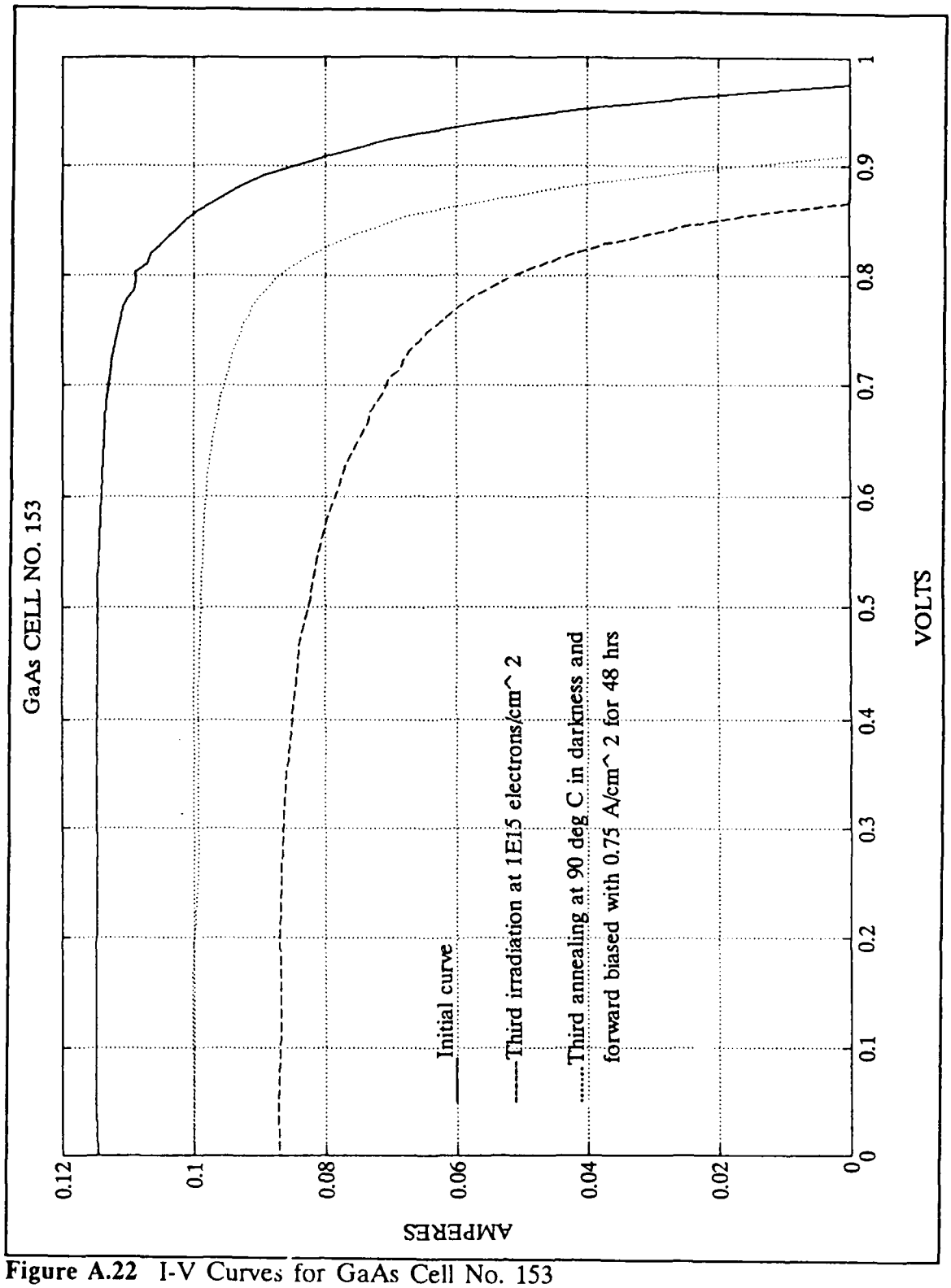

Figure A.22 I-V Curves for GaAs Cell No. 153

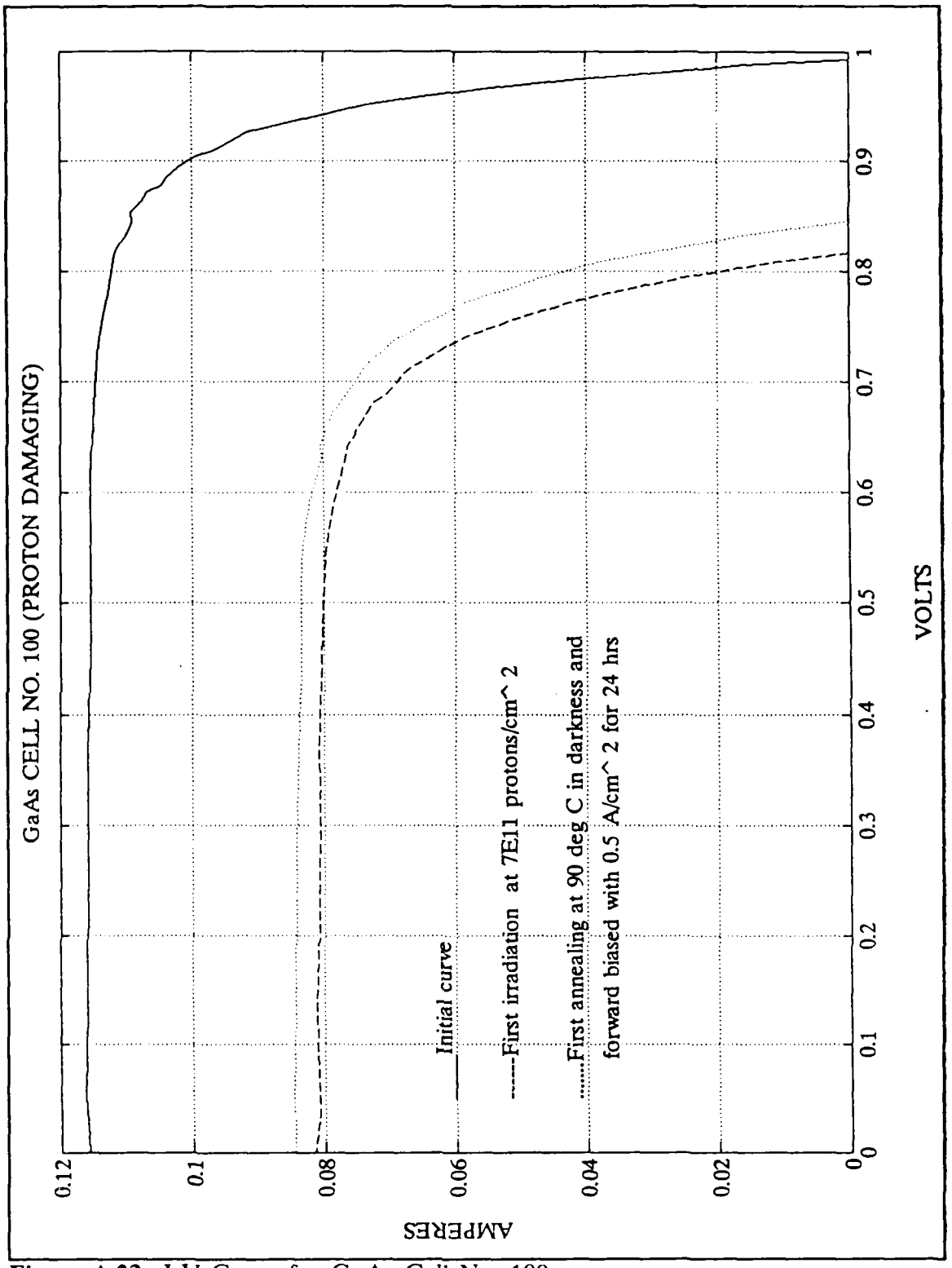

Figure A.23 I-V Curve for GaAs Cell No. 100

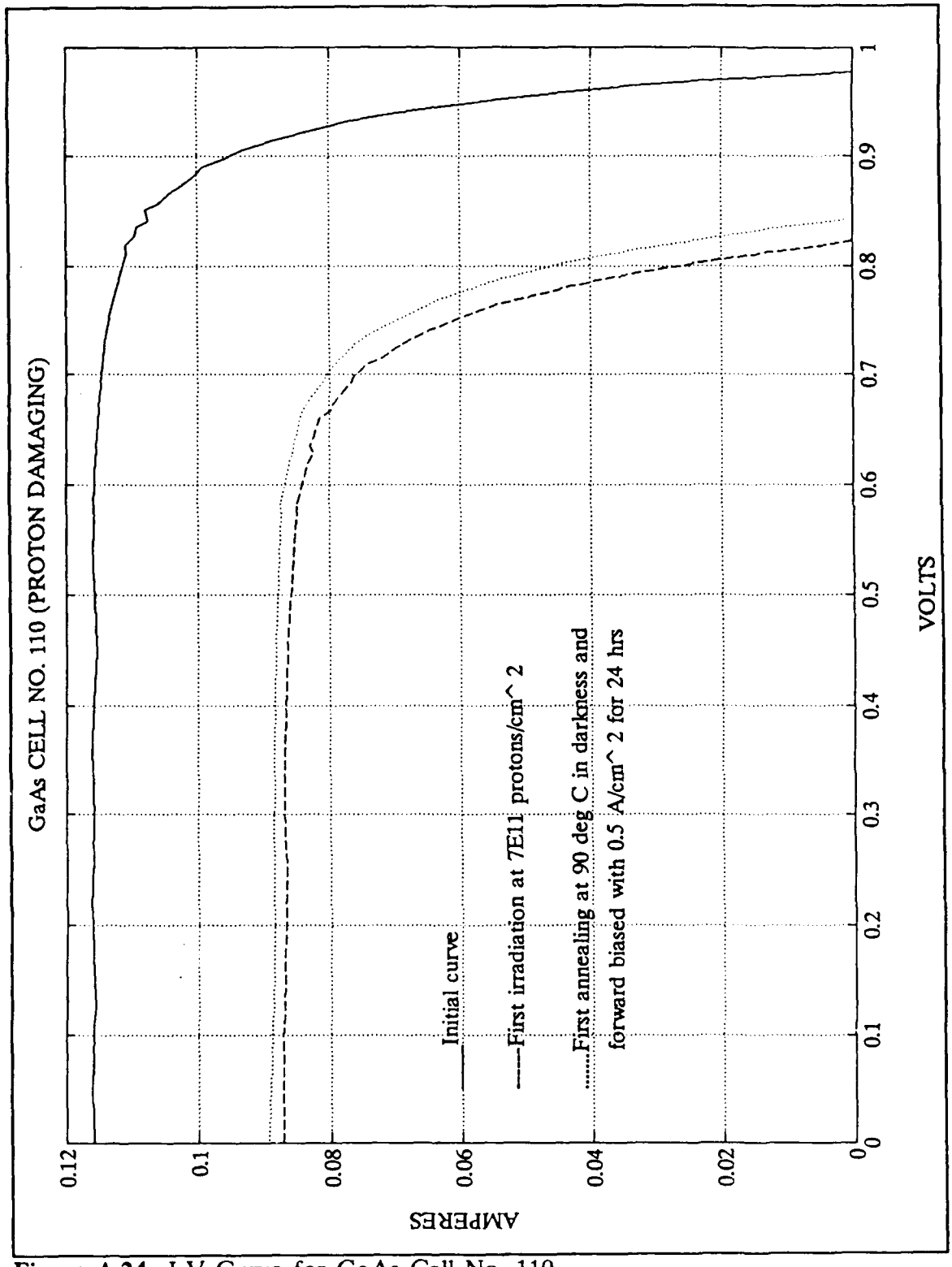

Figure A.24 I-V Curve for GaAs Cell No. 110

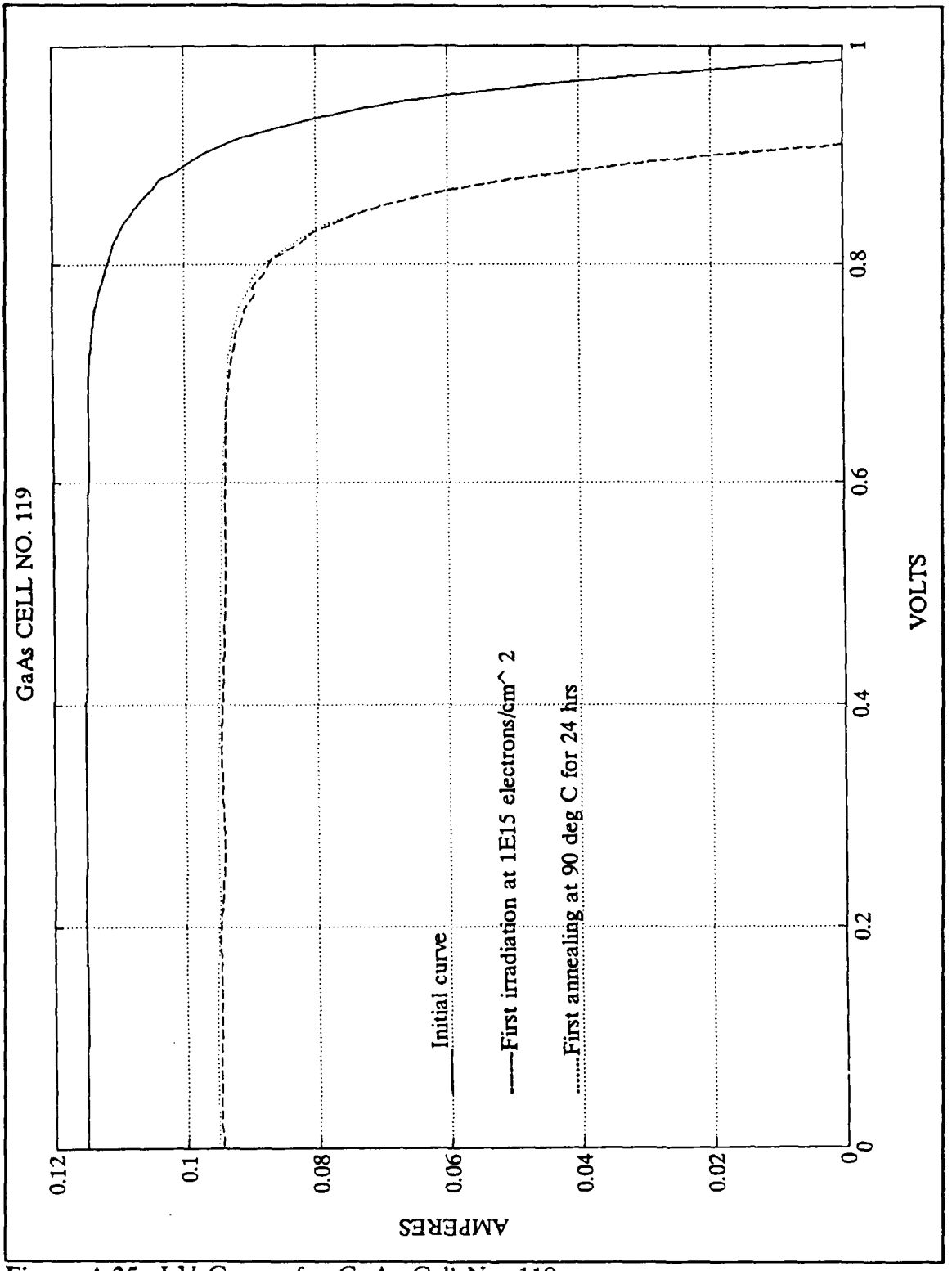

Figure A.25 I-V Curves for GaAs Cell No. 119

APPENDIX B. GaAs CELL DATA PLOTS

Voc, Isc, Pmax, and % Eff was plotted for every stage in the multiple irradiating and annealing cycle of every cell. These graphs are point plots which have been connected with lines and illustrate the degradation and recovery with every stage.

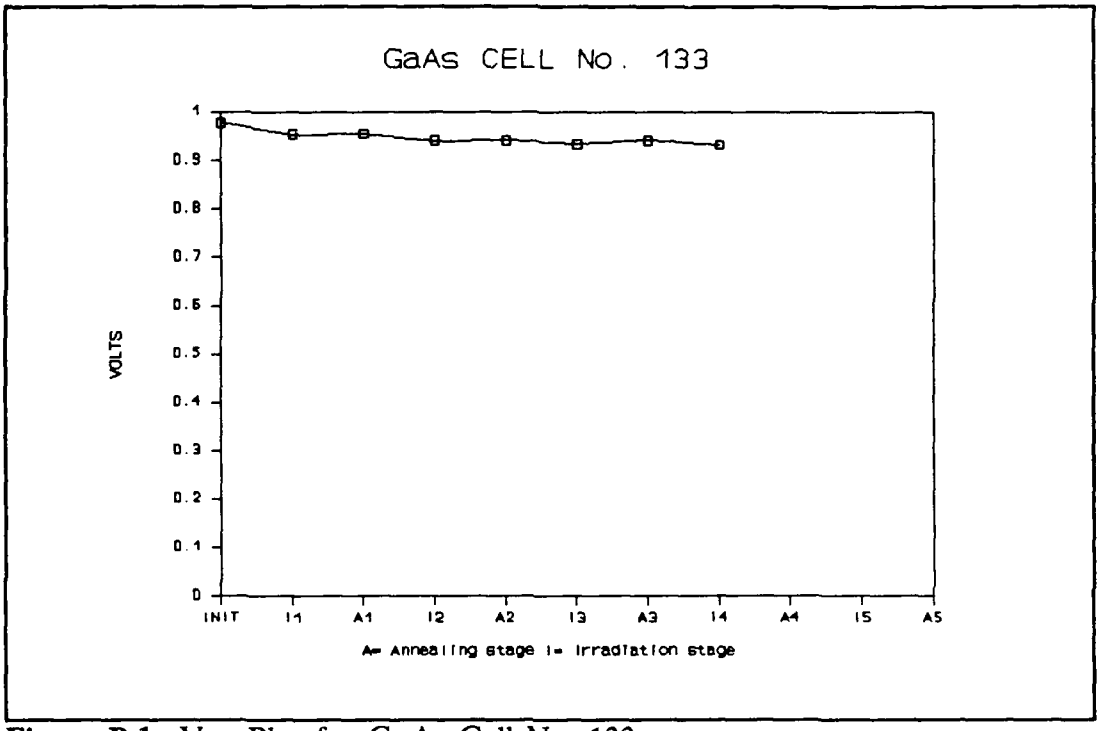

Figure B.1 Voc Plot for GaAs Cell No. 133

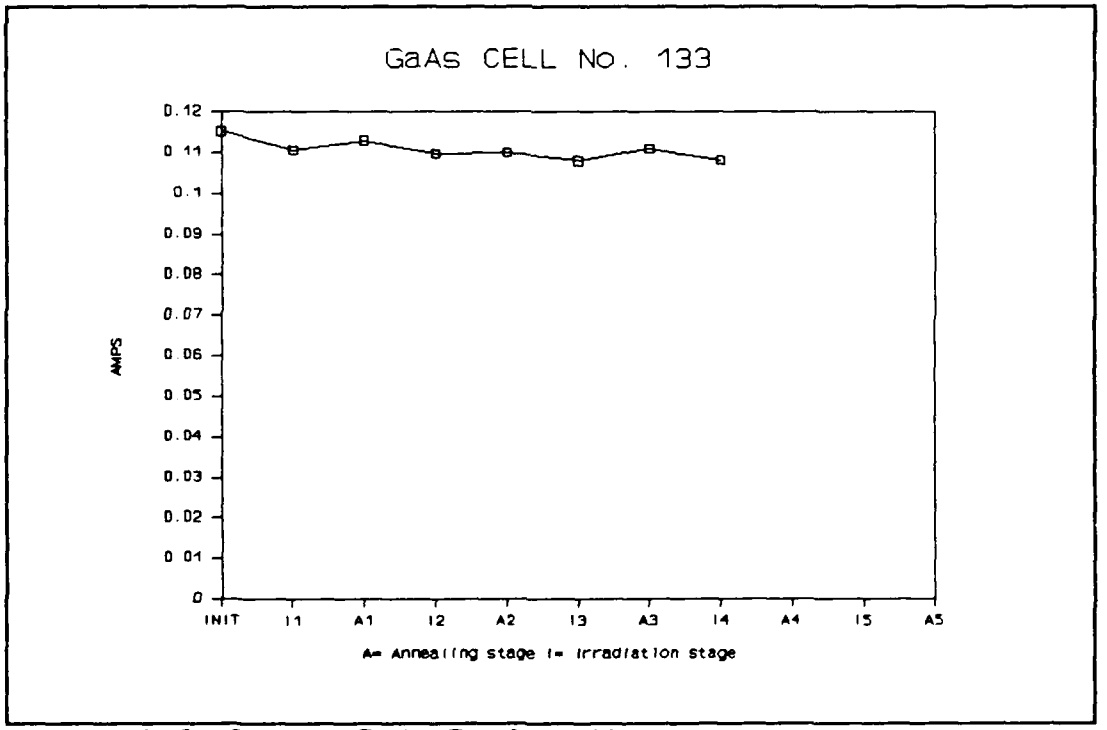

Figure B.2 Isc Plot for GaAs Cell No. 133

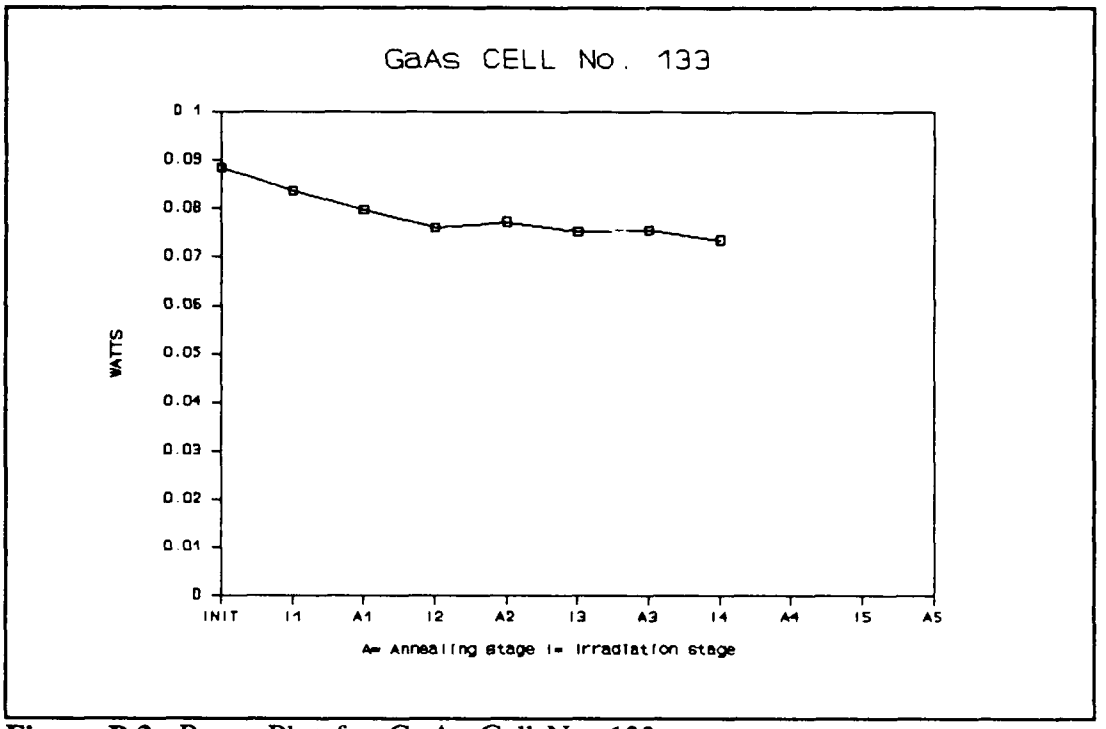

Figure B.3 Pmax Plot for GaAs Cell No. 133

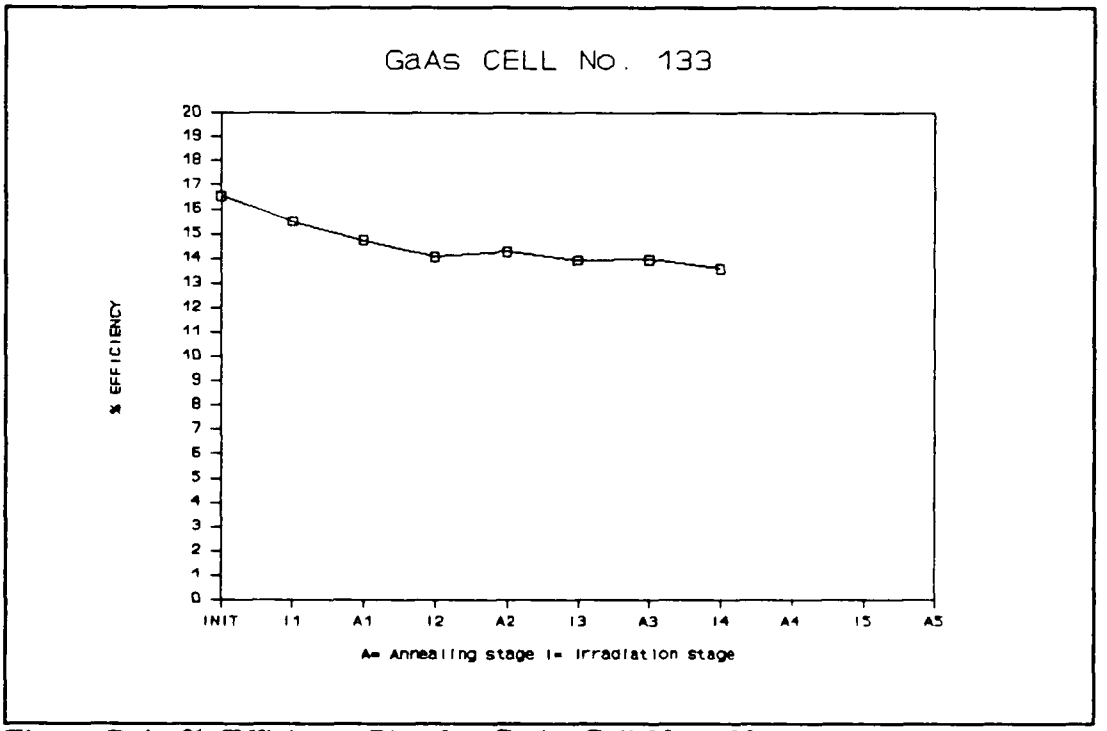

Figure B.4 % Efficiency Plot for GaAs Cell No. 133

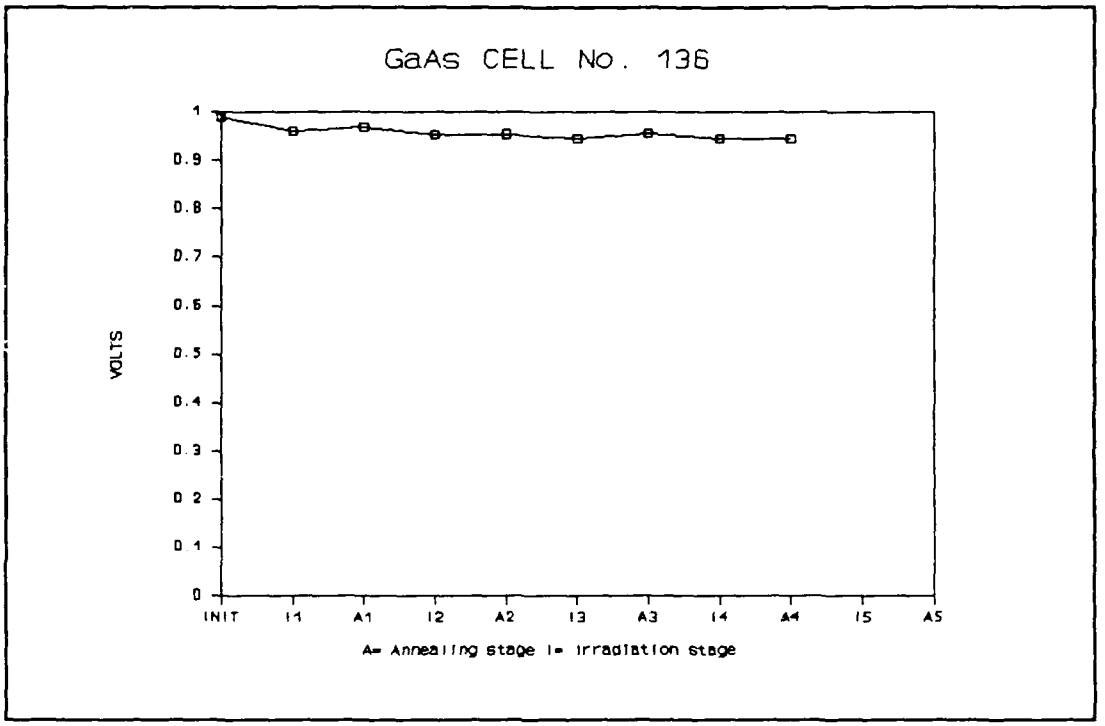

Figure B.5 Voc Plot for GaAs Cell No. 136

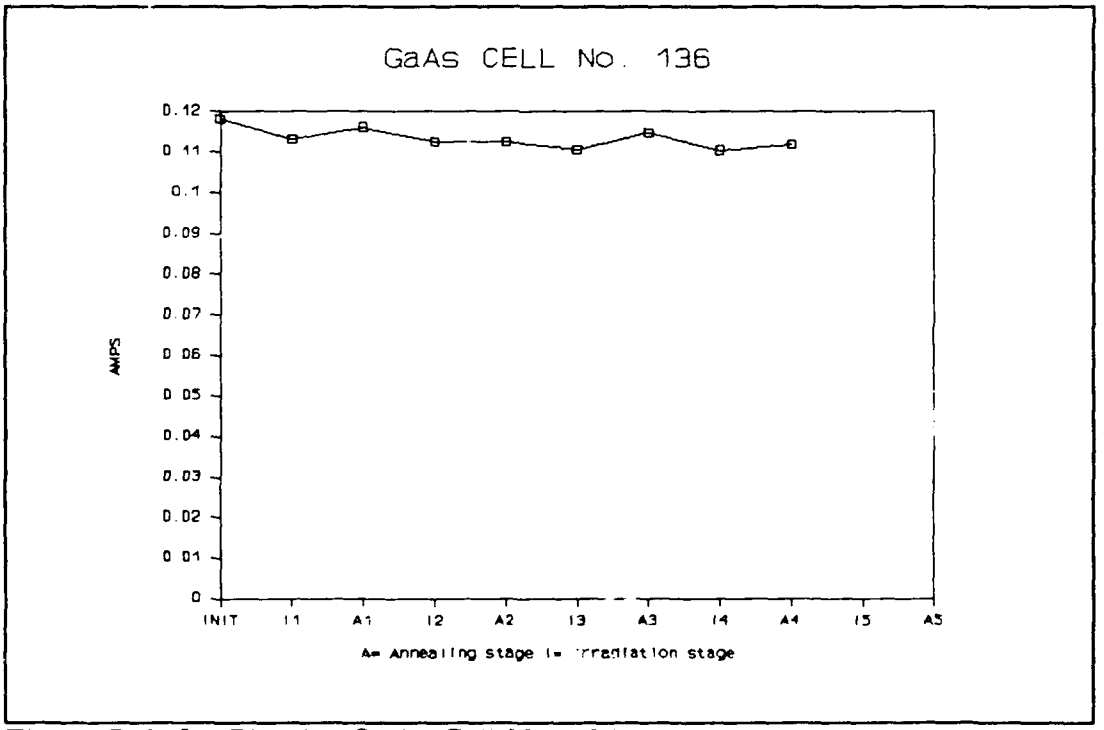

Figure B.6 Isc Plot for GaAs Cell No. 136

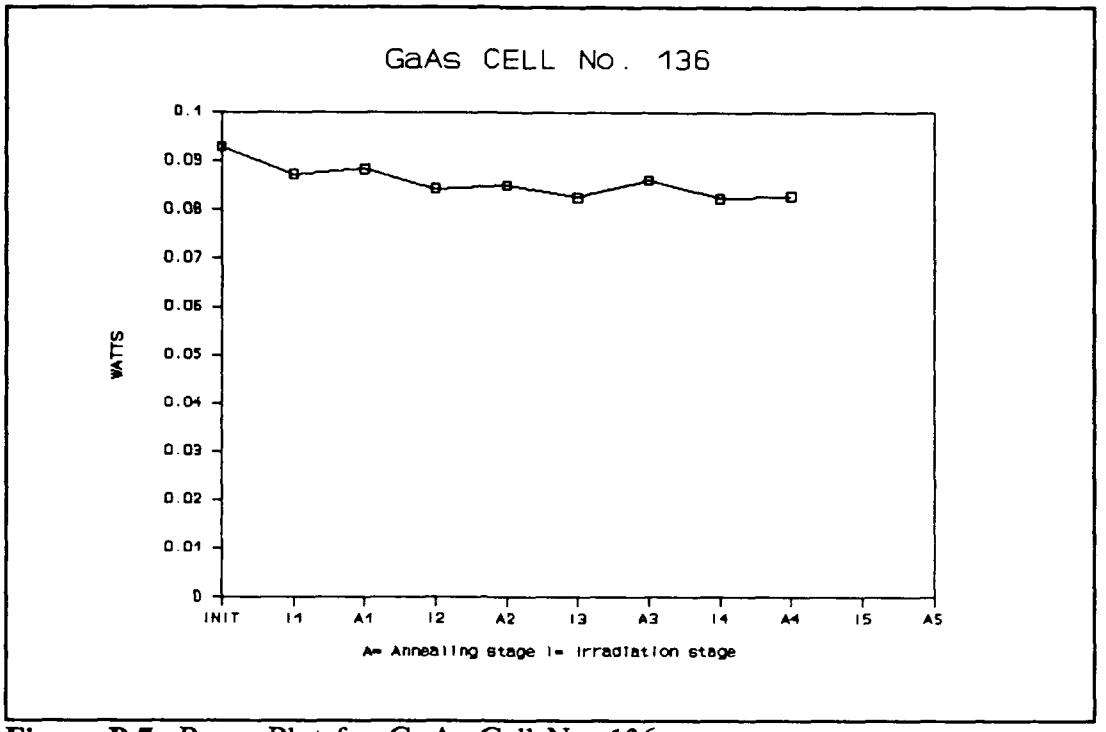

Figure B.7 Pmax Plot for GaAs Cell No. 136

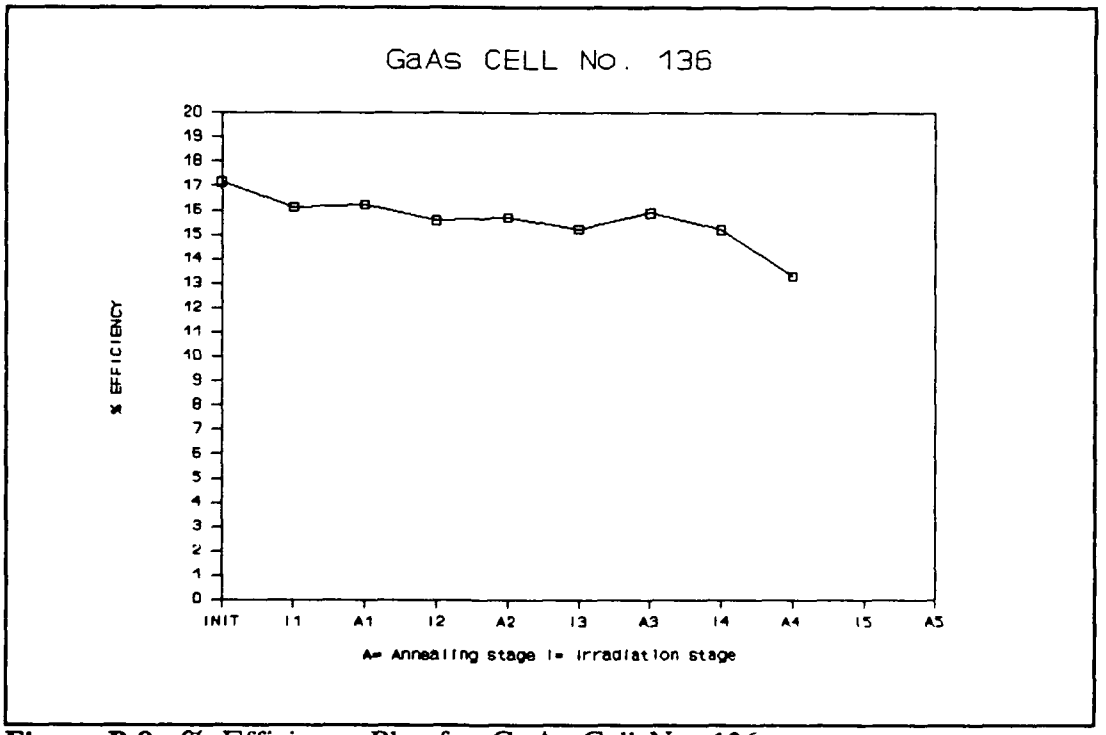

Figure B.8 % Efficiency Plot for GaAs Cell No. 136

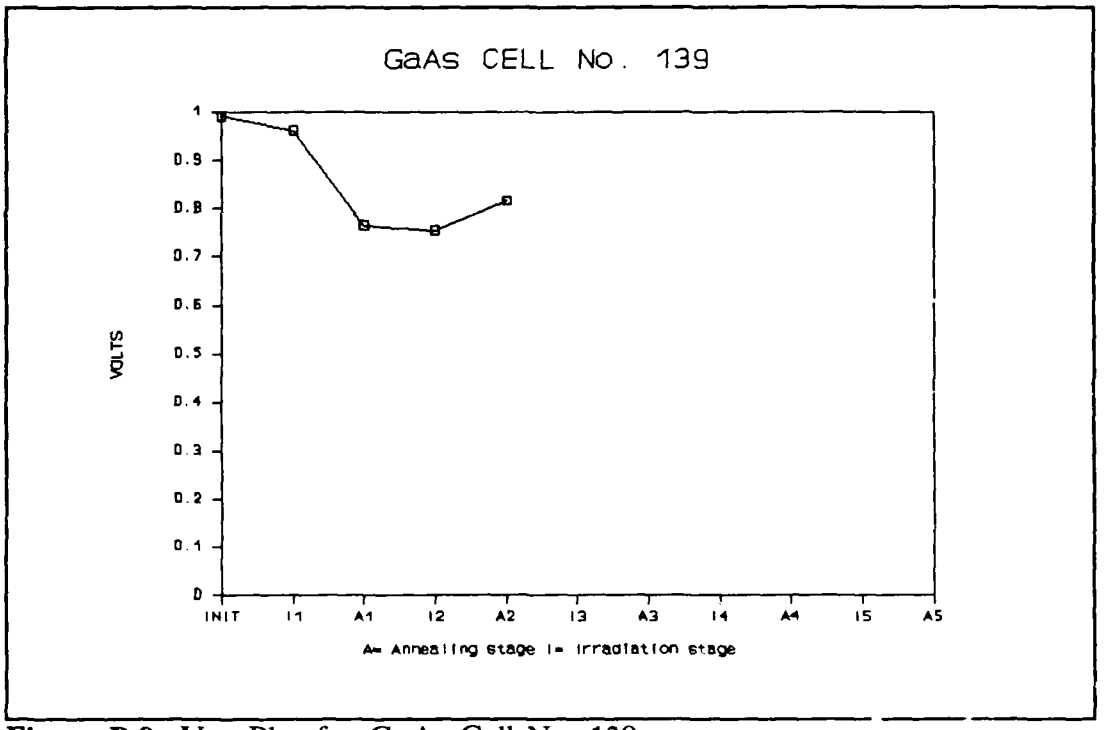

Figure B.9 Voc Plot for GaAs Cell No. 139

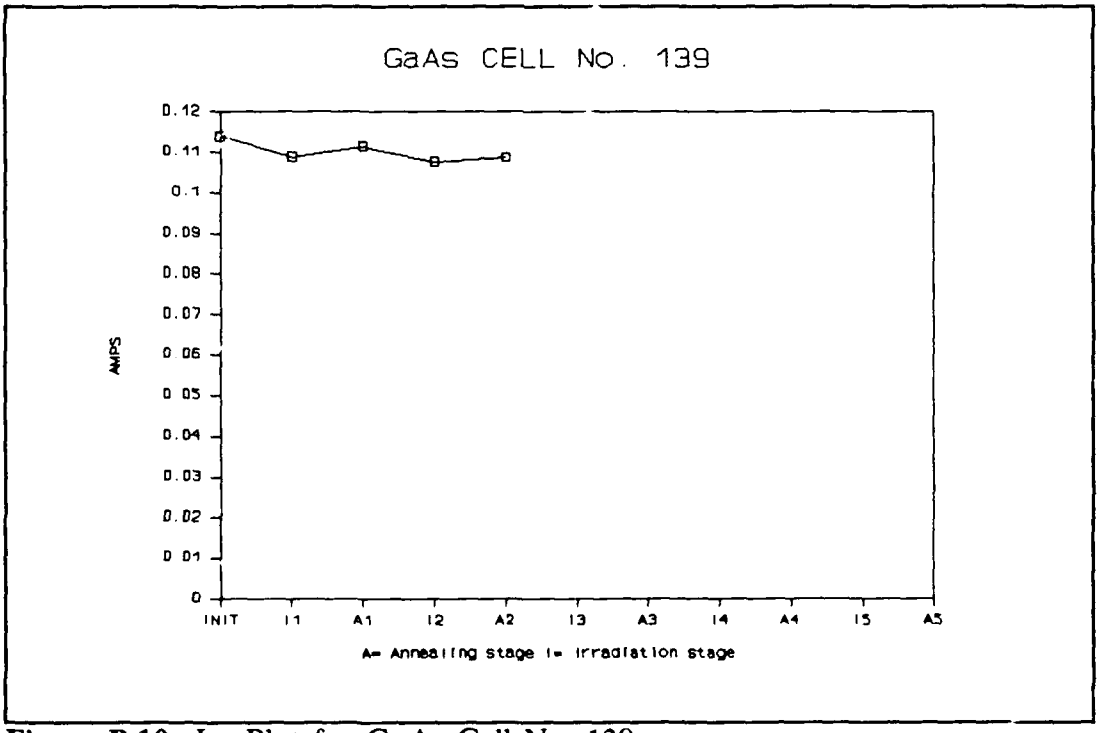

Figure B.10 Isc Plot for GaAs Cell No. 139

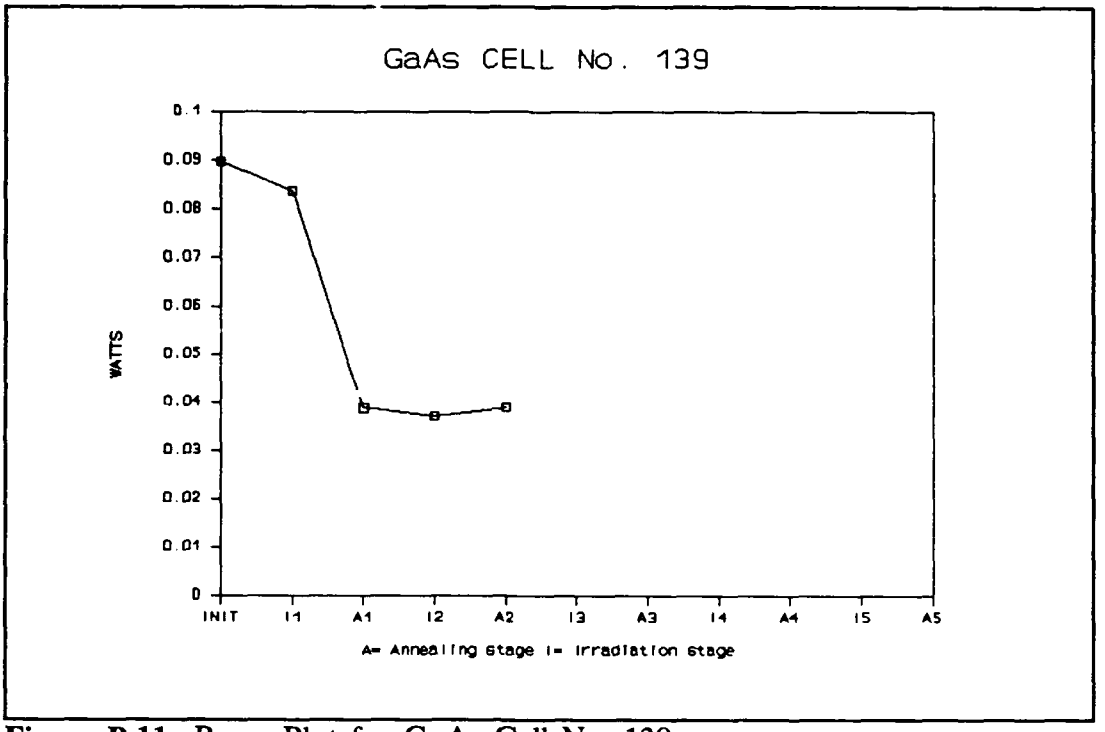

Figure B.11 Pmax Plot for GaAs Cell No. 139

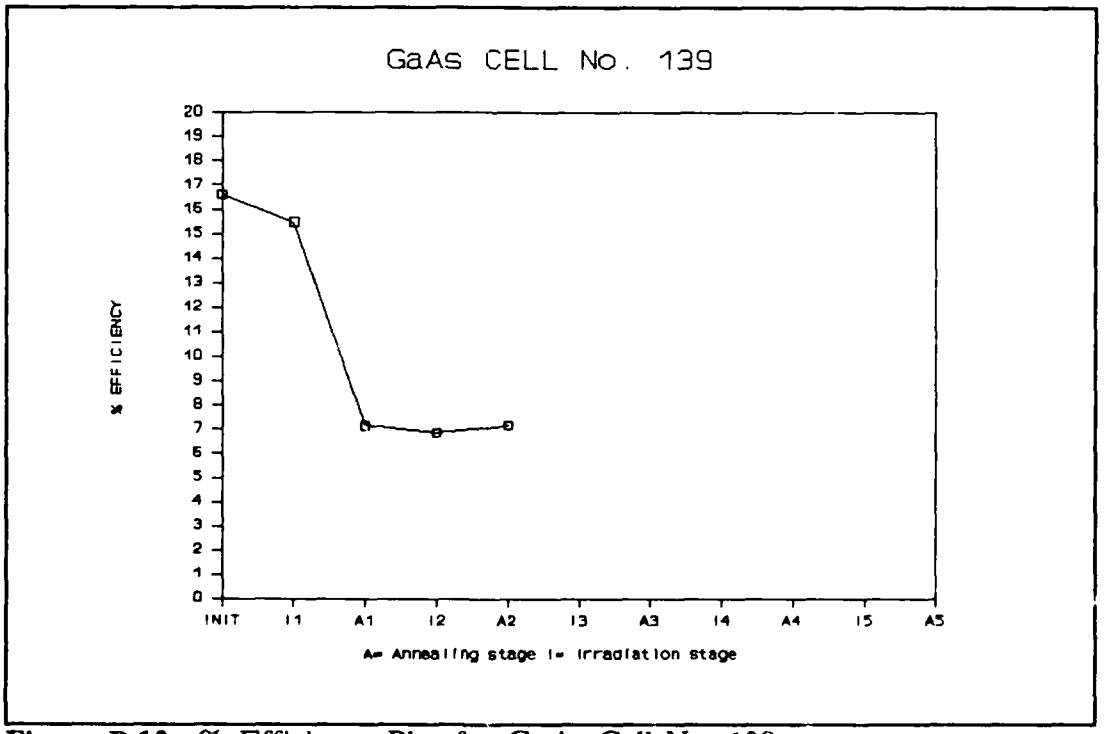

Figure B.12 % Efficiency Plot for GaAs Cell No. 139

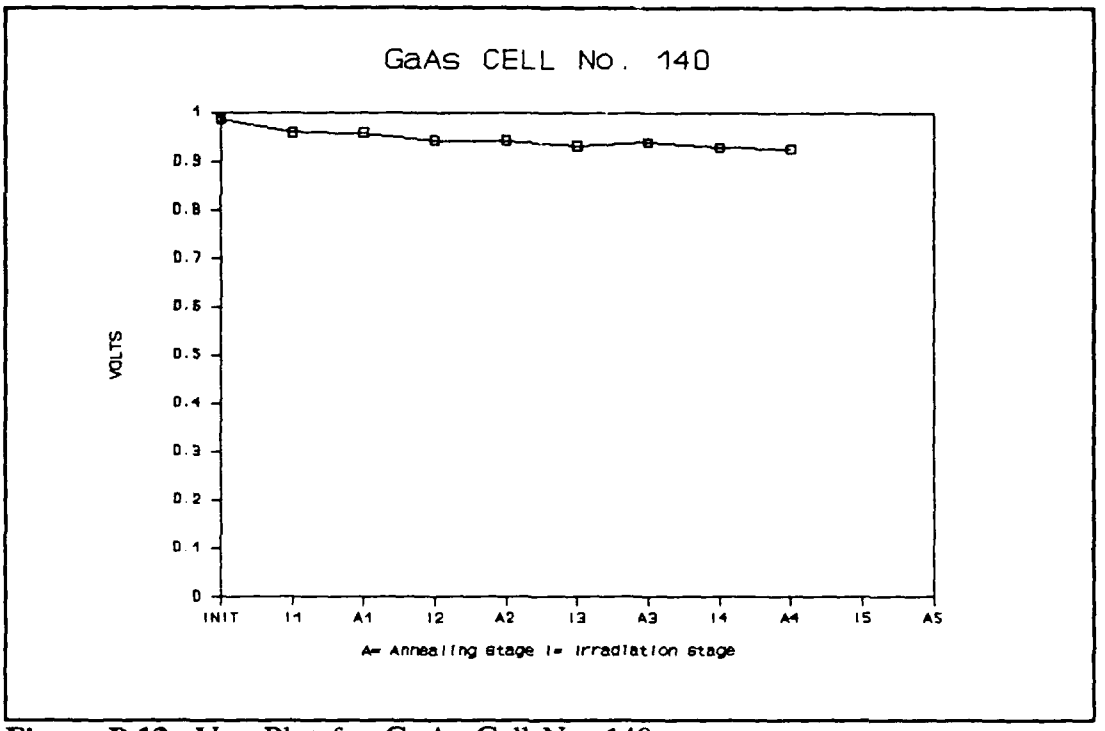

Figure B.13 Voc Plot for GaAs Cell No. 140

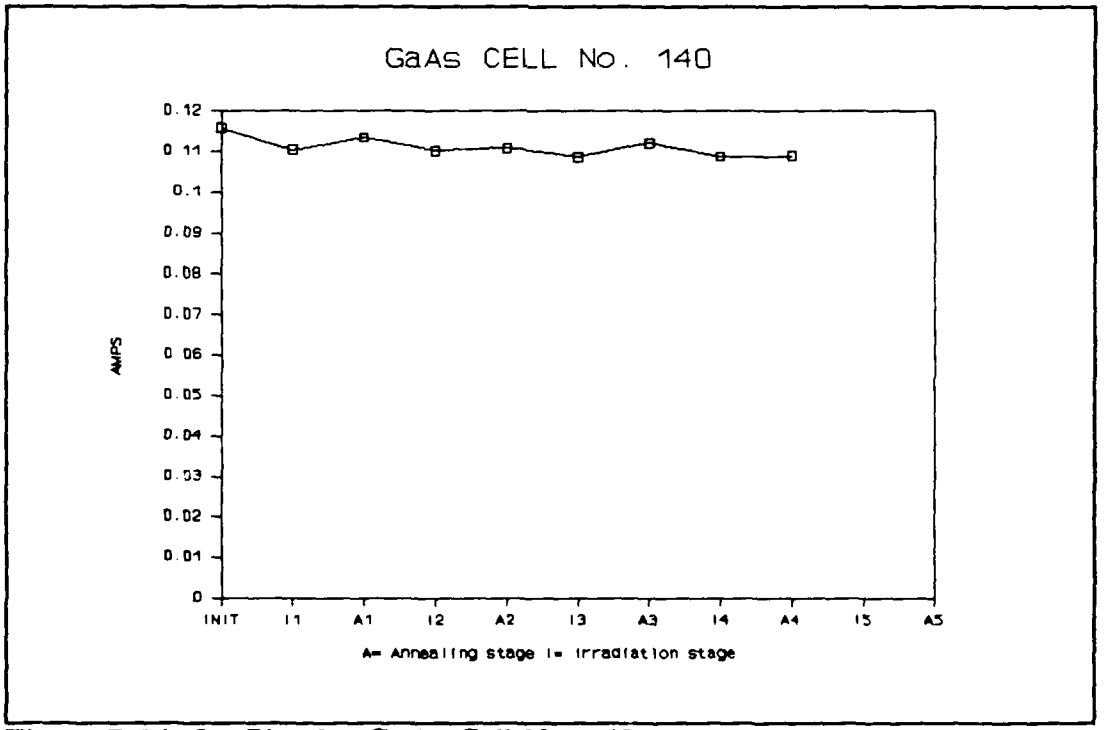

Figure B.14 Isc Plot for GaAs Cell No. 140

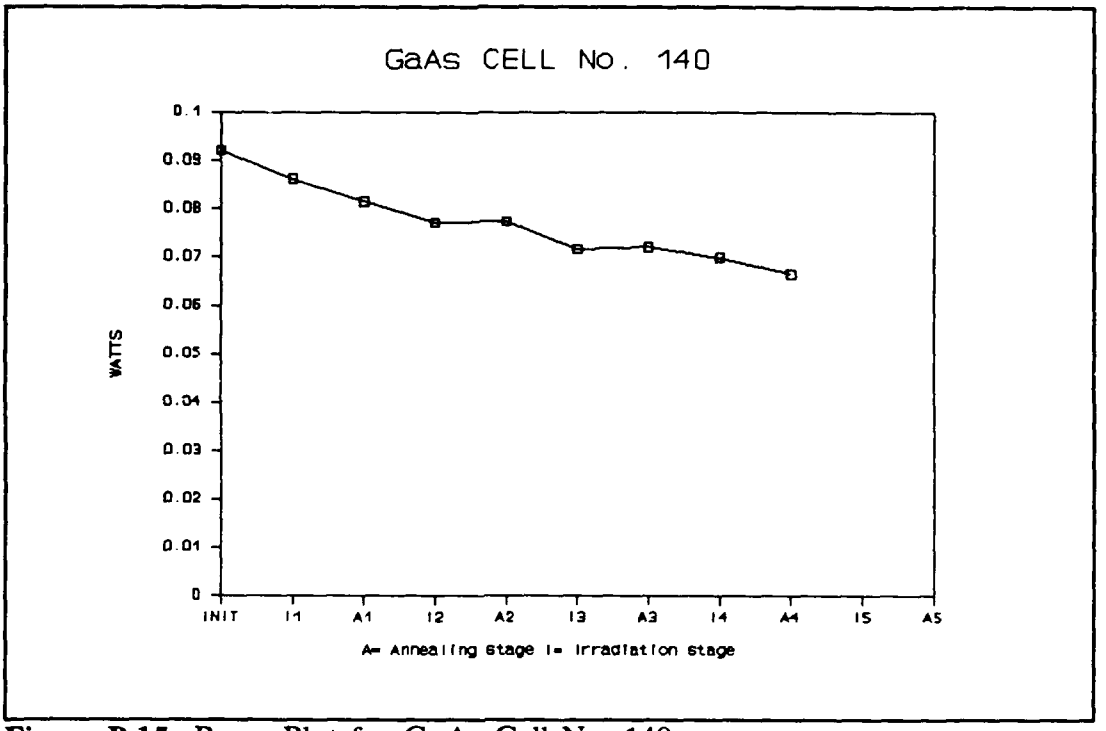

Figure B.15 Pmax Plot for GaAs Cell No. 140

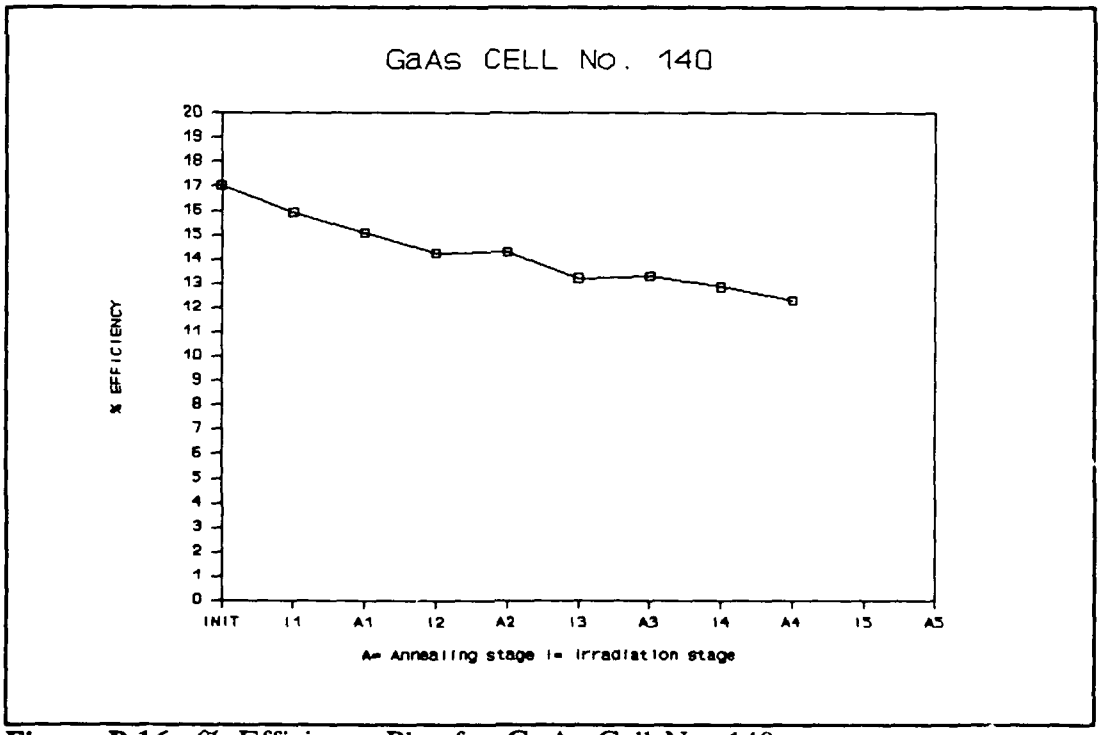

Figure B.16 % Efficiency Plot for GaAs Cell No. 140

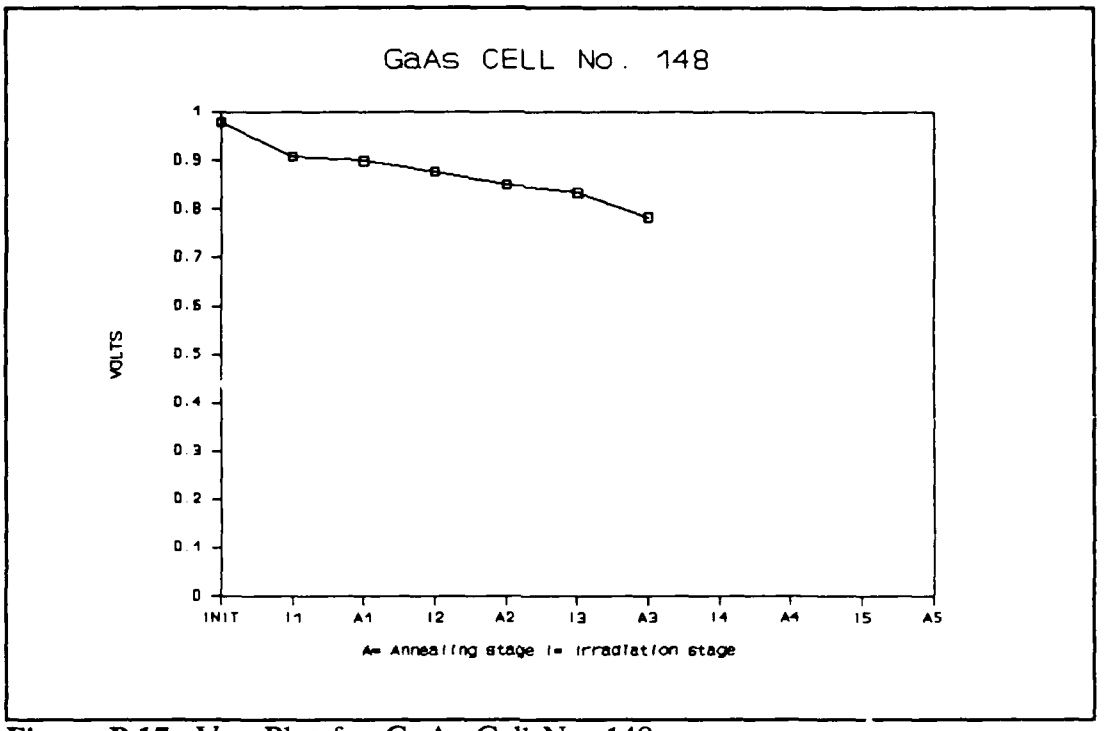

Figure B.17 Voc Plot for GaAs Cell No. 148

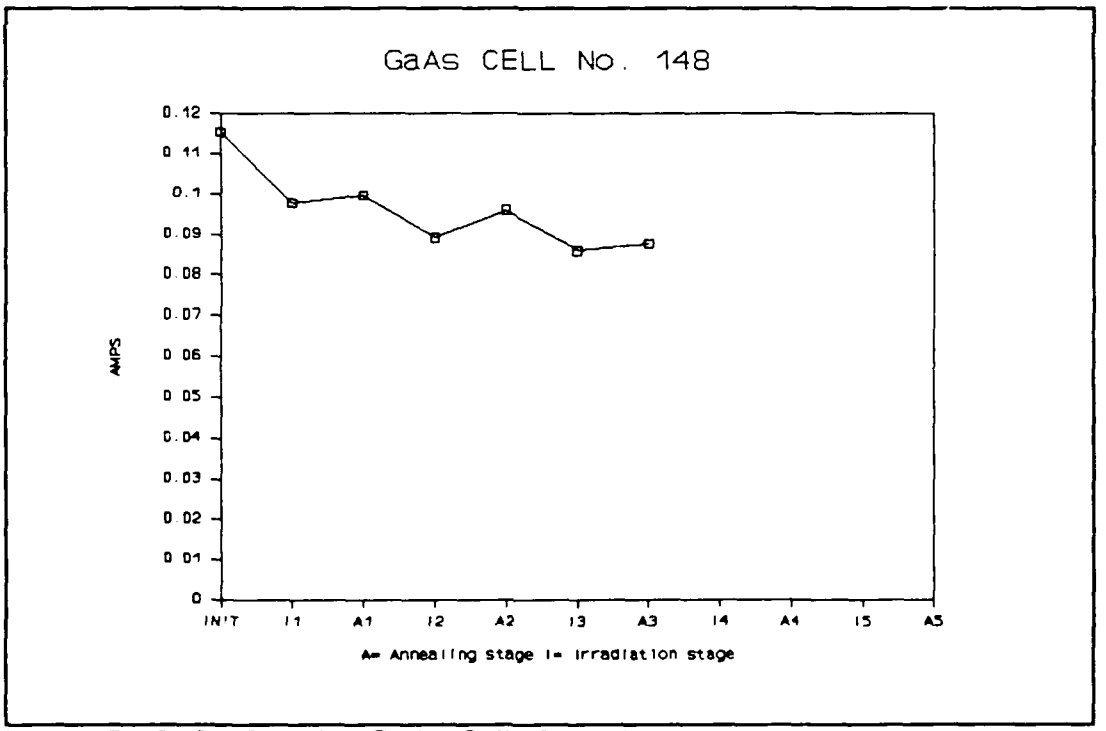

Figure B.18 Isc Plot for GaAs Cell No. 148

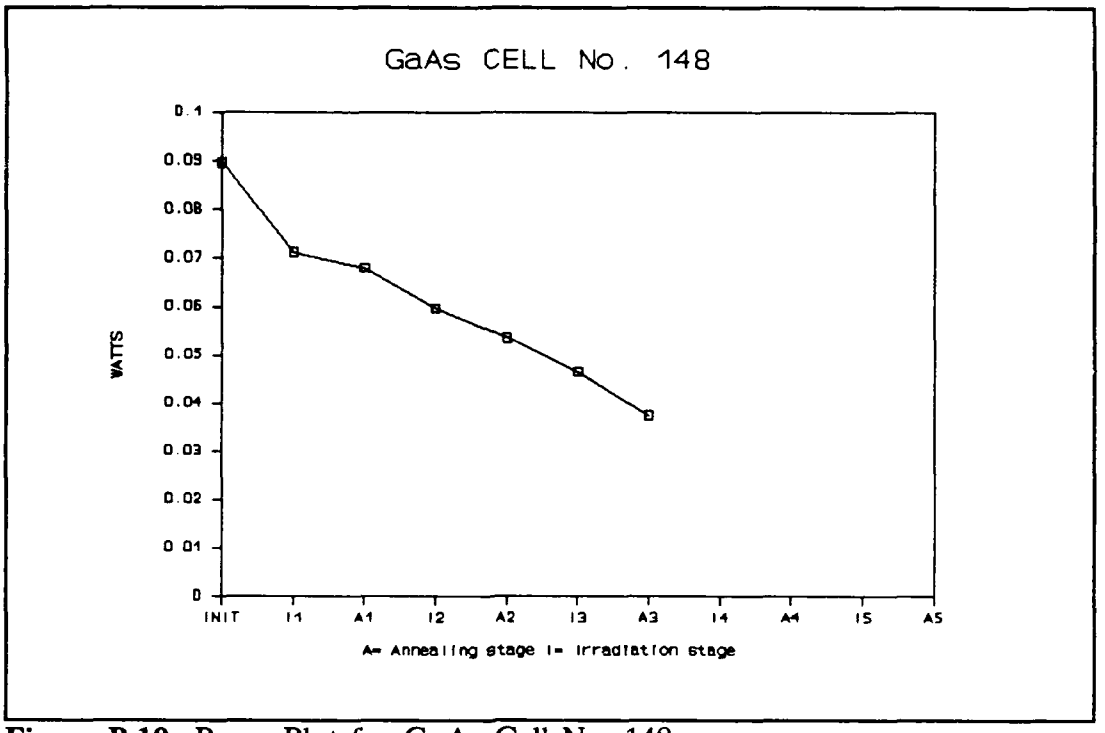

Figure B.19 Pmax Plot for GaAs Cell No. 148

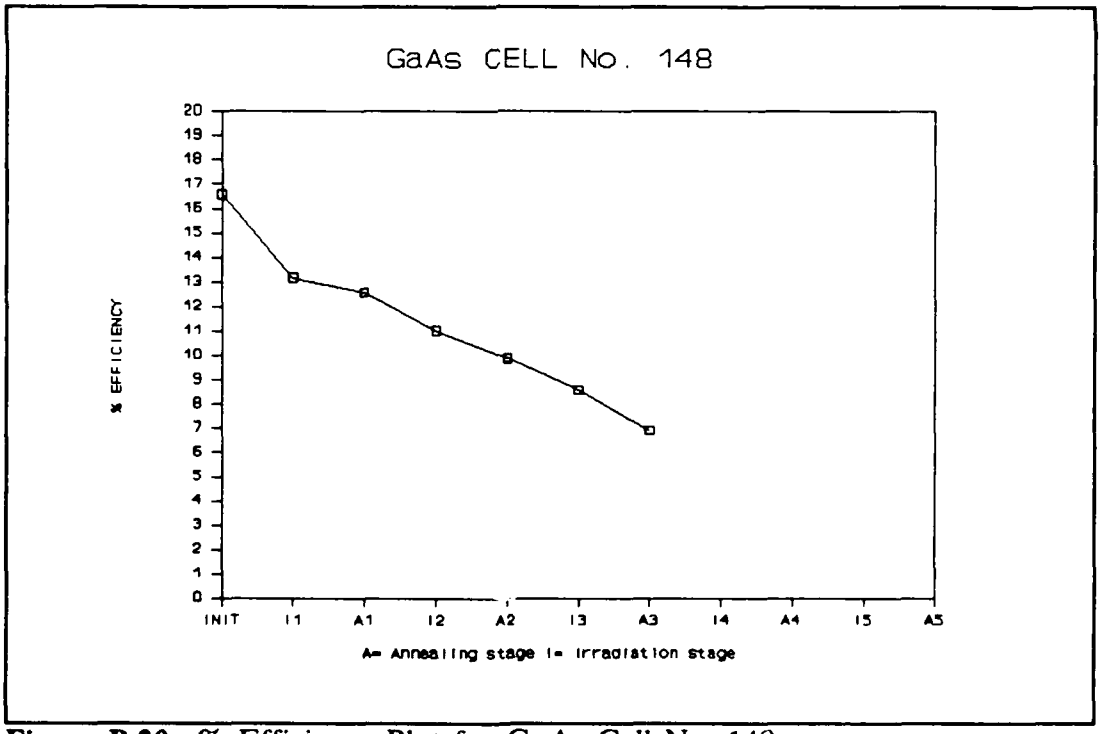

Figure B.20 % Efficiency Plot for GaAs Cell No. 148

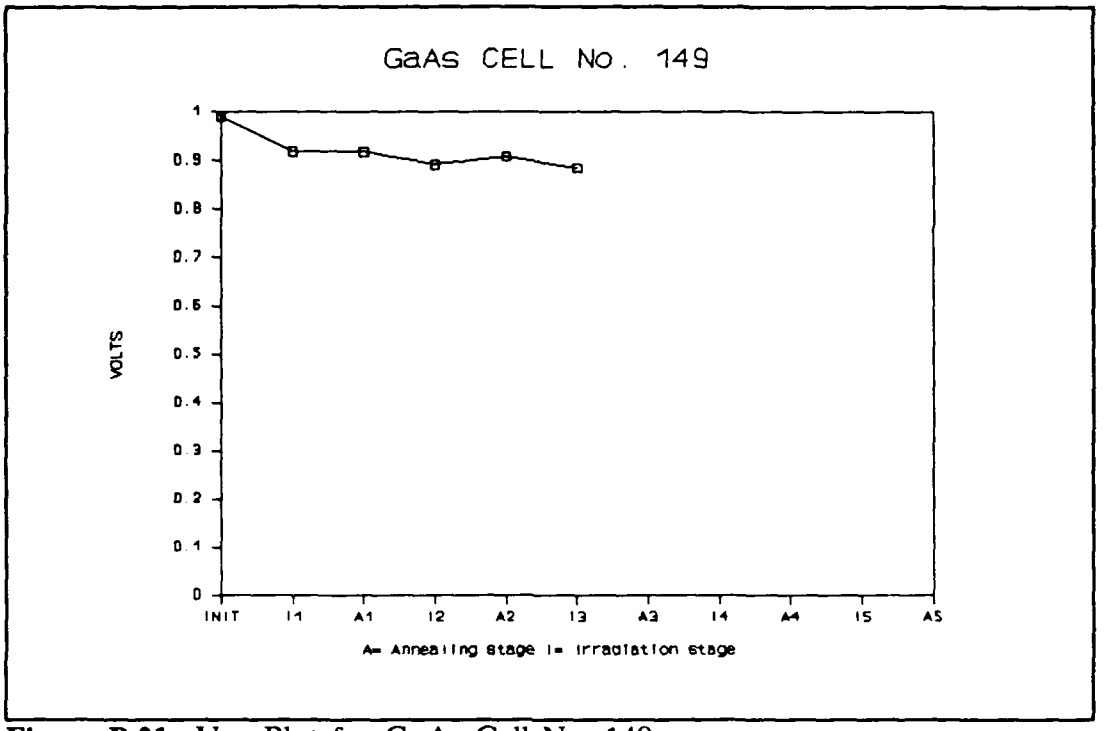

Figure B.21 Voc Plot for GaAs Cell No. 149

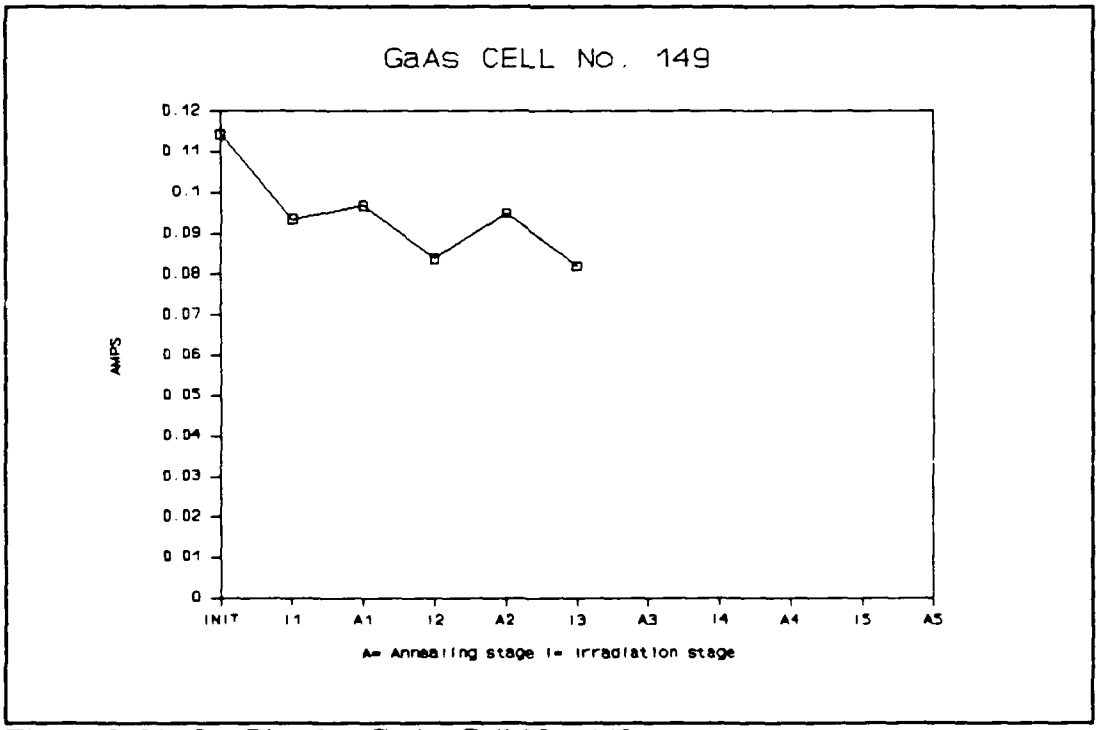

Figure B.22 Isc Plot for GaAs Cell No. 149

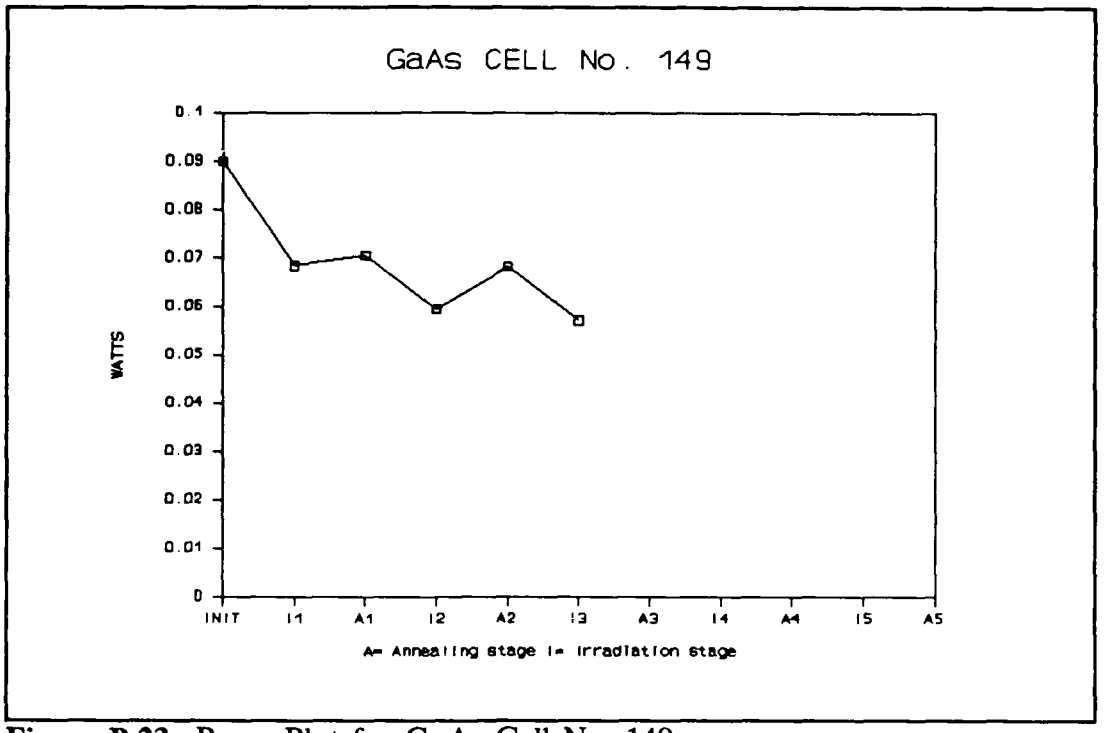

Figure B.23 Pmax Plot for GaAs Cell No. 149

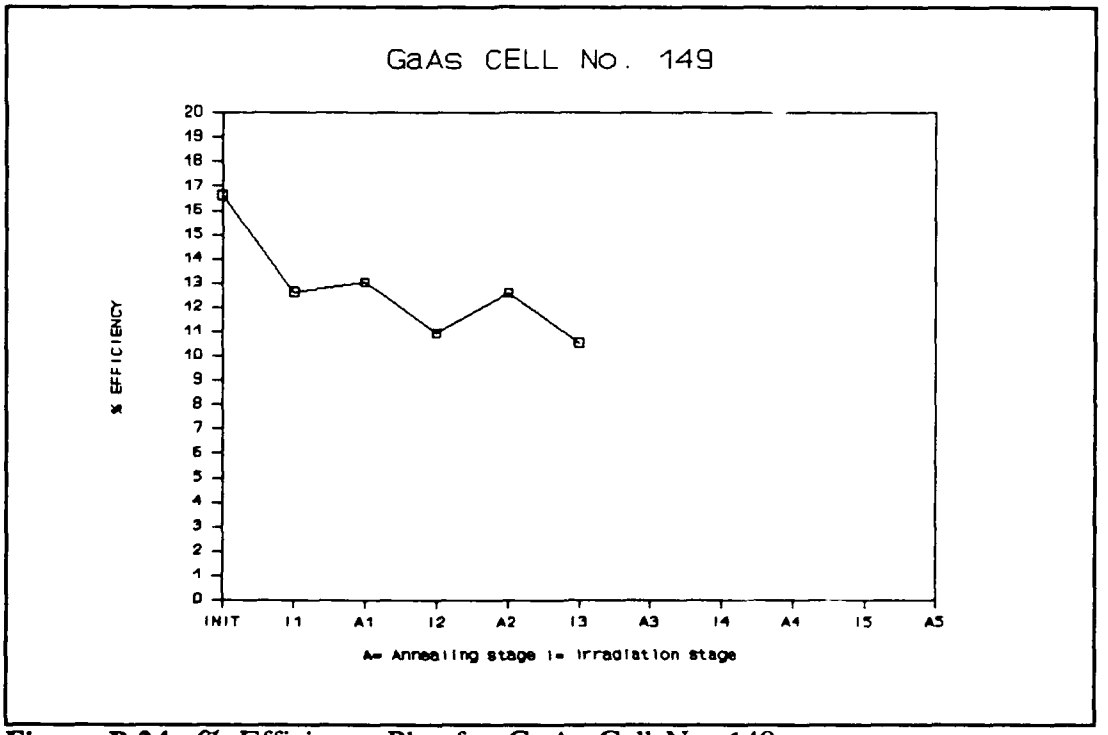

Figure B.24 % Efficiency Plot for GaAs Cell No. 149

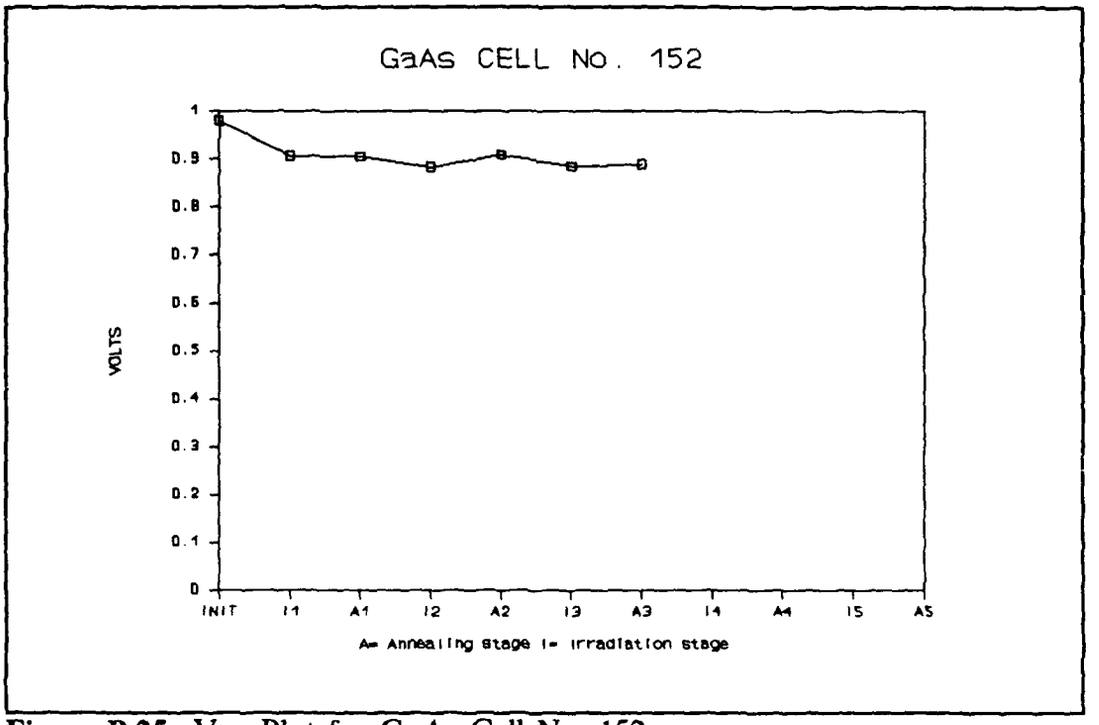

Figure B.25 Voc Plot for GaAs Cell No. 152

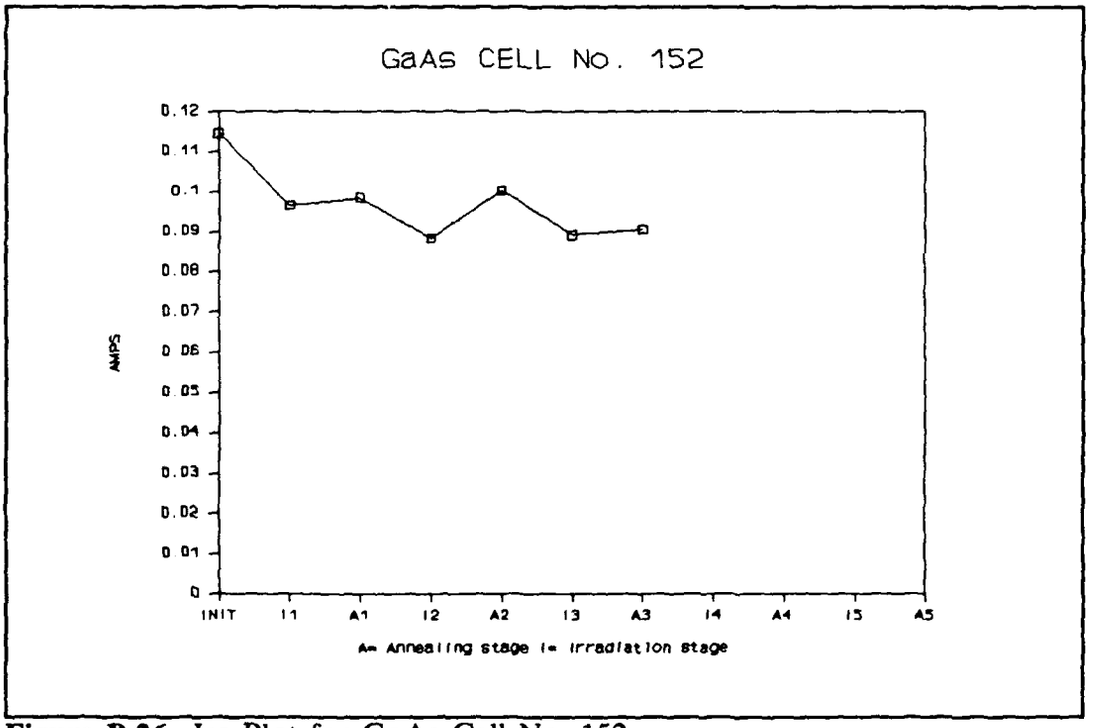

Figure B.26 Isc Plot for GaAs Cell No. 152

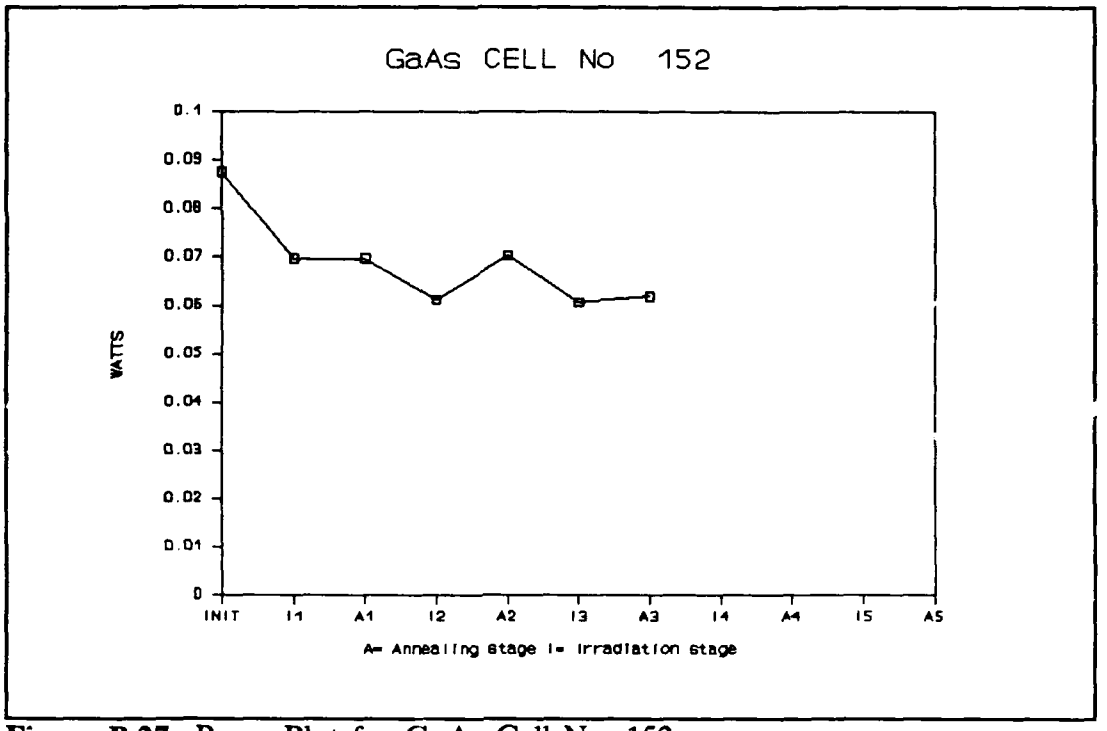

Figure B.27 Pmax Plot for GaAs Cell No. 152

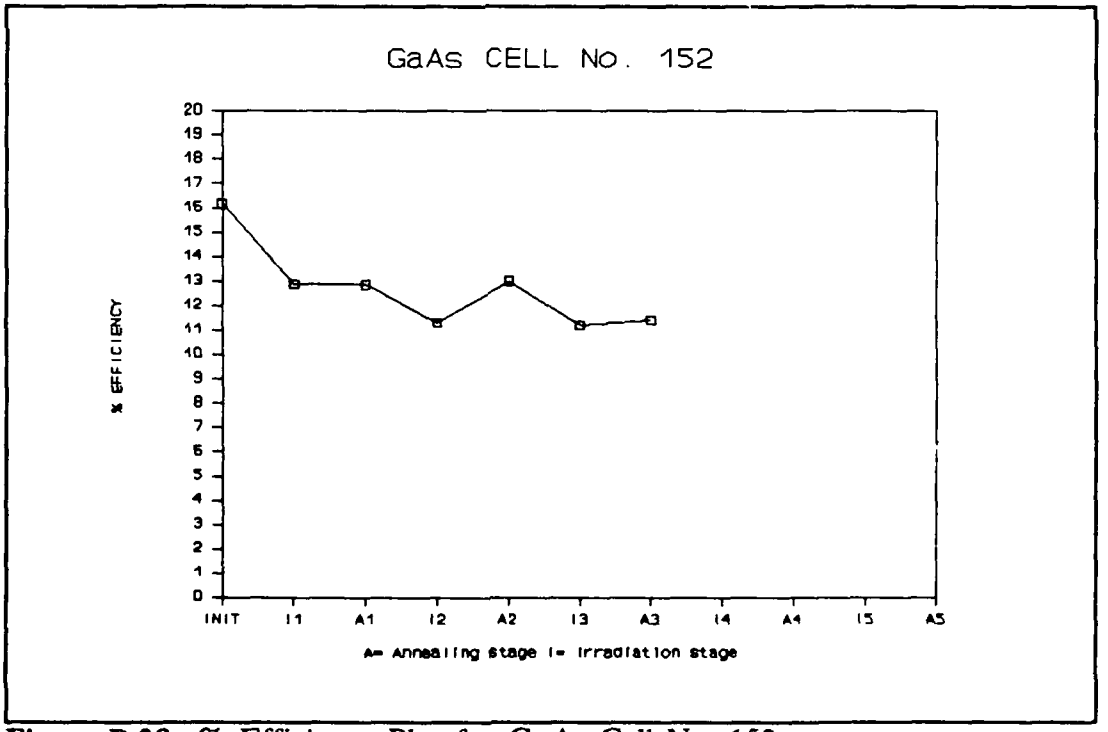

Figure B.28 % Efficiency Plot for GaAs Cell No. 152

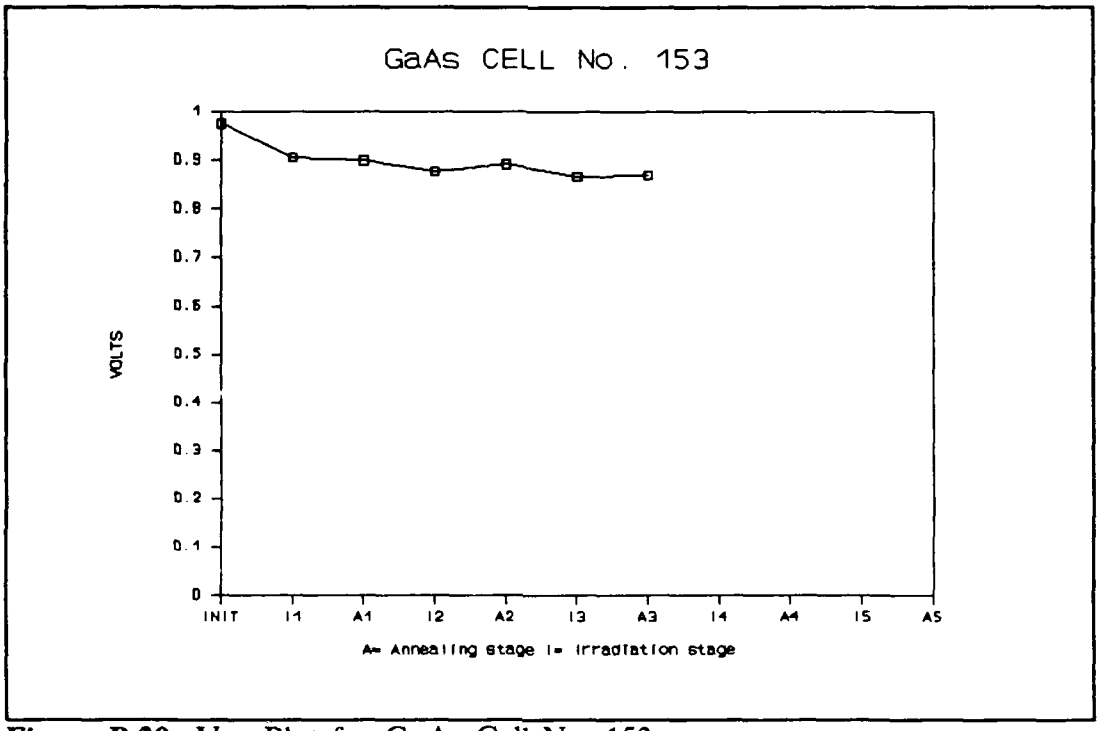

Figure B.29 Voc Plot for GaAs Cell No. 153

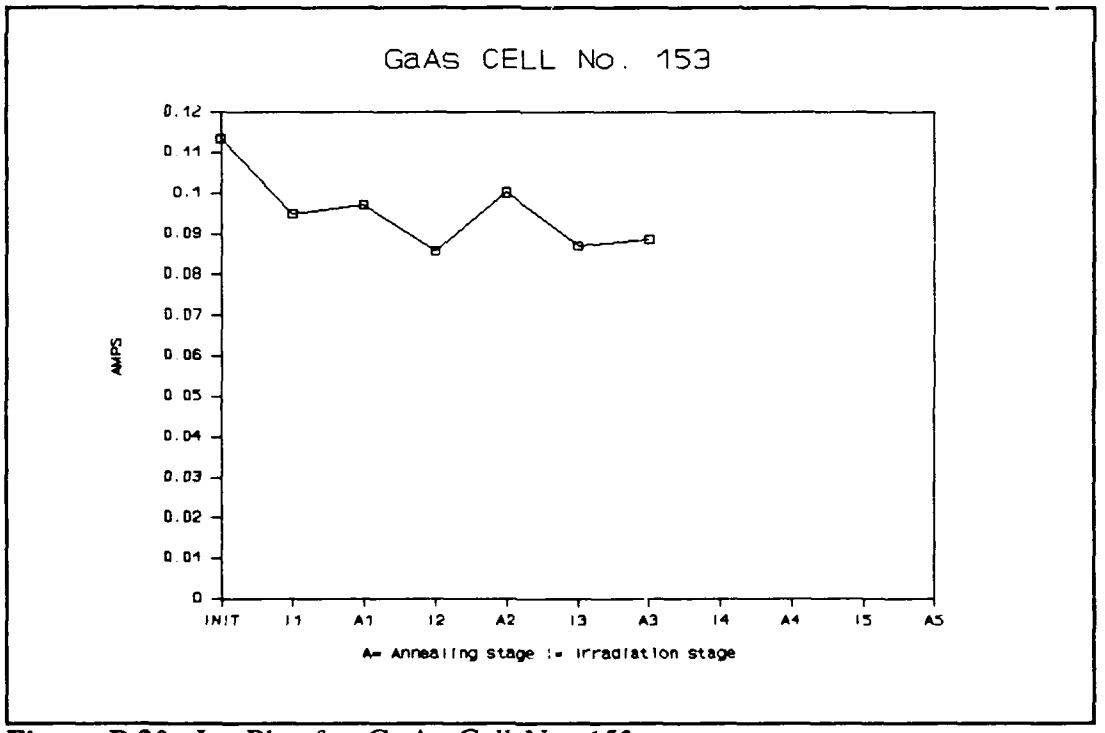

Figure B.30 Isc Plot for GaAs Cell No. 153

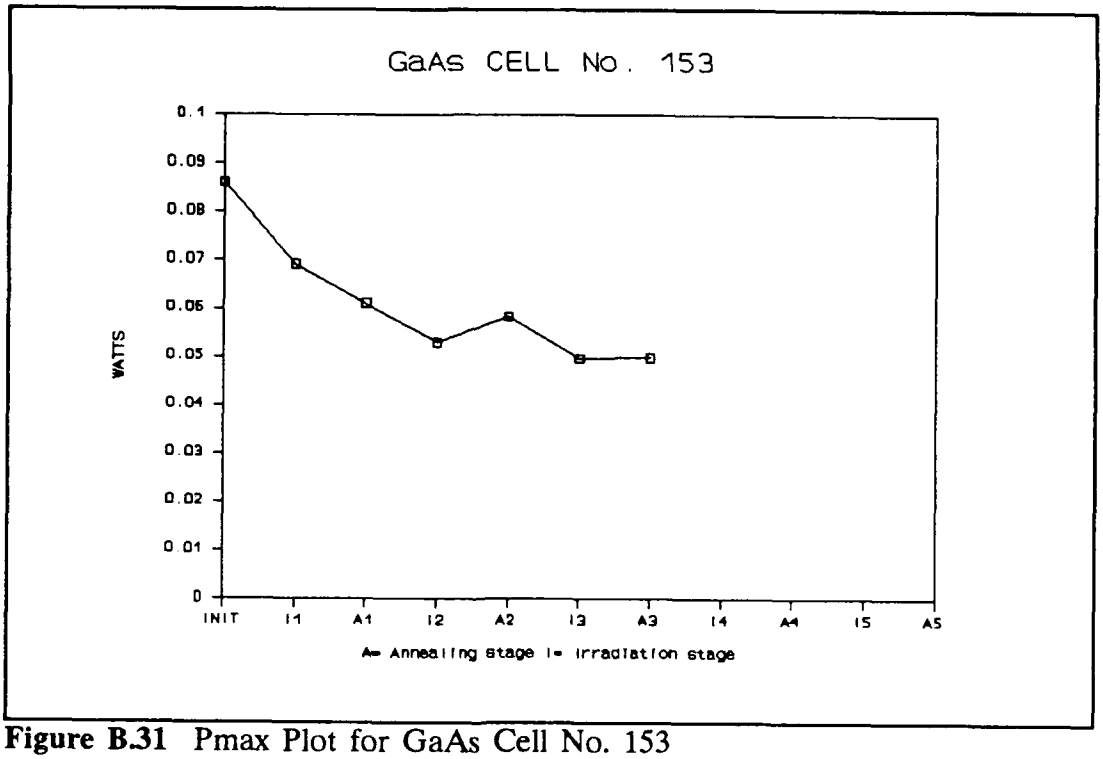

Figure B.31 Pmax Plot for GaAs Cell No. 153

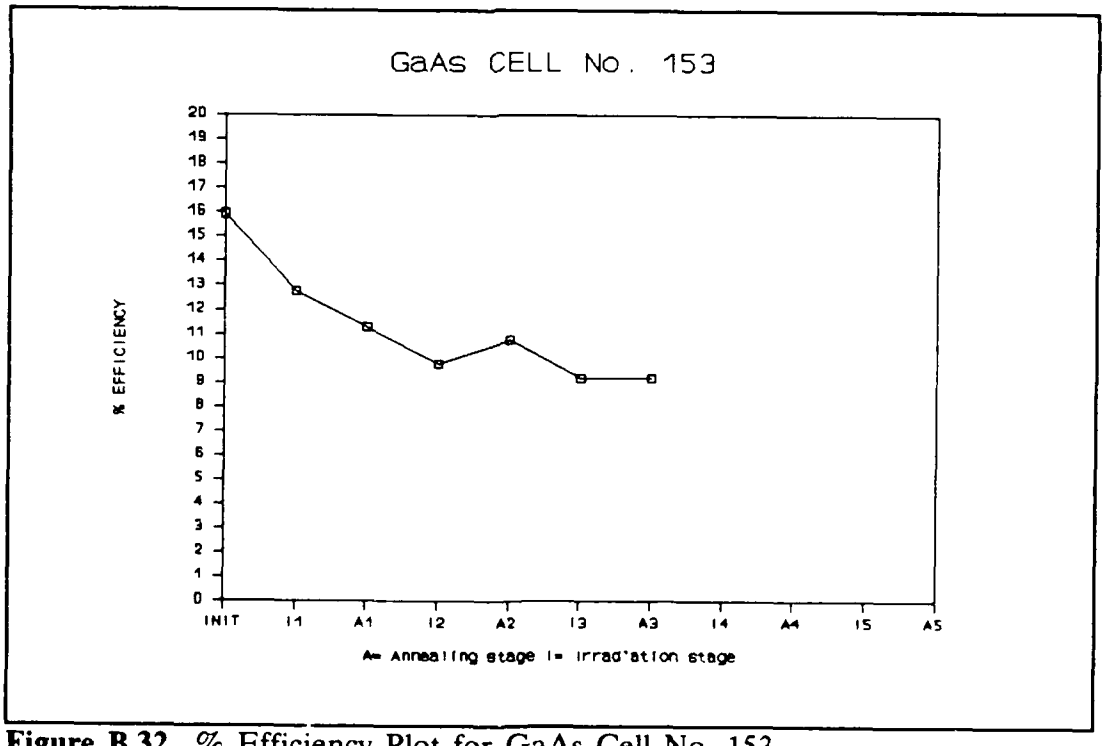

Figure B.32 % Efficiency Plot for GaAs Cell No. 153

APPENDIX C. InP CELL I-V CURVES

This appendix contains the I-V curves for multiple cycles of irradiating and annealing of the individual cells. Each curve is labeled with the amount of irradiation the cell was subjected to and the conditions of annealing.

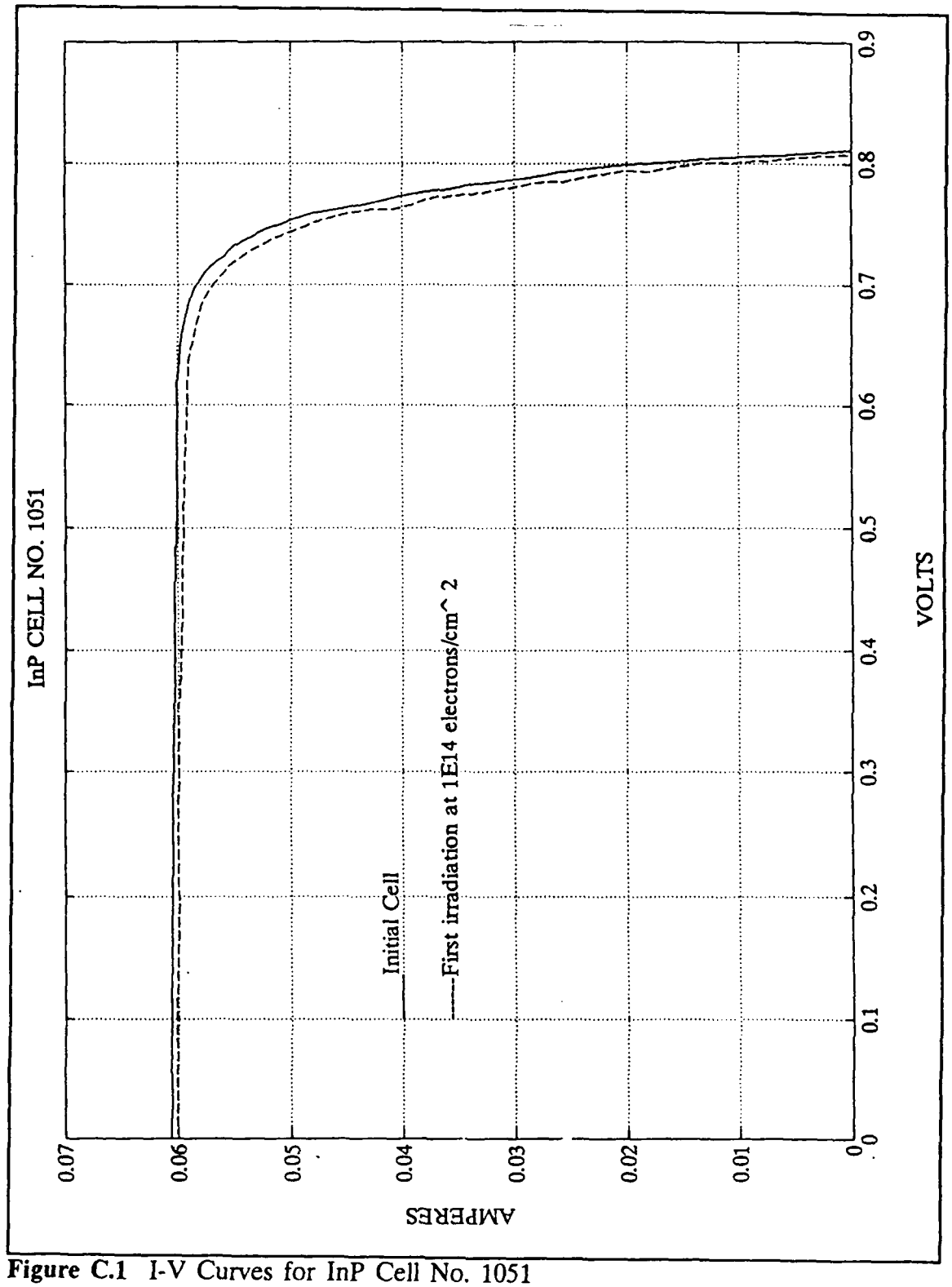

Figure C.1 I-V Curves for InP Cell No. 1051

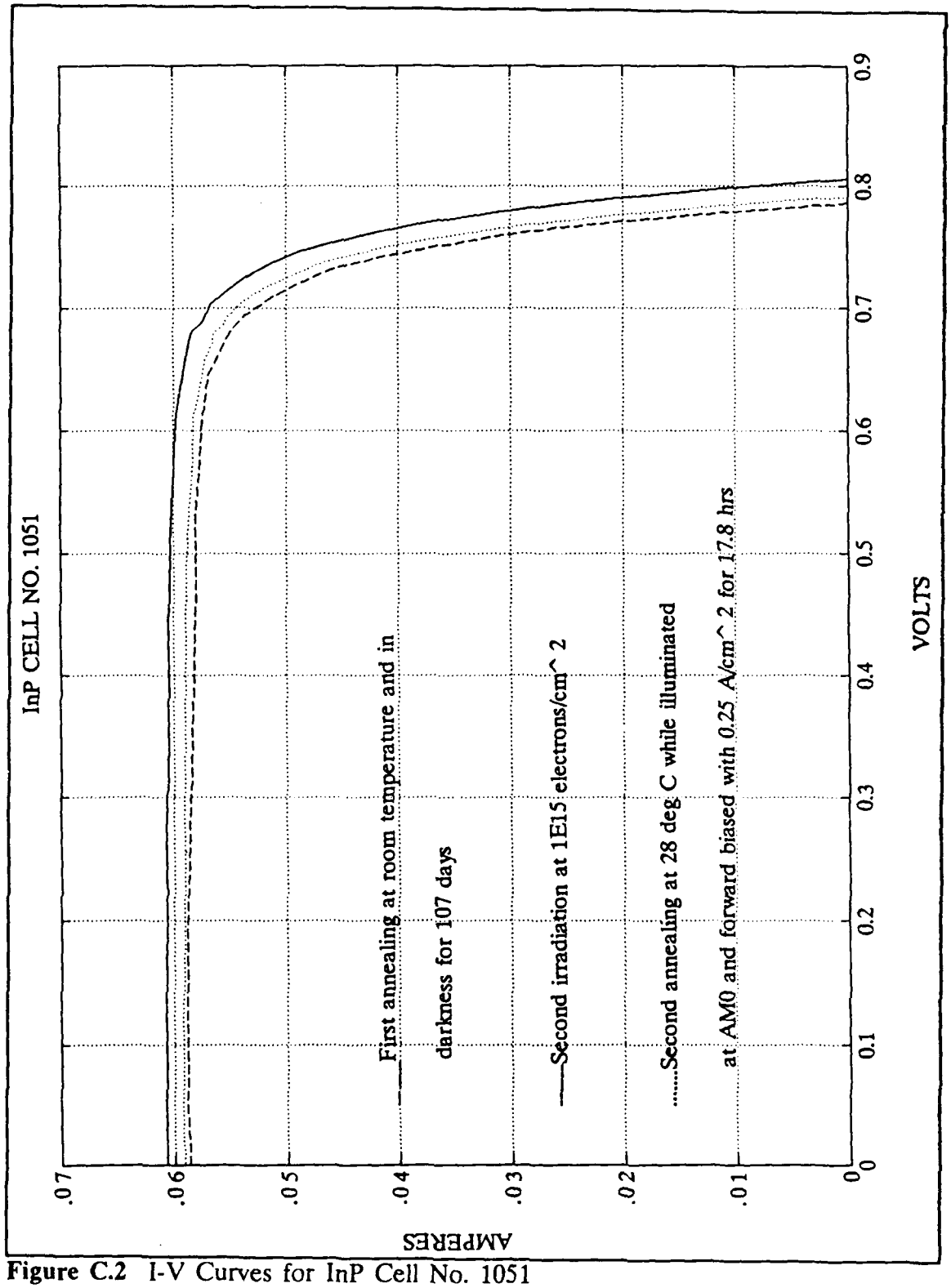

Figure C.2 I-V Curves for InP Cell No. 1051

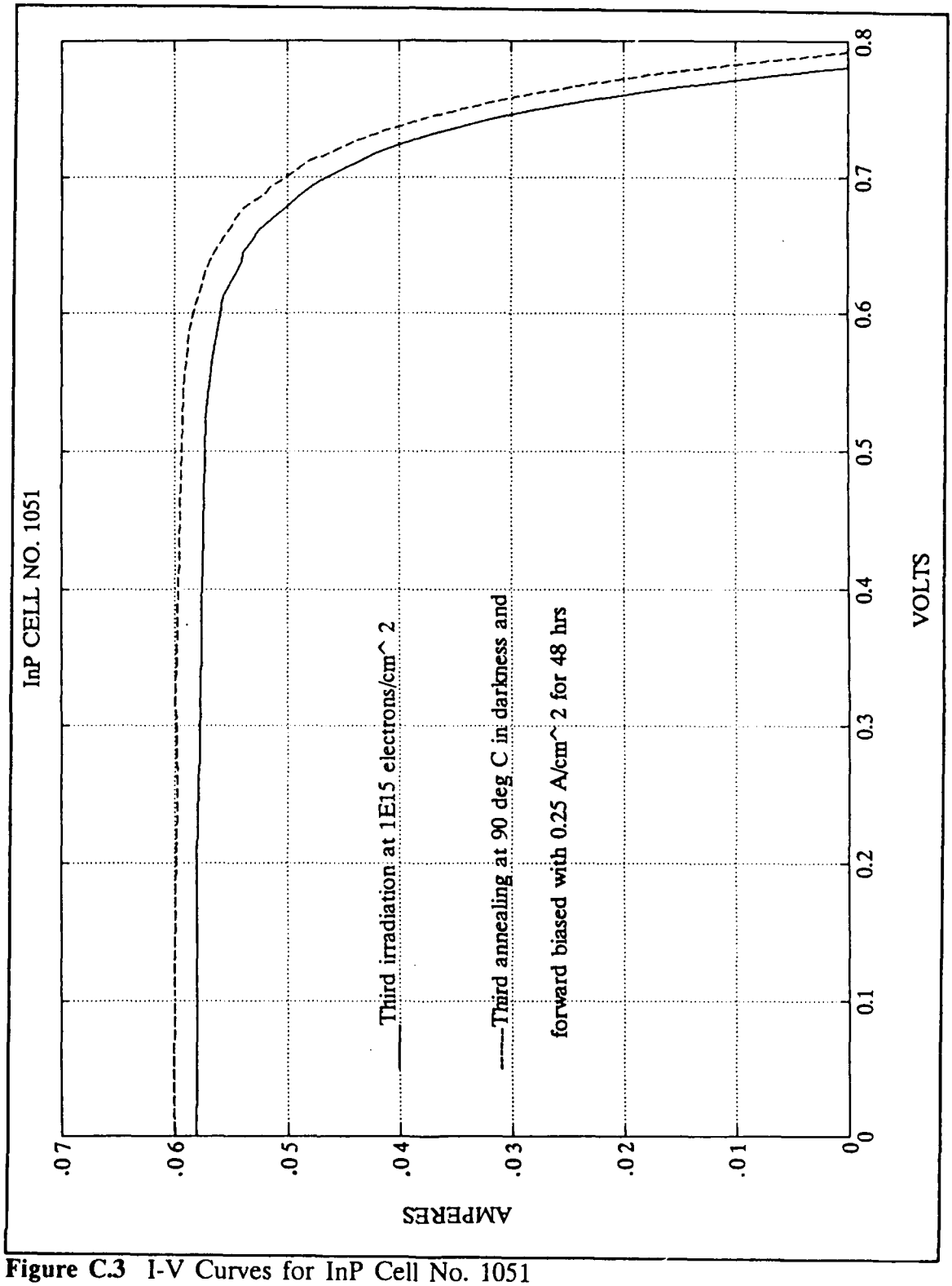

Figure C.3 I-V Curves for InP Cell No. 1051

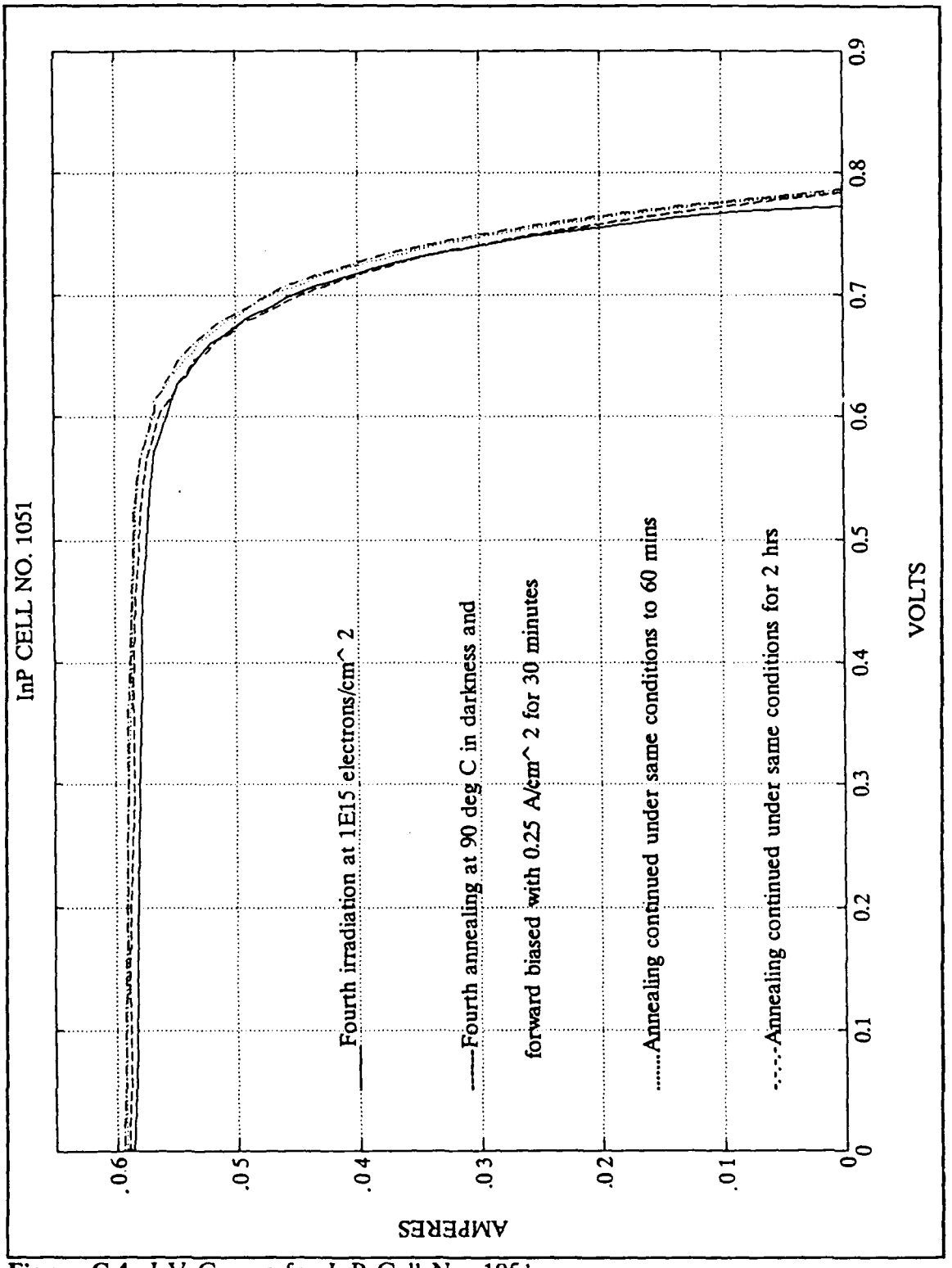

Figure C.4 I-V Curves for InP Cell No. 1051

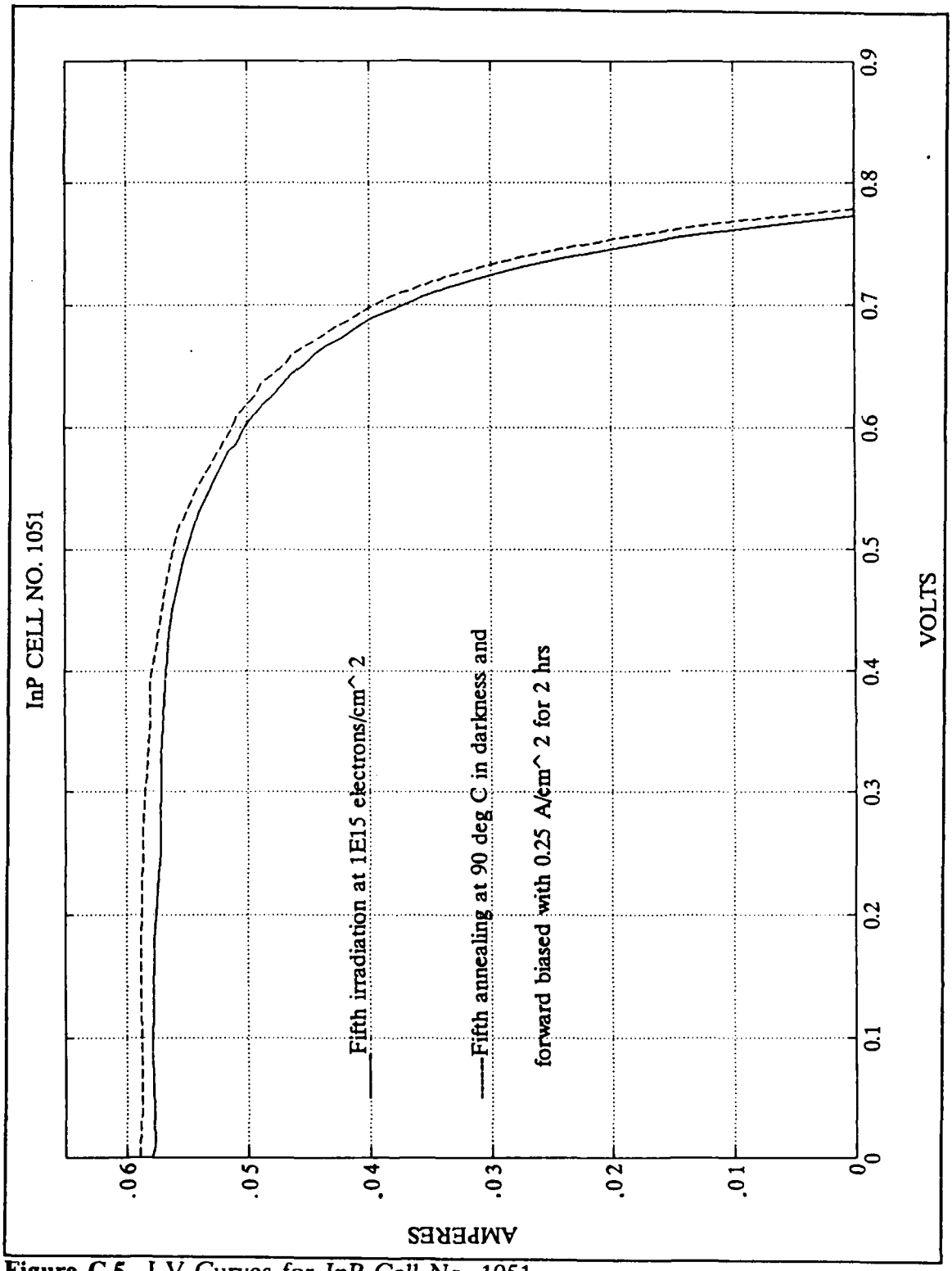

Figure C.5 I-V Curves for InP Cell No. 1051

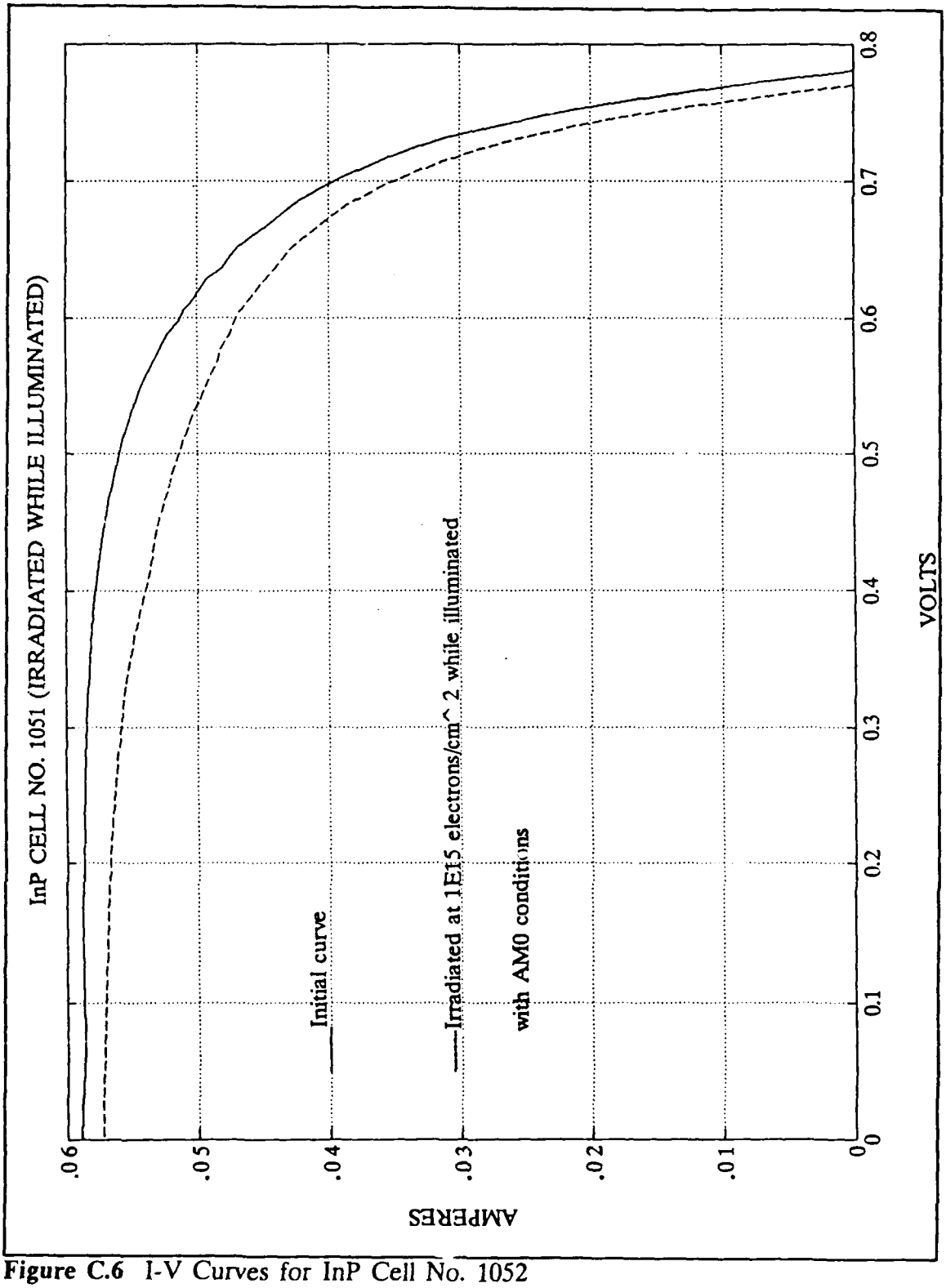

Figure C.6 I-V Curves for InP Cell No. 1052

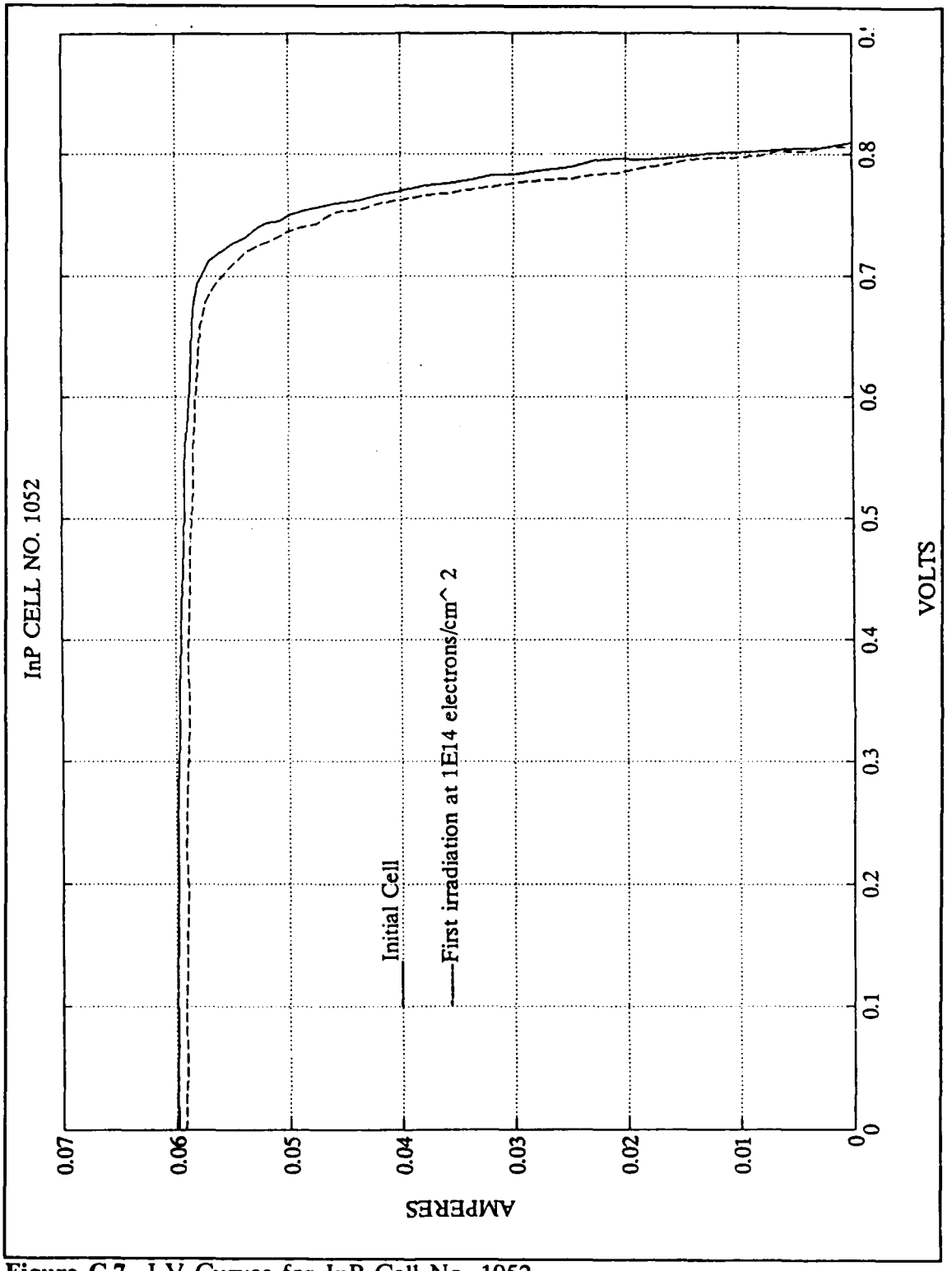

Figure C.7 I-V Curves for InP Cell No. 1052

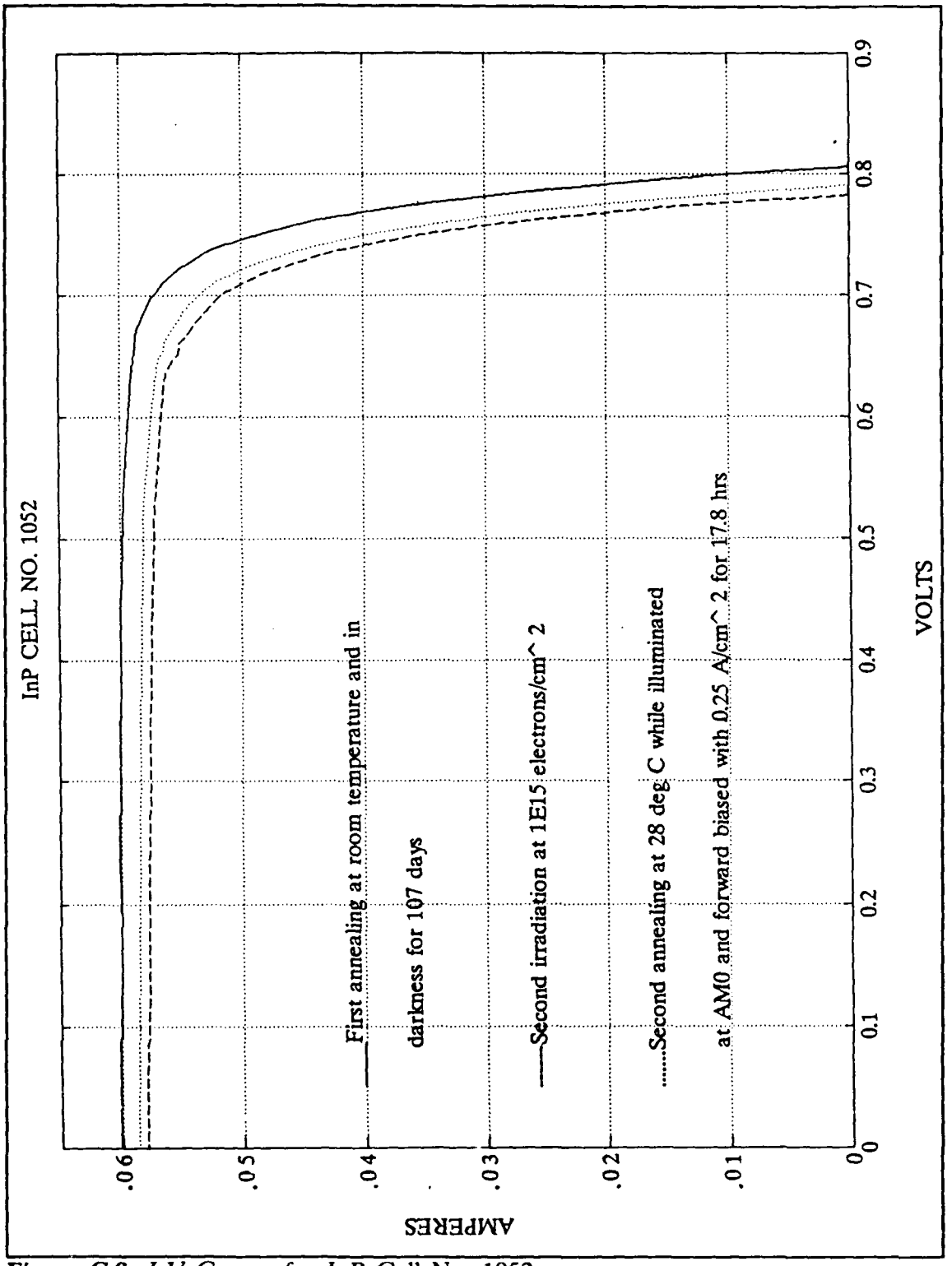

Figure C.8 I-V Curves for InP Cell No. 1052

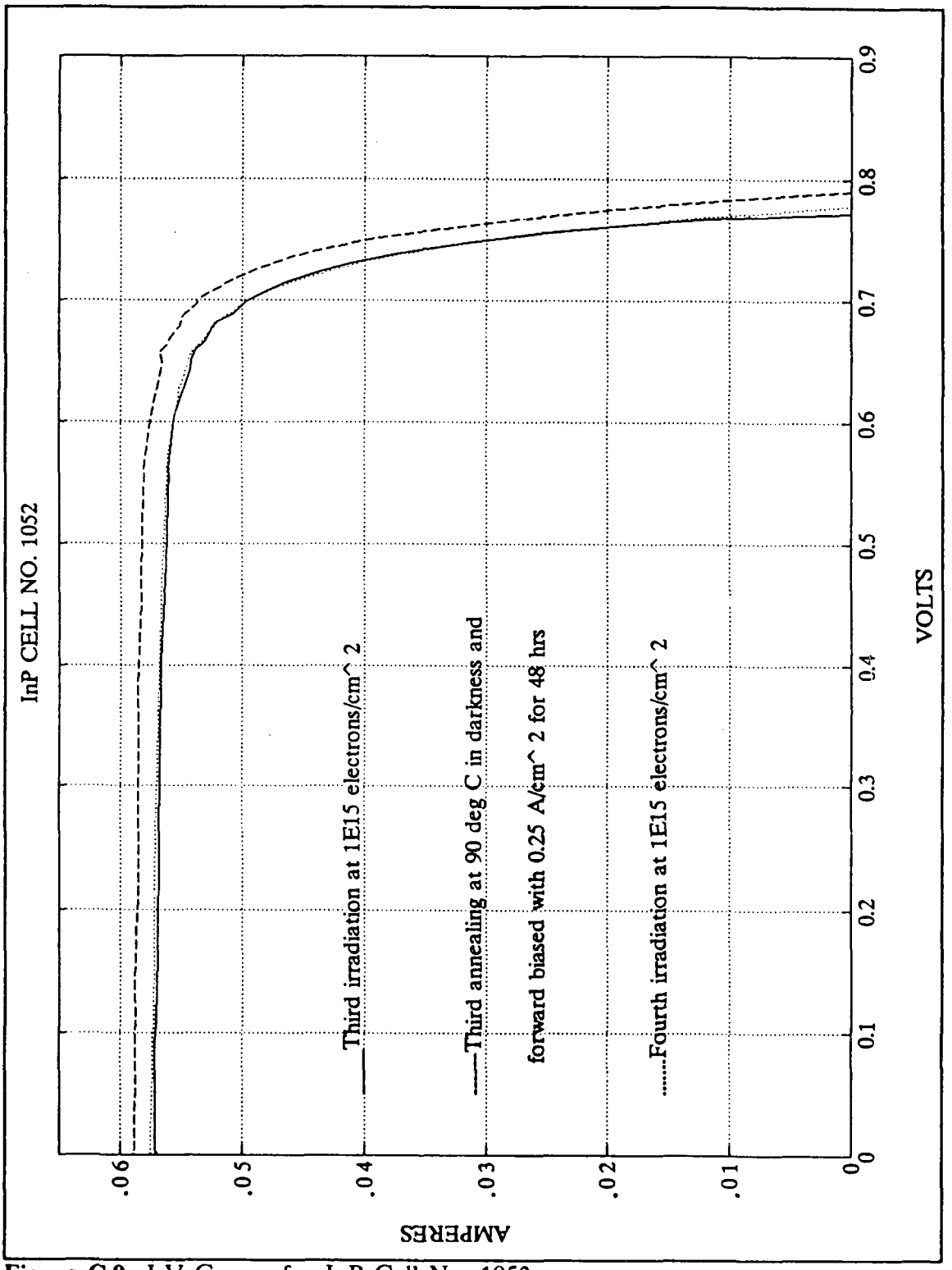

Figure C.9 I-V Curves for InP Cell No. 1053

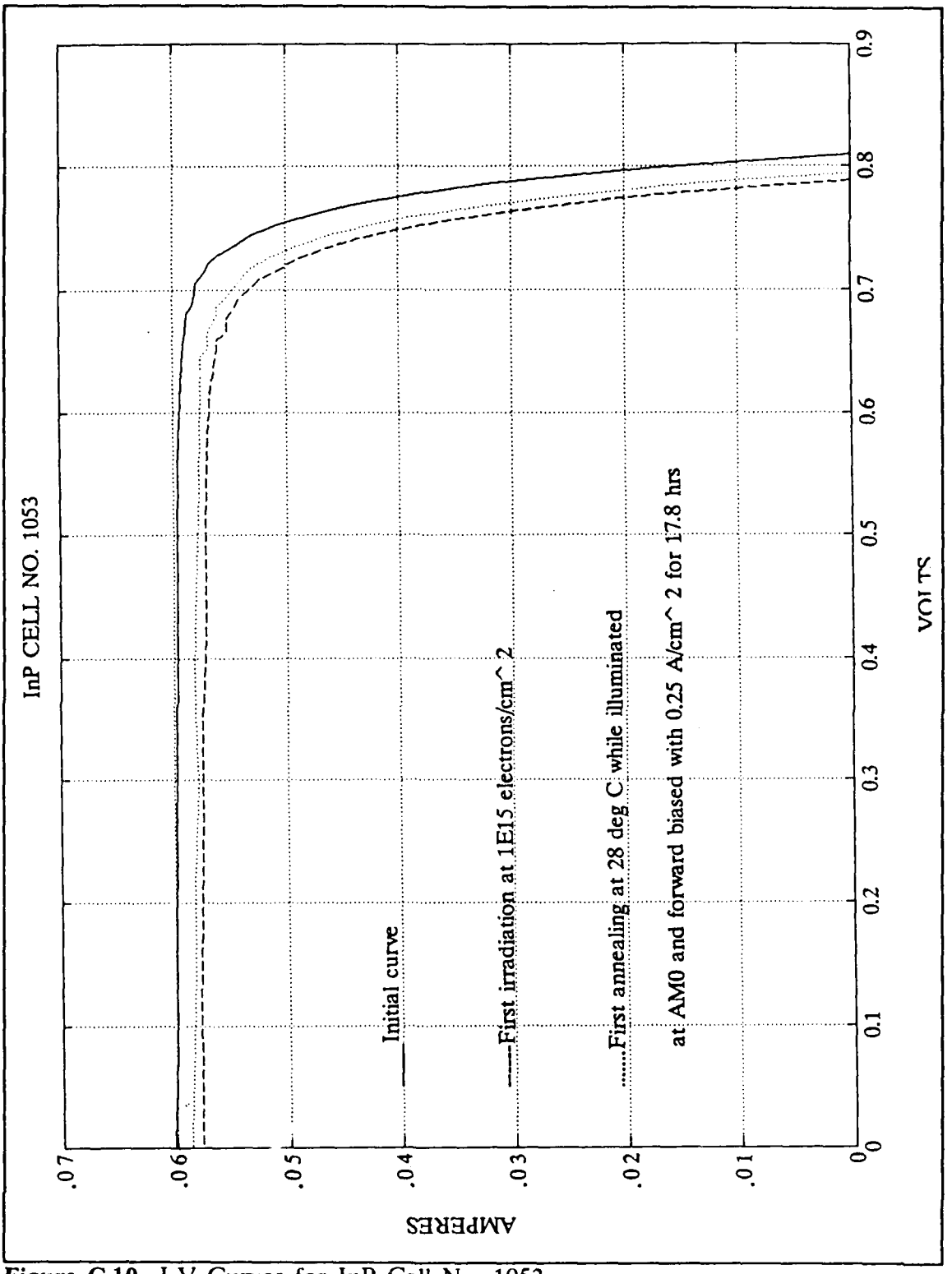

Figure C.10 I-V Curves for InP Cell No. 1053

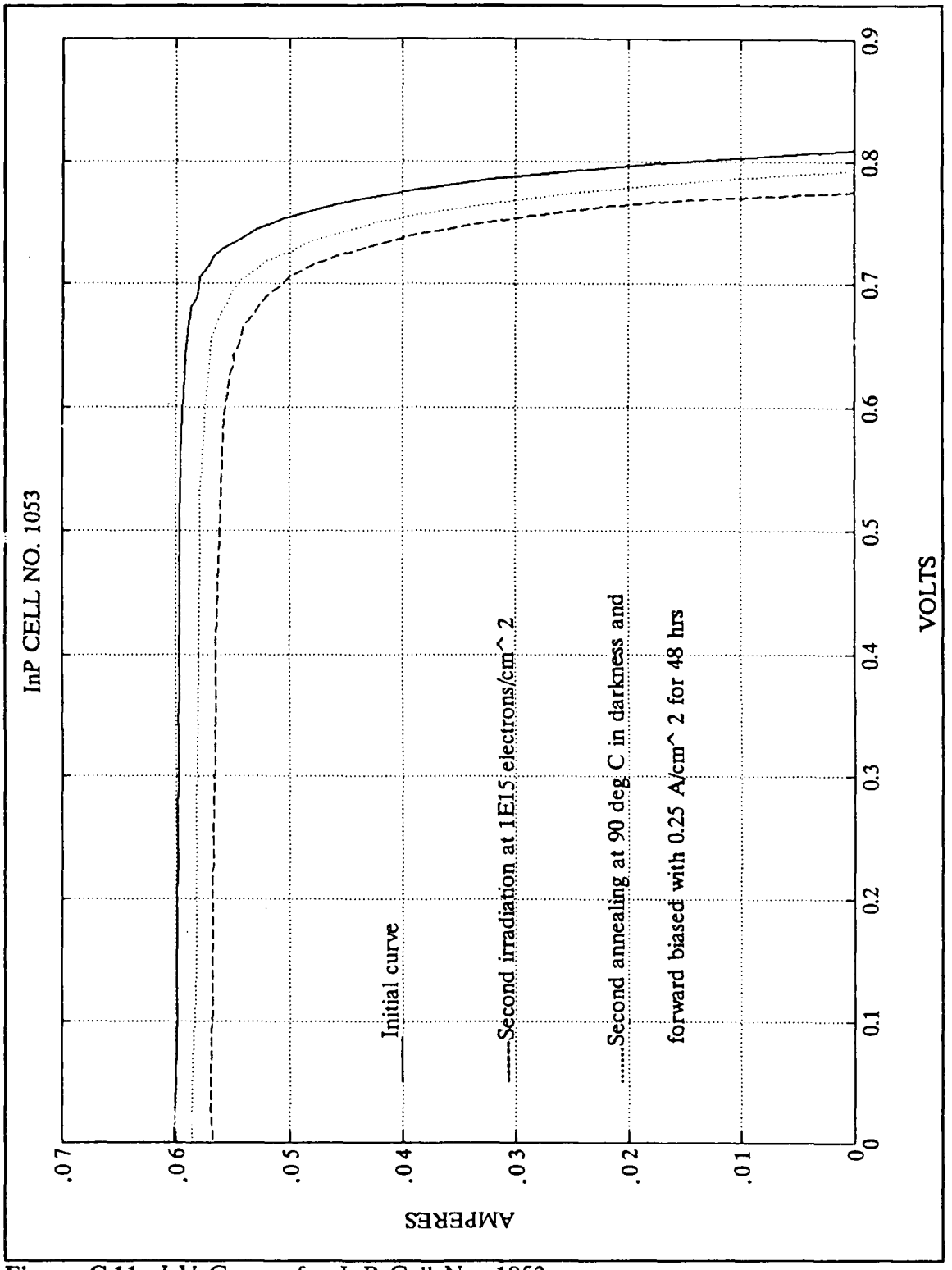

Figure C.11 I-V Curves for InP Cell No. 1053

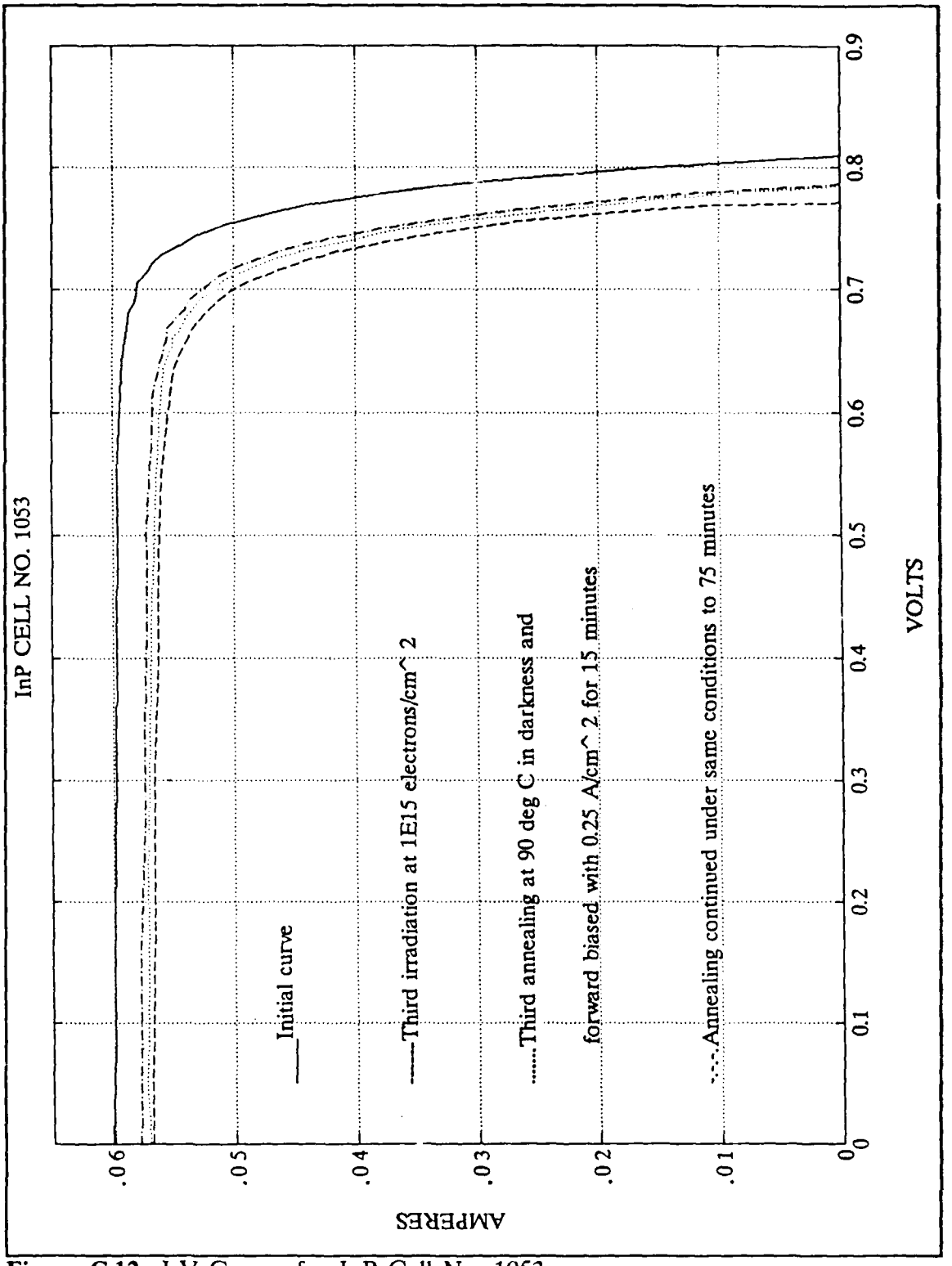

Figure C.12 I-V Curves for InP Cell No. 1053

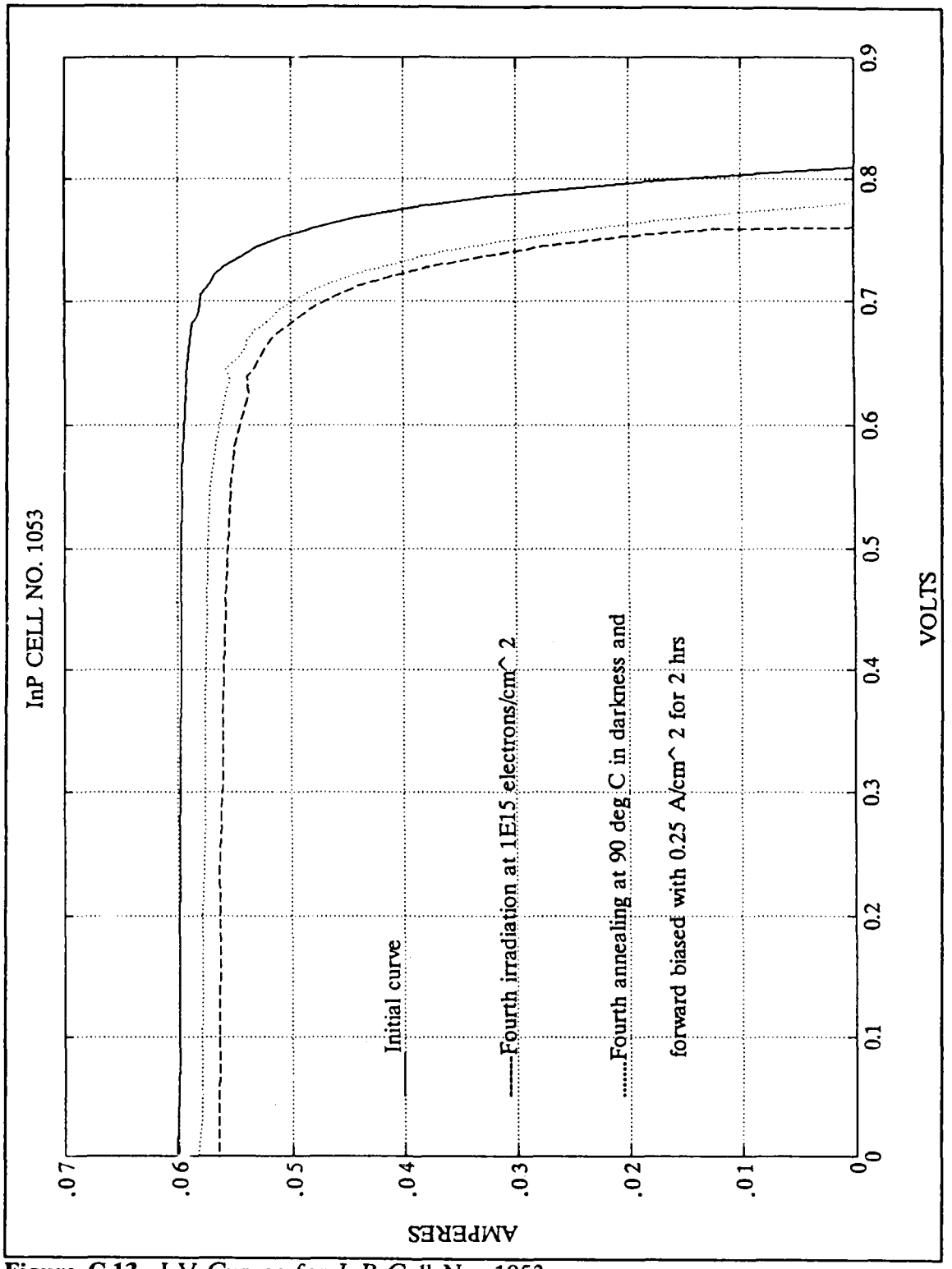

Figure C.13 I-V Curves for InP Cell No. 1053

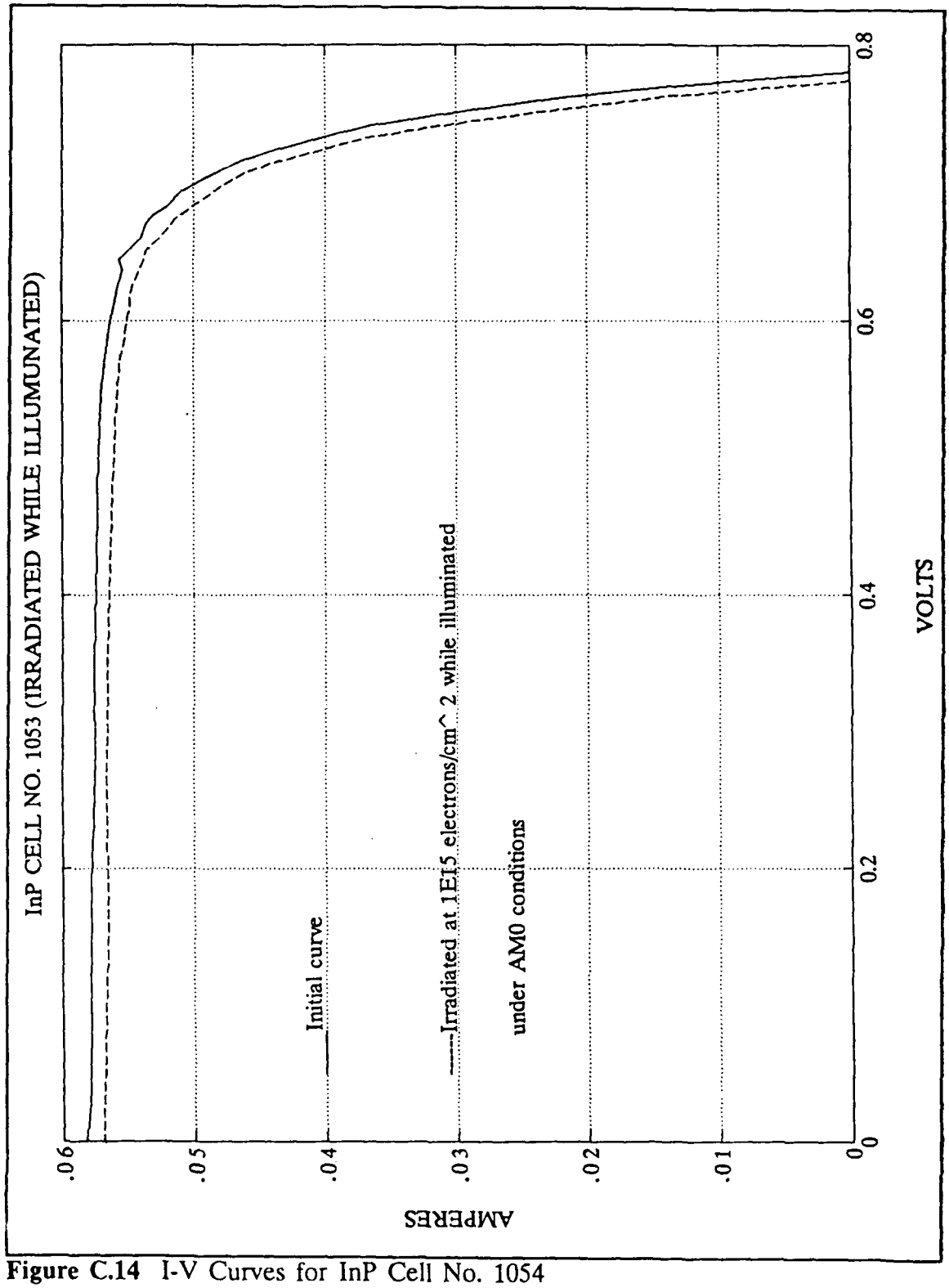

Figure C.14 I-V Curves for InP Cell No. 1054

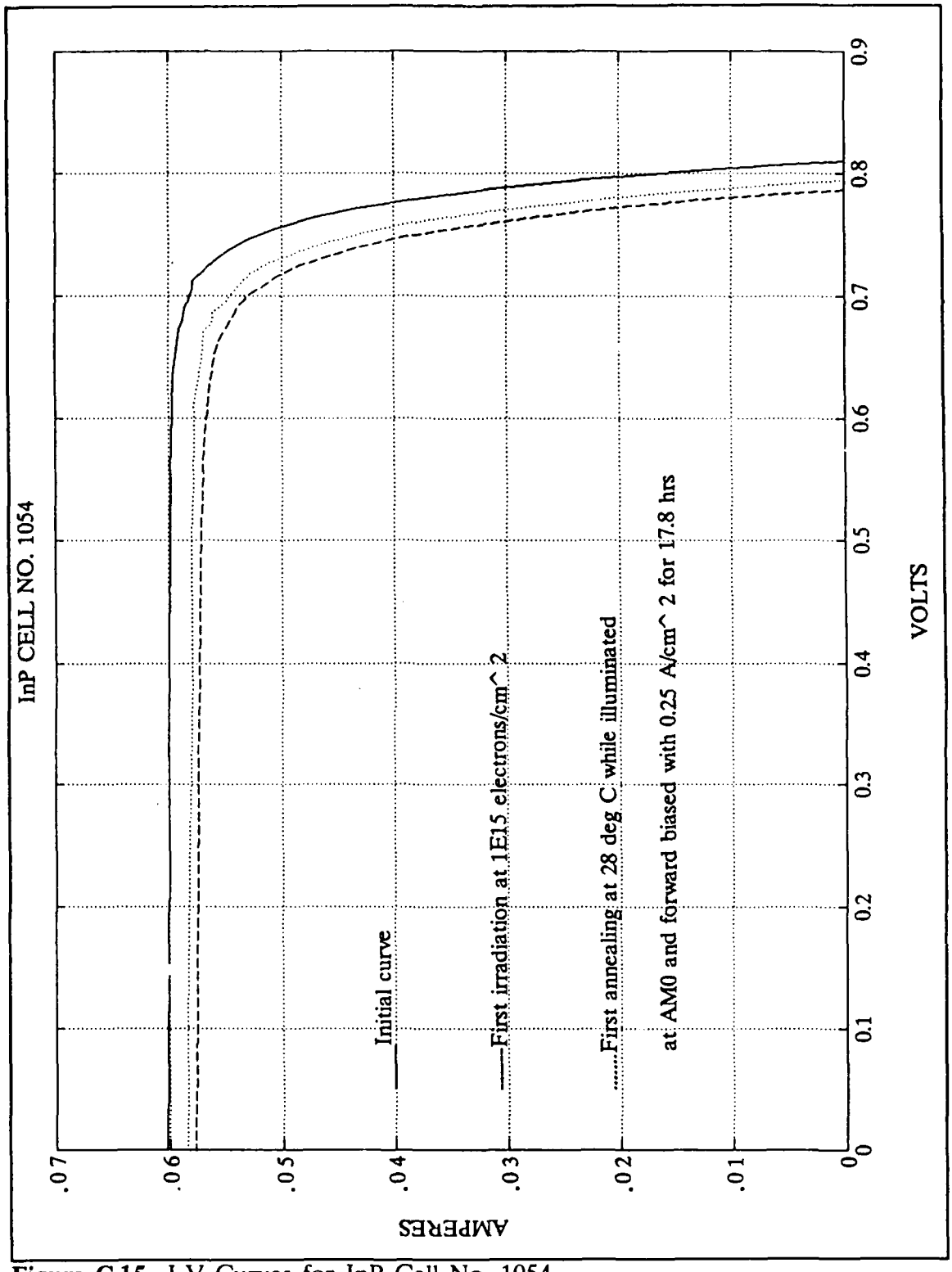

Figure C.15 I-V Curves for InP Cell No. 1054

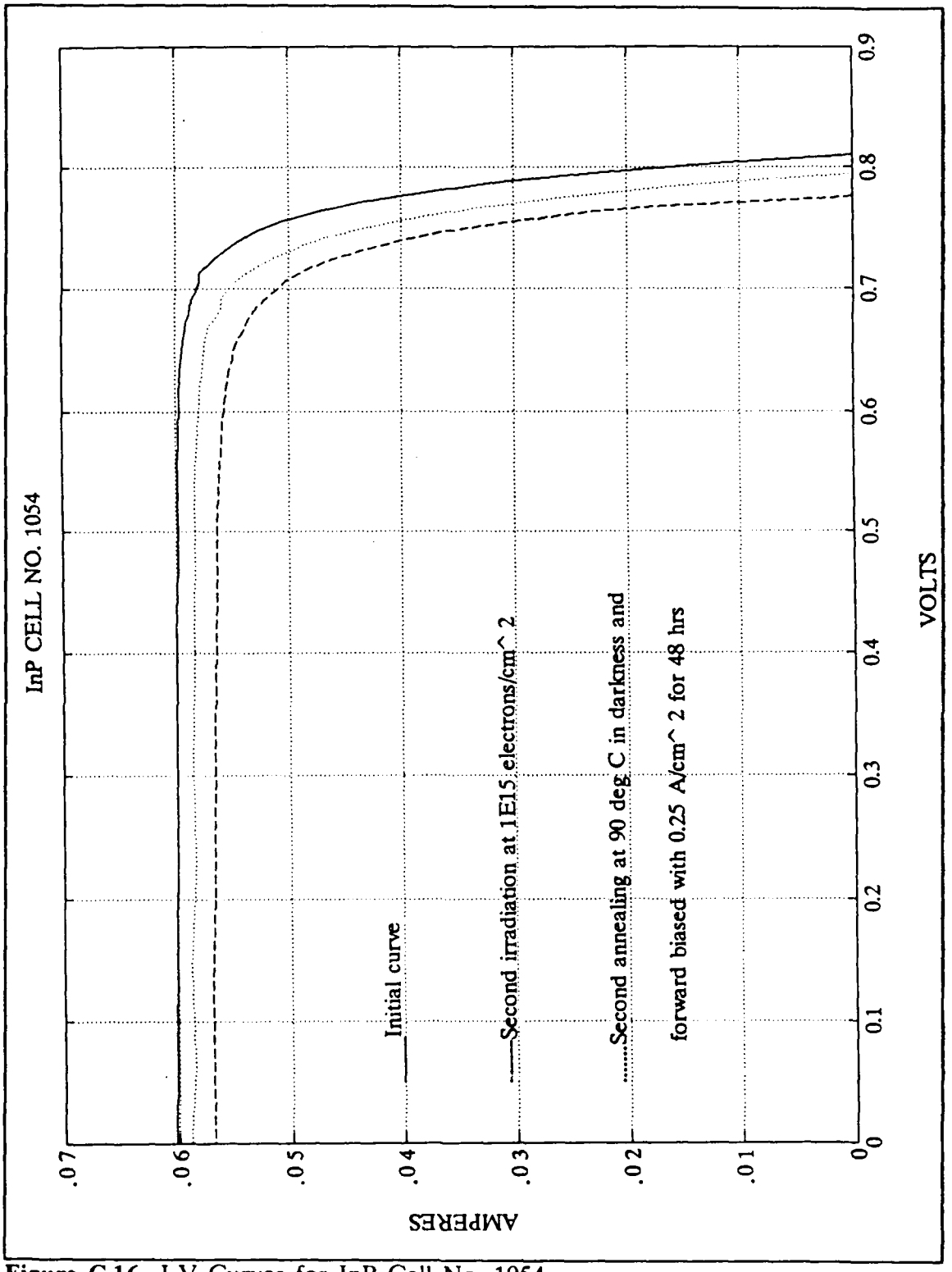

Figure C.16 I-V Curves for InP Cell No. 1054

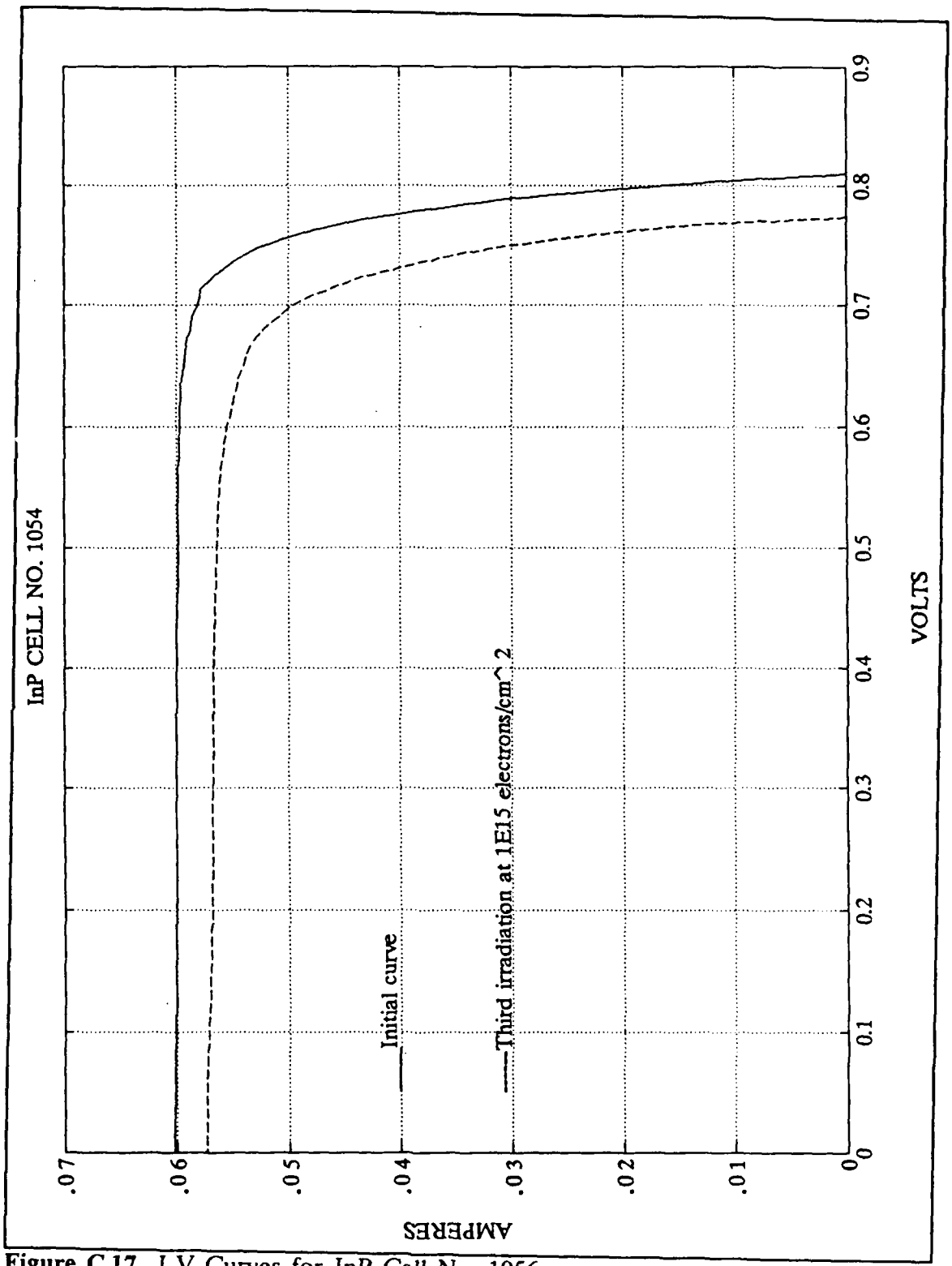

Figure C.17 I-V Curves for InP Cell No. 1056

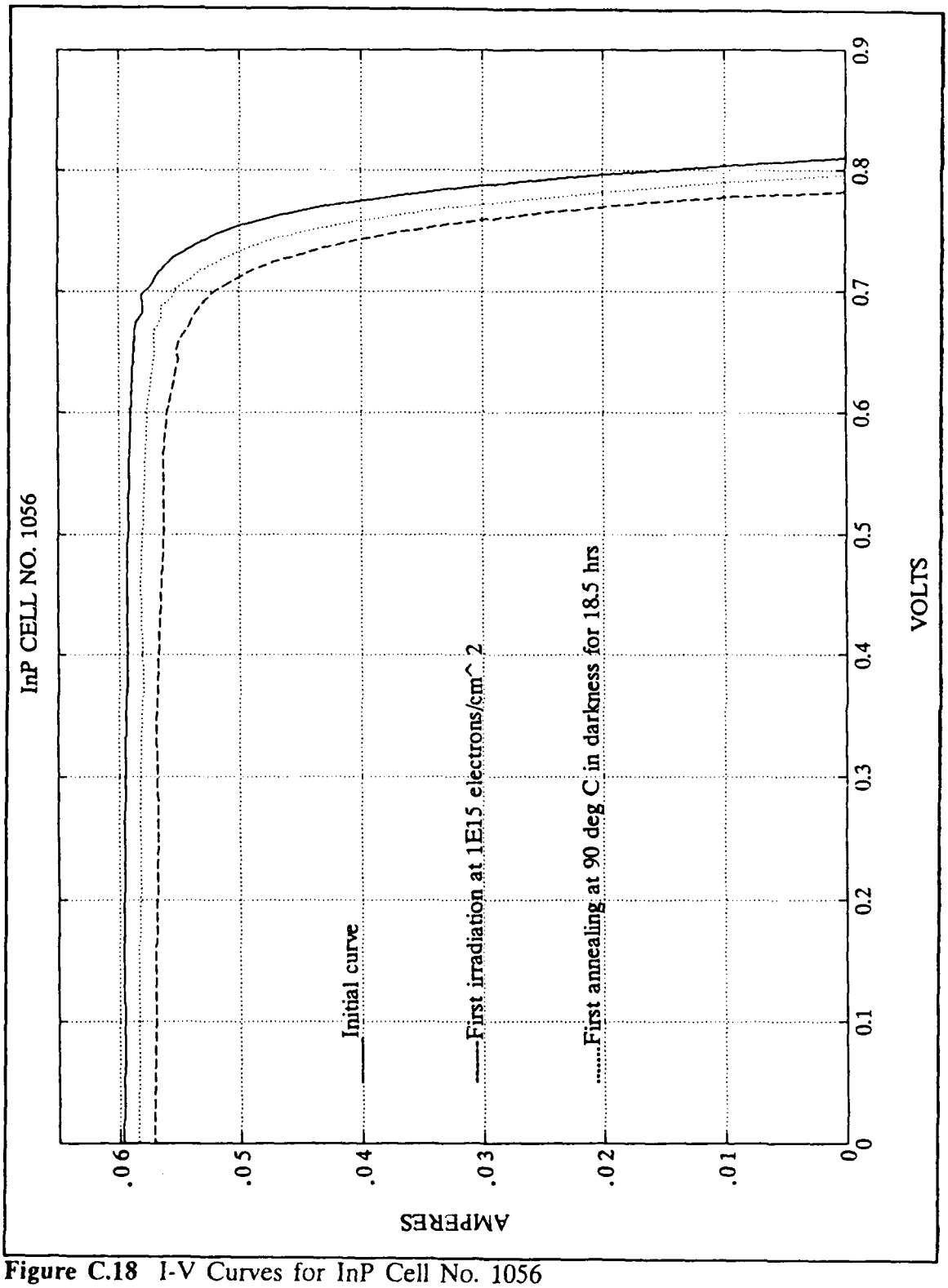

Figure C.18 I-V Curves for InP Cell No. 1056

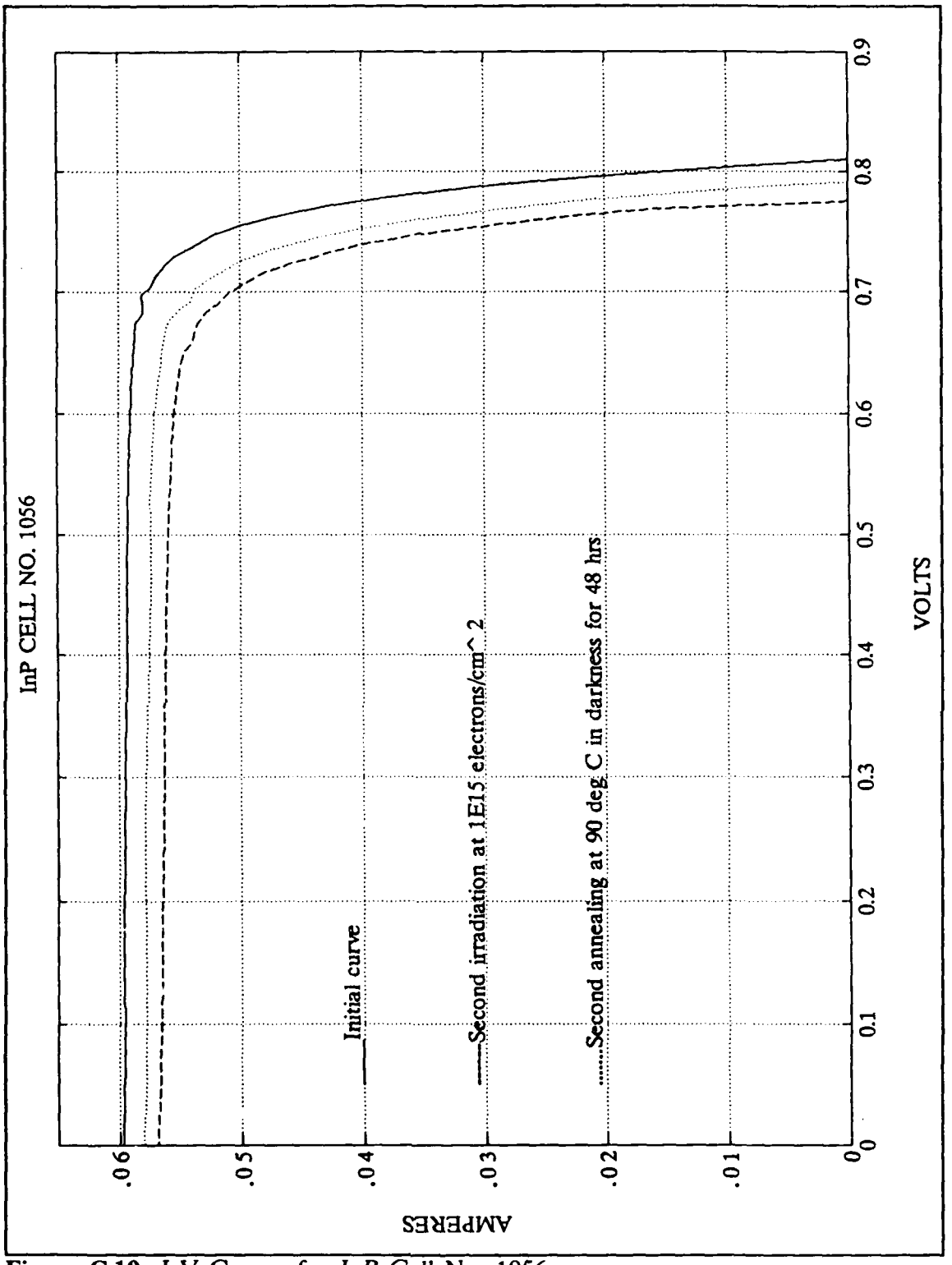

Figure C.19 I-V Curves for InP Cell No. 1056

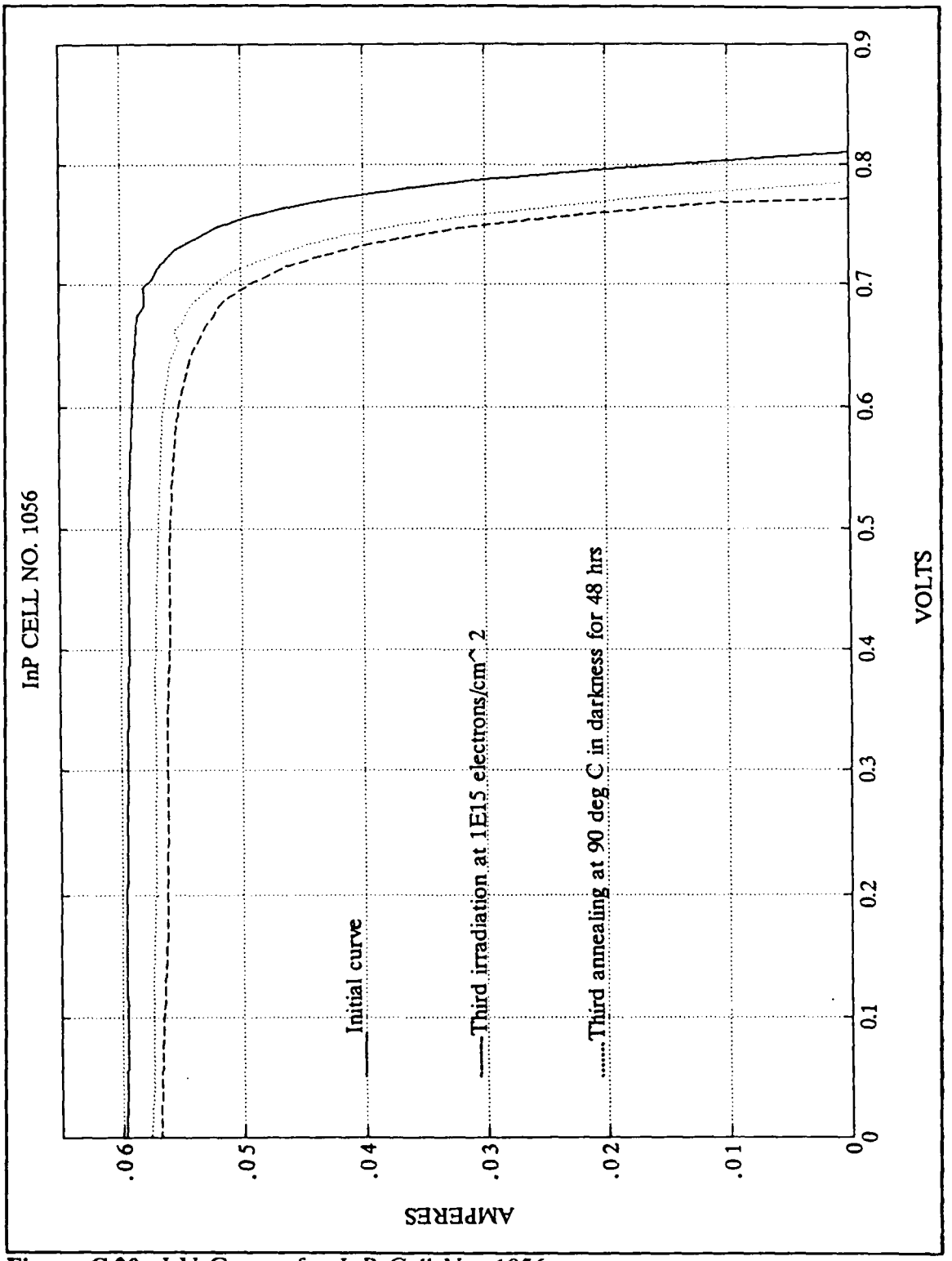

Figure C.20 I-V Curves for InP Cell No. 1056

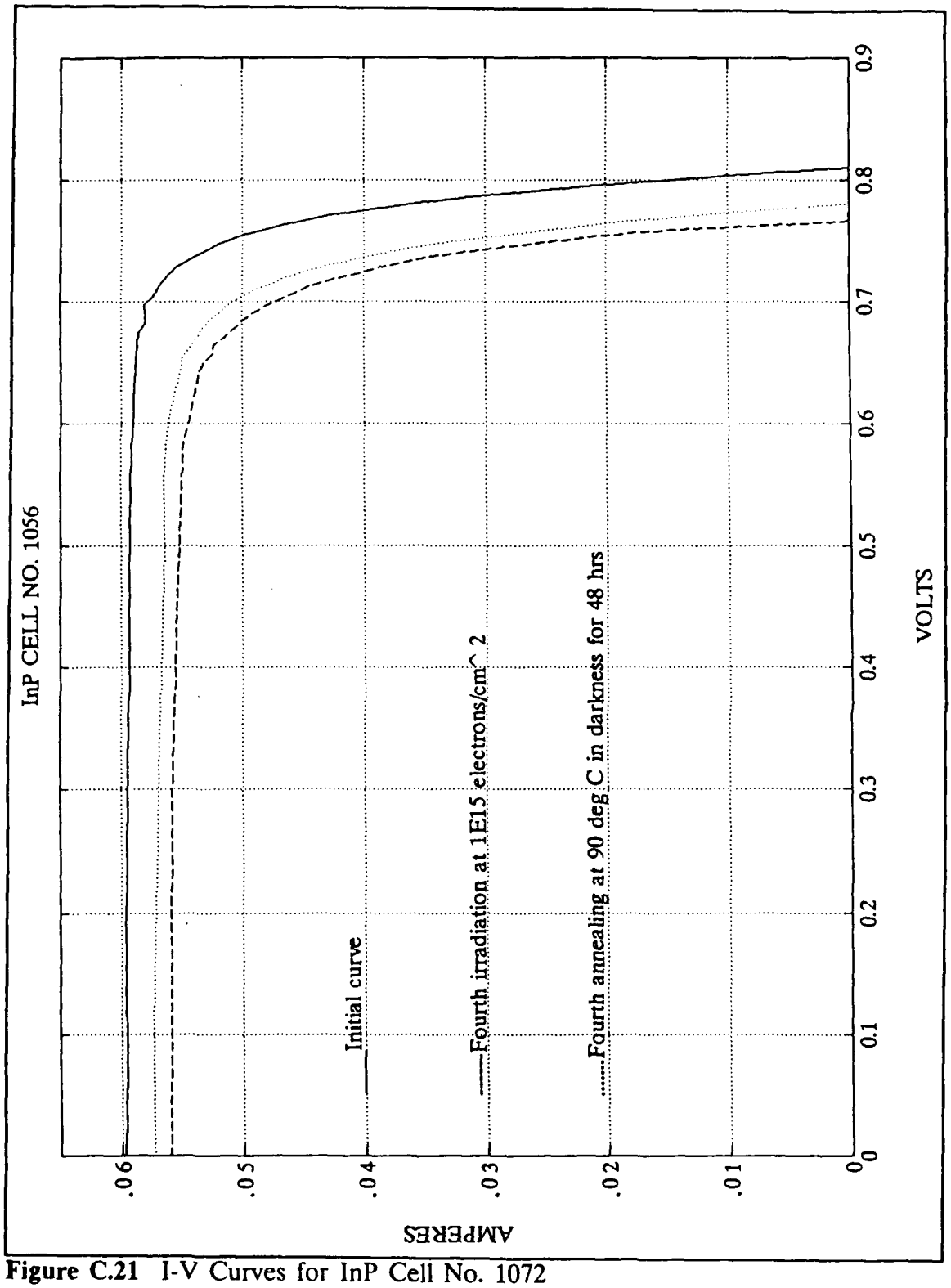

Figure C.21 I-V Curves for InP Cell No. 1072

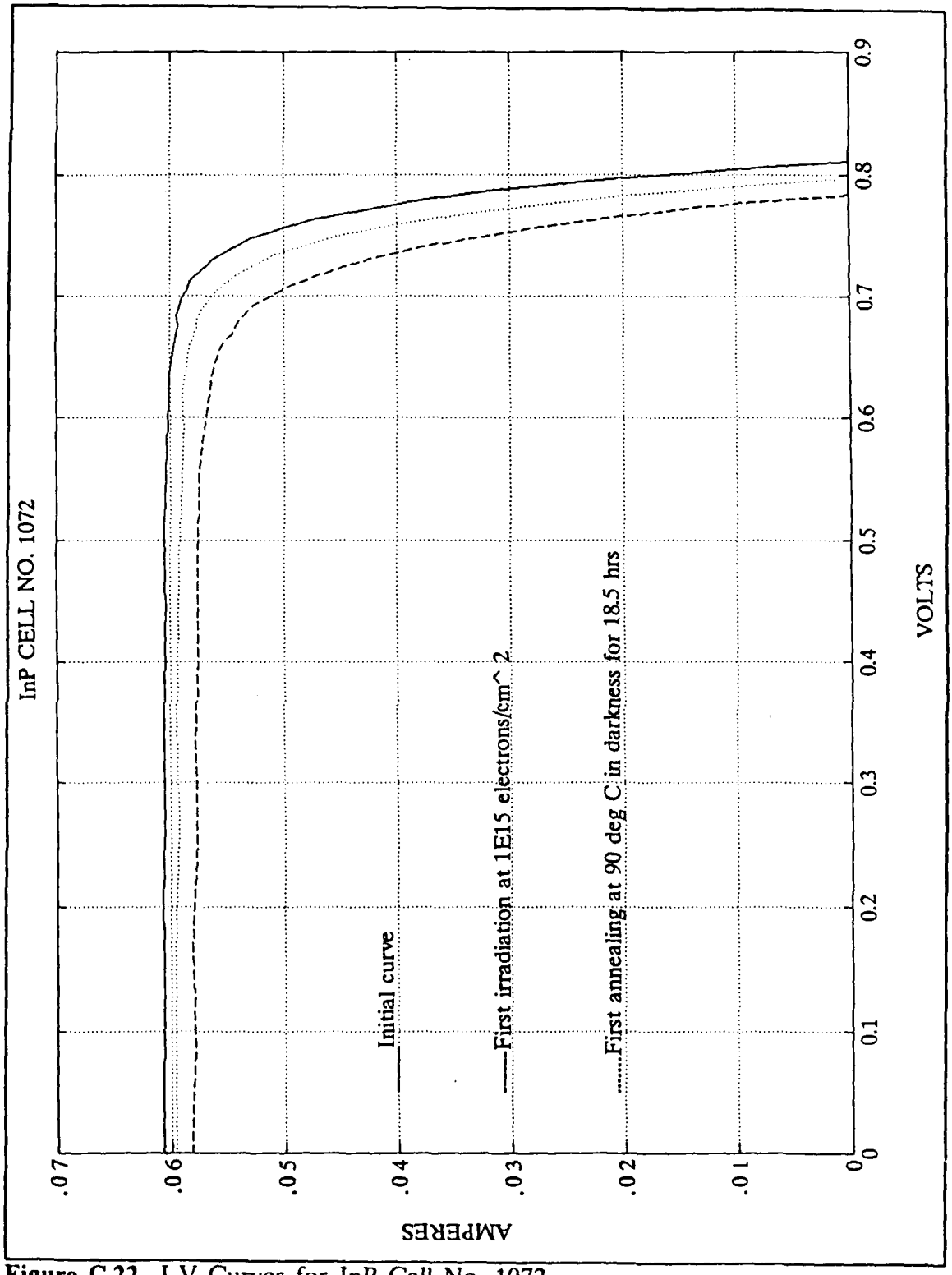

Figure C.22 I-V Curves for InP Cell No. 1072

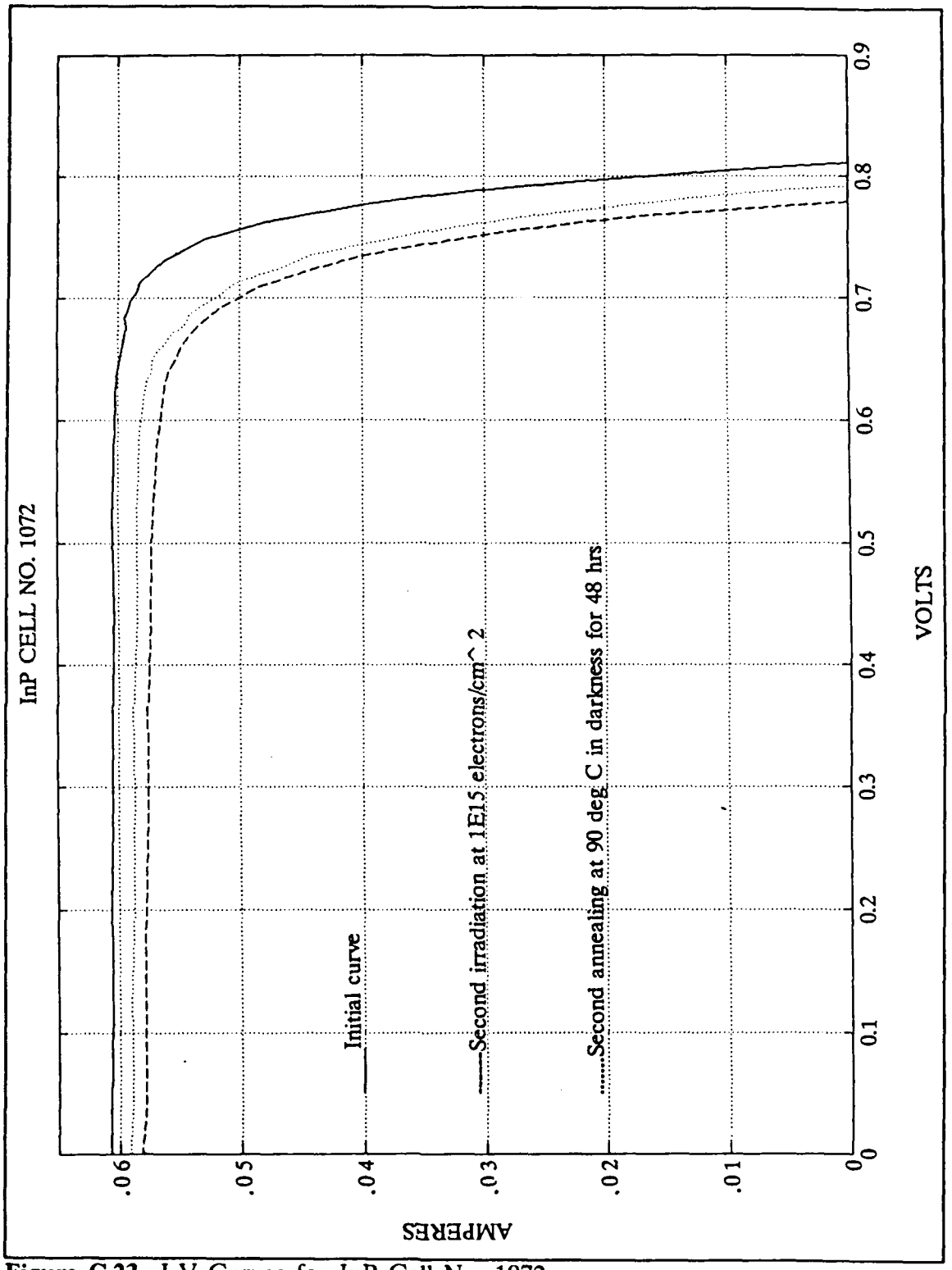

Figure C.23 I-V Curves for InP Cell No. 1072

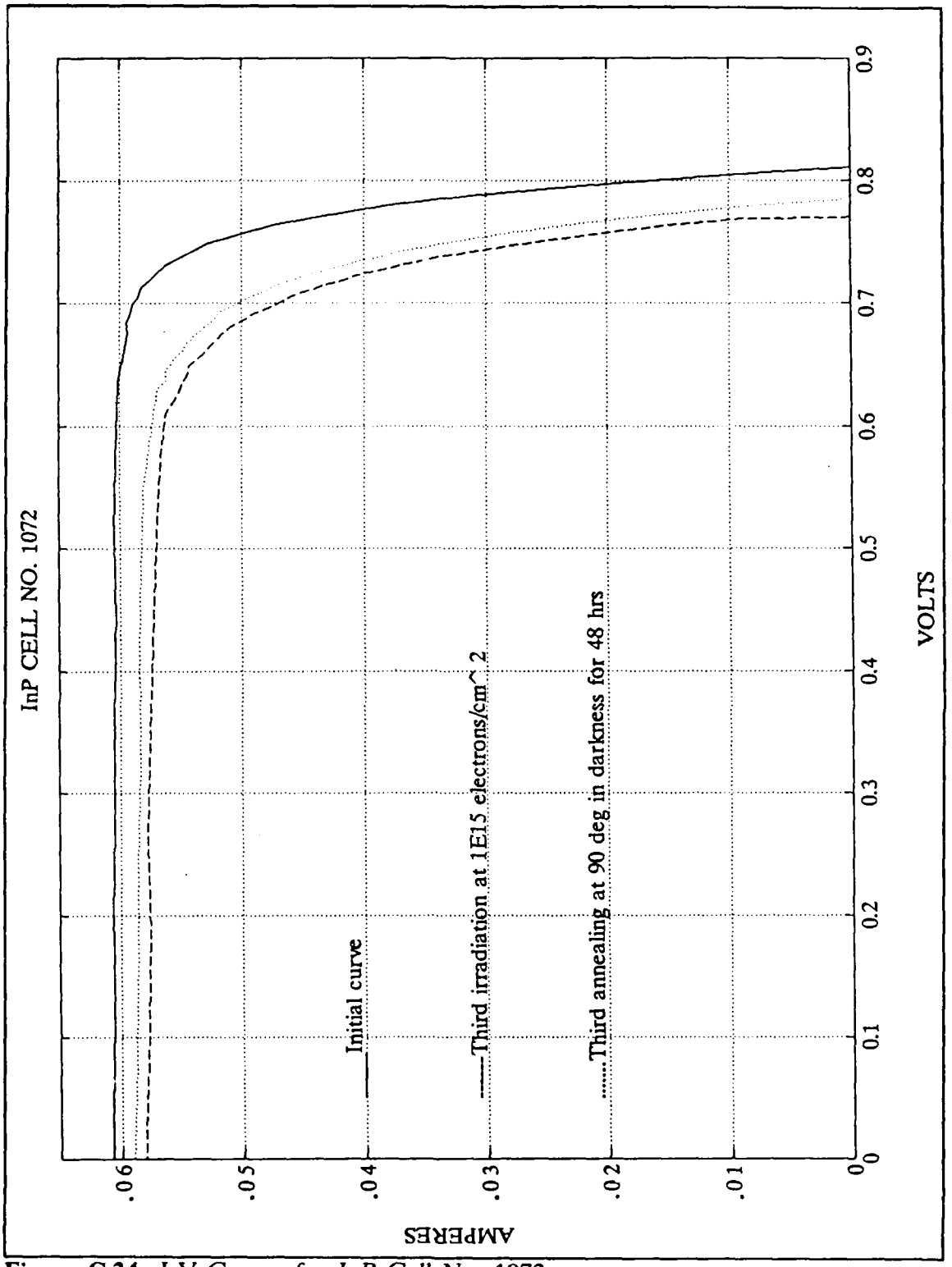

Figure C.24 I-V Curves for InP Cell No. 1072

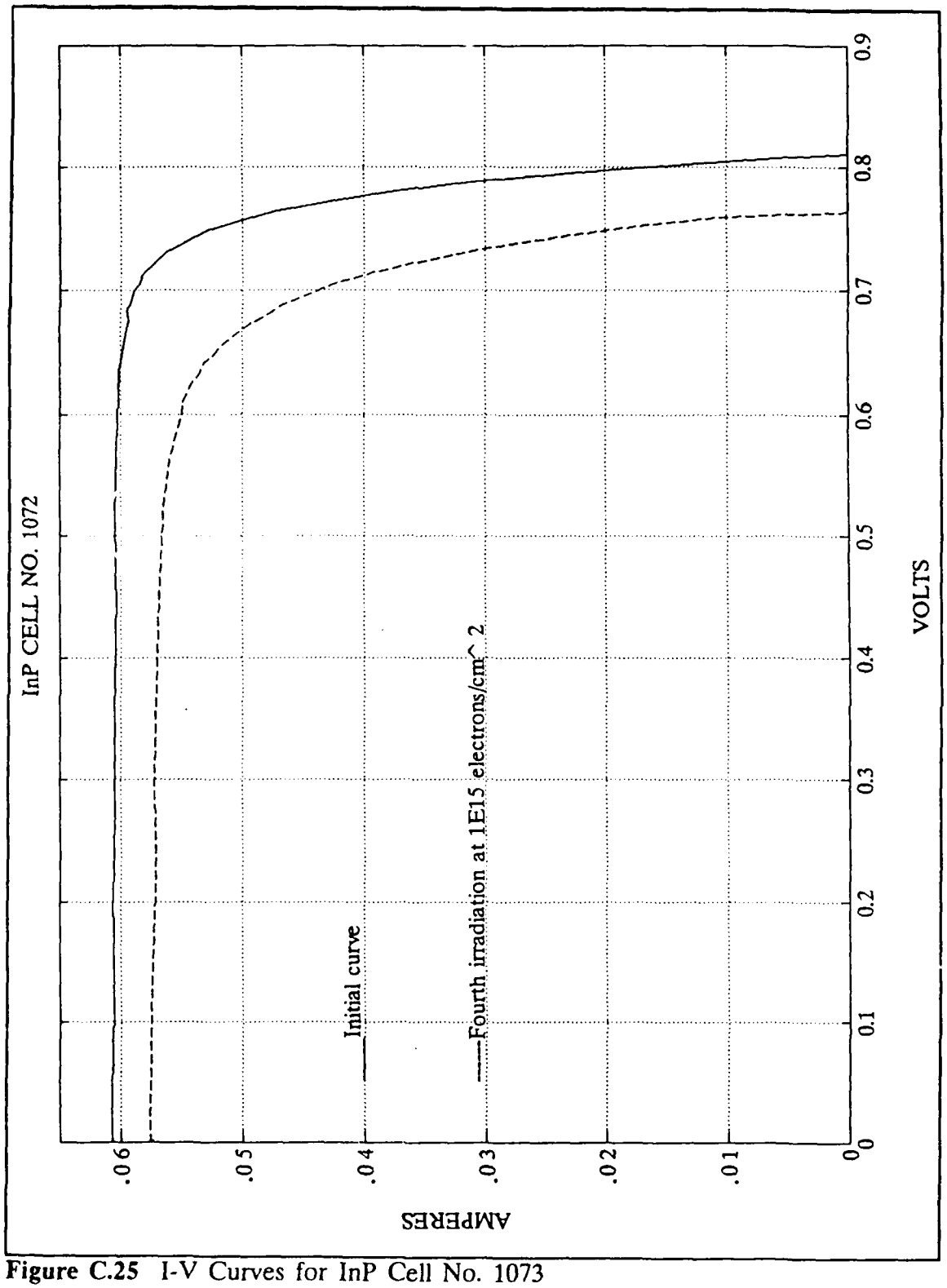

Figure C.25 I-V Curves for InP Cell No. 1073

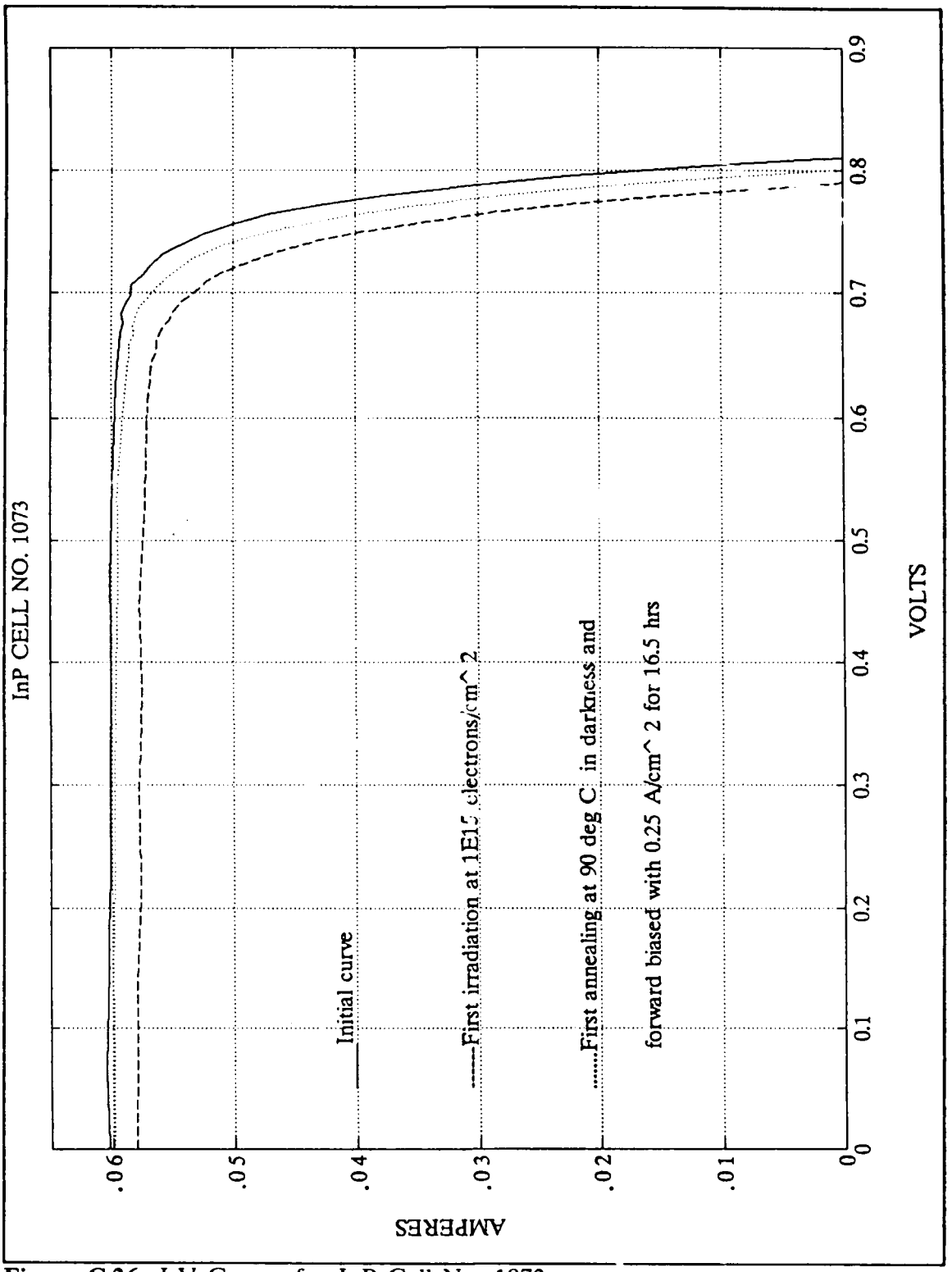

Figure C.26 I-V Curves for InP Cell No. 1073

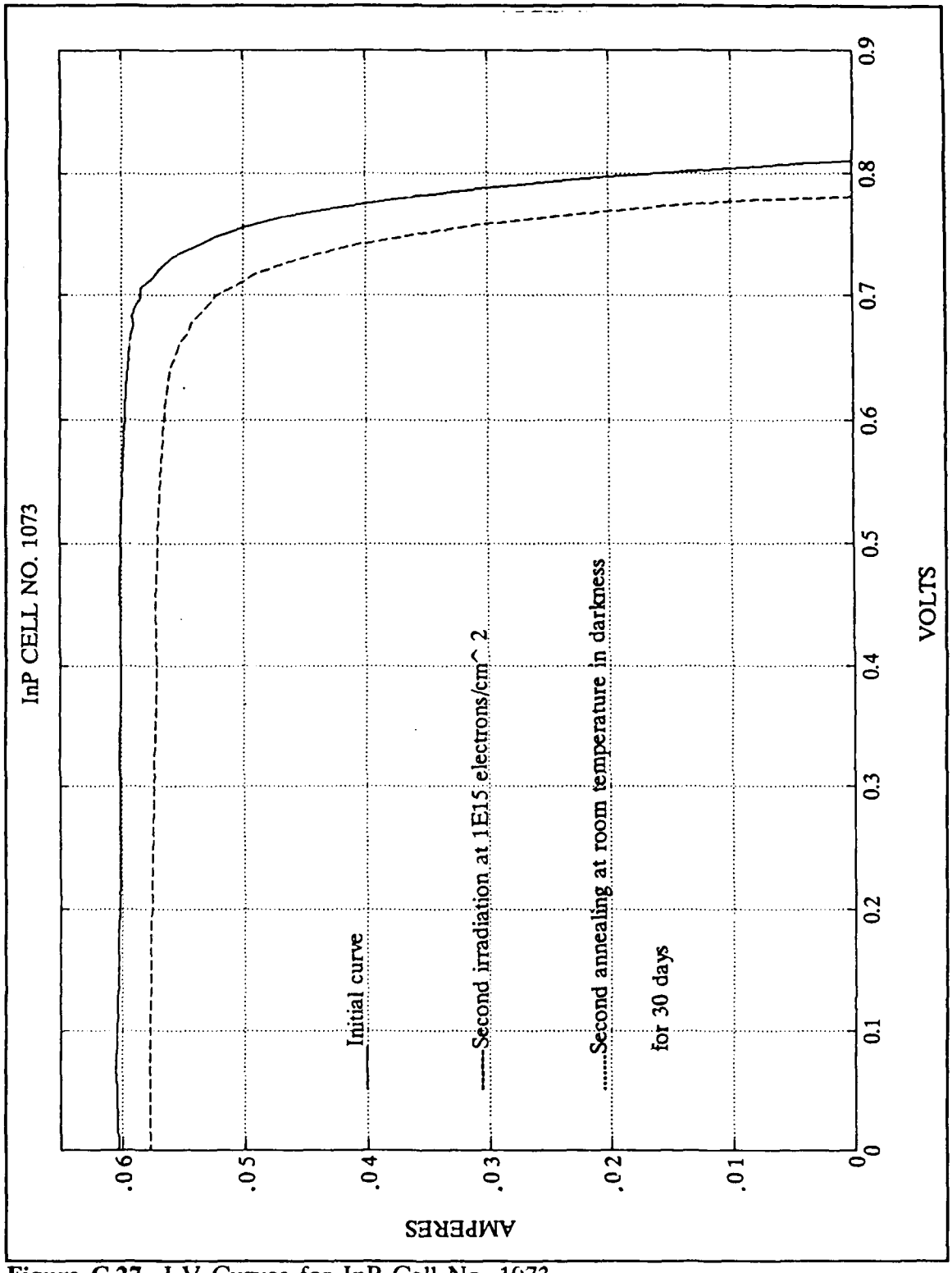

Figure C.27 I-V Curves for InP Cell No. 1073

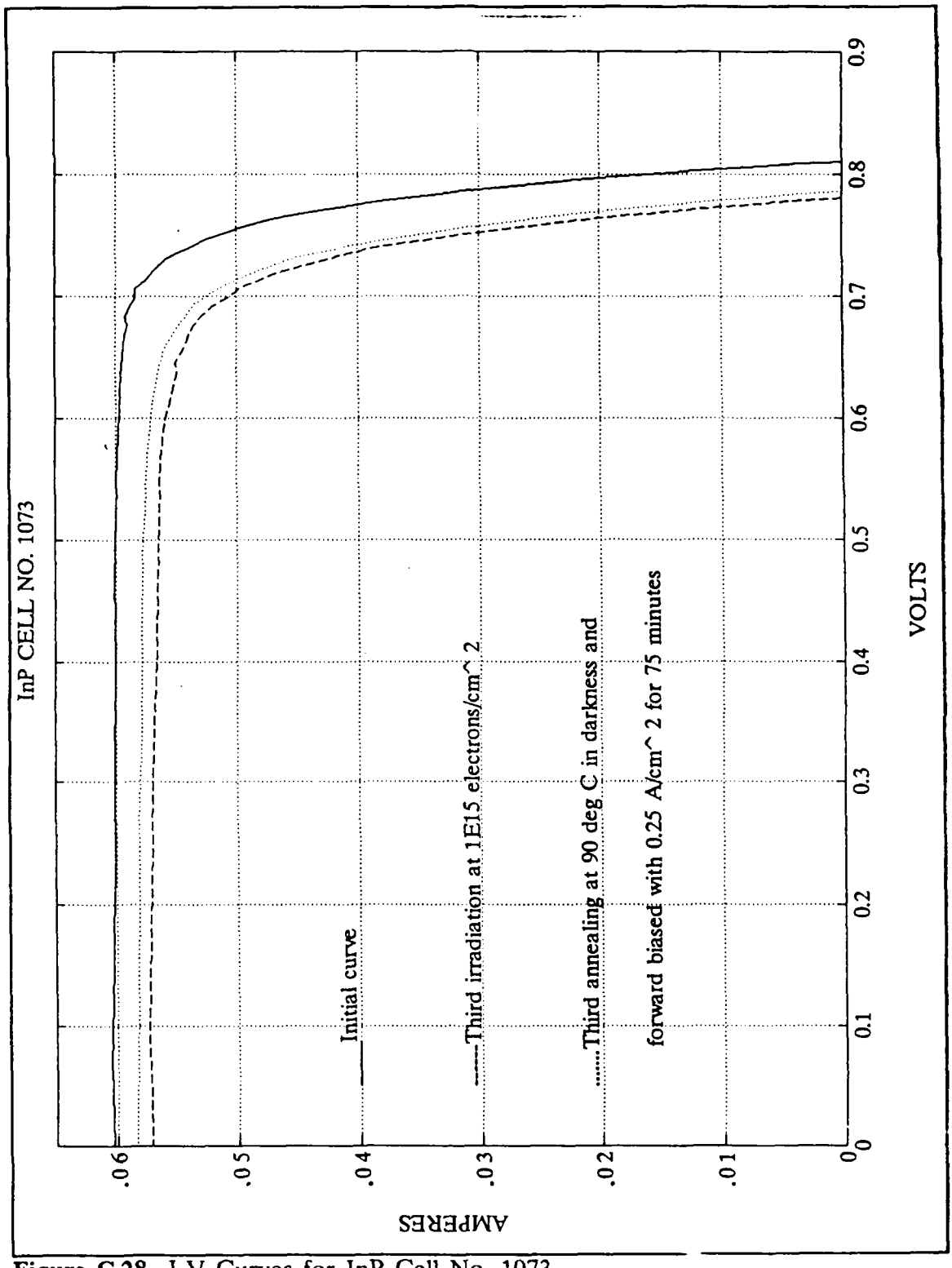

Figure C.28 I-V Curves for InP Cell No. 1073

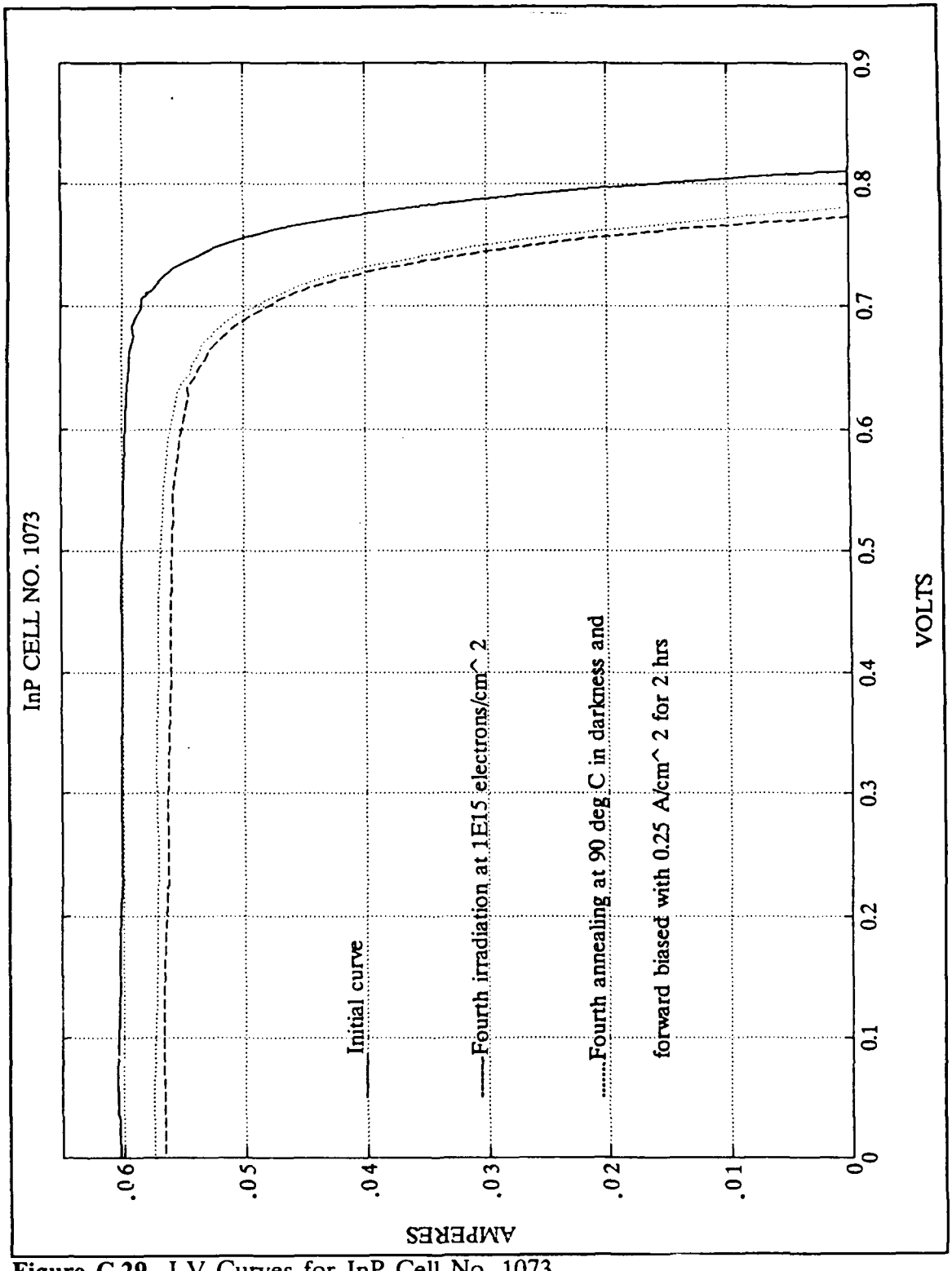

Figure C.29 I-V Curves for InP Cell No. 1073

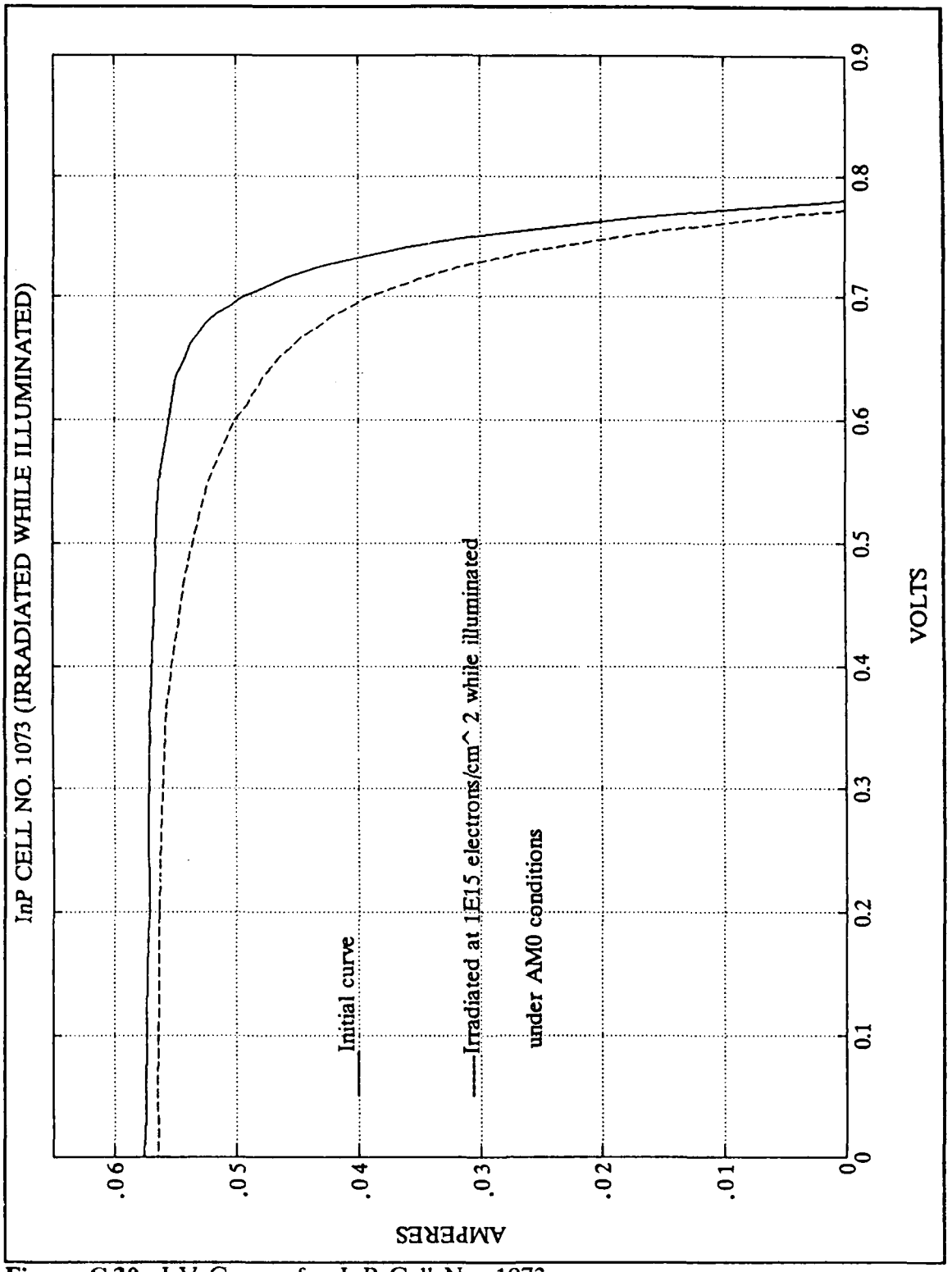

Figure C.30 I-V Curves for InP Cell No. 1073

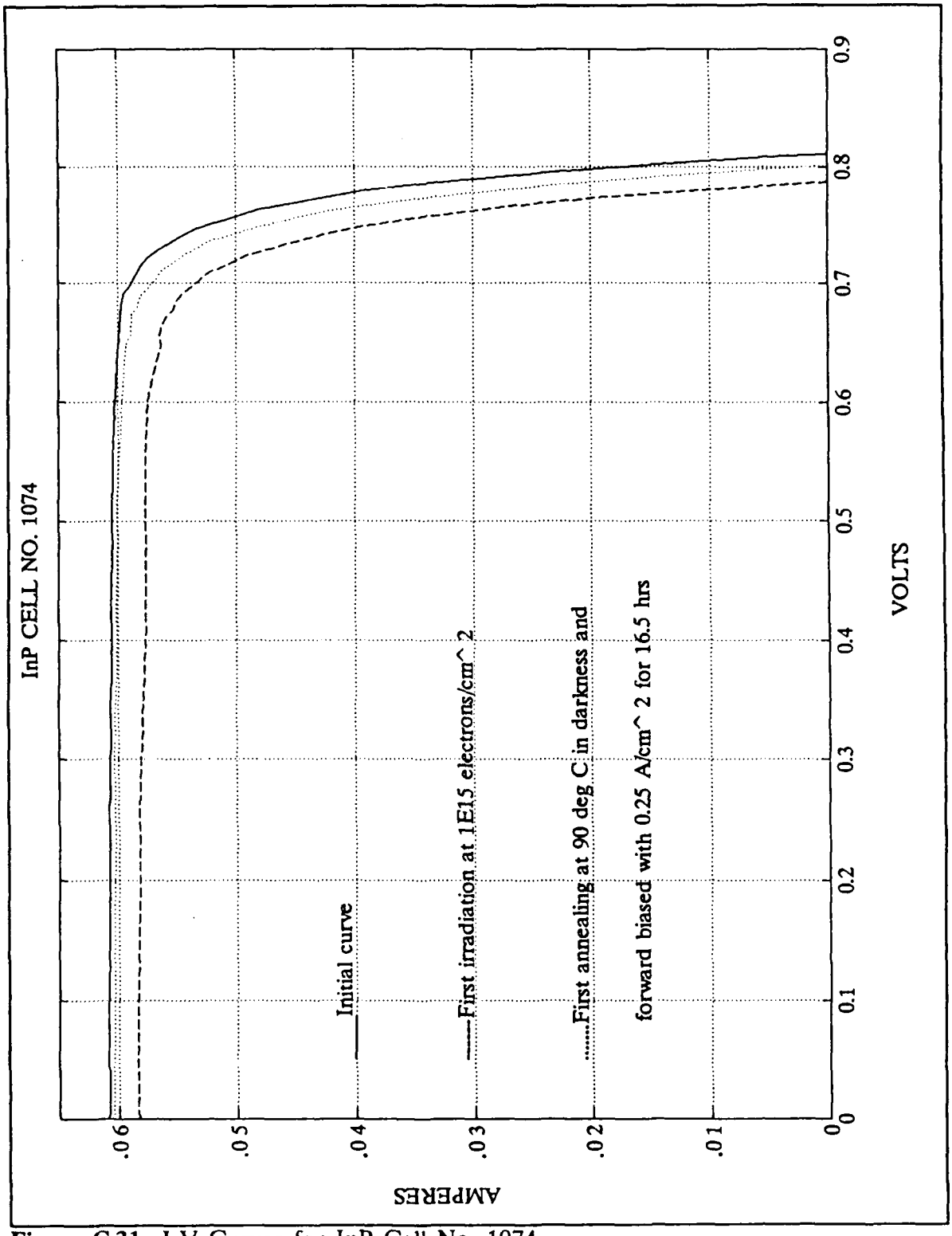

Figure C.31 I-V Curves for InP Cell No. 1074

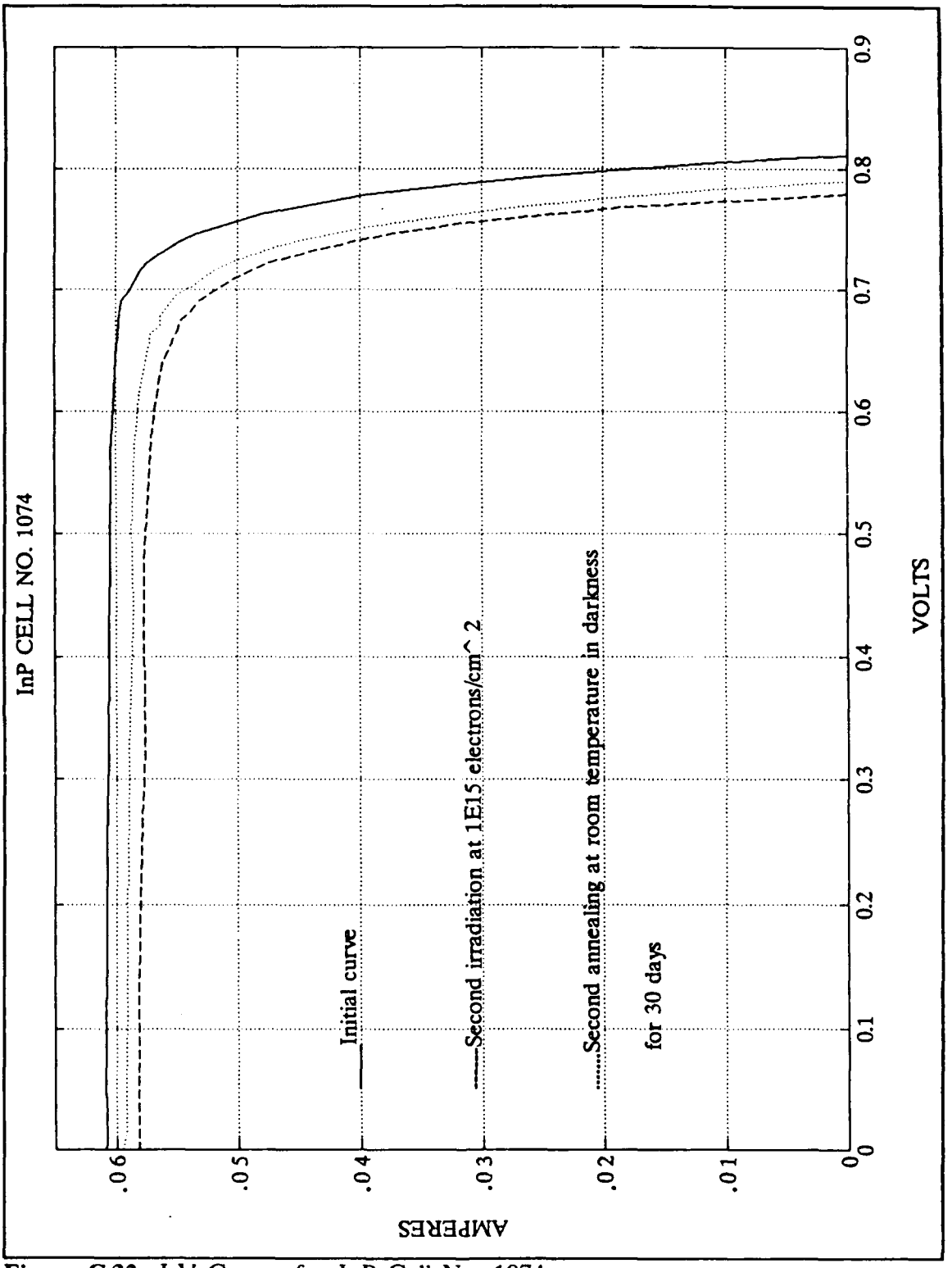

Figure C.32 I-V Curves for InP Cell No. 1074

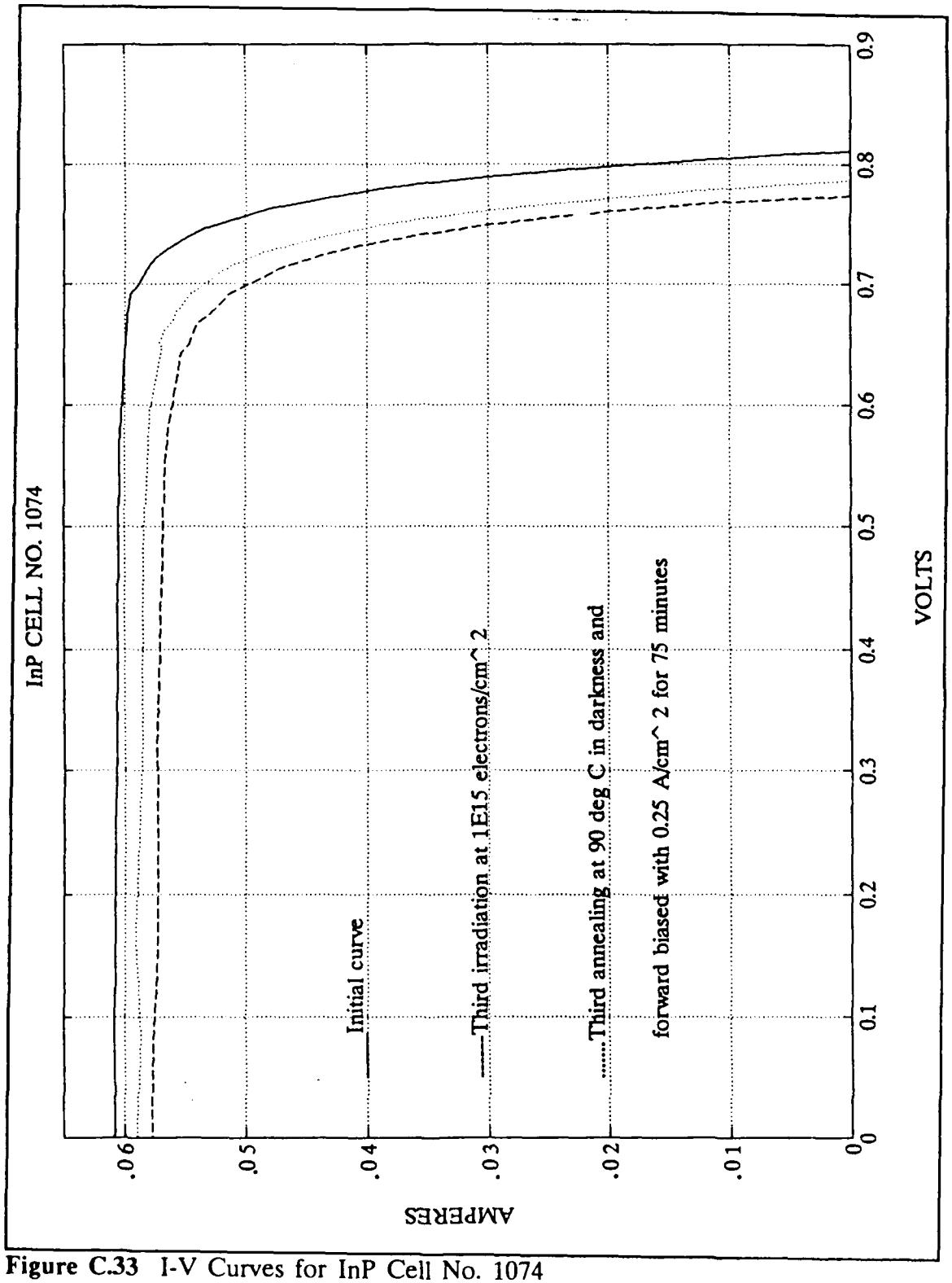

Figure C.33 I-V Curves for InP Cell No. 1074

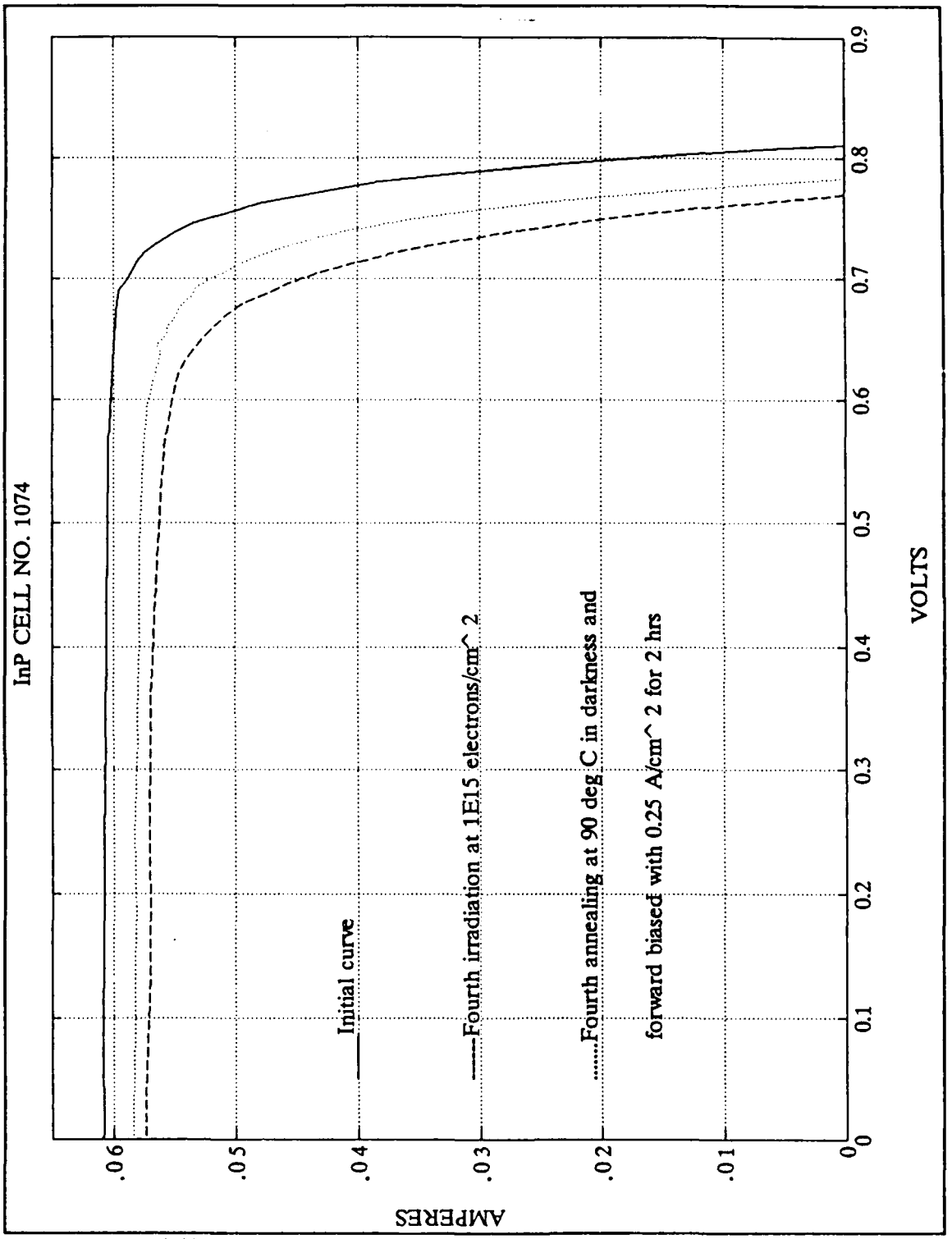

Figure C.34 I-V Curves for InP Cell No. 1074

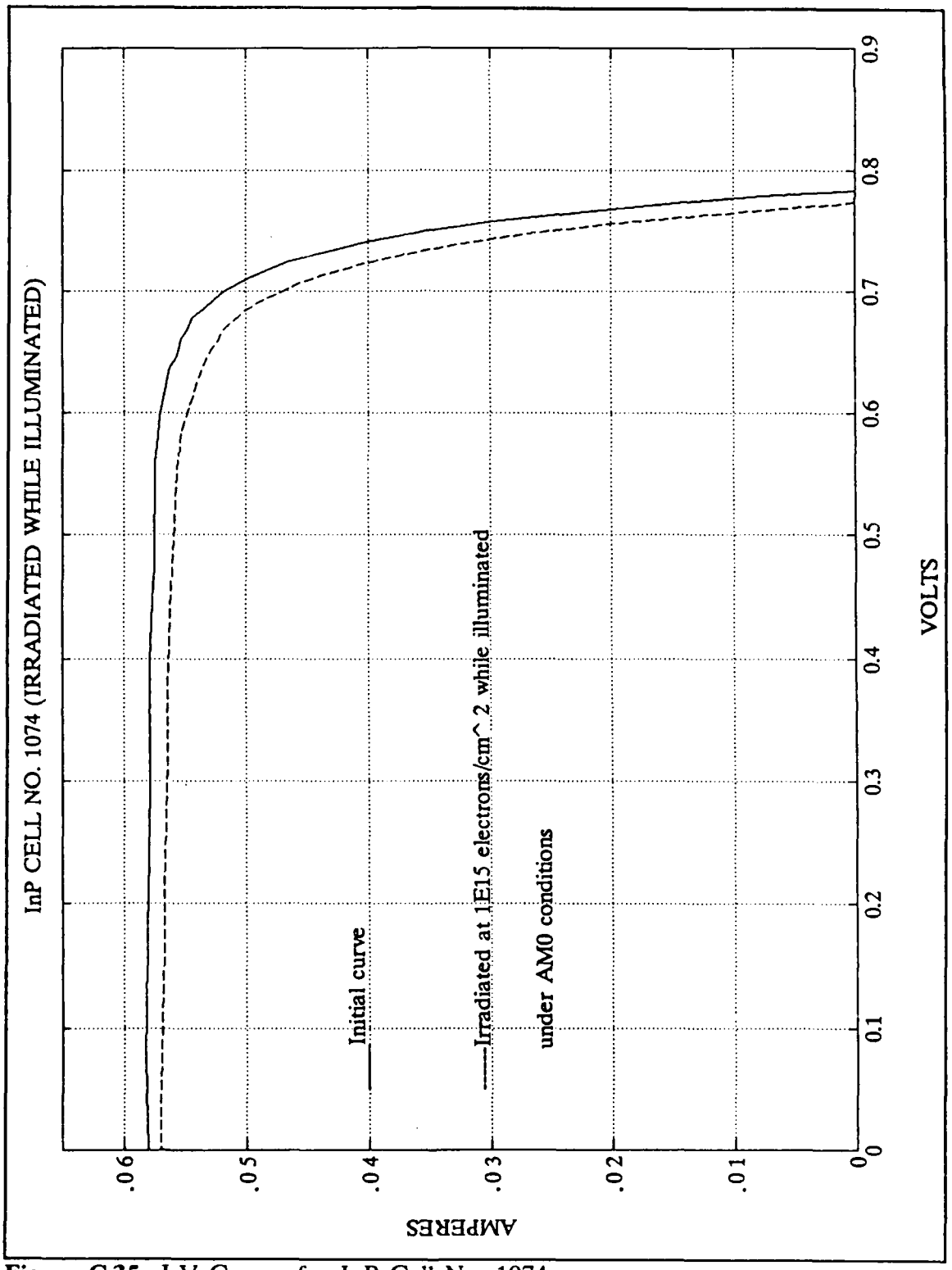

Figure C.35 I-V Curves for InP Cell No. 1074

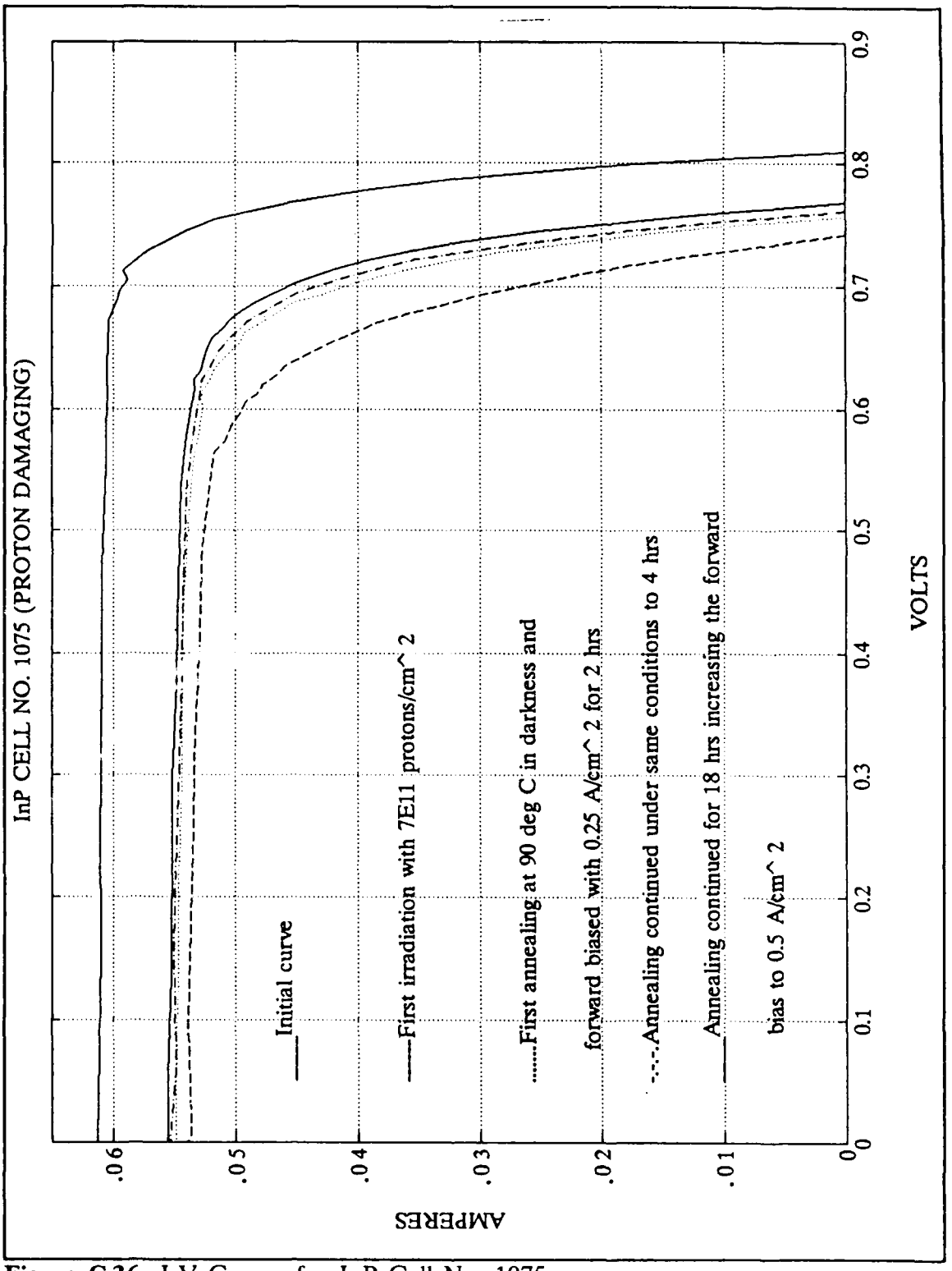

Figure C.36 I-V Curves for InP Cell No. 1075

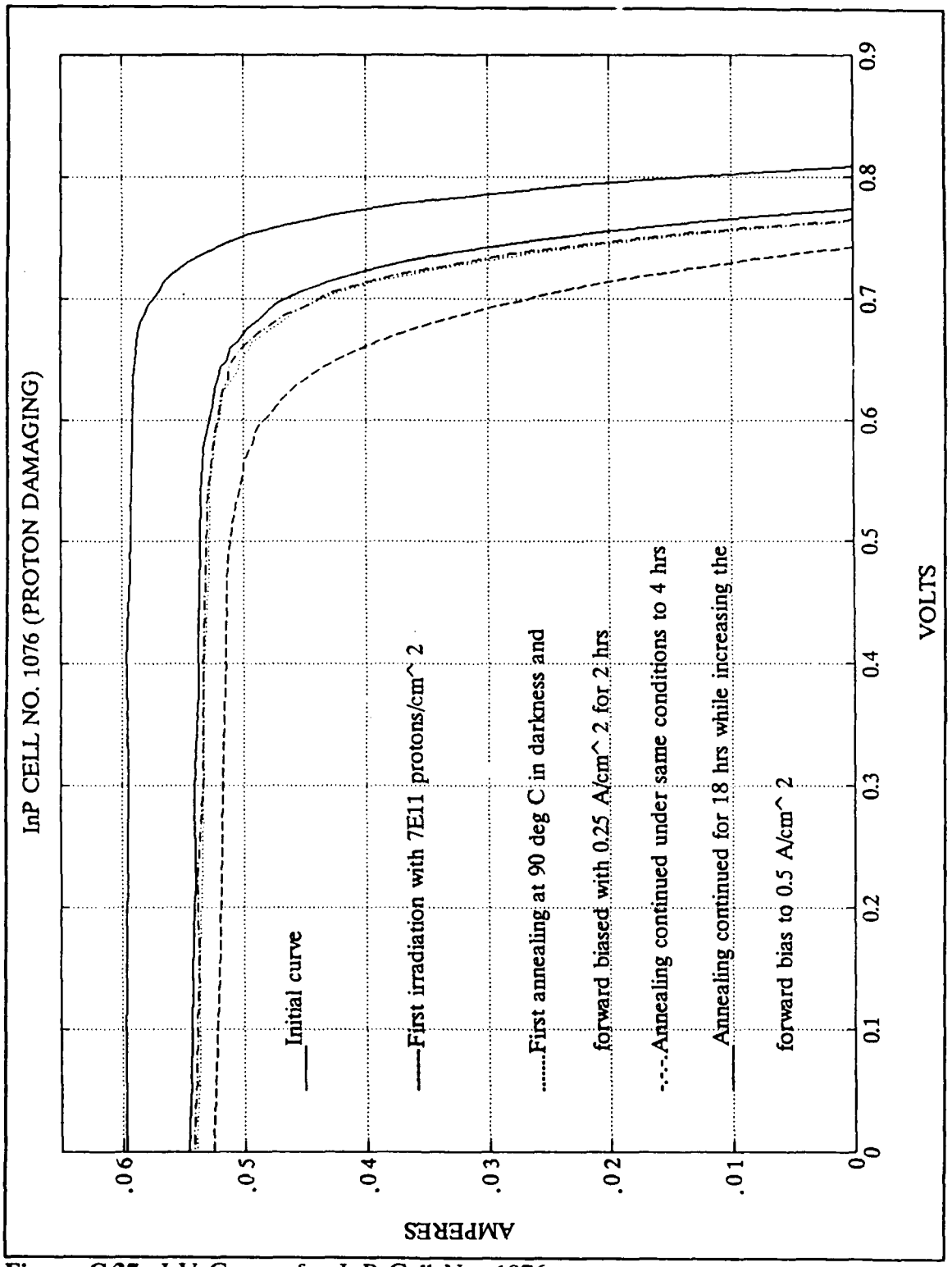

Figure C.37 I-V Curves for InP Cell No. 1076

APPENDIX D. InP CELL DATA PLOTS

Voc, Isc, Pmax and % Efficiency was plotted for every stage in the multiple irradiating and annealing cycle of every cell. These graphs are point plots which have been connected with lines and illustrates the degradation and recovery with every stage.

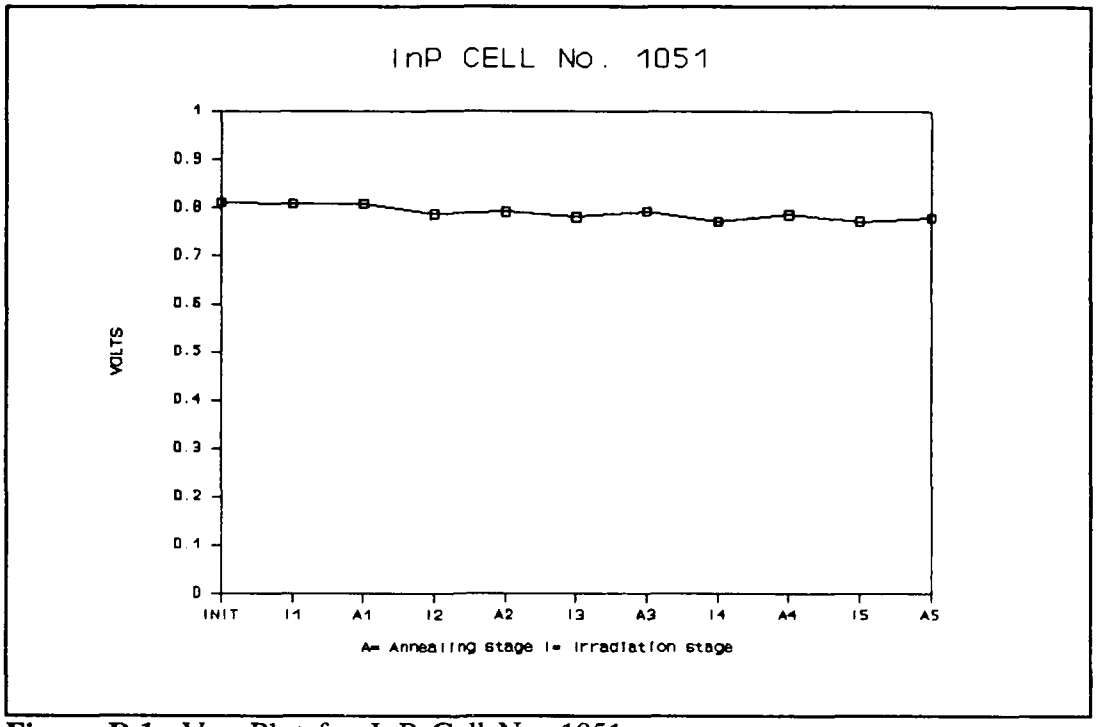

Figure D.1 Voc Plot for InP Cell No. 1051

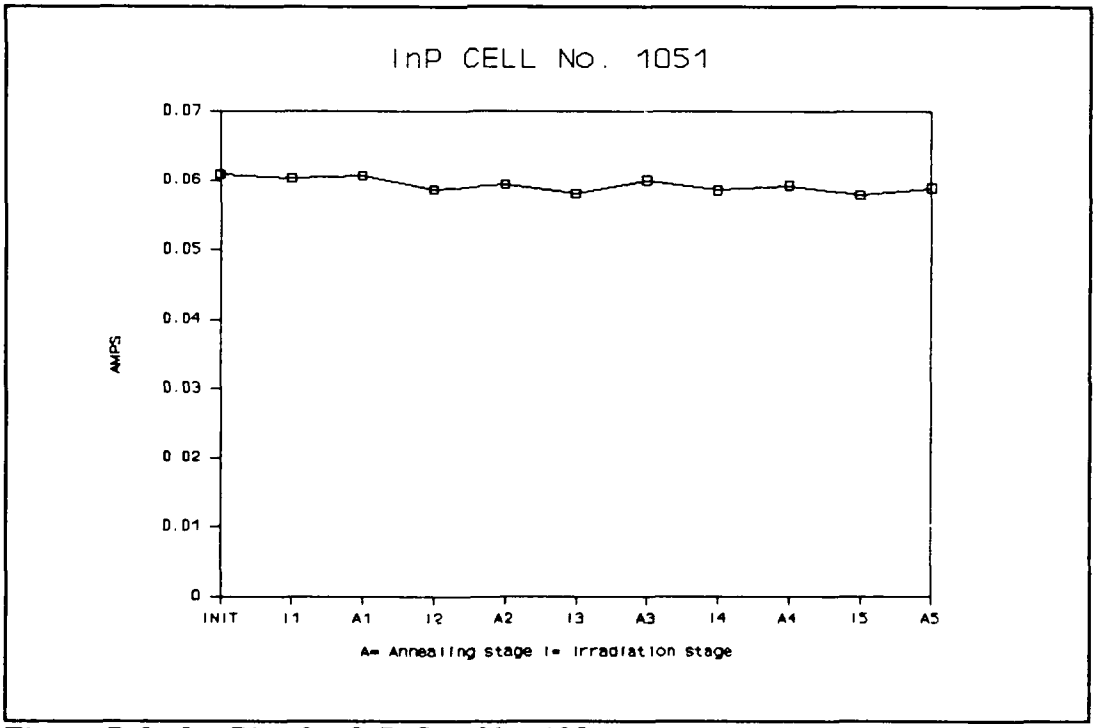

Figure D.2 Isc Plot for InP Cell No. 1051

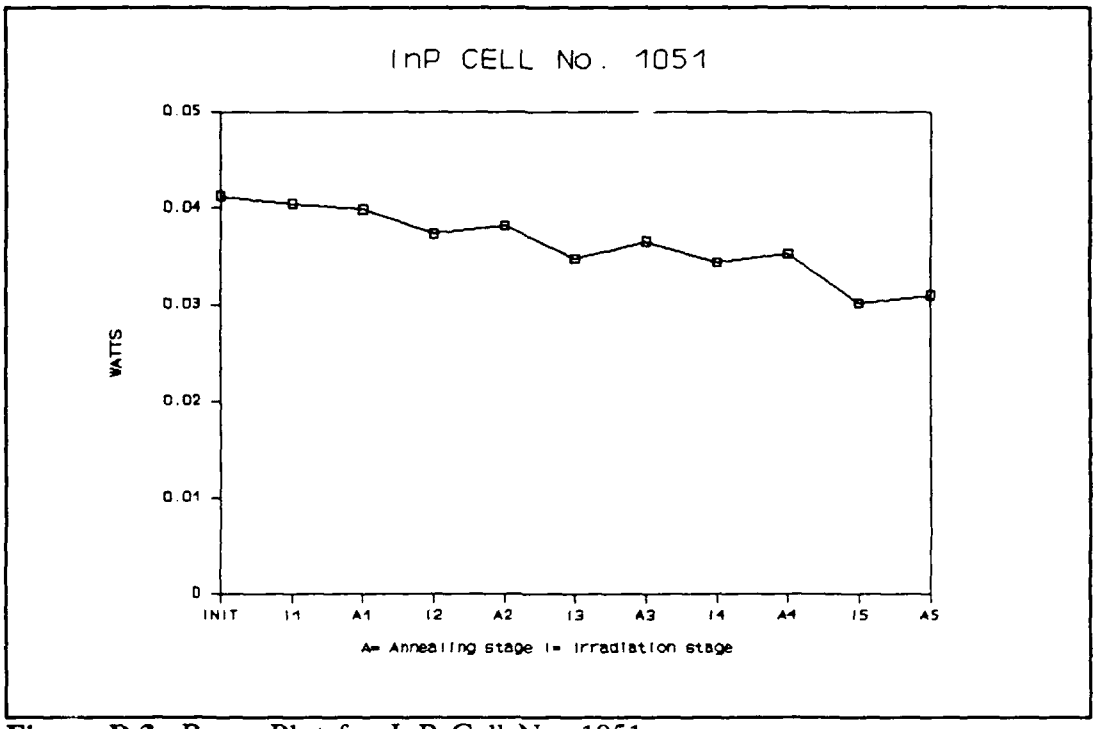

Figure D.3 Pmax Plot for InP Cell No. 1051

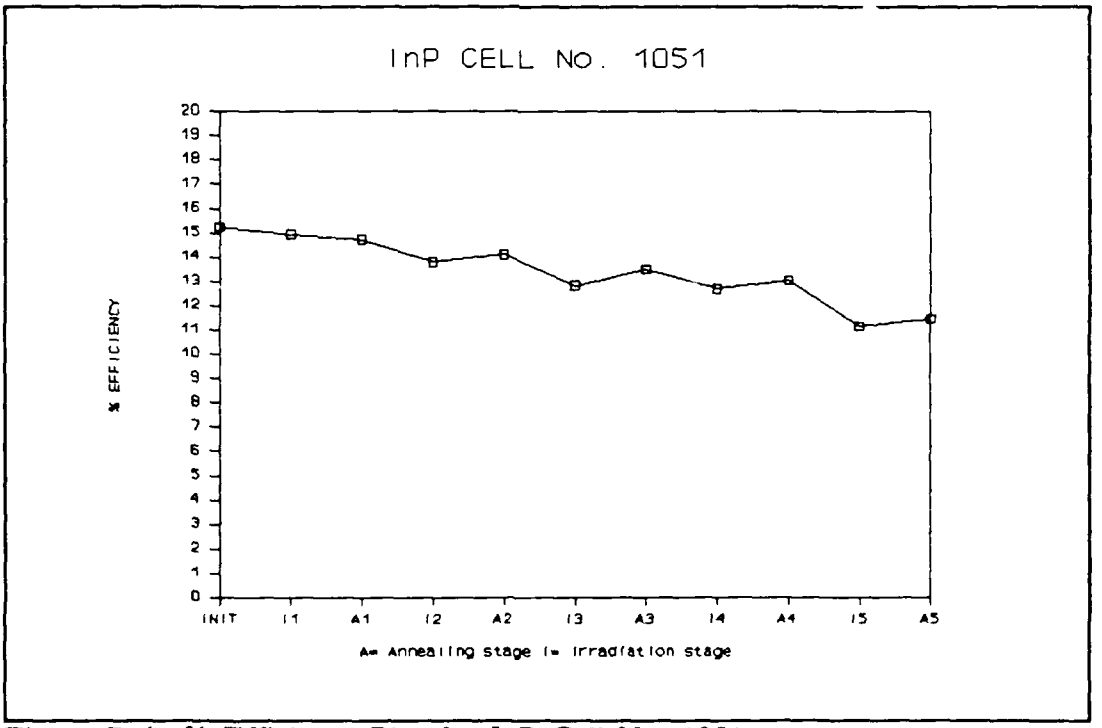

Figure D.4 % Efficiency Plot for InP Cell No. 1051

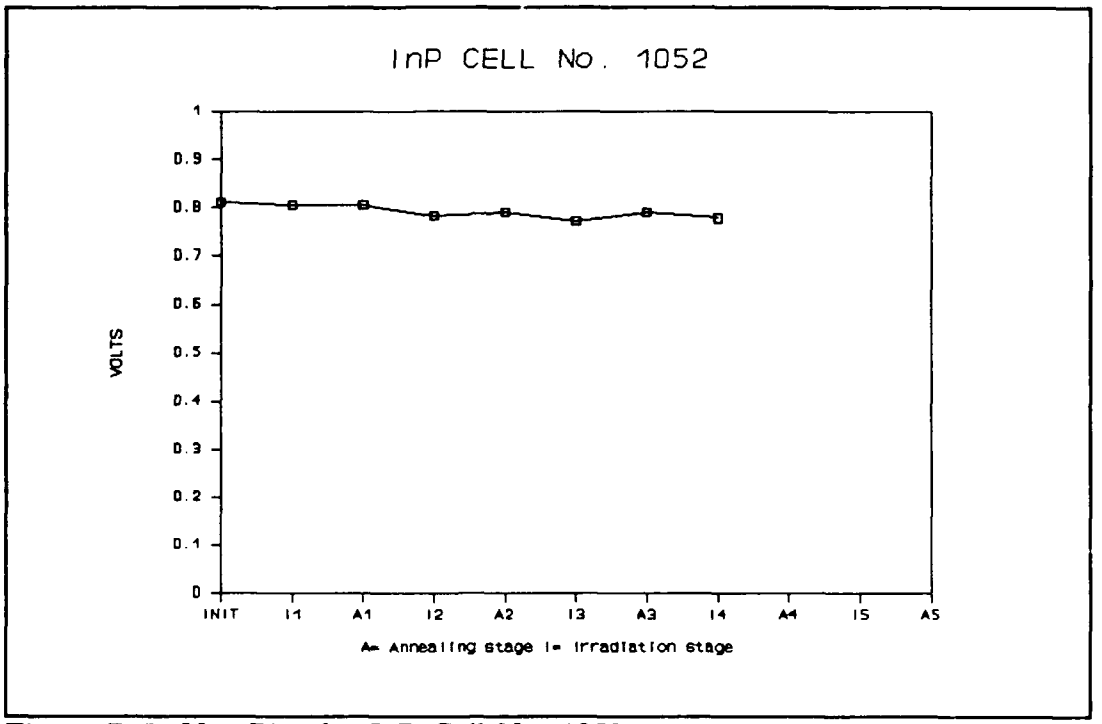

Figure D.5 Voc Plot for InP Cell No. 1052

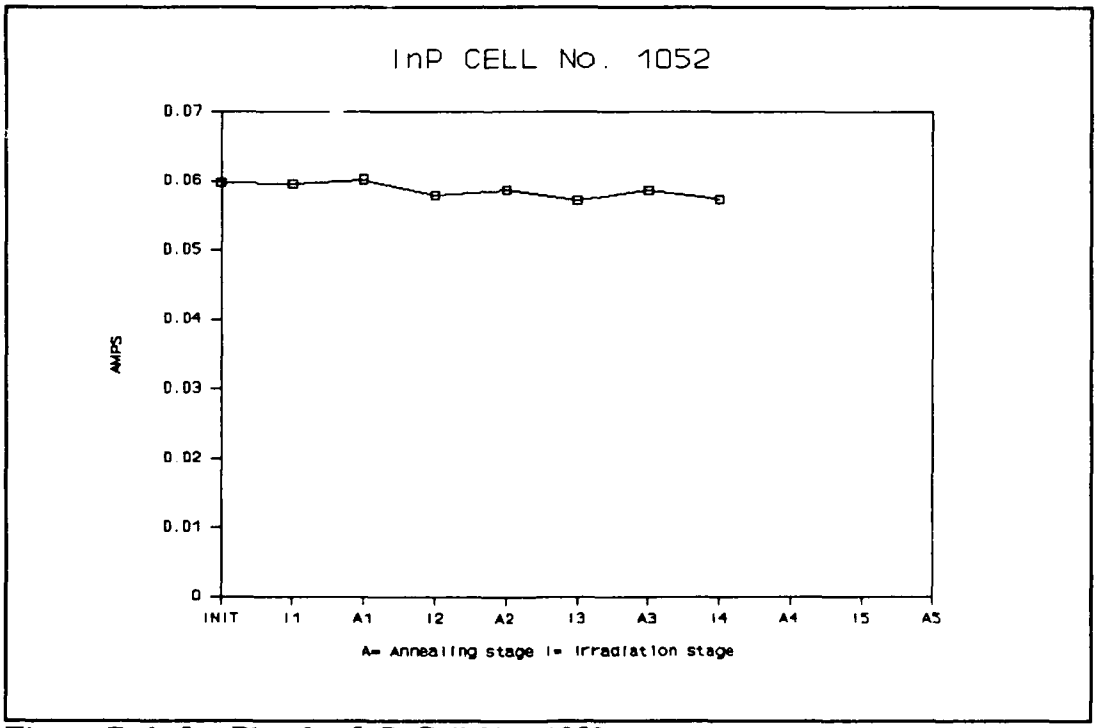

Figure D.6 Isc Plot for InP Cell No. 1052

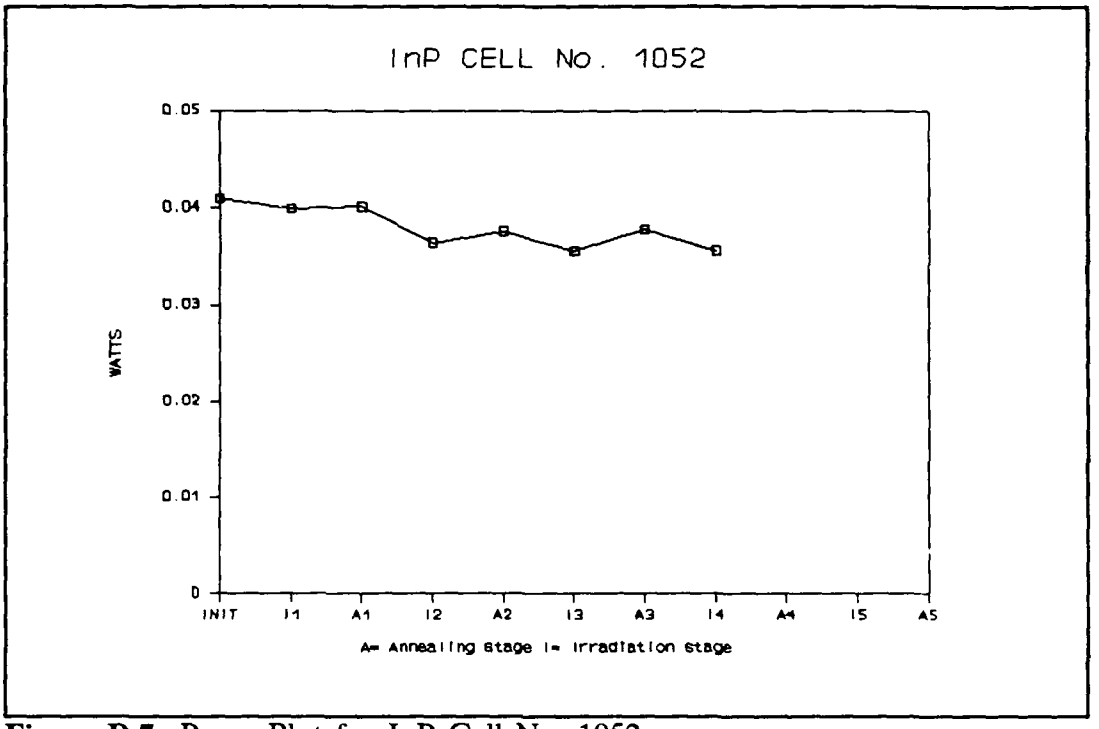

Figure D.7 Pmax Plot for InP Cell No. 1052

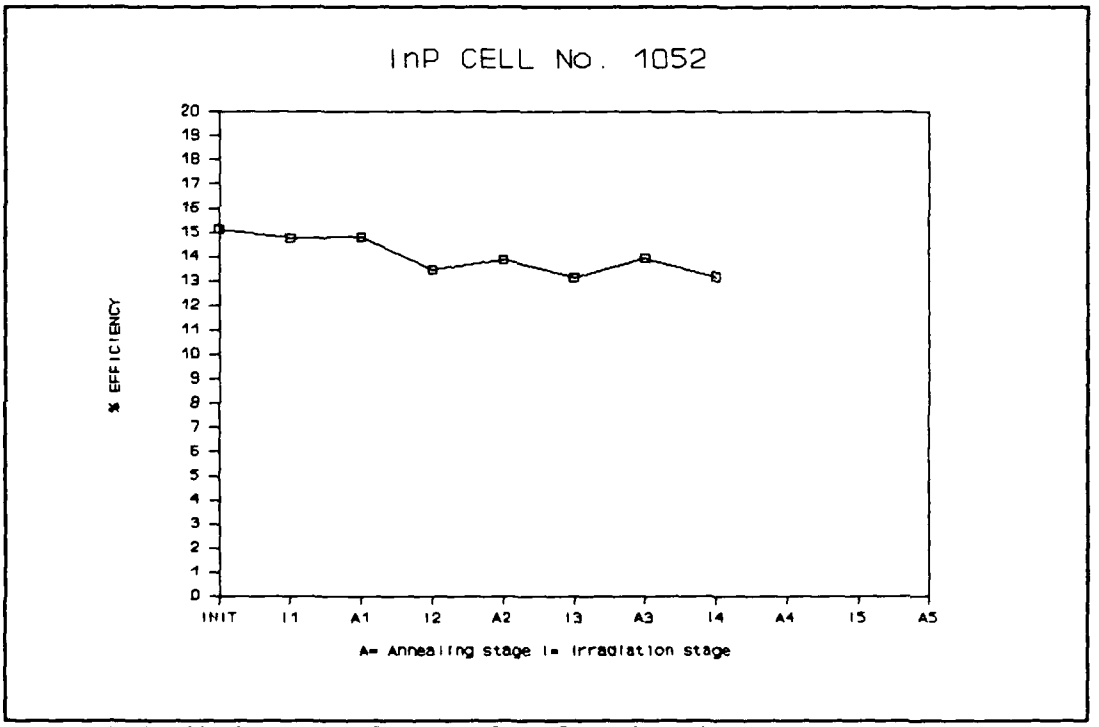

Figure D.8 % Efficiency Plot for InP Cell No. 1052

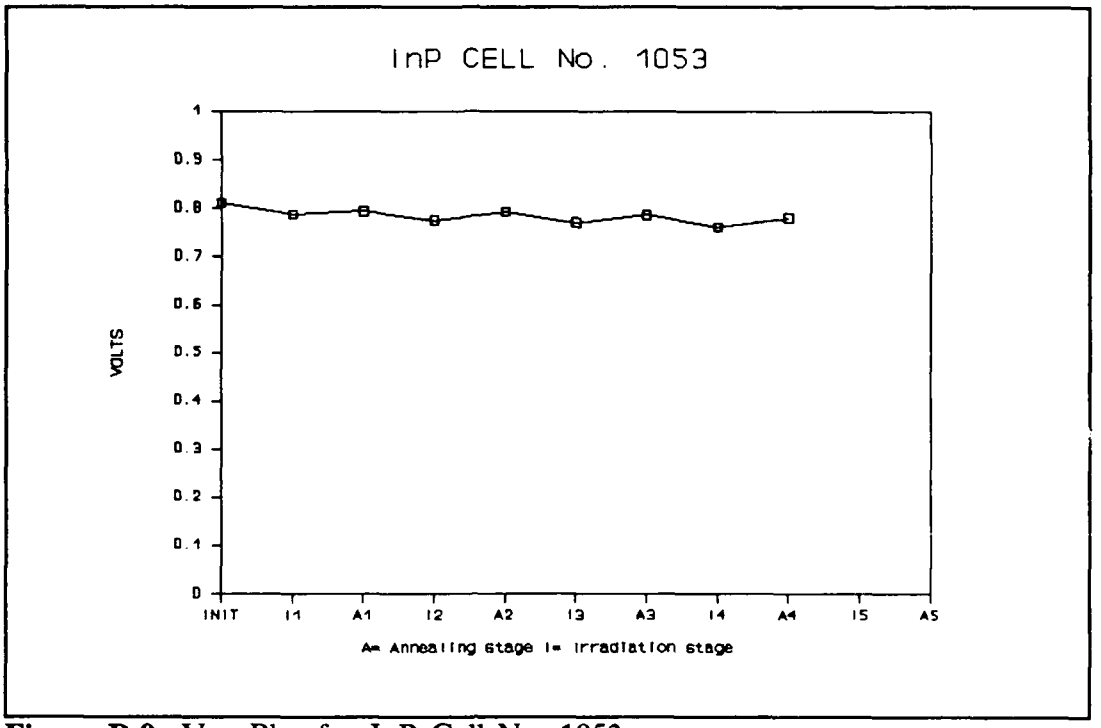

Figure D.9 Voc Plot for InP Cell No. 1053

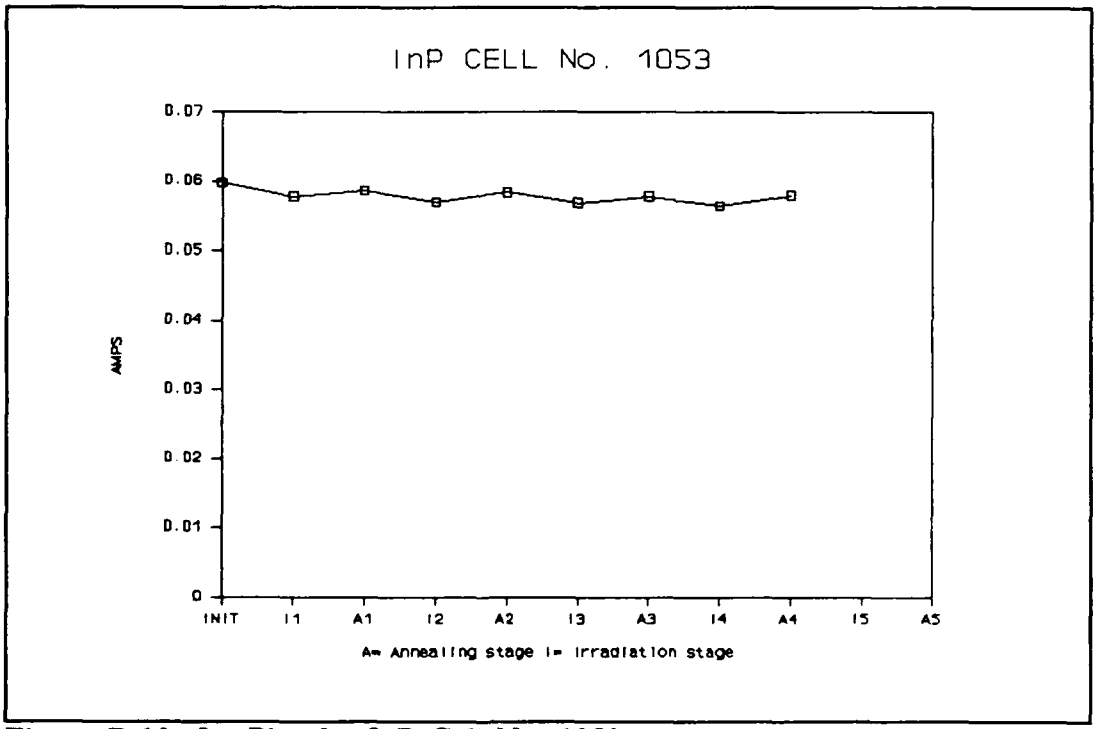

Figure D.10 Isc Plot for InP Cell No. 1053

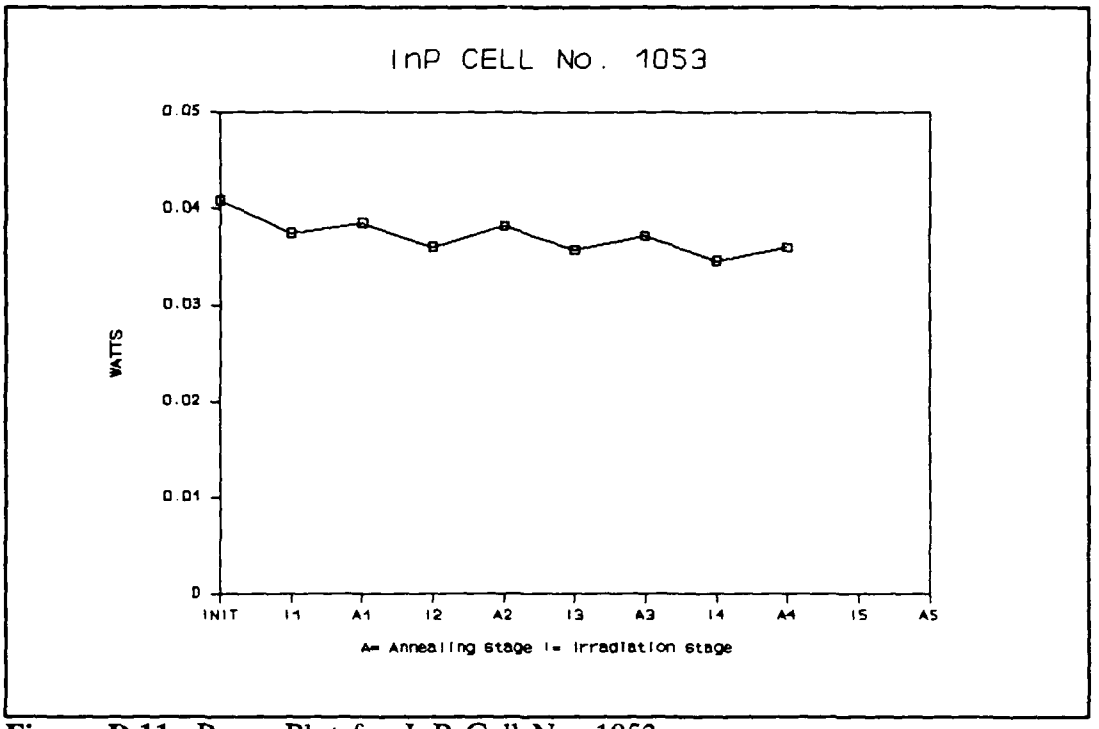

Figure D.11 Pmax Plot for InP Cell No. 1053

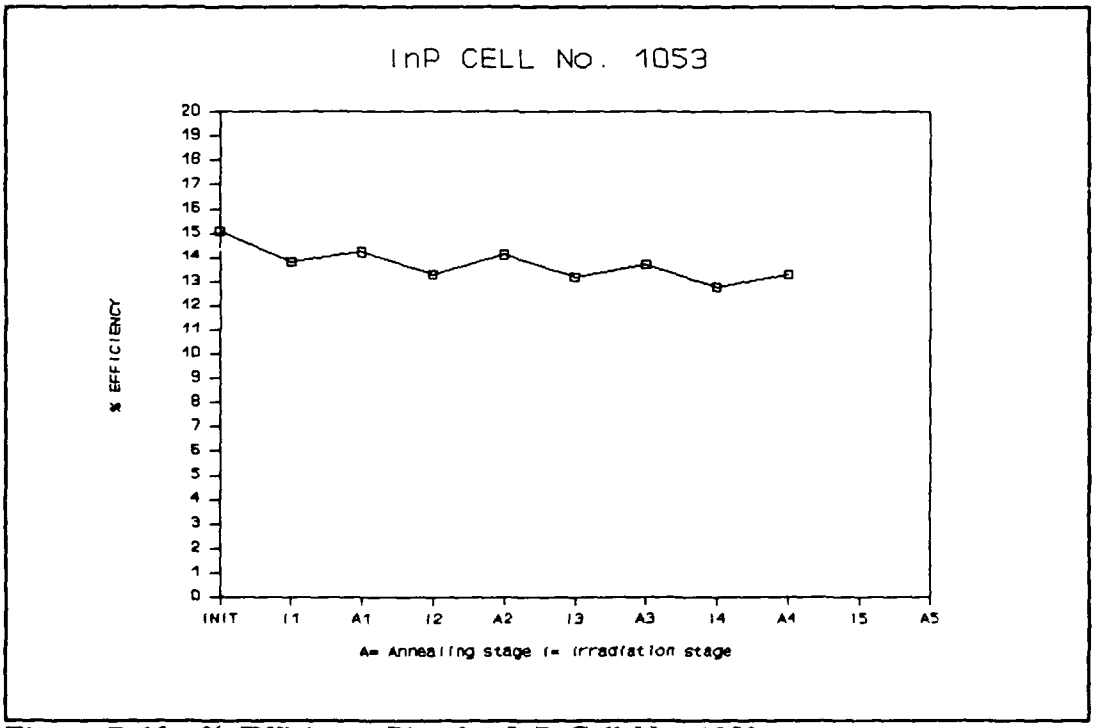

Figure D.12 % Efficiency Plot for InP Cell No. 1053

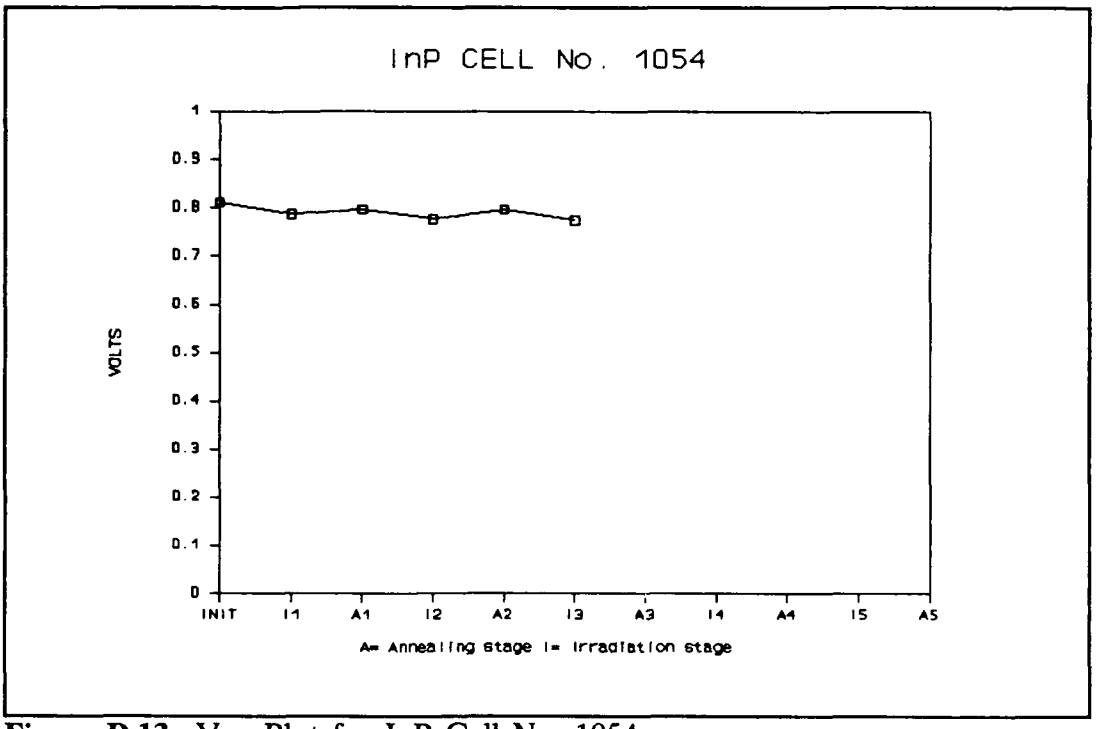

Figure D.13 Voc Plot for InP Cell No. 1054

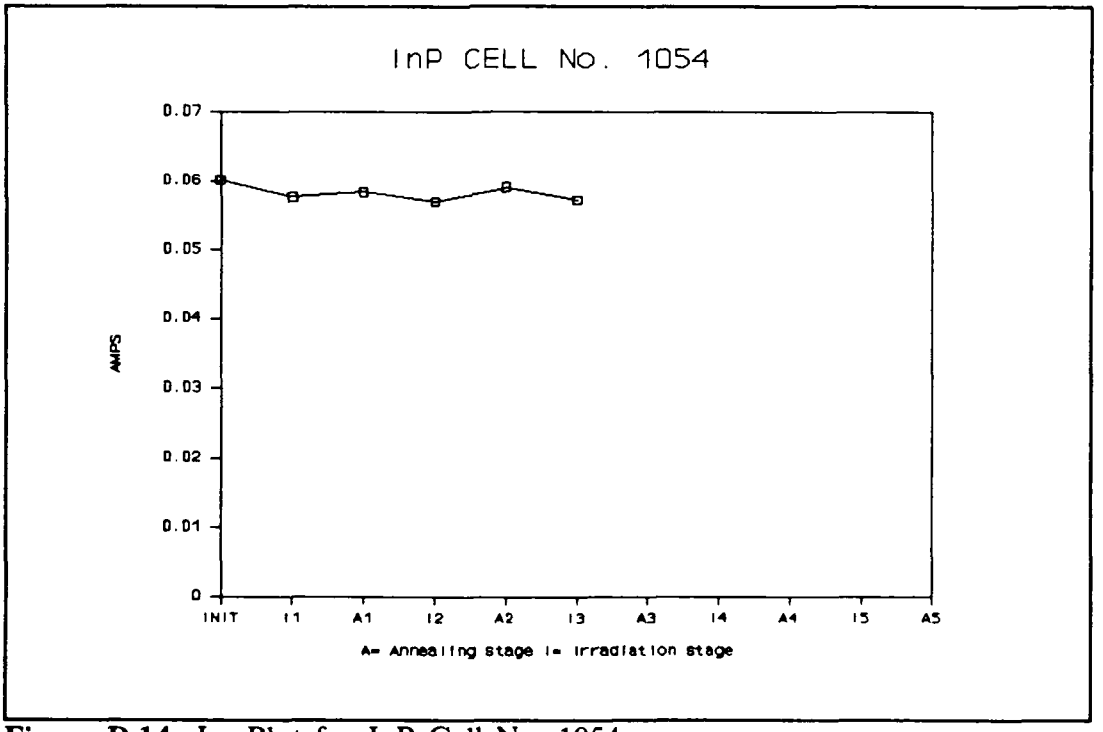

Figure D.14 Isc Plot for InP Cell No. 1054

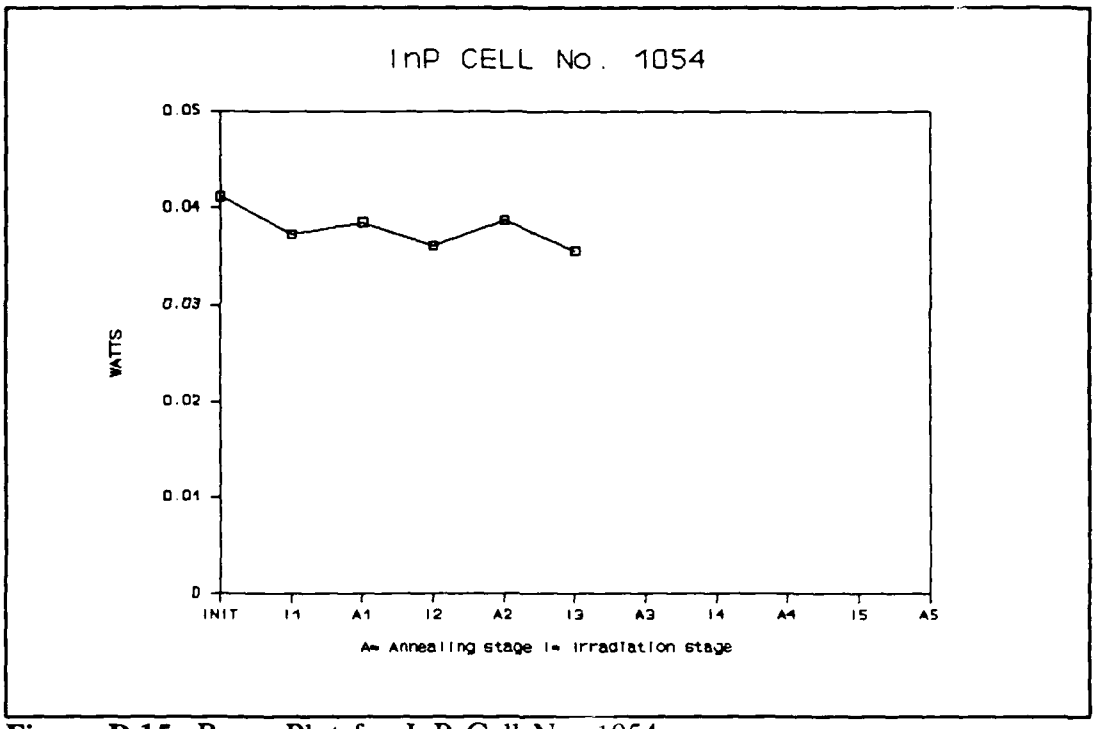

Figure D.15 Pmax Plot for InP Cell No. 1054

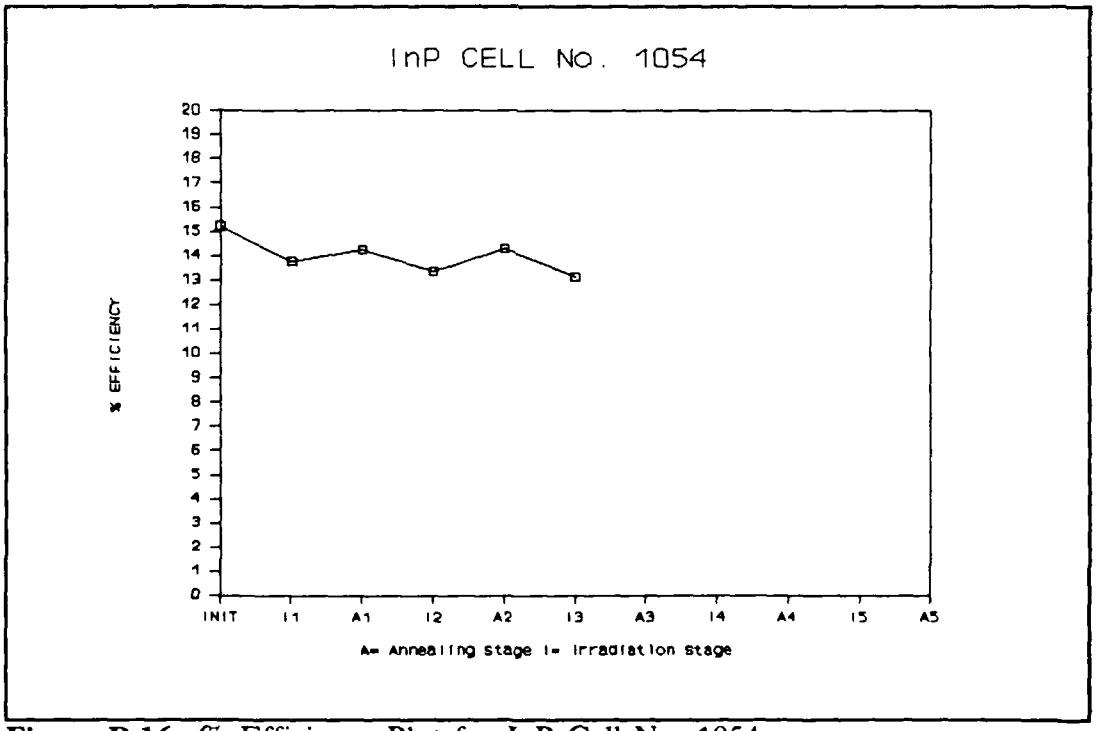

Figure D.16 % Efficiency Plot for InP Cell No. 1054

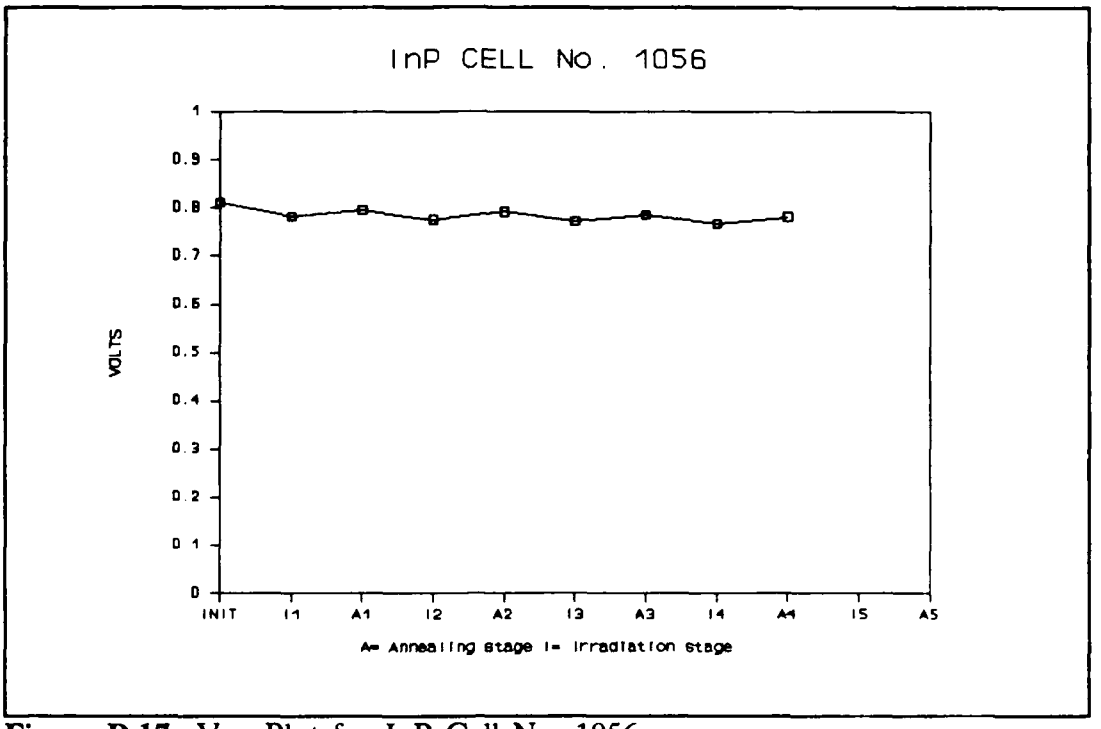

Figure D.17 Voc Plot for InP Cell No. 1056

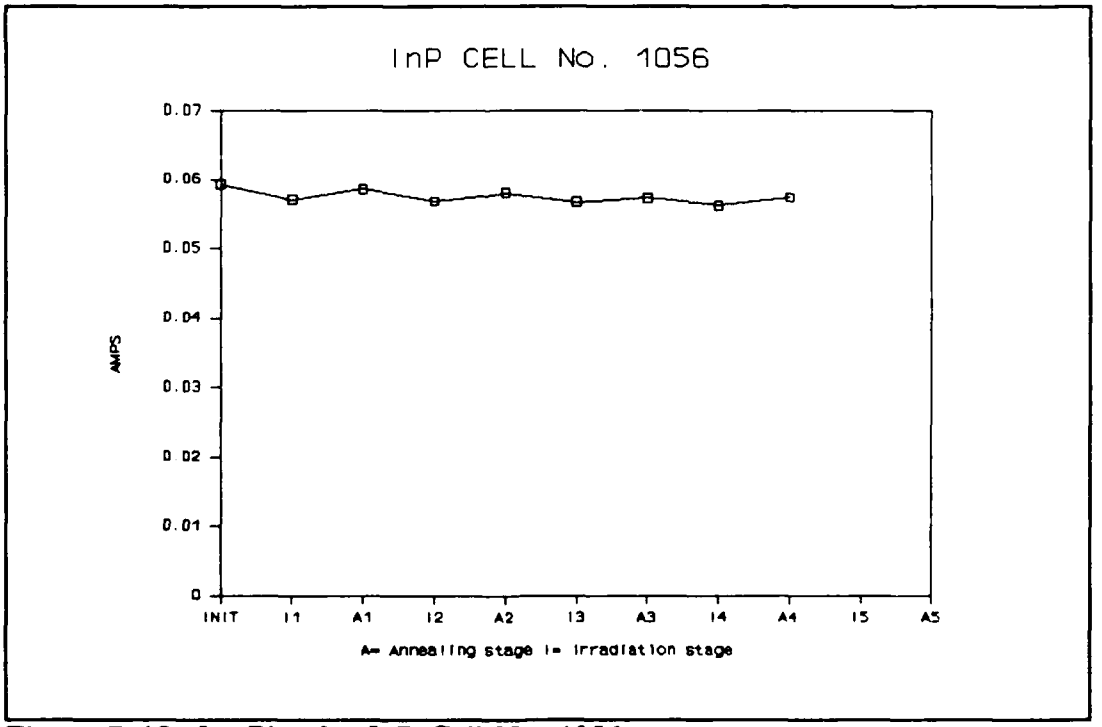

Figure D.18 Isc Plot for InP Cell No. 1056

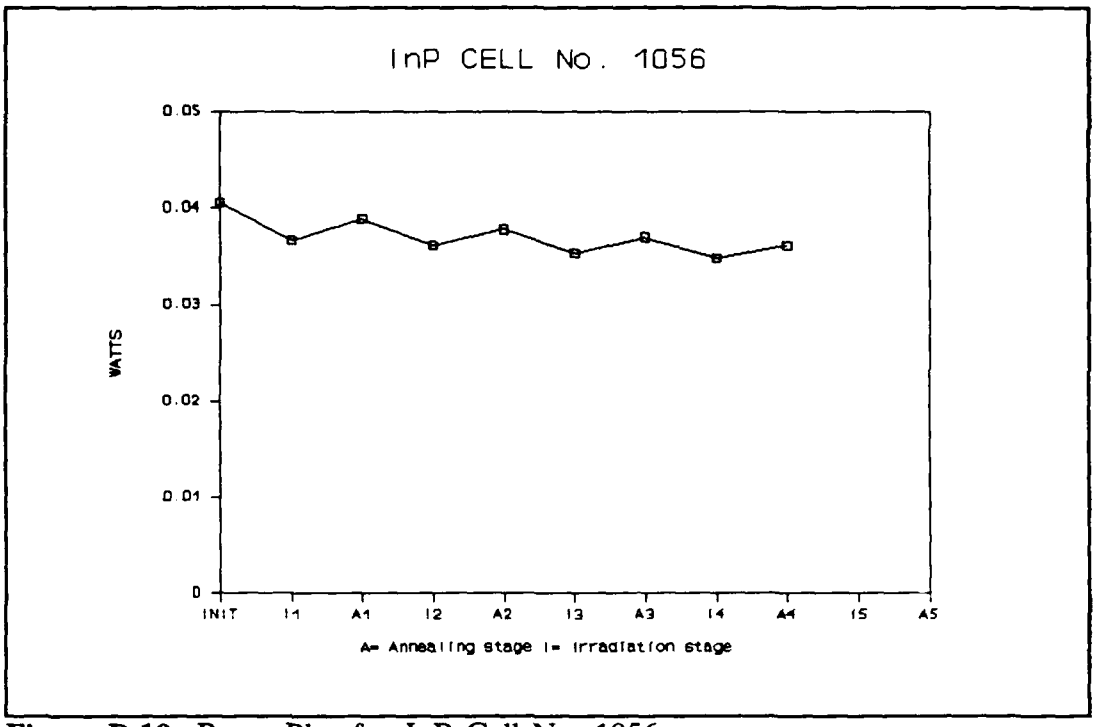

Figure D.19 Pmax Plot for InP Cell No. 1056

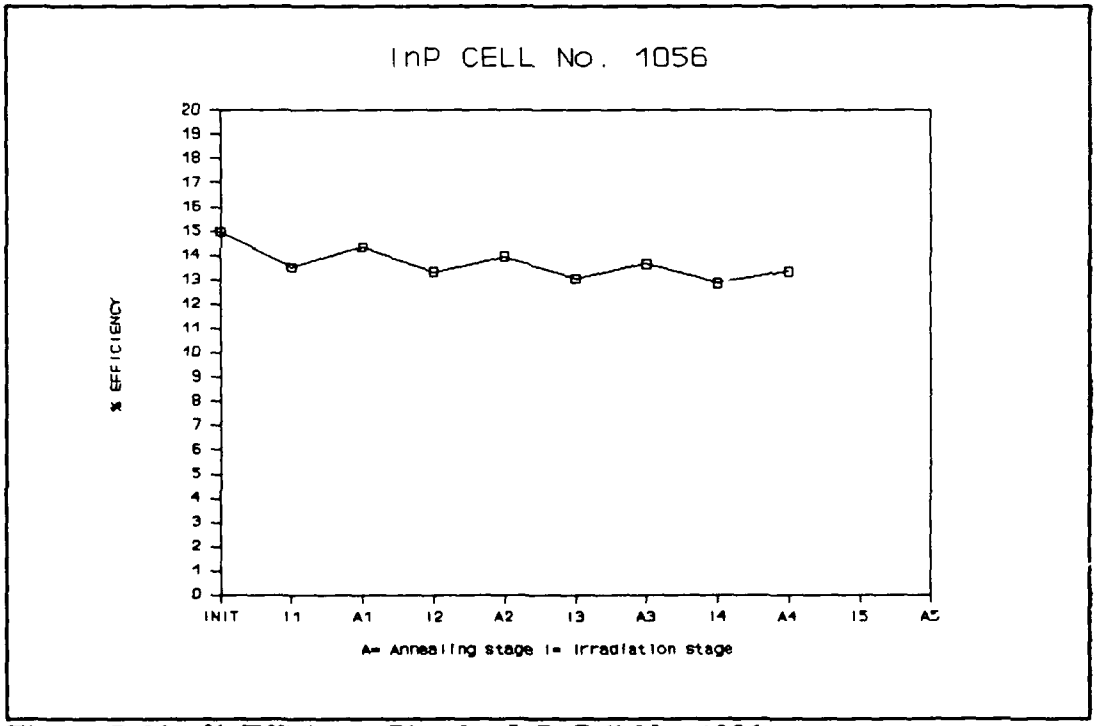

Figure D.20 % Efficiency Plot for InP Cell No. 1056

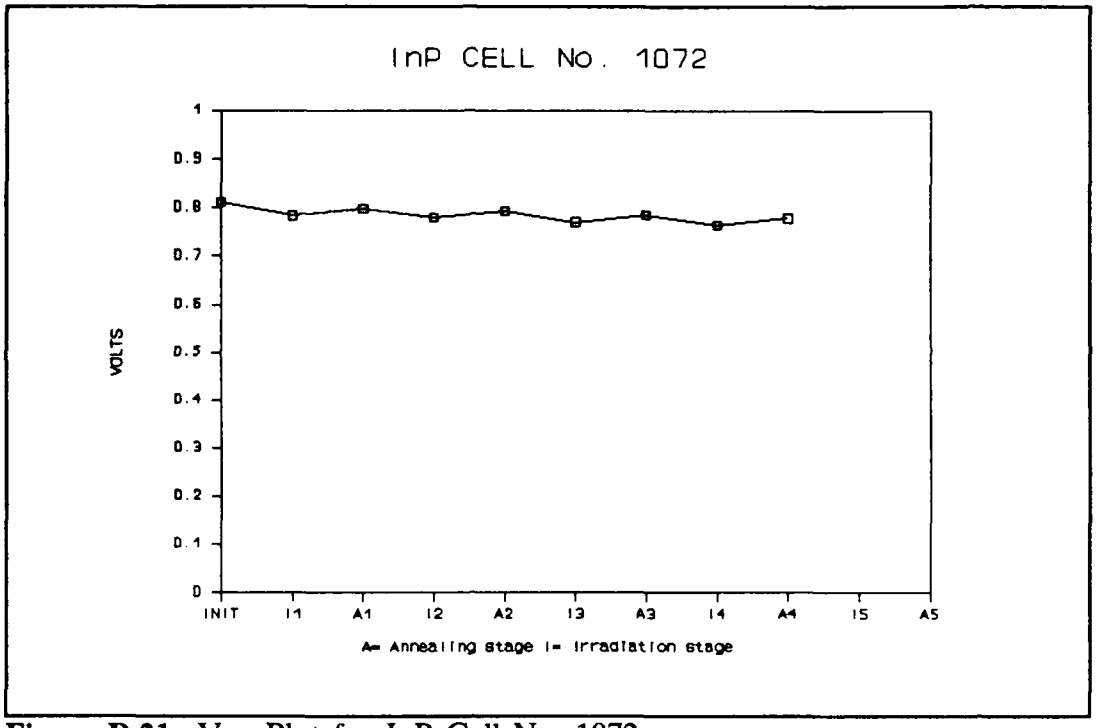

Figure D.21 Voc Plot for InP Cell No. 1072

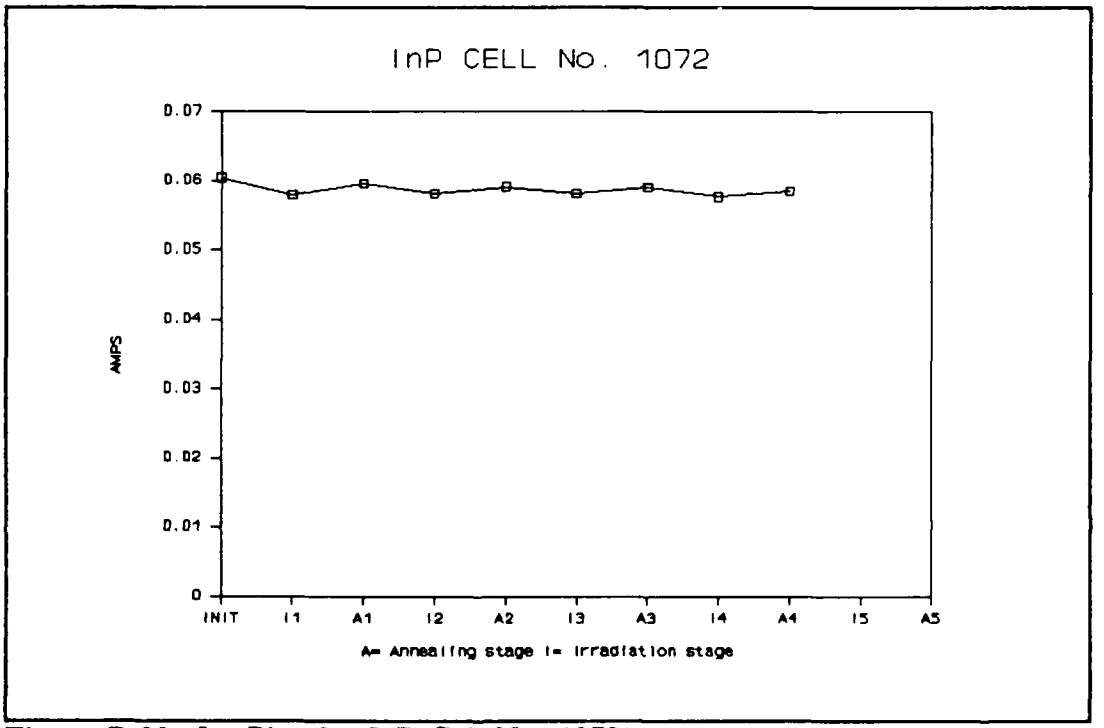

Figure D.22 Isc Plot for InP Cell No. 1072

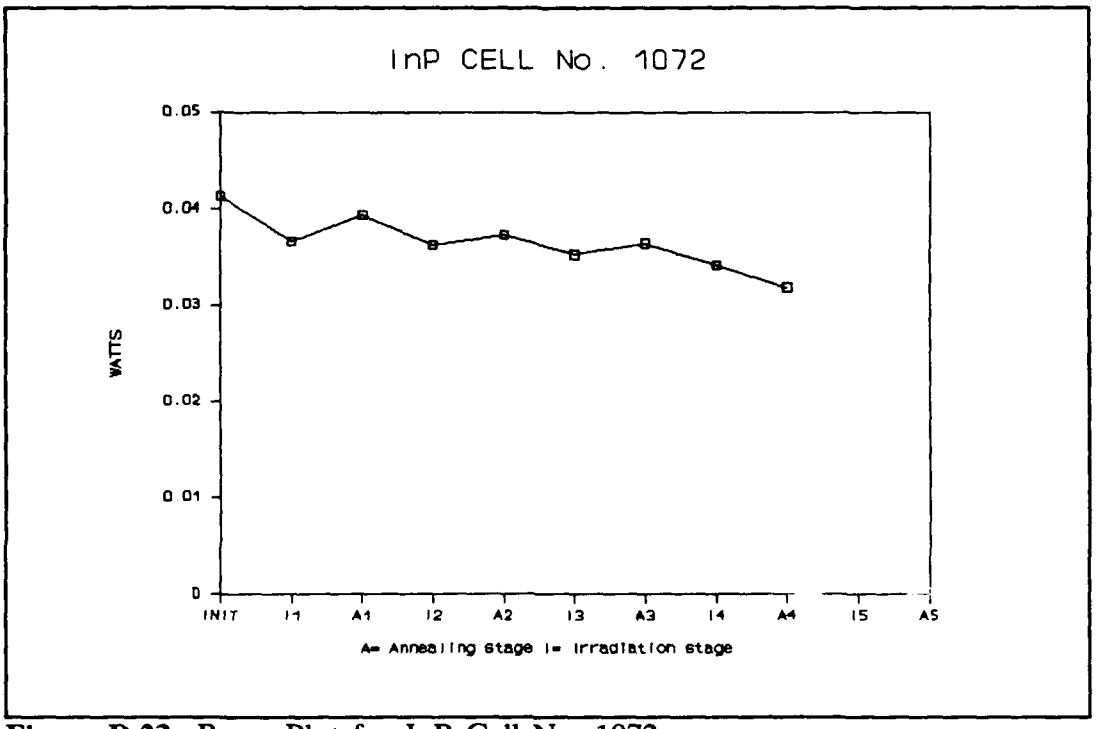

Figure D.23 Pmax Plot for InP Cell No. 1072

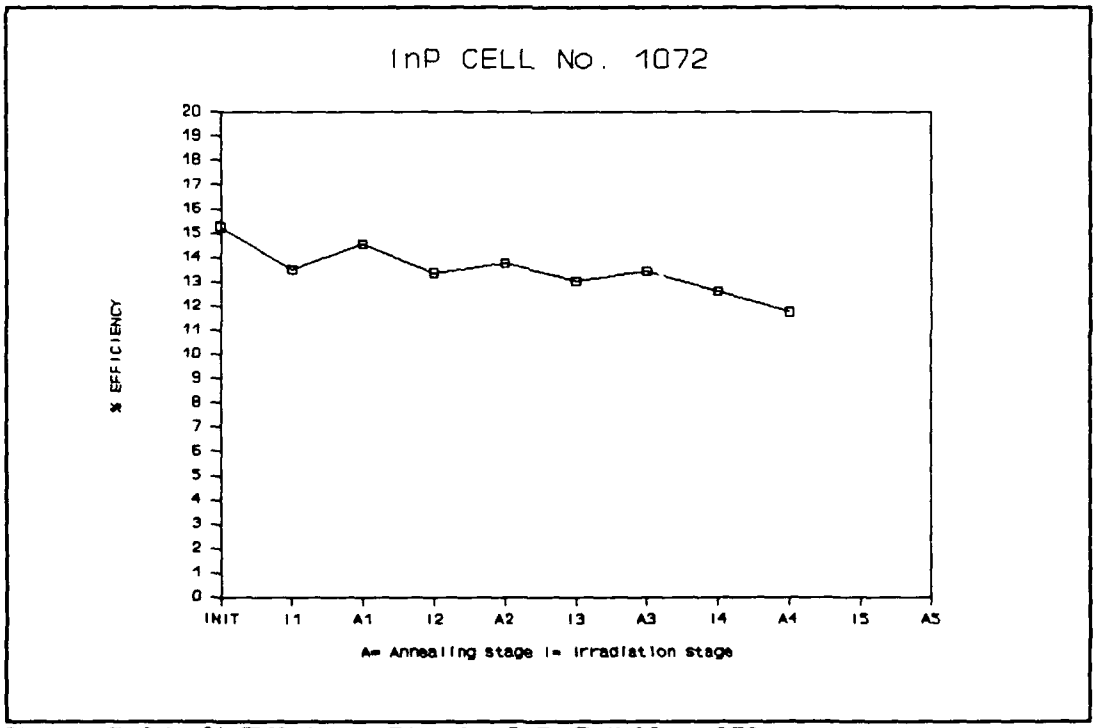

Figure D.24 % Efficiency Plot for InP Cell No. 1072

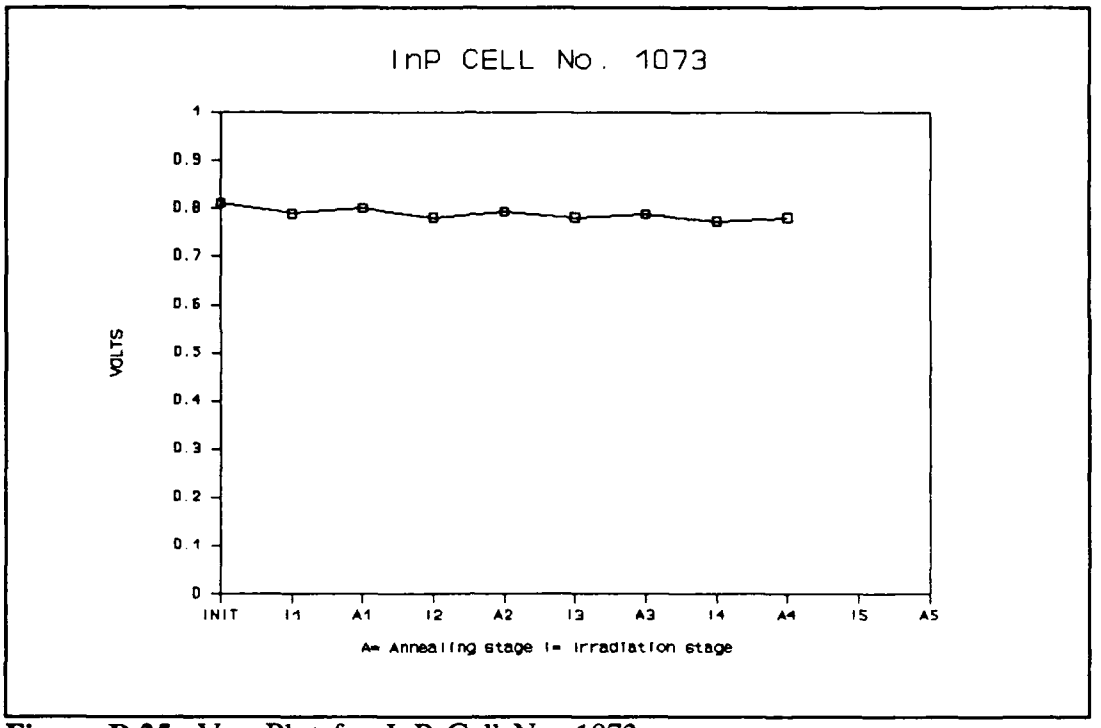

Figure D.25 Voc Plot for InP Cell No. 1073

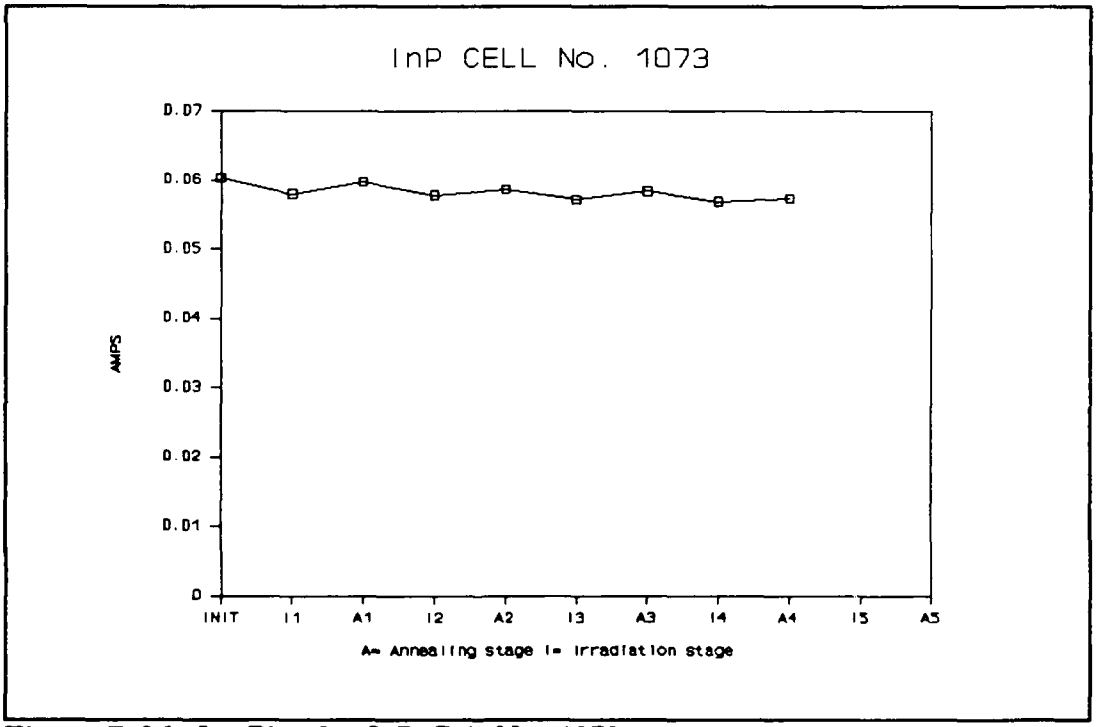

Figure D.26 Isc Plot for InP Cell No. 1073

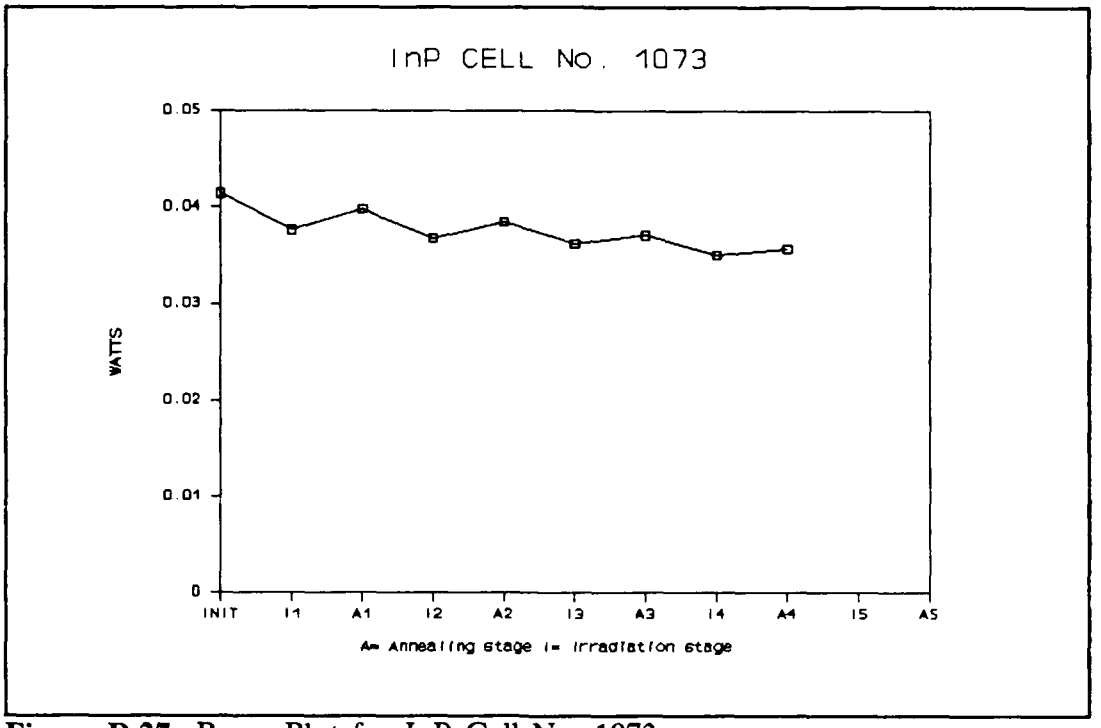

Figure D.27 Pmax Plot for InP Cell No. 1073

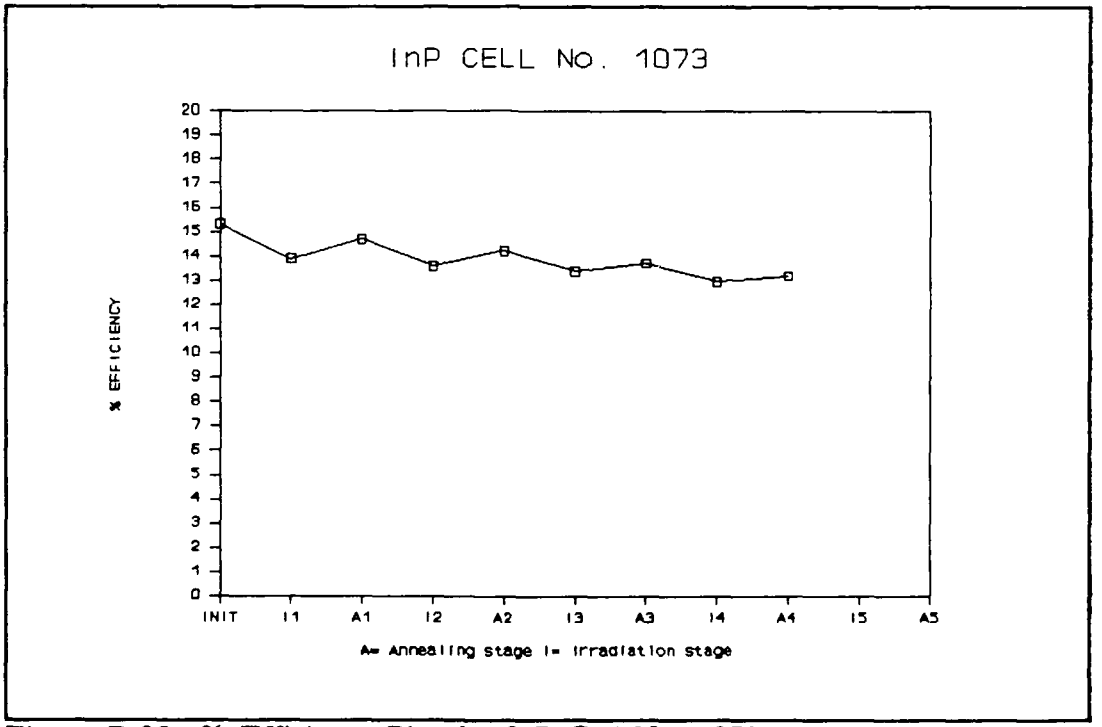

Figure D.28 % Efficiency Plot for InP Cell No. 1073

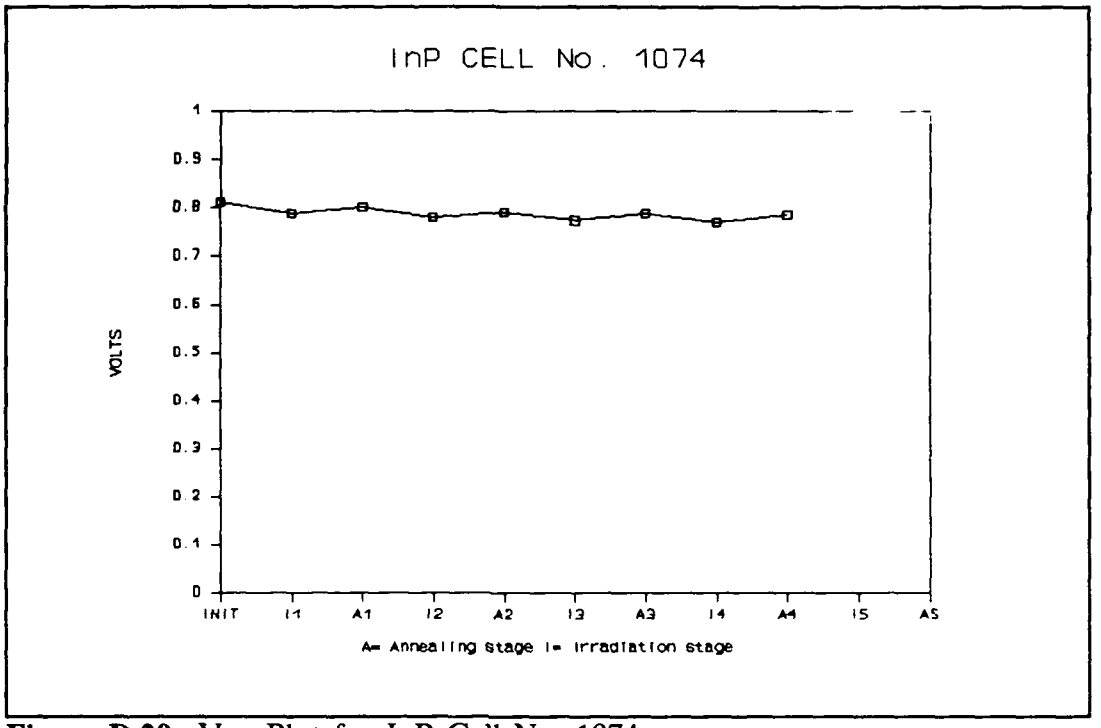

Figure D.29 Voc Plot for InP Cell No. 1074

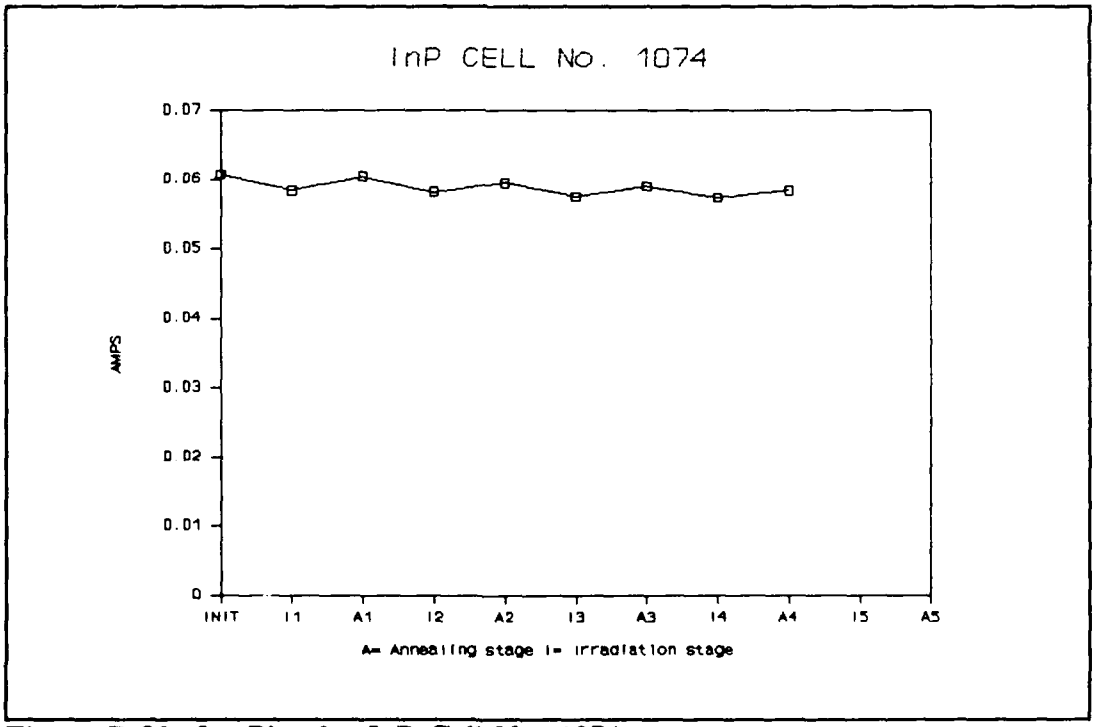

Figure D.30 Isc Plot for InP Cell No. 1074

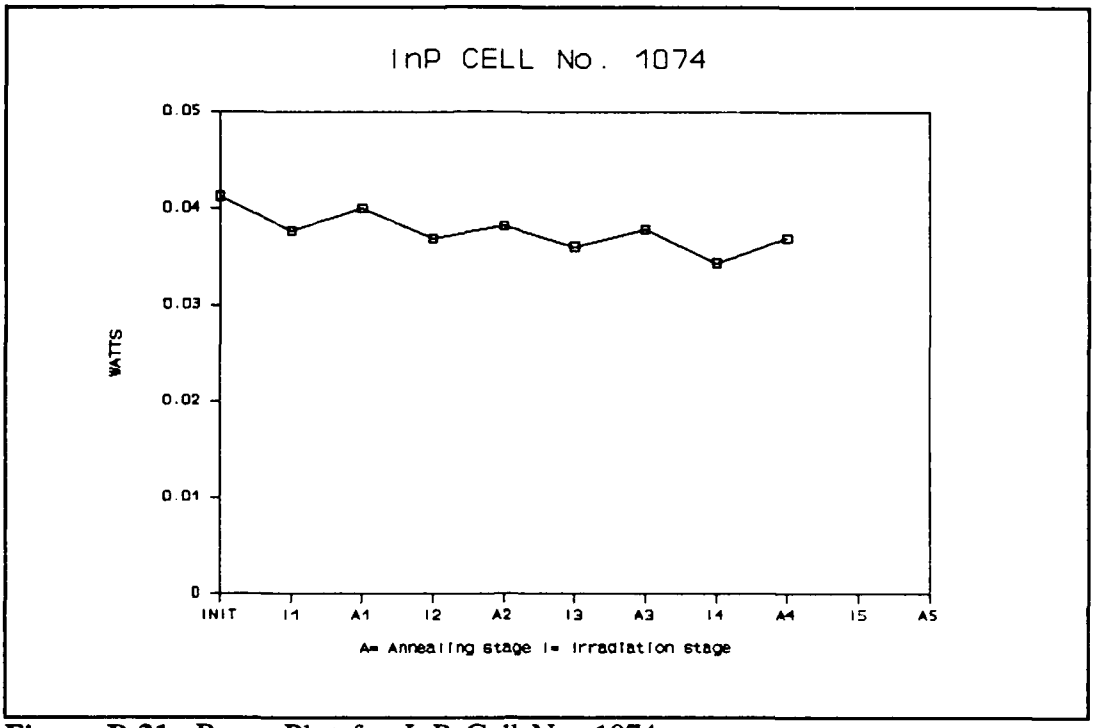

Figure D.31 Pmax Plot for InP Cell No. 1074

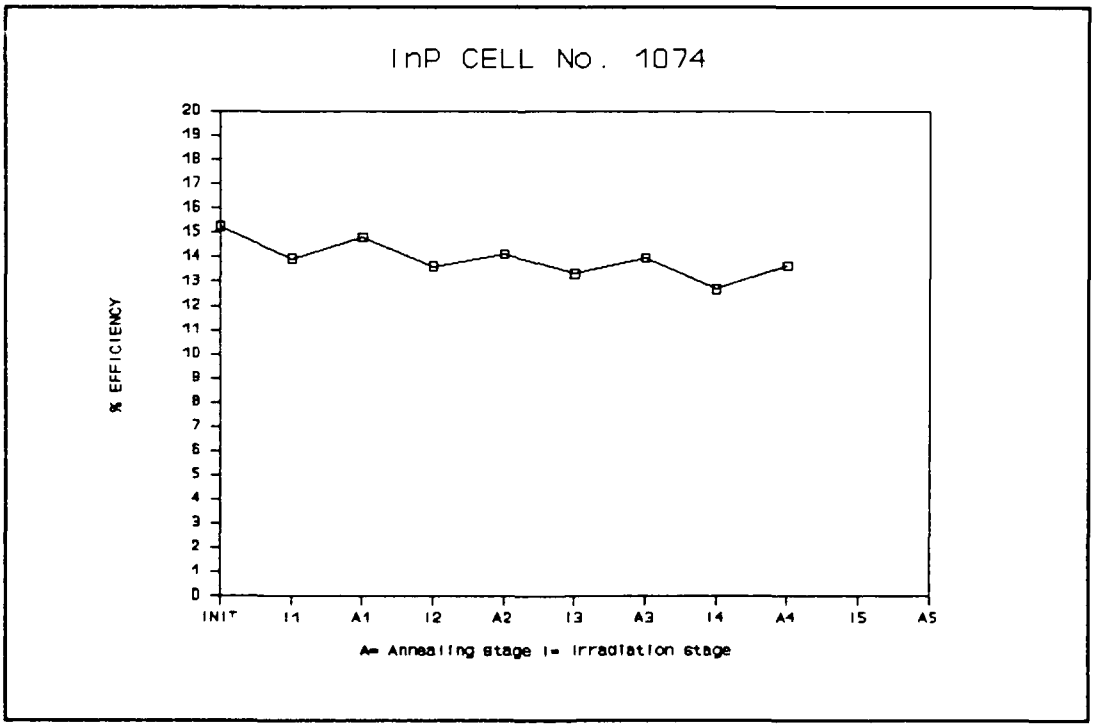

Figure D.32 % Efficiency Plot for InP Cell No. 1074

LIST OF REFERENCES

1. Jet Propulsion Laboratory Publication 43-38, Solar Cell Array Design Handbook, Volume 1, October 1976.

2. Rauschenbach, H.S., Solar Cell Array Design Handbook, Van Nostrand Reinhold Company, 1980.

3. Clark, T.F., An Experimental Test of Minority Carrier Annealing on Gallium Arsenide Solar Cells Using Forward-Biased Current, Master's Thesis, Naval Postgraduate School, Monterey, California, September 1986.

4. Staats, R.L., Forward-Biased Current Annealing of Radiation Damaged Gallium Arsenide and Silicon Solar Cells, Master's Thesis, Naval Postgraduate School, Monterey, California, September 1987.

5. Friedman, H., Sun and Earth, Scientific American Library, 1986.

6. Tascione, T., Introduction to the Space Environment, Orbit Book Company, 1988.

7. Jet Propulsion Laboratory Publication 82-69, Solar Cell Radiation Handbook, Third Edition, by H.Y. Tada, J.R. Carter, Jr., B.E. Anspaugh, R.G. Downing, November 1, 1982.

8. Hovel, H.J., Semiconductors and Semimetals, Volume 11, Solar Cells, Academic Press, 1975.

9. NATO Team, U.S. Air Force Space Division, NAVSTAR GPS Joint Program Office, Introduction to NAVSTAR GPS User Equipment, June 1987.

10. Weinberg, I., Swartz, C.K., Hart Jr., R.E. and Statler, R.L., Radiation and Temperature Effects in Gallium Arsenide, Indium Phosphide and Silicon Solar Cells, Nineteenth IEEE Photovoltaic Specialists Conference, pp. 548-557, 1987.

11. Rahilly, W.P. and Anspaugh, B., Status of AL GaAs/GaAs Heteroface Solar Cell Technology, Fourteenth IEEE Photovoltaic Specialists Conference, pp. 21-24, 1982.

12. Goradia, C., Geier, J.V. and Weinberg, I., Modelling and Design of High Efficiency Radiation Tolerant Indium Phosphide Space Solar Cells, Nineteenth IEEE Photovoltaic Specialists Conference, pp. 937-943, 1987.

13. Nippon Mining Company NS-12B NS-22B: Indium Phosphide Solar Cells: Space Power of the Future.

14. Yamaguchi, M., Ando, K., Yamamoto, A. and Uemura, C., Minority-Carrier Injection Annealing of Electron Irradiation Induced Defects in InP Solar Cells, American Institue of Physics, February 1984.

15. Yamaguchi, M., Itoh, Y. and Ando, K., Room-Temperature Annealing of Radiation Induced Defects in InP Solar Cells, American Institue of Physics, December 1984.

16. Agrawal, Brij N., Design of Geosynchronous Spacecraft, Prentice-Hall Inc., 1986.

17. Yamaguchi, M., Uemura, C. and Yamamoto, A., Radiation Damage in InP Single Crystals and Solar Cells, American Institute of Physics, March 15, 1984.

18. Loo, R., Knechtli, R.C. and Kamath, G.S., Enhanced Annealing of GaAs Solar Cells Radiation Damage, Fourteenth IEEE Photovoltaic Specialists Conference, pp. 33-37, 1981.

19. Chung, M.A., Meier, D.L., Szedon, J.R. and Bartko, J., Electron Radiation and Annealing of MOCVD GaAs and GaAs/Ge Solar Cells, Twentith IEEE Photovoltaic Specialists Conference, 1988.

20. Stievenard, D. and Bourgoin, J.C., Degradation and Recovery of GaAs Solar Cells Under Electron Irradiation, Seventeenth IEEE Photovoltaic Specialists Conference, 1984.

INITIAL DISTRIBUTION LIST

1.	Defense Technical Information Center Cameron Station Alexandria, Virginia 22304-6145	2
2.	Library, Code 0142 Naval Postgraduate School Monterey, California 93943-5002	2
3.	Professor Sherif Michael Code 62Mi Naval Postgraduate School Monterey, California 93943	4
4.	Chairman, Code 62 Department of Electrical and Computer Engineering Naval Postgraduate School Monterey, California 93943	1
5.	Professor Rudolph Panholzer Code 62Pz Naval Postgraduate School Monterey, California 93943	1
6.	Dr. Bruce E. Anspaugh Jet Propulsion Laboratory 4800 Oak Grove Drive Pasadena, California 91109	1
7.	Mr. Terry Trumbull AFWAL - POOC - 2 WPAFB, Ohio 45433-6563	1

8. Space and Naval Warfare System Command — 1
LCDR Richard Harding
WMOSS/SPAWAR/US NAVY
P.O. Box 2825
EADS Street Station
Arlington, Virginia 22202

9. LT Brian Kosinski — 1
Naval Research Laboratory
Code 9110-52
4555 Overlook Avenue, S.W.
Washington, D.C. 20375

10. Richard Statler — 1
Naval Research Laboratory, Code 4612
Washington, D.C. 20375-5000

11. LT Corinne Cypranowski — 4
P.O. Box 5451
Virginia Beach, Virginia 23455